The University Of Sheffield.

Leak Detection in Long Pipelines Systems

Hossen Saleh Alharbi

Thesis submitted to The University of Sheffield in partial fulfilment for the Degree of Doctor of Philosophy in the Faculty of Engineering

December 2018

Summary

Leakage in any fluid distribution network or conveying systems results in consumption of resources and time, and its impacts affect the on the environment and the profits for any asset owner. Moreover, a sufficient and applicable leak detection system, especially, in the oil/gas industry, comes at a high cost and time consuming, sometimes affects the system's productivity.

Because of its simplicity and encouraging results from the theoretical, experimental and real field tests, the water hammer phenomenon promises shows great benefits. This work has tried to utilise the routine transient events, raising the pump flow rate, to detect the leak. Also, it attempted to draw on some successful theoretical techniques, the cross-correlation and its second derivative, to apply on a real field system. To achieve that, some theoretical and experimental stages had to be carried out first.

The real system was scaled theoretically to form a laboratory apparatus, so it could be fitted in a Contaminant Ingress into Distribution Systems (CID) laboratory at the University of Sheffield. The leak approach was tested by means of a numerical code for this design before construction of the rig. Then, the experimental rig was completed and the data collected from it.

In the real field system, the shortage in the data frequency is an obstacle to applying the approach. The researcher's colleagues tried their best to improve the data acquisition system to meet the requirements. Although the improvement made to the system in terms of the time precision was impressive, the sample frequency increment was under the desirable level. The signal analysis approach was worked as expected theoretically, empirically the results were limited. Some trials were conducted to enhance the signal features. Later, some issues were raised and clarifications were added.

Table of Contents

List of figures

List of Tables

Nomenclature

Acronyms

CALM	Catenary Anchor Leg Mooring
CID	Contaminant Ingress in distribution Systems) laboratory Location (CID) laboratory, Civil Engineering, University of Sheffield.
CP	Cathodic Protection
DWT	Discrete Wavelet
EO	Export Operation Team
GC	Gathering Centre
HSDLS	High Speed Data Logging System
ITA	Inverse Transient analysis
KOC	Kuwait Oil Company
MOC	Method of Characteristics
NPP&MS	North Pier Pumping & Metering station
NRA	Noise-Removal Algorithm
OWT	Orthogonal Wavelet (OWT)
PLC	Programmer Logic Control
PLEM	Pipe Line End Manifold

SCADA	Supervisory Control and Data Acquisition System	
SA	Sample array matrix	
SF	System features matrix	
SFEE	Steady-Flow Energy Equation	
US	Upstream	
WH	Water hammer	
WT	Wavelet transform	

Greek Symbols

Δ	Change in parameters	
ψ	Localised oscillatory wavelet function	
Ψ	Fourier transform or the mother wavelet	
ρ	Fluid density	kg/m^3
μ	Fluid Dynamic Viscosity	$N.s/m^2$

Roman Symbols

a	Scale parameter	
A	Area	m^2
b	Translation parameter	
c	Wave speed	m/s

C	Coefficient	
C_r	Courant number	
d	Characteristics length	m
Eu	*Euler number*	
f	Darcy-Weisback friction factor	
F	Frequency start steepness	Hz
g	Gravity acceleration	m/s^2
h	Head	m
H	Pressure head	m
i	Index	
j	Index	
K	Increasing parameter number	
L#	Leak position number #	
M	Number of data	
n	Number of data	
P	Pressure	Pa
P#	Pressure transducer number #	

Q	Flow rate	m^3/s
r	Cross correlation	
Re	Reynolds number	
S	Transient and reflection wave ratio	
t	Time	*seconds*
V	Velocity	*m/s*
w	Frequency	*Hz*
W	Discrete wavelet transform	
x	Length	*m*
x	Input Signal	
y	Input signal or filter output	
Δx	Grid cell in x-direction	*m*

Scripts

C	Cut-off frequency	*Hz*
d	Discharge	
l	loses	
L	Leak	
O	Initial condition	
p	Pressure parameter	

R	Reflection Wave
v	Kinematic parameter
z	Potential parameter

Acknowledgments

Life is a journey of knowledge, and as long as the human being lives, he/she still continues to acquire new experiences and knowledge. Having the chance to work with knowledgeable and experienced people; saves lot of effort and time in gaining new knowledge.

During my PhD research period I could not have reached the end without being surrounded by such capable and sincere people, who supported me from the beginning until the end. First, I wish to thank my supervisor Professor Stephen B. M. Beck for sharing his experience and knowledge; additionally, his advices and patience always supported and encouraged me to continue working and keep my motivation. Second, I thank his co-supervisor Dr. Richard P. Collins, who helped me on many occasions. His precise remarks and inquiries highlighted a lot of details in various the research aspects.

Also, I extend the thanks and appreciations to the mechanical, technical, and laboratory supervisors for their support in building and maintaining the experimental rig.

I would like to thank engineer Shujaa Al-Otaibi (Team Leader Export Maintenance, Kuwait Oil Company) and his staff for their efforts and time in enhancing the real field data acquisition system to meet the research requirements as far as possible.

I really appreciate what they have done so far, for their hard works and sincere efforts. Their unfailing cooperation in the face of unexpected changes and challenges was greatly appreciated.

Finally, many thanks to my family members, parents, my dear dad (passed away during my studies), mom, and siblings; for their understanding and patience while I have been away from them, and for my wife and children for their accompanying me and bearing the separation.

Chapter 1 Introduction

1.1 Background

The use of conduits to convey fluid to end users is the main delivery method worldwide. These are constructed in different configurations to fulfil various operational requirements and form different kinds of networks. They generally consisting of long pipelines that transfer the fluid from one point to another, for example, the submarine export pipeline, the delivery of water from its source to a distribution pump station or the networks for distribution of water to residential properties. The operational flexibility of the system requires various fittings, such as valves, manifolds, and instrumentation to control the fluid flow and avoid any troubles.

In addition to water, the fluid of life, oil and gas have also become vital crucial for the recent civilizations and the development of industry. Because of their hazardous nature of these hydrocarbons, regulation codes and specifications to control the design, construction and operation circumstances of the pipelines networks have become a crucial safety issue in terms of minimising leakage to the lowest possible level.

Preserving non-renewable resources is an aim for the modern society in addition to minimising the destructive impact on human health or the environment. Fluid leaks are dangerous for all people dealing with oil and gas products and in some cases for the environment as well. The oil and gas companies and related vendors are therefore working hard to prevent and detect leakage. Attention to the possibility of leakage begins with the design stage and selecting the proper materials to carry the fluid. Afterwards, many approaches and techniques are utilised prior to and after operating the conveying system. Some of these techniques will be described in the following sections.

There are various approaches to finding leaks and there is no single ideal solution for all cases. Consequently, selecting the appropriate detection method is based on a variety of factors. In some situations, a survey is necessary to evaluate all the techniques and choose the most suitable and reliable one. In addition, leak cases can be used as case studies and the conclusion can be presented in the form of recommendations to minimise similar events.

It is well known that leaks in oil and refined products networks accounts for a very small percentage compared to the annual transfer amount [1], while water systems have a high percentage of leakage globally [2]. Oil and water network data show that these leaks in the oil industries are hazardous in respect of the high-risk impact, which explains why the number and quantity of oil leaks need to be lower than those of water leaks in number and quantity. Sustaining a high level of pipeline integrity to prevent any failure causing a leak is a highly essential issue for the pipeline operators. As a result, leak prevention measures such as 'leak detection methods' are applied to avoid consequences such as fluid loss, increased operational cost, environmental impact or hazardous fluid disasters.

The literature shows that, in Europe, leaks in oil and refined products networks compared to the annual transfer amount were reduced from 0.00019% in 2013 to 0.00006% in 2017 [3, 4]. Meanwhile, as reported in a 2017 report, 87 cases out of 93 were related to third party activity. Leaks in the oil industry are particularly hazardous due to the related high-risk impact. Restrictions imposed by design codes and the monitoring of normal operations have led the oil and gas industries to adopt the latest technology to detect leaks and carry out periodic inspections internally and externally to define their conduits' condition. An over-reliance on these methods means that detection of leaks based on the 'pressure surge phenomena' has been given less attention.

Leak detection methodology has developed over the last century, starting with visual inspection and progressing to detecting leaks by utilising different techniques based on modern technology. Methods of leak detection are divided into external

and internal forms. Examples of the former include visual inspections and acoustic leak finding, while the internal detection methods, which depend on fluid parameters, pressure, temperature and fluid properties, include: mass balance, pressure point analysis, intelligent pigging, transient wave, fibre optic, chemical based systems and others.

Utilising the pressure wave phenomenon to find leaks is robust, cheap and requires little operational effort compared to other methods. This method includes various approaches, but mainly well-presented numerical modelling is required to simulate the system. Indeed, no single approach is universally appropriate, since each system is distinctive in its configuration and operational requirements [1]. In the next chapter, this will be explained in more detail.

For evaluation, using the transient method to detect the leaks requires less effort, manpower and operational cost compared with other internal detection methods like intelligent pigging [5]. This could be integrated into continuous monitoring of the network system, making effective use of instrumentation and software for detection and measurement of any leakage. That being the case, the response time and operational efforts are sufficient in general when comparing this with other methods. Continuous monitoring can define the leak directly, and probably any changes in other features that may cause the leakages, such as changes in pipe topography and blockages, which may well, contaminate the water. Settled water in oil pipelines is a major source of internal corrosion.

As an introduction to the thesis, this chapter consists of the following sections: Oil and Gas Industry Pipelines, Leak Causes, Leak Consequences in the Oil and Gas industry, Leak Prevention and Protection in the Oil/Gas Industry, Pressure Surge Phenomena and Research Aims and Objectives.

In this dissertation, it is proposed to use and test the water hammer phenomena on a real-life system for exporting oil to vessels. The research consists of different stages and will begin by modelling the system and evaluating the numerical solver.

Then an experimental rig is designed based on the numerical code and scaled to mimic the real system. More details about aims and modelling will be explained in the next chapters.

1.2 Oil /Gas Industry Pipelines

An oil/gas network consists of the production wells which produce the crude oil/gas that is then transferred to the Gathering Centres (GC) by pipelines. The oil/gas from many different wells is collected at the GC where it is treated mechanically and chemically and then the collected fluid is conveyed through the pipelines again by pumping or gravity fed flow to the tank farm, the oil is further enhanced through separation of the water from oil using a sufficient settlement time. The tank farm also stores the daily production and when a cargo is requested, the crude oil is conveyed through gravity or pumped pipelines to the export terminals before being loaded onto the tankers or supplied to the refineries. In other words, the crude network could be divided into segments or a transient network and export network and the tank farm is the middle junction between the two. The network utilises a lot of facilities such as isolation or flow control valves, manifolds, instrumentations and others which allow operational flexibility and reduce operational difficulties. Most of the pipelines are equipped with pigging facilities to provide both the cleaning and intelligent pigging services.Geographically the production fields are located in various positions and normally are not adjacent. Pipelines pass through secured and unsecured areas and convey different fluids like crude oil, High Pressure (HP) Gas, Low Pressure (LP) Gas, Low and High Fuel Gas and condensate. Although in pipeline transportation the possibility of leakage is present, it is still the most efficient, secure and inexpensive conveyance method for these hazardous hydrocarbon materials [6].

Figure 1-1 presents a diagram of a typical oil production system.

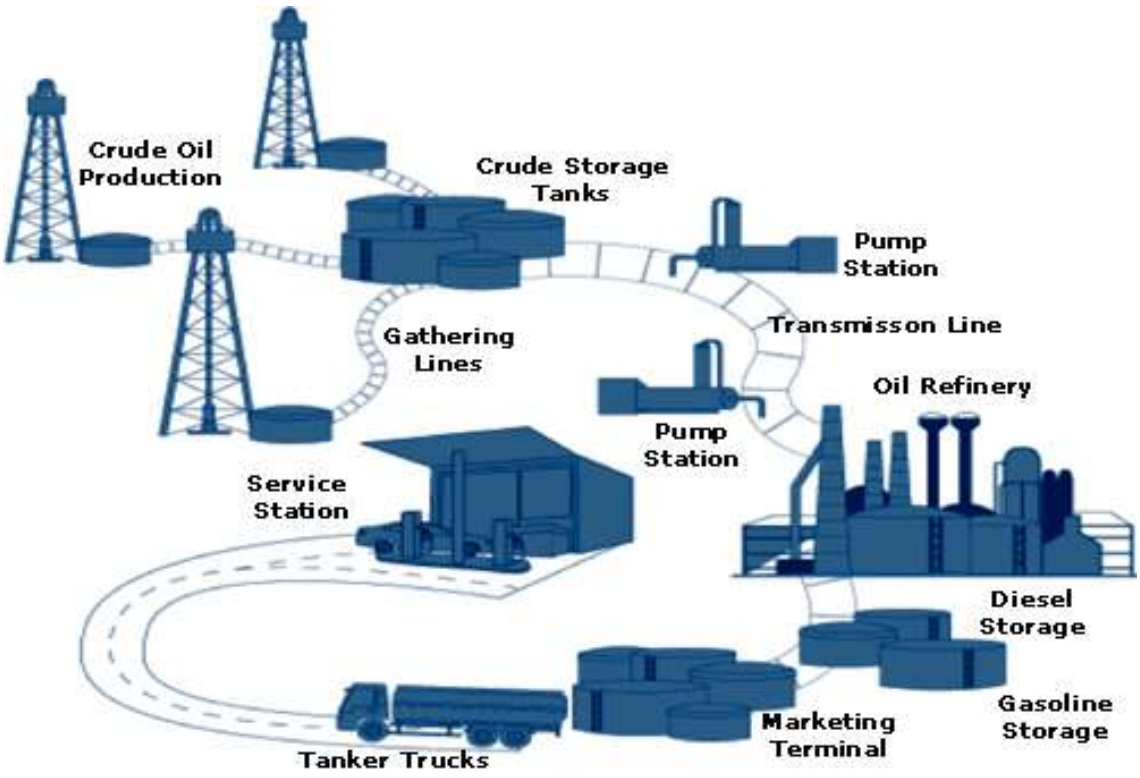

Figure 1-1: Crude oil System [7].

Since there is a high risk of impact on the environment and society, pipelines used in crude/gas industry are strictly required to incorporate safety features into the design of operating parameters (pressure, temperature and flow) in order to avoid any uncontrollable faults that could lead to leaks. In addition, the latest technology, and on average, highly expensive techniques are normally employed.

1.3 Causes of Leaks

There are several possible causes of damage in the pipelines which can lead to fluid loss. These causes include:

1) Corrosion of the pipeline.
2) Erosion due to mechanical effects.
3) Failure of equipment or components like valves or gaskets.

4) Improper equipment criteria, for example, use of pipeline or fittings of lower class than the operational parameters for the pressure, temperature or flow rate.

In some situations, poor installation of the proper equipment by untrained technicians can cause leaks. For instance, incorrect installation of metallic gasket could damage it and prevent it from holding the pressure of the fluid.

However, corrosion is the main reason for leaks in oil/gas industry networks. Corrosion in the pipelines could happen internally or externally. The first form occurs mainly because of water stagnation in some pipeline segments due to topography or insufficient flow like pipe dead legs. As a result, the corroded part will be generally in the 6 o'clock position [6]. In some cases, such as when the gases condense, the pitted part is on the top of the pipe because of the vapour phase of the liquid. In addition to water, the presence of Hydrogen Sulphuride (H_2S) also accelerates the corrosion [6]. On the other hand, external corrosion is a result of damage to the external coating, failure of the cathodic protection system (widely used in oil/gas industry, as will be explained later), or damage could be caused by a third party such as contractor who is not directly employed by asset owner.

Crude oil is variable in composition and, consequently, requires precautions in pipeline design. The two most common components known to cause corrosion are water and Sulphur. High concentrations of both components increase the probability of corrosion, particularly in parts of the network where fluid can stagnate due to topography, flow rate or sediments. At these locations there is a probability of stagnation and, therefore the likelihood of the separation between oil and water is likely to occur [6]. In some systems, the engineers in that location suggest installing an internal lining layer coating of an internally by suitable substance like fibre-glass.

The aforementioned reasons may individually cause leaks but occasionally two or more of these reasons may combine to contribute to pipeline failure and hence fluid loss.

Figure 1-2 to Figure 1-5 illustrate some of the kinds of leaks that can occur. Figure 1-2 illustrates a leak in a D-filling line in the South Tank Farm of a Kuwait Oil Company due to corrosion at the welding joint. The pinhole pitting can be seen and the maintenance team is stopping the leak by fixing a piece of wood in order to repair the damaged pipeline segment temporarily until the pipeline can be drained and

Figure 1-2: Leak due to internal corrosion in D-Filling line in South Tank Farm, Kuwait Oil Company (Original/Fieldwork).

a permanent repair can be made . Figure 1-3 shows a gasket failure leak where the valve pit has become filled with crude oil and is beginning to overflow from the pit. This incident occurred in the Cross-Over Manifold at the Export facilities of a Kuwait Oil Company.

Figure 1-3: Gasket Failure leak in Cross-Over Manifold, Kuwait Oil Company (Original/Fieldwork).

Another example of a leak caused by internal corrosion can be seen in Figure 1-4, which shows the pitting inside condensate pipelines. Corrosion due to vapour is clearly shown in the right hand picture, while the left hand one shows the corrosion due to water stagnation at the bottom of the pipe.

Figure 1-4: Corrosion in Condensate pipelines [6].

A third party can also cause some of the damage to conduits. Unfortunately, all accidents due to this reason have been noticed to happen within the restricted area

for the company as mentioned in a KOC leak report [6]. Also, damage can be caused by the owner company itself. Due to lack of supervision, poorly trained personnel, lack of demarcation facilities, markers or other reasons, there has been a noticeable numbers of such occurrences in the company.

Figure 1-5 shows damage to an HP gas pipeline caused by an excavator.

Figure 1-5: Third party damage by excavator on GC-20 HP Gas pipeline [6].

1.4 The Consequences of Leaks

Although both oil and water are fluids, because of their different components, the different design criteria, and the severity (riskiness level) of the fluid the leaks will vary in nature; firstly as mentioned earlier the size of the leak, or to be more specific, the size of the harm to the property, the public and the environment may differ. Also, the consequences of the leak differ from one case to another.

Most of the leaks in oil pipelines are due to corrosion which probably culminates in a small quantity of loss; however, these leaks could enlarge, for example, a slow leak such as a the pinhole size crack could become larger with time without any

significant forewarning of its existence due to, for example, such as a sudden pressure surge.

Another noticeable consequence of leaks is the suspension of flow in production or transmission pipelines to rectify the pipeline, which leads to daily losses for the oil/gas companies as they focus their maintenance efforts internally or externally on rectifying and resuming the operation of the damaged part. In addition to suspension of the production, repairing the damaged facilities requires manpower which in turn might have an impact on people and even cause fatal accidents.

Regarding the environment, leaks of oil/gas products have harmful effects and the cleaning, recovery and rehabilitation of the environment could incur very high expenditure. Consequently, companies in this industry could lose their good reputation with one massive leak. For instance, one recent disaster had a huge economic and environmental impact is the leak which occurred in the Mexican Gulf in 2010. This adverse incident resulted in 11 fatalities and cost two companies billions of dollars, British Petroleum and Halliburton (the drilling company), with about 9 billion US dollars paid to the fishermen in the region and to settle the criminal charges [8].

1.5 Leak Prevention & Protection in Oil/Gas Industry

Owing to the high risk of leak impacts in the oil/gas industry, many approaches and techniques are used in all facility stages, beginning as early as the design stages through analysing the product contents, selecting suitable material for conveying it; and continuing during construction and after completion and starting the operation of the network to control the leak causes. In this section some techniques and processes used to prevent and reduce the possibility of leakage will be demonstrated. These include brainstorm type analyses which including the Risk Assessment and the Hazard and Operability Analysis (HAZOP) [6, 9], modifications of the pipelines, for example, using the internal and external coating to reduce the corrosion/erosion opportunity or monitoring methods like instrumentation, control systems and the intelligent pigging.

Leak detection systems will be explained in detail in the next chapter in order to set the scene for the research subject.

As aforementioned, pipeline corrosion is the major reason for leakage. Manufacturers and operating companies are working hard to increase pipelines' operational age by reducing the corrosion influence on the conduit. That is achieved by installing internal or external coating or using the inhibitors as well as installing a Cathodic Protection system which significantly reduces the corrosion.

An external coating prevents the external pipeline layer from interacting with the substances which cause the corrosion. The coal tar tape system has been used for decades and has been very successful when installed efficiently. Recently, use of the three-layer Fusion Bonded Epoxy coating system has become popular and is widely used [6]. Similarly, to control corrosion, injection of the fluid with inhibitors like wet crude (crude with high content of dissolved and free water) is another implemented technique. From the signal point of view, the coating increases the noise dissipation [10]. The internal coating produces additional reflection waves.

A further active method to reduce corrosion in metal pipelines is the Cathodic Protection (CP) system. After the primary protection of wrapping and coating, the CP system is considered as a secondary protection. CP systems supply the metal with electrons to enable it to work as a cathode, so the direction of the corrosion will be reversed. Kuwait Oil Company (KOC) as an oil/gas company example has utilised this method since the 1950s [6]. For underground pipelines, the Impressed Current Cathodic Protection is used, while for the offshore assets the Sacrificial/Galvanic Anode Cathodic Protection is installed. A survey is carried out periodically to check the function of the system on every designated pipeline length, typically 1-2 km, thereby allowing for any faults or breaks in the system to be identified and fixed.

Moreover, some systematic analytical risk evaluations are carried out on networks to recognise possible influences on employees, property, public and the environment and in the following the risk assessment and the HAZOP process will

be clarified. Risk Assessment is a tool to manage the pipeline system's integrity by identifying the probability of a circumstance that leads to a leak. Loss of the pipeline's integrity (pipeline failure) causes the hazardous products to leak and increases the risk consequences. The risk is different from one location to another and depends on the surrounding environment that may contain residential housing or risky locations.

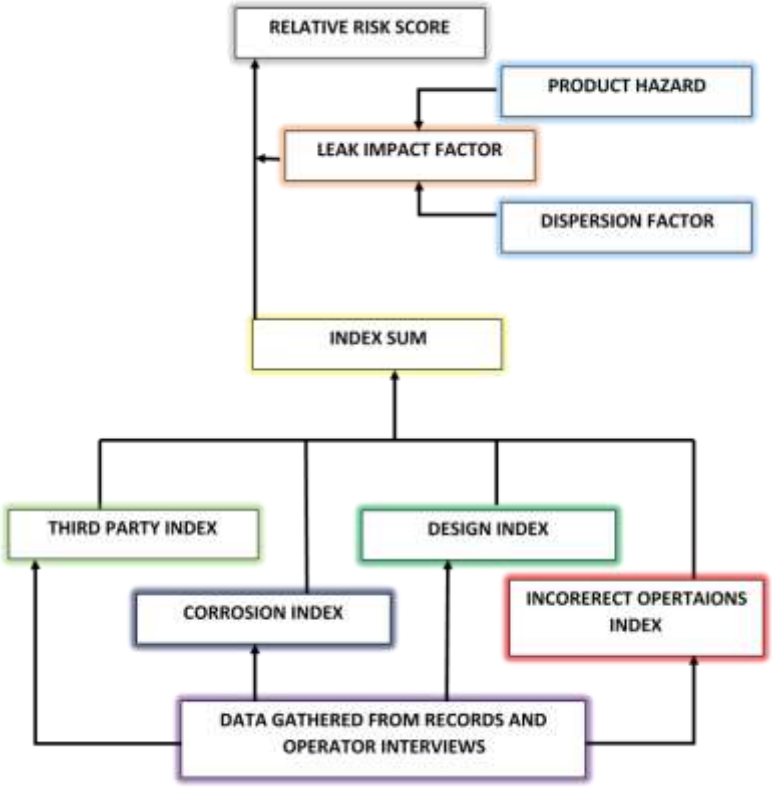

Figure 1-6: Basic Risk Assessment Model [6].

In this case, the costs will be highly expensive on both an economic and human basis. A risk assessment study will discover what could go wrong, how frequently it is likely to happen, and finally the consequences of each undesirable event. The event will be scored based on its likelihood of occurrence and its severity. The final results focus the decision makers on the most critical events. Figure 1-6 shows a basic risk assessment model. The other approach is based on a brainstorming among multi-disciplined members of the team with sufficient experience in their field to predict the hazards based on operational and related activities like maintenance that could create a hazard or incident, known as the Hazard and Operability Analysis (HAZOP) [6, 9]. The analysis is performed in meetings of the groups/teams who study the

system components individually and assess the risks; for example, closing a valve improperly could cause high pressure. Then the next step is to discuss of the likelihood and severity and thereby to rank the event in terms of its likelihood of occurrence. Finally, the recommendations for each event are highlighted and applied either during construction and by modifying the system at later stages of the project. All new projects should include the HAZOP study after the design stage and before construction to provide the ability to fulfil the safety requirements. This is necessary in the design stage to avoid any catastrophic operating or maintenance case in the future [11].

During operation, monitoring for leaks can be established by the following different methods: accounting processes like tank gauging and metering devices which use different kinds of meters such as positive displacement, turbine or ultrasonic meters; intelligent pigging and network instrumentation and control systems such as the Supervisory and Control Acquisitions System (SCADA) which gives the operator good monitoring and control access to the network. The SCADA system will be described within the real field data in Chapter 5.

Regarding pigging, the intelligent pigging method could be considered as the only method of comprehensive inspection and it will be explained in the next chapter among other leak detection methods, while the cleaning pigging method is designed to reduce the corrosion factors by removing sediments and contaminated water. As a result, scheduled cleaning pigging, inhibitor injection and corrosion monitoring can control corrosion of the pipeline.

Another effective method included in this section is the leak report; it is based on real events and lessons learned which allow the use of experience to deal with similar situations. As a normal procedure in an oil/gas industry, after each leak a task force team is delegated to investigate the event, which can then improve operation and avoid any similar cases. After sufficient research on the incident from all aspects, like interviewing the asset operators, maintenance teams and all related personnel, visiting the site, collecting evidence and other investigations,

recommendations are produced that try to focus on the main reasons. They also aim for improvement which might involve reviewing the operational or maintenance procedures, the safety regulations, design codes or any related instructions or activities.

1.6 Pressure Surge Phenomena

In this section a fluid dynamic phenomenon is presented, which could be a cause of or contribute to leaks in pipelines networks. This is where a pressure pulse is created, which, when it reaches an under-designed pressure pipeline segment, can cause the maximum permissible pressure to be exceeded. Due to corrosion or equipment failure, the pressure rise may be less than anticipated. As this is the basis for the current research, it will be later described in more detail; it is called a Pressure Surge, Pressure Transient or Water Hammer.

For this event, the maximum head, once it has been calculated between the higher allowable speed and the stationary moment, can be calculated by the Joukowski equation [12]

$$\Delta H = -\frac{c}{g}\Delta V \qquad (1\text{-}1)$$

Where:

ΔH: change in pressure head (m)

c: wave speed (m/s)

g: gravity acceleration (m/s^2)

ΔV: change in velocity (m/s)

The subject behaviour of the fluid becomes known when the kinetic energy of the fluid is converted to elastic energy and that happens when the fluid velocity comes to rest from the steady state condition [12]. The pressure, in this case, will transfer at the speed of sound from the point in the system that triggers the water hammer phenomenon, normally because of the rapid closure of a valve, the start or stop of a

pump, conveyance of different fluids in sequence, and other reasons mentioned in Thorley [13] and Wylie and Streeter [12]. Pump starting is selected to be the water hammer trigger. It has less interesting research [14]. In order to provide an explanation through a simply configured system, the typical simple reservoir valve system is considered. When the valve is closed, the pressure head of the fluid upstream of the valve is elevated and this increment in pressure is transferred through the conduit by wave action until it reaches the upstream boundary condition, in this case the reservoir with its fixed head. The wave always moved at the speed of sound in the pipeline and the time taken to reach the reservoir can be calculated by dividing the length of the pipe by the acoustic speed. When the wave reaches the valve again, the time now is described as the 'periodic time'. The new wave, which is the first reflection, now will have a negative valve and it will take the same period of time to complete a round trip and return back to the valve. See Figure 1-7 below.

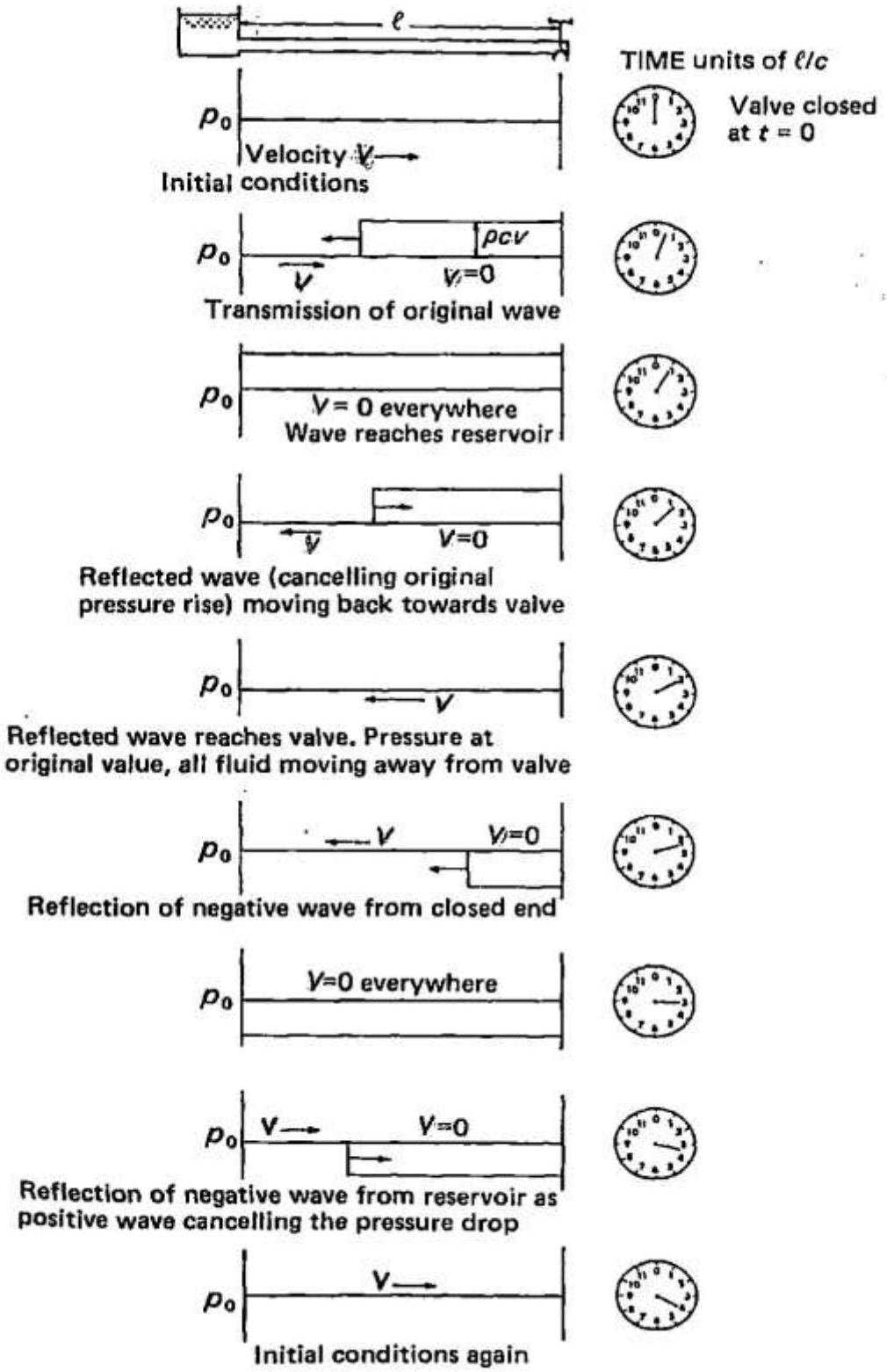

Figure 1-7: Pressure diagrams showing transmission waves [15].

Figure 1-7 shows a theoretical pressure trace and assumes, for example, an ideal fluid, but in real systems, the response is different which affects the wave amplitude and sometimes its shape. Several factors that should be considered include pipe friction, pipe material, pipe supports, fluid properties, system configuration and topography. Many factors attenuate the head amplitude and force the wave to dissipate quickly. That is the case in a single pipe system; however, in a complex system with a probable water hammer, some boundary conditions like the partial steady state load could accentuate the wave amplitude [16]. Also, some boundary conditions could amplify the reflected pressure wave [15, 17, 18]. In general, the wave propagation is affected by system geometry, fluid properties, the flow features, present of gas, and other factors.

The study of this phenomenon has developed from defining the maximum pressure surge for any system to the analysis of the pressure waves to identify the conduit features such as leakage, blockage, variation of the cross-sectional area and other related parameters. To achieve that, many researchers have contributed to a greater understanding of this phenomenon by applying suitable numerical modelling for the systems and developing numerical models representing different transient aspects, for example, the unsteady friction term, which is more important for high velocity systems like the real system in this research. More details about the numerical aspects will be explained in the forthcoming sections.

In this research, fluid transients will be used to try to detect the leakage in a real-life system. This objective will be established by: firstly, modelling the real-life system and checking if the numerical outputs are presented in the system. The provisional solver will allow addition of any modification terms which can improve the numerical code and reduce the variations between the collected data and the numerical results. Then the code will be used to design the scaled experimental rig.

1.7 Research Aims and Objectives

1.7.1 Research Aims

The research aim is to find a reliable, rigorous and cheap method to detect leakage in real field systems. The study will be based on a method utilising the normal operations procedure with the available instrumentation. The surge pressure waves will be used to diagnose the system features by analysing the wave attenuation. That will help to identify the system features and especially the location of the leak. Signal analysis will be applied through techniques such as analysis of the cross-correlation between two points or reduction of the noises in the rig and the real field system. In addition, the cross-correlation has not been used practically for long distances [19]. A Signal filtering should eliminate unnecessary signals without affecting the essential information. Also, as Taghvaie [20] and Ghazali [21] recommend, in this research several measurements points will be used rather than just one. Another recommendation adopted from Ghazali [21] is the use of more complicated numerical method (MOC) rather than Transmission Line Modelling (TLM). Additionally, whereas most of the empirical and real research has been conducted in a single cross-section area [22], this study's real system uses three different cross-sectional areas. In real field applications, the oil/gas industry has been of less interest to researchers than the water networks [23, 24].

The approach will first be tested theoretically, and then be applied in the scaled rig experiment before applying the technique in a real system. The scaled apparatus is essential because large networks are badly affected by numerical errors [2], and it will be easier to validate any technique in the laboratory before using it in the real field. Furthermore, most of the water hammer research has been carried out using small apparatus [13], and long apparatus is more applicable study pressure surge in real field networks [25]. Finally, the real field data will be verified with experimental approach [26].

In relation to the oil/gas industry it is recommended by API-1130 to use three parallel leak detection techniques[27], one of which can be the water hammer approach.

1.7.2 Research Objectives

The objectives of the research are as follows:

- A Hydraulic Transient Solver will be written to simulate leakage in pipelines. Also, this will aid in the design of the experimental rig. In this research, the solver will be created in Matlab® (2018a) [13].
- An Experiment Rig will be designed and constructed as a scale model of the real field system. The numerical model will be validated and tested on it before applying it on the real system. The rig will be constructed in (Contaminant Ingress in Distribution Systems) laboratory Location (CID), Civil Engineering, University of Sheffield. The rig was designed to simulate long pipelines at different locations to fit the pressure transducers or simulate a leak with valves.
- Signal processing is to be used to reproducing the pressure wave data from the numerical code and the rig. The different kinds of noises will be a source of uncertainty, and these can be treated by the signal processing techniques.
- After validation through the previous steps, the numerical model will be applied on measured data from the real system.

1.8 Thesis Structure

The thesis consists of nine chapters. Chapter 2 conducts a literature review of leak detection techniques and discusses the characteristics and limitations of each technique. Then, Chapter 3 demonstrates signal processing, including the different filters to be used for smoothing the raw data, and the cross-correlation and its second derivative. Chapter 4 describes the basic numerical tools used in the thesis. It presents the basic equations from fluid dynamics that are used in the scaling, design, and simulations. The next section demonstrates the Method of Characteristics as a solution tool for the partial deferential equations from governing equations for the rig and the real field. Finally, the last section presents the auxiliary code design that is used to align the data from different runs. Chapter

5 explains the real field system, its components and the development of the data acquisition system. This chapter also presents some numerical results and describes the enhancements carried out on the real field data collecting system to meet the water hammer criteria. Chapter 6 describes the different stages of constructing the experimental rig, the scaled parameters used to mimic the real field system and its physical dimensions and components. It later explains the operating procedures, initial runs, and how the system pressure wave calculations were done. It additionally describes the tests carried out for the leak simulations. Finally, Chapter 6 discusses the challenges in constructing and operating the rig.

Chapter 7 presents the signal analysis and its results for the numerical and experimental rig, including the main signal analysis, cross-correlation and its derivatives, also the power spectrum and spectrogram. Some discussions and explanatory examples are provided. Finally, some signal processing improvement trials that can enhance the results are presented. Chapter 8 discusses the results and tries to give reasonable explanations. Chapter 9 presents the thesis conclusions and proposals for further works that can be derived from different aspects of the thesis.

Chapter 2 Literature review

2.1 Leak Detection Systems

Leak detection systems are divided into two main methods: internal and external [10, 28] as API 1130 second ed. [29]. Another classification categorises them into hardware-based methods that require distinct sensors to operate, and those that utilise conventional fluid sensors [30]. In this thesis, the categories are explained as follows: the first depends on the fluid state and requires sufficient measurements to find the leak while the other is applied on the pipe surrounding to specify the pipe condition. In the following sections, some examples will be provided for each method. The various methods differ in leak detection factors. Those factors include: the response time between leak occurrence and its detection, accuracy, reliability, practicability and the cost.

In addition, the leak characteristics also influence the detection method's performance. For identification purposes, leaks can be categorised into two types: either slow or sudden. The first of these is the leak that takes a long time to discover due to its unnoticeable size. As an example, leaks happen due to pipeline corrosion, and mostly start from pin head size over a period of time [10, 31], or occur due to the failure of a gasket or joint and are considered as leaks, particularly in hazardous product systems [6]. The second kind is called the sudden leak and it causes an instantaneous change in the flow properties and could cause a transient wave [6]. This happens due to instantaneous pressure loss in the conduit. Mostly, sudden leaks are sufficiently large to be noticed by the operator and also by the current detecting methods because of their size and the event singularities.

It is important to mention that there is no leak detection method that is ideal for all networks [1, 26].

2.2 External Detection Methods

These methods depend on the observation of the pipeline's condition from the outside. This can be done by simple visual inspection or utilising specialised equipment to monitor the conduit.

2.2.1 Visual Inspection

This is one of the oldest leak detection methods and is still considered an effective one. It is based on frequent patrols to monitor the network and the pipelines' corridors. Depending on the network, the operators follow either a daily schedule, weekly schedule or another appropriate period to check the network conditions. On many occasions, the operator's experience is significant in discovering leaks effectively [20, 32].

2.2.2 Temperature Profile

This external leak detection method is based on monitoring the temperature of the surrounding environment specifically for the underground pipes and when there is a significant temperature difference between the fluid and the conduit surroundings [10]. This can be done using suitable sensors or a fibre optic attached cable.

2.2.3 Acoustic Leak Detection Technique

In the presence of a leak, turbulent flow characteristics through the hole produce noises and these can be measured to detect the leak [10, 30]. Sounds of leaks are proportional to the nominal flow and the applied pressure. However, these detectable sounds could be attenuated for different reasons, for example, non-pipe components or if the conduit is internally coated (anti-corrosion) in a network carrying highly corrosive fluid networks [10]. The leak can be detected by installing two sensors which measure and calculate the noise distance by identifying the acoustic speed (the distance between the sensors and the time difference between the two identical frequencies) using cross-correlation techniques. Furthermore, the leak noise is a wide band signal ranging from 1MHz to below 1 kHz. Since the subsea pipeline is highly turbulent, a leak will act as a sound source [10].

2.2.4 Intelligent Pigging

One of the most important methods in detecting leaks in the oil/gas industry is intelligent pigging. Despite the operational effort required, it is a highly reliable method for detecting small leaks or predicting possible ones by measuring the thickness of the pipeline wall and it can locate small leaks or weak pipe portions which may need repair [6, 33]. Running the pig through the pipe allows it to measure the ultrasonic noise of small leaks by using by these acoustic markers, the position of the leak can be detected. However, not all the pipelines are piggable, even in oil/gas networks. In a report for KOC buried pipelines[6], 80% of the pipelines are described as piggable. However, not all piggable pipes accept intelligent pigging. Normally, the first 'intelligent' survey is done ten years after construction and then at periods of 8 years unless any circumstances require the test to be accelerated. In oil/gas companies, this survey is done by reputable international contractors, which are specialised in intelligent pigging, particularly for offshore pipelines where special equipment such as vessels is required to access the pipelines and the signals. Figure 2-1 illustrates a typical intelligent pigging device and its components. The main component in the detection of leaks is the magnetic flux leakage (MFL) detector [6].

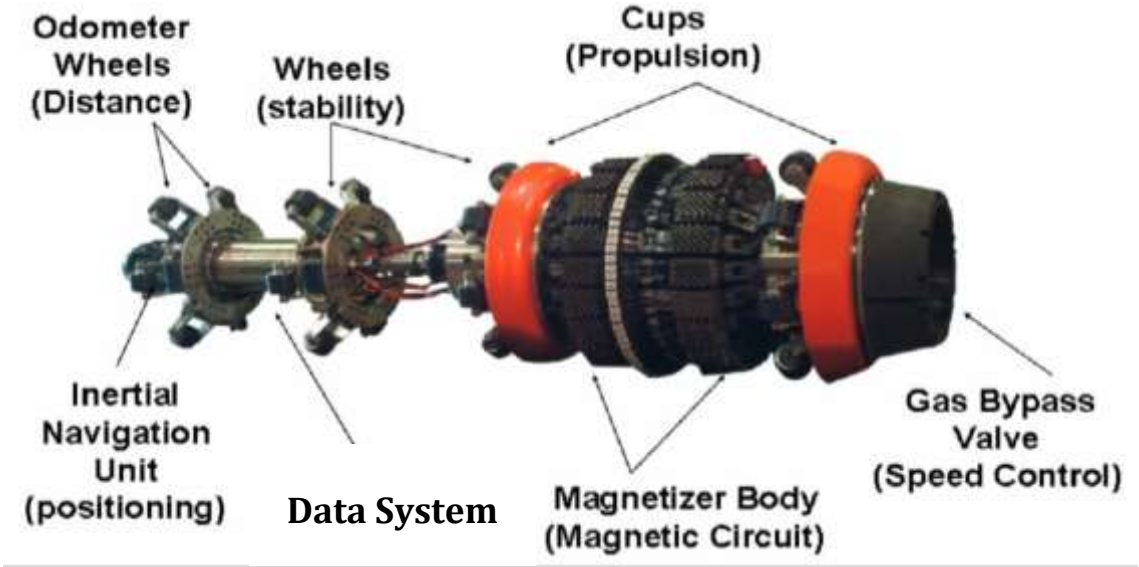

Figure 2-1: An intelligent pigging device and its components [34].

2.3 Internal Detection Methods

These methods rely on monitoring the fluid's condition internally, and the identification of possible leaks is based on the measurements of the fluid variables like pressure and flow. Examples of these methods include: mass (volume) balance, pressure point analysis and pressure wave (transient) method. Since these methods depend on fluid measurement, knowledge of the instruments' uncertainties and the measurement noise is essential to prove their sensitivity for conduit features analysis [10, 30]. The fluid viscosity does not seem to have a noticeable effect on the leak detection [10].

2.3.1 Mass (Volume) Balance

This method derives from the principle of conservation of mass. The difference between the entry and the exit flow in a pipeline is calculated by taking into account the line packing volume. Therefore, the sensors measure the flows, pressures and temperatures. However, this method cannot locate the leak [10].

2.3.2 Pressure Point Analysis

In this technique, a static trace is recorded for one point to create a threshold. Later, leaks can be detected by comparing the current pressure with the historical data [10, 30].

2.3.3 Water-Hammer Method (Transient)

As explained earlier in the introduction chapter, the water hammer phenomenon produces waves, which travel at the speed of sound inside the conduit [12, 13]. When measuring the pressure at one point, it will be noticed that the pressure will oscillate between a range of values until, after a certain time, it reaches the steady state. The pressure waves attenuate because of pipe characteristics. It has been found that by developing a robust numerical model of the studied system and accurate measurements, the system features could be defined as changes in the cross-sectional area, blockage, topography and other characteristics [22, 35-39]. One of these features which affects the pressure wave is the leakage [38, 40, 41].

In the following section, the water-hammer phenomenon will be critically analysed and discussed in further detail. Different approaches will be demonstrated by describing several works in this field. Also, some research studies which used the water hammer phenomena as a method to detect singularities, including leakage, will be demonstrated.

Before demonstrating the contribution of leak detection by this method, it is necessary to refer to three tools that are fundamental to achieving an approach to find new leak detecting techniques which can represent the system robustly and can be used in combination to avoid some limitations of each one, and to apply the transient leak detection method. These three tools are: numerical modelling, data from experimental rigs and signal processing. The following sections present a definition of each tool, its implementations, limitations and significant features.

a) Numerical Modelling

The response of any physical system which is described by mathematical equations for defined boundary condition can be predicted. Such a mathematical models could include the following equations: conservation of mass, conservation of momentum, first or second thermodynamic laws and equation of state. As a result, some variables will be constant, and some will be a function of other variables like time or space thus providing differential equations. Consequently, the governing equations will be ordinary differential equations with one or more unknown variables. Kreyszic [42] summarises the modelling process in three steps: firstly, converting the physical system into mathematical formulae; then, solving those equations; and finally, evaluating the outcomes. While the second step is fundamentally a process which can be done on a computer (PC), the first and the final steps are completely dependent on human experience and expert knowledge.

More specifically, some issues have been raised by researchers about modelling hydraulic transients and these include the boundary conditions or other parameters. For instance, Kosstaz [43] used the steady state to adjust the friction

losses. He also recommended that to detect leaks, the model should be tuned to adjust some parameters like pipe thickness. Another major issue in leak detection and fluid transient modelling is the acoustic speed. Some researchers have measured the actual speed from the studied system [44]. Conversely, Vardy [24] estimated it to find the difference in the cross-sectional area and the system friction factor. Furthermore, Liou [45] limited the uncertainties that are produced from pumps by refraining from modelling this. Stoianov [27] took the pressure values directly from a file, thereby making the numerical solution easier to handle. Liou & Tian [46], meanwhile, took the pump discharge pressure and other boundary conditions directly from the Supervisory Control and Data Acquisition System (SCADA). They mentioned an important weakness of the water-hammer technique, namely, that is, in the case of high friction or of high inlet Mach number: the outcomes will not be as accurate. This point is critical as it is could be applicable to the field system in this study.

b) Experimental Measurements

Generally, an experimental rig gives a well-controlled environment to test many approaches when the researcher is trying to pilot or test a method before applying it in the real field. The flexibility of the laboratory apparatus allows for a variety of modifications and it is not expensive compared with field trials. Also, in large networks like a research field system, the errors in numerical models can be significant [2]. So a scaled experimental rig will enhance the study's results. However, some techniques can be followed to mimic the field system, such as using the dimensionless parameters. The similarity can be divided into three categories: geometry, kinetic and dynamic [15]. The geometry similarity can be controlled by the scale factor between the real system and the rig components. The kinetic similarity is the motion similarity, and the dynamic is the forces' similarity. Some useful dimensionless figures can be used in the rig design. As an example, the dimensionless Reynolds Number (Re) (4-3) measures the ratio between the inertia and viscous forces and the Euler number (E) (4-6) is a factor between the drop in pressure and the kinetic energy.

c) Digital Signal Processing

Features such as leaks or blockages in a fluid system create a discontinuity that produces a reflected wave [47]. Digital signal processing gives a powerful tool for analysing the signals collected from the field by using appropriate processes to select the desirable parameters. Cross-correlation and Cepstrum Analysis are two example approaches to analyse the collected signals. The former measures similarity of two signals and it is commonly used to find the time lag between the signals [27, 39]; hence, it can identify any spikes on the measurements despite its accuracy limitations. Most studies were implemented to compare the two signals at the same point between two systems, for example with/without leak. The second approach, Cepstrum Analysis, involves the Fourier transform of the logarithm of the Fourier Transform [47, 48] and it is used in water-hammer phenomena to avoid the dispersion of the wave [47], which is an obstacle when applying this technique in the field. The power of these tools as techniques for analysing the collected signals is obvious [49].

On the other hand, signal noise or uncertainties represent a major factor that limits the signal processing technique [2]. The noise sources are the transducers, data acquisition system and the hydraulic conditions. This noise can be monitored for a reasonable time period to account for each value or variation in reading when collecting data. So, applying the signal processing in combination with good error analysis can greatly improve the accuracy of this leak detection technique. One such realistic method is wavelet transform (WT) [19, 50, 51]. This method employs time or frequency scale transforms for de-noising, compression and extraction of the signal. Both the rapid and gradual signal deviations can be monitored by WT when measuring the hydraulic variables.

2.4 The Water Hammer Phenomenon

The water hammer phenomenon is caused by different reasons, including: closing valves, stopping or starting a pump and pipe motion [12]. In this case the kinetic

energy will be converted to elastic energy affected by the conduit and the fluid characteristics. The plastic-elasticity of the pipe combined with the friction of the fluid in the pipe will ultimately attenuate the pressure wave. Features in the system, and many other factors will damp or reflect the pressure wave, including friction, pipeline leakage, and blockage.

Additionally, changing the cross-sectional area dissipates the pressure wave as part of it is reflected. Of course, not all the system features attenuate the pressure wave; some boundary conditions may amplify the pressure wave [15, 52]. As examples: Bergant *et al.* [53-56] show the discrete vapour cavity, discrete gas cavity, and fluid-structure interaction models increase the pressure wave heads in comparison with the first pressure wave. In addition, in real system studies, Duan *et al*. [57] stated that the protection devices may enhance or weaken the system's integrity. This occurs because of the interaction between the network components during the transient phenomena. Further real system investigation, conducted by Zhang *et al*. [16], has been showed that the maximum head for water hammer event could be caused by the partial load.

2.5 Water Hammer in the Oil/Gas Industry

This thesis is a first step to utilise the water hammer phenomenon to detect leaks in fluid transient networks in general. Further to the experiments in this field, many studies have been conducted on real water networks [24]. Despite the similarity of the fluids, fewer studies have been carried out on petrochemical networks, primarily due to the hazardous nature of the products. Moreover, in the oil and gas industry more advanced techniques are utilised to detect the leakage, such as intelligent pigging; in other words such networks rely on more reliable detection methods. According to Stafford & Williams' survey [10], conducted on submarine oil/gas pipelines, the intelligent pigging can detect a leak of a minimum of a few litres per hour, while for the transient method the minimum is tens of metric tons per hour. Another possible reason for the lack of oil/gas network studies is limited accessibility for the researchers and developers to the facilities and also the

restrictions which need to be complied with when modifying the real system to implement new approaches. In reality, most of the suggestions for network modification requests are rejected. The author has personal experience of this during his career with KOC.

This problem is particularly relevant when dealing with the configuration of essential components for constructing a pipeline; for example, installing new instrumentation, branches or valves. In other words, changing the original pipe network configuration may increase the probability of failure; for instance, whereas installing many isolation valves would help to control the fluid, at the same time, it could increase the possibility of leakage due to gasket failure. For that reason, most suggestions for changing the network configuration are likely to reject.

In addition, by its nature, the oil and gas industry has a variety of characteristic, which do not apply to water networks, and which can be summarised as the following:

1. Most of the oil and gas networks are recent constructions and have sufficient documentation about the networks' components like pipe dimensions, valves or pumps characteristics compared to the water networks. As an example, Stoianov [27] highlights that the main 36" diameter water pipeline in Oxford Street, London was constructed in the 1840s and little information exists on its geometry and location.
2. Generally, the technology in this field is constantly being updated and has the latest devices like signal transmitters, acquisition systems and flow rate meters, which, combined with adequate calibration and maintenance efforts, make the data acquisition analysis more reliable [58, 59]. Compared to the oil/gas real networks, management procedures relating to the water systems are inadequate [36]. In addition, this technology helps to define pipe properties [27].

3. Most of the studies particularly at laboratory scale have been on networks of small dimension , in the field, pipelines are significantly larger in geometry [60].

The water hammer method is an economical [2] way of detecting leakage compared with other methods like intelligent pigging. So, this study attempts to find a method that is practical and reliable when used in real systems.

The following part of the literature review discusses the main research subject, leak detection. Firstly, the works (leak detection research) related to the oil/gas industry will be highlighted and the previous efforts in this field will be identified. The aim is to demonstrate how to apply a suitable approach for numerical modelling, avoiding the aforementioned obstacles and anticipating the limitations, whether in terms of modelling results, system instrumentation or rig configuration. Secondly, detecting leakage as a feature of any pipelines system cannot follow any individual approach. Much of the research that will be discussed have used different methods to detect the various singularities of the pipe system, such as blockage, branches and in-line devices, and to compare their effects on the transient waves

Furthermore, the review will consider some contributions from oil/gas industry field, and some pipe diagnosis techniques using the water hammer method to detect leakage will be reviewed. The study by Kaplan *et al.* [61, 62] on the validity of method of characteristics (MOC) was one of the first to use computers for the numerical calculations [63]. These studies included the friction term in the governing equations and found the results were reliable. The study was conducted on long oil pipelines and suggested that the wave speed should be measured after the construction of the system. Once again, although water and oil are fluids and tend to exhibit similar behaviour under comparable conditions, there still are some differences in response based on the oil components which should be recognised. Some points which have been highlighted in previous studies need to be accounted for during the stages of this research study. In general, oil is more compressible due to the gas content (dissolved and free gas) and that leads to more attenuation of the pressure surge wave. Thorley [13] suggests that the oil could be considered a multiphase fluid. This conclusion was also reached by Bergant *et al*. [64] who

reported that in long oil pipelines it is essential to measure the gas released since it presents a challenge and will be a source of noise and uncertainties. Furthermore, the viscosity and temperature are unstable oil properties [16] and have an obvious effect on the oil's behaviour.

As explained in the previous chapter, corrosion of pipelines is one of the main reasons for leak and is currently monitored by the intelligent pigging. However, some efforts have been made to monitor the pipeline's condition from the blockage point of view. Vardy and Mackenzie [24] followed an approach of defining the area through the Joukowski equation by assuming all the parameters are known. They started by triggering the event from zero flow, then measured the flow and the pressure, and finally evaluated the outcome in the time domain. In conclusion, they were able to predict a blockage of 50% of the cross-sectional area. In other similar research, Makenzie and Vardy [60] tried to locate and remove blockages in offshore pipelines. They stated that, due to gas bubbles and fluid properties changing nonlinearly with pressure and temperature changes, the oil is more difficult to deal with. Also, the pipe is much more difficult to deal with, because of locations, hazards, and sometimes the weather. Despite, the pipe being rigid, the floating hoses, swivel joints, valves and other components are a source of noise. To locate the blockage, the use of the negative wave is more effective. Another blockage detection and localization study was done analytically and experimentally by Wang *et. al* [65]. Their experimental test identified 20% of the cross-sectional area. However, they expected some limitations for the approach when it was applied in complex systems.

In another aspect, Kosstaz analysed different relief systems to protect a marine terminal [66]. He used a commercial software package and the analysis was satisfactory.

2.6 Leak Detection Approaches

When an event such as closing a valve, pump shutdown or start-up occurs, different fluids consequently dispatched along the same pipe, and a sudden rupture can cause a water hammer event. A pressure wave is produced which will be affected and attenuated by the pipe friction until the flow returns to a steady state flow. However, that only happens in the case of a single pipeline without any components, changes in the cross-sectional area or topography of the conduit, as shown in Figure 2-2.

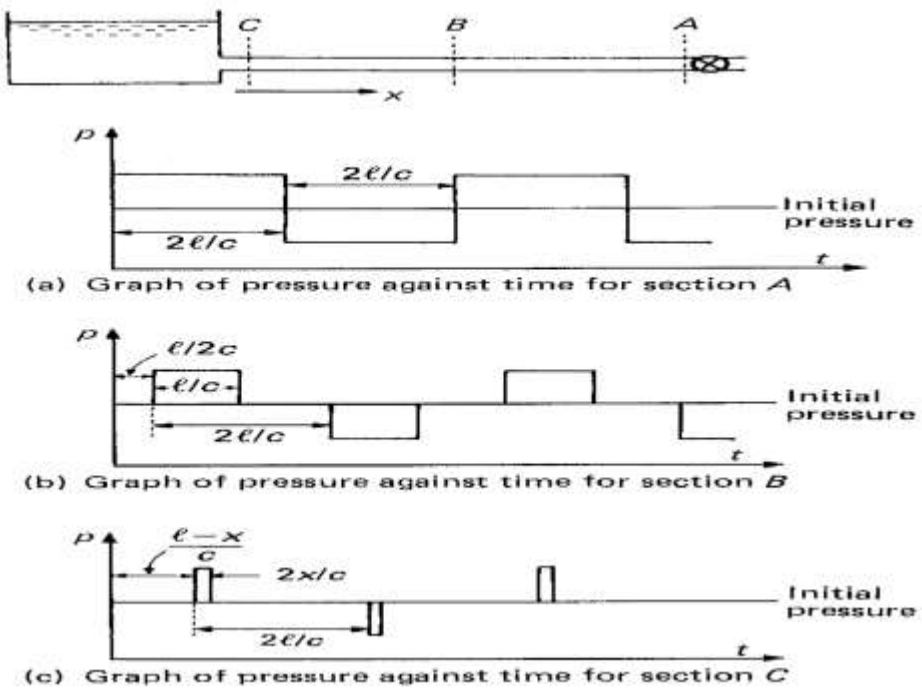

Figure 2-2: Simple Reservoir-Valve system and its pressure head at different sections [15].

Figure 2-2 demonstrates the simple reservoir-valve system. In the case of sudden valve closing, the pressure waves will travel between the reservoir and the valve. On each round trip the sign for the pressure head will change from positive to negative sign and vice-versa. Based on the location of the measurement point, the pressure wave graph will change as in Figure 2-2 b and c.

In contrast, various anomalies can affect the pressure wave when it passes the singularities, such as in line valves, a blockage, branches or, in general, any change in the physical structure of the pipe. Many researchers have distinguished between

these factors, including a leak being one of them. It is a feature of the hydraulic system that it alters the pressure waves, which travel through the conduit. Detecting the leaks using the water hammer phenomena is based, as mentioned by Colombo *et al*. [2], on the properties of the reflected signal (wave) and how it increases the transient damping as a result, or presents leaks.

In Figure 2-3, when the incident wave is passing the leak it will produce two waves; the first will be the transmitted wave and will travel in the same direction as the original wave. The second, the reflected wave, will flow in the opposite direction.

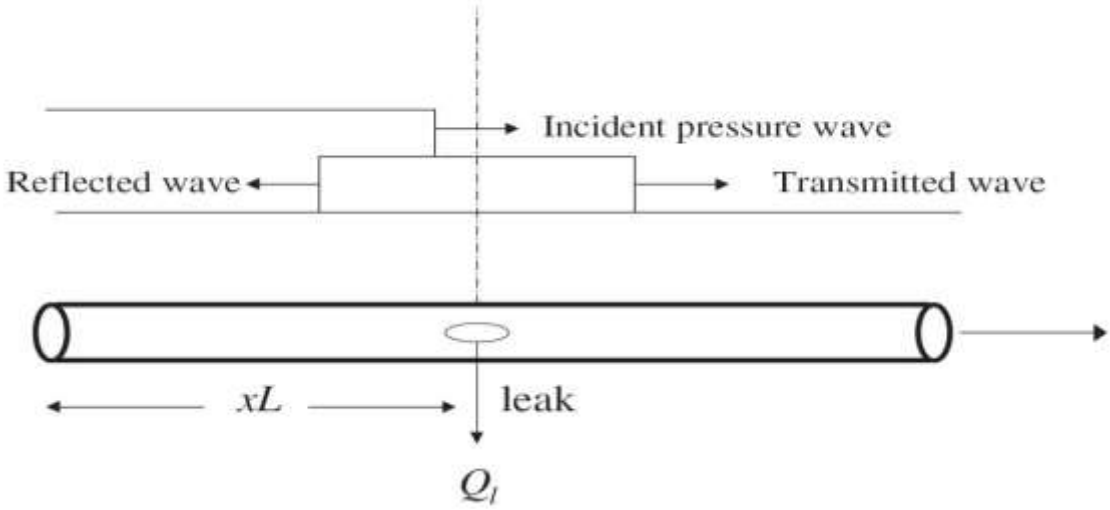

Figure 2-3: Conceptual wave reflections at a leak [67].

Figure 2-4 shows the reservoir pipe valve system will demonstrated to explain the difference between the water hammer event with and without leak. The total pipe length is *L* and the leak location is *X* from the valve. If the water hammer is triggered from the valve, the pressure traces have different behaviour between the system with and without leak. As seen, the pressure trace for the system with leak is presented in the dashed line. The effect of the leak reduces the pressure value at the time of *2x/C*, where is *C* is the system wave speed.

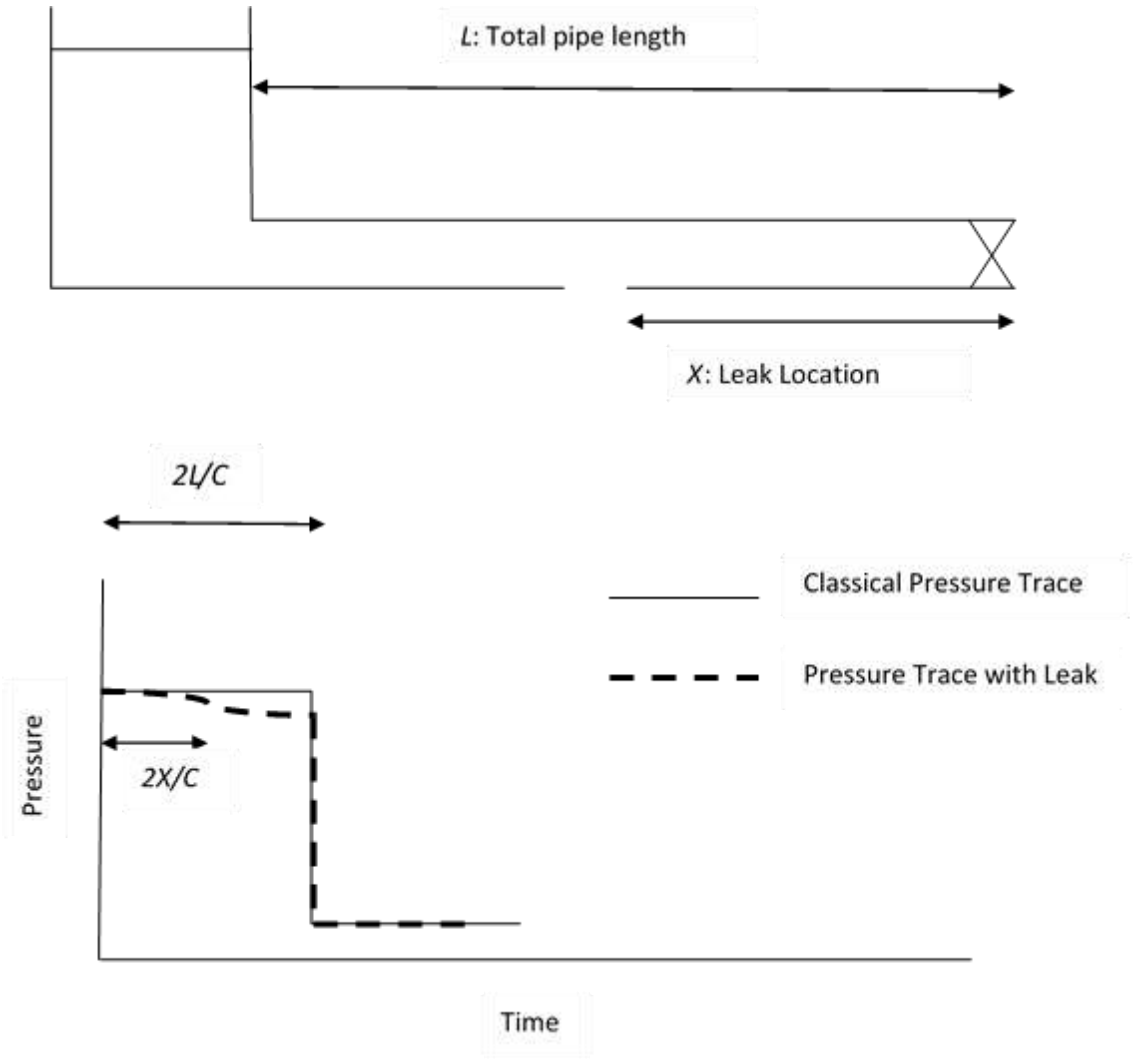

Figure 2-4: Reservoir-pipe-valve system and pressure traces against time with/without leak.

When the in-line valve is closed, in a simple-reservoir-pipe- valve system with a leak, the transient wave travels through the conduit and a reflected wave from the leak will have the effect as shown in Figure 2-5. The head response will continue to be damped until the fluid returns to its steady–state condition. In other words, the leak affects the transient wave by increasing the damping and creates a reflected wave [2].

The ratio between the reflected and incident waves can be obtained from Chaudhry [68]

$$S = \frac{\Delta H_R}{\Delta H_0} \qquad (2\text{-}1)$$

The numerator is the difference in the reflection wave, while the denominator is the Joukowski head.

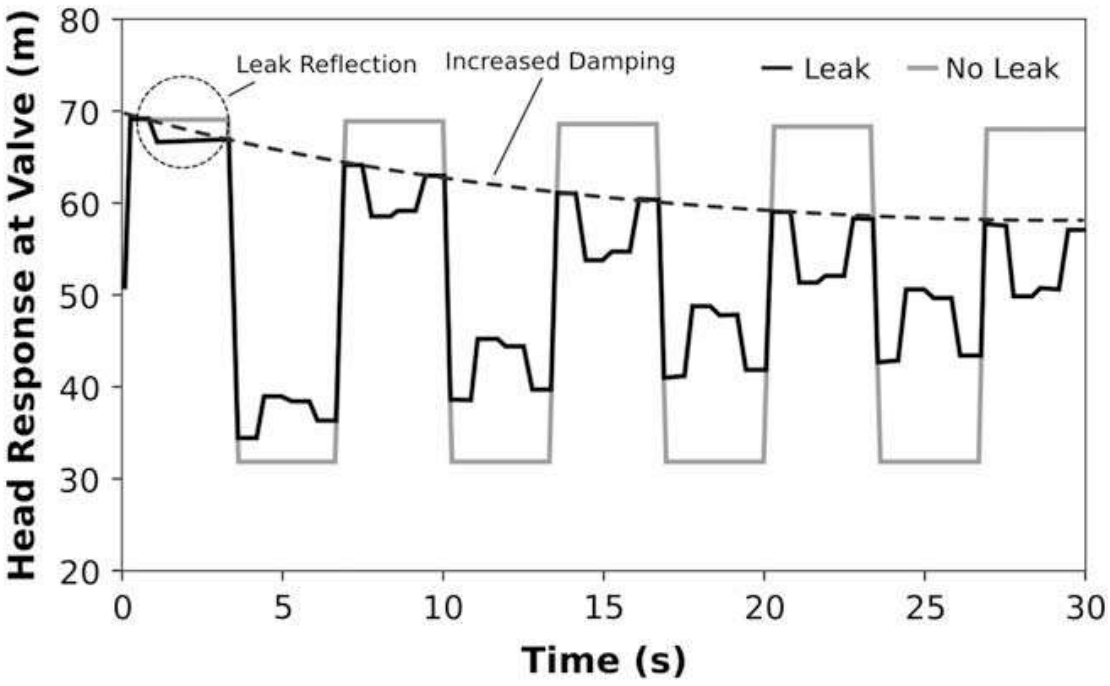

Figure 2-5: Comparison of transients in intact frictionless and leaking pipeline [2].

2.6.1 The Direct Transient

The direct approach is based on the history of pressure measurements from one or different points on the system. That leads to dependence on a significant amount of information gained from the field despite the many uncertainties deriving from measurements or hydraulic aspects. Contractor [35] used the water hammer method to define minor losses in a pipe, and was one of the first researchers to use pressure surge in the diagnosis of a system [36]. Contractor did his research numerically by MOC and using an experimental setup, producing encouraging results. Brunone [69] detected leakage in outfall pipes by finding the relationship between the time taken for the initial and reflected wave to arrive from the leak. Due

to its simplicity, this method struggled to cope with hydraulic and instrument noises. In order to improve the technique and avoid the undesirable measurements, Beck *et al.* [38] used cross-correlation analysis to examine the first and second derivatives of the cross-correlation. The former was used to get the magnitude of the gradients, while the latter defined the gradient change peak points. Stoianov *et al.* [70] also used discrete wavelet transforms to detect the reflected waves. Depending on the fact of the damping rate for leaks, the Fourier analysis was applied to adapt the governing equations in order to find the relationship between the harmonic and damping rates. Nevertheless, as with the two other techniques, it still has many limitations that prevent its application to a real system without further research. Complex systems consist of many system features such as: in-line components, branches, and topography, and these result in the production of many complicated waves that preclude the use of this simple technique [2].

2.6.2 The Inverse Transient Analysis

The second approach for leak detection which will be demonstrated is Inverse Transient analysis (ITA) [71-74]. In this technique measurements of the known variables (pressure, flow, etc.), are used to define unknown parameters (leaks, pipe length, etc.) in transient equations by reducing the differences between the numerical model and the field data. This approach starts by collecting the data during the transient event and then evaluating the singularities with numerical code results for both cases, with and without leak, until the corresponding pressure values are matched. Pudar and Liggett [71] suggested this method. In steady state condition, they minimised the sum of the square of the differences between the measured and calculated pressure heads. The analysis was innovative notwithstanding the effect of errors in head pressure measurement which affected the pipe friction factor estimation. Later, Liggett and Chen [75] applied this technique to unsteady analysis. Nash and Karney [76] used the technique to calibrate the friction factors.

In order to improve the technique, different researchers have put forward various modifications. Since this method depends on minimising the sum of the squared differences between the modelling and recording pressure readings, two

approaches are used to define leaks, the Levernberg-Marquardt (LM) (nonlinear derivative optimization) method and Genetic Algorithm (categorised the sampling and search) by Colombo *et al.* [2]. Viskovsky *et al.* [74] suggested using the Systematic LM to get the benefit of the LM algorithm and expedite it the by initially guessing the location, so the Shuffled Complex Evolution (SCE) algorithm works quicker when trailing the leak.

Covas *et al.* [77] evaluated the ITA by means of experimental tests. They provided some suggestions for improving this approach, including developing a 2D model, and highlighted that the success of ITA depends on the accuracy for all data inputs, such as system parameters and transient simulator

Also, Covas *et al.* [78] tested ITA for different features of a well-controlled laboratory apparatus. Many discrepancies were reflected by the system; as a result, they concluded the ITA is difficult to apply on a real system without first resolving the related obstacles. Some researchers have tried here to enhance this technique [79, 80].

2.6.3 Mass Balance

Another approach for detecting the leaks in pipeline systems is the mass balance method. It is based on the conservation of mass, measuring the mass flow between the inlet and the outlet and comparing those data. To get trustworthy results the system initially measures the steady-state condition to identify any discrepancies in the measurements, which may affect the readings. Then, when the water hammer is being initiated, the collected data could indicate the leak quantity and location as presented by the Liou [31] experiments to measure the fluid characteristic frequency of the pipeline and consider the allowable discrepancies of the system.

Some studies will be demonstrated as an example of this method. Nicholas [81] studied a real oil pipeline test for a leak in a short period of time based on volume balance principle. The pipeline was 290 Km long with a nominal flow rate of $1590 m^3/hr$, while the leak rate was 2%. However, in an earlier study Nicholas [82]

stated that pressure discrepancies for a leak depends on the pipeline length. Stouffs and Giout [1], meanwhile, identified the variations in temperature and pressure of fluid and their effect on the liquid density and the cross sectional area of the pipe. That is defined as Line Packing. They also postulated that the effectiveness of leak detection depends on the severity of the transient flow and computational mass balance.

Liou [31], in a study based on the data collected by a Supervisory Control and Data Acquisition (SCADA) system, utilised a software approach to create several leak detectability curves, accounting for the uncertainties in variables, and then compared these results with field leak tests. The results demonstrated reasonable estimations. The levels control the ability to detect the leak. Leak detectability has been defined as the ability to detect small leaks reliably [10]. The field tests were performed on real long pipe petroleum products with variation in thickness and topography. This paper's results have shown that this method is sufficiently reliable to detect very small percent leaks in the throughput of the pipeline.

Liou [46] later showed that water hammer equations at the steady state and the transient condition contains the same errors. That was investigated by using a petroleum products pipeline as an example. Again, he relied on the SCADA to obtain real simulation of the boundary conditions.

Liou & Tian [45] continued studying the mass balance approach and its ability to detect the leaks. In this paper, they modified the approach by data noise by detecting two test leaks, and illustrated their idea about generalizing the parameters of functions to govern similar cases with the same scale. The results are similar to those of the previous study, when determining the moderate leaks of a moderate life. Simplifying the parameters enables a dimensionless analysis to be undertaken which produces reasonable results.

2.6.4 The Frequency Domain Technique

The frequency domain technique is an alternative technique for monitoring the pipe system at one location rather than collecting the data from different locations. It is

based on measurements of the pressure history from one point, and with periodic triggering of the transient the system can be analysed in the frequency domain. The leaks change the resonance pluses in the frequency domain; therefore, it can be analysed numerically [2]. One of the researches works suggested that the leak properties can be found by using the Fourier spectrum [83]. In this approach, the signal processing technique is strongly presented as will be seen in the following research study. In the following chapters, related techniques will be explained in depth. Beck *et al.* [39] monitored the pressure wave and then the leak by generating a pressure wave signal, and the reflected wave history was recorded. They then used signal-processing techniques (like wavelet transforms, cross-correlation) to ascertain the actual time delay to the event. Finally, the system wave speed was used to calculate the anomaly distance. In other words, it is a nonparametric technique in which the numerical model is described in functions or curves: impulse response, frequency response or cross-correlation. The second derivative amplifies noise in the signal. They used the cross-correlation approach that has the advantage of looking for spikes rather than trusting the accuracy of the measurements. Their hypothesis is that any change in the cross-correlation gradient represents an event. By applying the second derivative of the cross-correlation, these gradients will be deformed into spikes. They concluded that the main system features, such as open and closed ends, give the largest spikes. Additionally, the open end reflects a negative pressure wave. It was notable as a measurement issue that the high pressure and the small pipe diameter added noise to the signals. In other work [38] they applied the technique on experimental apparatus. Also, they enhanced the technique for detecting the leaks. This enhancement was achieved by using the Matlab software to acquire the data, repeating the runs to reduce the noise, smoothing the data, re-trending the data by moving the mean value, and treating the reading of the pressure wave, before applying the second derivative cross-correlation. Experimentally, they defined the leak and other features with reasonable tolerance. More theoretical and detailed information about the cross-correlation technique is provided in section 3.2.1

Lee et al. [84] used the frequency response method (FRD) to detect leaks in single pipes numerically. The leak was found by identifying the steady friction and unsteady friction. Despite their promising results, the approach has some restrictions: some specific leak locations were not identified, accuracy of the measurement devices is essential, and the linear assumptions in the governing equations are disrupted. Other work using FRD on a single pipeline was presented by Lee [85]. The leak detection was carried out by the inverse resonance method and resonance peak sequencing method. While both presented good information, however the latter was faster and more efficient. For the same approach, the FRD, Duan *et al.* [86] concluded that it can be applied to complex systems rather than the single pipe systems. The analysis by Brounone and Ferrante [87] used the wavelet transform in a simple pipe apparatus and waste water outfall to find the leak. The data for this simple conduit was collected from one point. The frequency domain analysis detected the leak, despite the high pressure head variation.

Wang *et al*. [88] expressed the governing equations in terms of Fourier series. Since the leak damping is different for different Fourier components, they suggested this can be used successfully to detect the presence of a leak. Their detected leaks were of small size.

Taghvaei *et al.* [47] used Cepstrum analysis to obtain the time delay between the initial wave and the reflected one. This was based on the fact that any change in the steady-state conditions can provide a pressure wave, and those alterations could derive from the system geometry, hydraulic components and the flow characteristics. However, there is difficulty in finding small leaks since they could be considered as false peaks. In real systems, the dispersion (spreading of waves and smoothing) is an obstacle to applying the Cepstrum technique. Later, Taghvaei *et al*. [89] continued their work and showed the capabilities of the wavelet transform and Cepstrum analysis through their use of low-profile piezoceramic transducers for transient pressure monitoring. Despite the weakness of this device in recording an accurate history, the measurements were sufficient to define the system features and the leaks by the transient. After that, Taghvaei *et al.* [19] applied their aforementioned techniques (Orthogonal wavelet analysis for filtering and Cepstrum

analysis for detecting the leak) to signal processing, on a real field system belonging to Yorkshire Water Services Ltd, to define a noticeable leak with unknown exact location. Although the test was conducted over a short distance (32m of pipeline) in the network, it could potentially be applied on longer networks.

Other new techniques were used by Ghazali *et al.* [90] to detect the pipe leaks and features by analysing the instantaneous phase and the frequency of the signals by Hilbert transform (HT) and Hilbert-Huang transform (HHT). The HT detects the leak location with small error while the HHT identifies the pipe end.

Another field study was implemented by Arbon *et al.* [91] to check in-line valve isolation conditions (fully closed) by transient analysis instead of by normal inspection, which is more costly in operational and the manpower terms. The test was carried out for two days on a 20 *km* length of pipeline length with diameter of 600 *mm*, and the outcome was to change three out of seven valves.

Other researchers applied the water hammer approach to diagnose various pipe features including leaks. Meniconi *et al.* [36] found the pressure drop for in-line devices is hard to measure due to slow flow rate and errors in hydraulic grade line. However, by using short period analysis they identified the reflected wave changes by varying the in-line device. They applied it to ball, butterfly valves and different orifice devices. In addition, Meniconi *et al.* [36] used a portable device to trigger the transient and analysed the pipe system in order to diagnose and define the system based on the small amplitude sharp wave. The pipe anomalies they checked included leaks, branches (they tried to detect the anonymous ones), partial blockage and semi open in-line valves. For each case of the four, they changed the parameters to distinguish between the same case conditions. For instance, for the in-line valve they tested using different percentage closing of the valve, while in the branches they analysed a dead and an active branch. The evaluation of the entity was based on applying water hammer theory for a short period and using wavelet analysis to locate that by finding the arrival time of the pressure wave. The results showed that it was possible to use transient pressure techniques to diagnose the pipe system.

Meniconi *et al.* [22] conducted a similar study on finding the blockage, using an in-line device and altering a cross-sectional area in complex viscoelastic pipe systems. The behaviour of the three systems, different cross-sectional areas, partial blockage and in-line valve, produced different outcomes. The partial blockage was presented by a small-bore pipe. The difference between the single cross-sectional area change and the in-line valve is the local head loss.

Standing wave difference method is another leak detection technique that was used by Covas *et al.* [26]. This method utilises an electrical cable to identify cable defaults. They achieved promising results but advised applying some additional parameters, also that attention should be paid to the antinodes.

The research by the water group at Sheffield of University on water hammer phenomena is still ongoing, in particular leak detection, and has resulted in recent leak detection research being published. The vibro-acoustic emission technique is commonly used in real water distribution systems to detect and quantify leaks. This would allow prioritisation of maintenance and repair activities. The research utilised the vibro-acoustic emission signals approach to detect the leak. Butterfield *et al.* [92] tried in addition to detecting the leak, to find the leak flow rate and distinguish between the leak and background noise signals. In signal processing, wavelet analysis was selected and focused on selecting the mother wavelet function to optimise the outputs. They concluded that by selecting the proper mother wavelet function, leaks and other system properties can be identified. However, issues relating to selection of the mother wavelet and the plastic pipe properties limit the approach.

Later, they noticed the leak flow rate had an effect on their results, Butterfield *et al.* [93] looked for a signal processing technique to quantify the leak flow rate through using the vibro-acoustic emission. This could help water companies to prioritise their leak flow rate. To achieve that, four signal techniques were tested: vibro-acoustic emission accounts, root mean square, peak in magnitude of the power spectral density, and octave banding. The root mean square produced the best evaluation.

The work was continued by the same group and for the same purpose, to identify the leak rate and leak area and their effect on spectrum analysis [94]. In this work, the effects of leak rate and area were noticed on the leak spectrum. Hence, 24 features were applied to analyse the raw data. They achieved predictive results to identify the leak flow rate and area. Since there is no ideal technique that is valid for all cases, they suggested for future work, to investigate the appropriate features for each system.

Chapter 3 Signal Processing

This chapter summarises signal processing and its importance in the analysis of experimental and real field data. After a general introduction, some techniques that have been used by previous researchers working on leak detection will be demonstrated, since the current research continues the work of previous studies. The work here will use different aspects in the experimental settings, boundary conditions, and the numerical handling, in addition to employing the work in a long pipeline.

3.1 Introduction

As the Oxford English Dictionary states, a signal is '' A sign or notice, perceptible by sight or hearing especially for the purpose of conveying warning, direction or information''. In transient events, the signal and its processing can make an essential contribution to detect the system singularities. During the analysis of a transient, the captured signals often need some treatment to capture the useful data from the sensors. Signal processing is of vital importance, particularly when dealing with the real system. As highlighted by many scholars [95], the numerical solution and assumptions are not always accurate. The parameters include pipe diameter, friction factors, and acoustics speed, cross-sectional area, steady and unsteady friction factors. From this point, the measured data can be enhanced by the signal processing, to become more reliable. Hence, the signal analysis will be more dependable and close to the precise.

Many researchers have found that the discontinuity in the signal indicates singularities of a pipe network system, including branches, leaks, blockages, and others, depending on signal processing techniques. One of these is cross-correlation and its second derivative. Sheffield University researchers have conducted many studies using this technique and others on different aspects of the studied systems, or variations in simulations, numerical, experimental, and real field systems [19, 38, 39, 47, 49, 89, 90, 92-94, 96-98]. In this work, the same techniques will be used in numerical coding, experiment rig, and real field data where possible. The new aspects in this research are: high flow rate, long pipeline system, and the transient

using some slow surge triggers, pump starting. In a recent research publication, Louati *et al.* [99] used a piezoelectric actuator to produce a high frequency wave and treated it by finite volume and a two dimensional numerical method to detect real networks features. However, the recorded data has the following constraints: it should be gathered over a long time, and the measurement point should be close to the wave source.

Two other researchers from the Sheffield University group, Taghvaei [20] and Ghazali [21], each presented a PhD thesis using different signal processing techniques. Although they both used one pressure transducer for pressure wave readings, and the same experimental rig, they produced different techniques to eliminate the noise effects from the collecting signals. Then, they identified the network's discontinuities by using a variety of signal processing methods. In the following paragraphs, their contributions will be described separately.

Taghvaei [20] filtered the raw data by using the Discrete Wavelet (DWT) method. The advantage of this method is the removal of the high/low frequency signal. He found that the Orthogonal Wavelet (OWT) is able to identify the system's features for the non-stationary signal. In addition, the Fourier Transform (FT) deals with the difficulty of the noisy environment. Selecting the levels of wavelet to remove the noise was based on the researcher's previous experience. Cepstrum is a non-linear technique also used by the researcher also to define the non-stationary signal. He found the latter an easier method for identifying the features. It requires only filtering of the wavelet. Furthermore, its amplitude has a linear relationship with the leak size. In the case of field data, he combined the Cepstrum and the OWT techniques, to enhance results.

Based on his literature view, Ghazali [21] concluded that the Standard Fourier Transform (FT) and the Short–Time Fourier Transform (STFT) have poor resolution in the time domain and that limits their capabilities to identify normalities in the signals. Regarding the Wavelet Transform (WT), he reported it is hard to adapt it for desirable applications. So, he used different techniques in seeking to develop leak

detection methodology. He presented the Empirical Mode decomposition (EMD) for filtering, and both Hilbert Transform (HT) and Hilbert-Huang Transform (HHT) for analysing the data to find the features. He claimed that both techniques could be more accurate than cross-correlation, Wavelet and Cepstrum technique. The EMD produced some undesirable low frequency spikes which passed the HT. The EMD showed good ability to deal with noise in the real field. In his analysis the EMD and Cepstrum produced the worst results.

Another addition introduced in this research is the creation of a hypothesis to treat the noise that is created. The Removal-Noise Algorithm is designed to deal with noise as unrepeated system features. This will be explained in the last section of this chapter and along with a description of how this improves detection of irregularities.

The friction factors (steady and unsteady) affect the wave attenuation but not the timing [100, 101]. Signal processing could enhance the numerical computational outputs by locating the singularities even after attenuation and lowering of peaks. Clearly, dealing with small peaks could identify some additional system features. Nevertheless, longer pipes exhibit higher effects of quasi-steady friction [39, 45, 101].

3.2 Basic Techniques

3.2.1 Cross-Correlation and it's second Derivative

Lange [102] developed the technique to compare two signals and how they are related to each other [38]. The relationship is given by this equation

$$r[k] = \sum_{n=-\infty}^{\infty} x[n] \times y[n+k] \tag{3-1}$$

The signals x and y will be moved over each other by increasing the k parameter for a number of data n. The result r fluctuates in value, k is the time shift integer which increases, and when it reaches a suitable time period, the r values will be at their

peak. Figure 3-1 shows the cross-correlation values between two signals and the delay time τ.

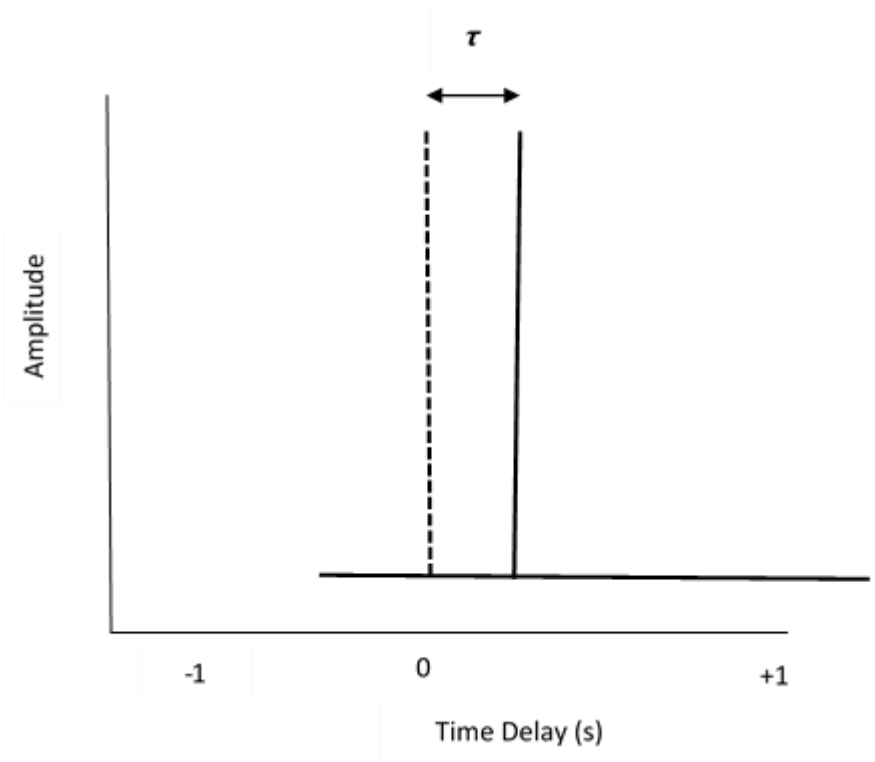

Figure 3-1: Cross-correlation between two signals.

The cross-correlation can find a leak between two sensors. Figure 3-2 shows a leak between two sensors. The total length between the sensors is L. The distance between sensor 1 and the leak is L_1 and between sensor 2 and the leak is L_2.

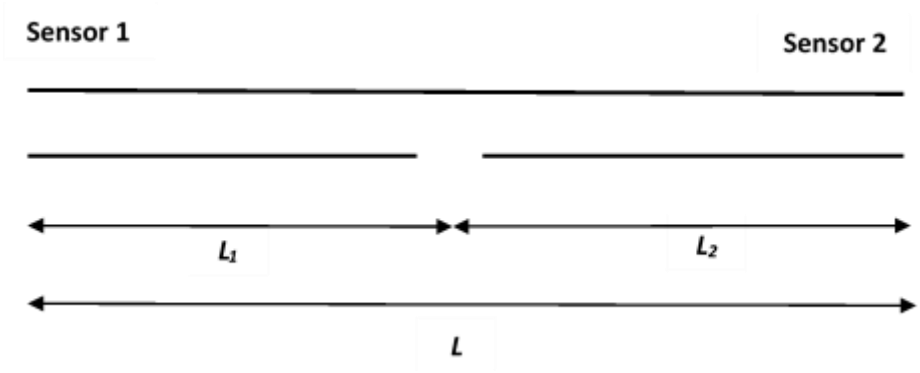

Figure 3-2: Leak between two sensors.

The time delay for sensor 1 and sensor 2 are τ_1 and τ_2, respectively. The distance of the leak can be calculated by the following steps:

$$L_1 = C\,\tau_1 \text{ and } L_2 = C\,\tau_2$$

$$\text{So, } L_1\text{-}L_2 = C(\tau_1 - \tau_2) = C\,\tau$$

$$\text{and since } L_1 + L_2 = L$$

$$\text{Then } L_1 = (L + C\,\tau)/2 \text{ and } L_2 = (L - C\,\tau)/2$$

In addition, the cross-correlation values are differentiated with respect to time, twice; the first gives the gradient and the second produces peaks at which the gradients changed. The cross-correlation value between the two signals is maximum when the two signals' features are aligned [103].

To illustrate this technique, an example which has been presented by Beck *et al.* [39], is introduced briefly here. They used an exponential signal with certain delays and added all the signals and the output to be the case study with the cross-correlation and its derivatives. The exponential function has a decaying property with time, and the reflections could exhibit a similar effect to the reflected wave in transient events. The three reflection functions have different delay sample times, and the third one has an opposite sign. Figure 3-3 shows the original signal and its sum and reflections after it has been cross-correlated. The difference in the gradients is because of the delayed reflections delayed is shown. Then, in Figure 3-3 (b) the first derivative shows each delay with different amplitude step. Finally, in (c), showing the second derivative, instead of steps, spikes have been created to represent the reflections. In addition, from Figure 3-3 (c) shows that the positive spike indicates the positive change and vice-versa.

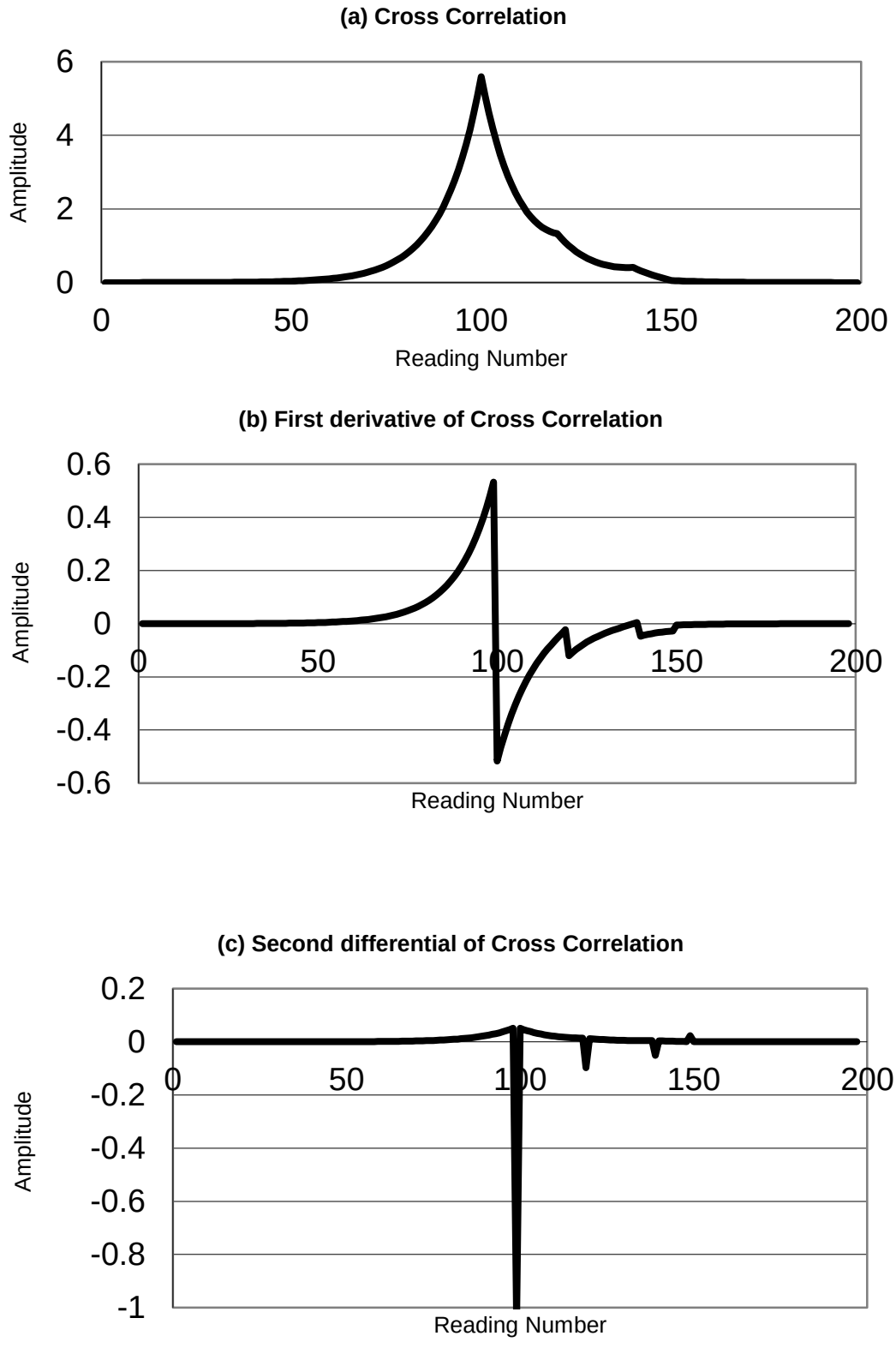

Figure 3-3 Cross-Correlation of signal with sum of signal and reflections in (a) and its first and second derivate in (b) and (c), respectively [39].

To highlight the points where the gradients change, Beck *et al.* [38, 39] used the second derivative for the values over the time period. The five point averaging filter was used to reduce the expected noise after applying the derivation algorithm. The sharp waves deriving from T-junctions, open and closed ends, and other features were detected by this technique. Later, Motazadi *et al*. [104] applied the analysis from two locations to improve the detection and avoid overlapping. This simulation was carried out using Computational Fluid Dynamic code, and testing of the location and shape of leaks produced satisfactory results.

In this research the same basic techniques will be used. They will be applied to find the features using slow waves created from pump start up or switch off. Other aspects to be tested will be decreasing the leak sizes to ascertain the minimum detected values, and the use of more than two sensors to record data numerically and experimentally.

Ultimately, all techniques are affected by signal noise. Noise is another phenomenon in real network system's features which could be considered; created features like blockage or leak may cause some small reflections and these could, initially, can be buried by noises [2], or considered as noise [105].

Noise presents severe challenges for any data collection process. It can seriously affect the data analysis and may even give false indications. Filters are used widely to improve the collected samples and then the analysis undertaken is similar to that of Taghvaei [20] and Ghazali [21]. The following section explains the methodology of filters.

3.2.2 Validation of Cross-Correlation and it Derivatives by using Sine Signals

Cross-correlation and second derivative technique is applied to a simple example to ensure that the coding was correct and to validate this process.. The sin function was selected and applied in Matlab. The time domain was created by $t = linspace(0{,}2 * pi, 100)$ Matlab statement.

The first and second signals were created by $a = sin(t)\ and\ b = sin(t - pi/4)$. In order to create two signals with spikes, the value at the twelfth point was changed

to be 0.8, and since the delay was 12 steps, the second signal at the twenty fourth point was changed to 0.8 to achieve coherence between the signals. Also, to understand the negative spike effects on cross-correlation and its derivative, the values at step 30 and 42 were reduced in the first and second signal, respectively. Figure 3-4 shows the six signals investigated.

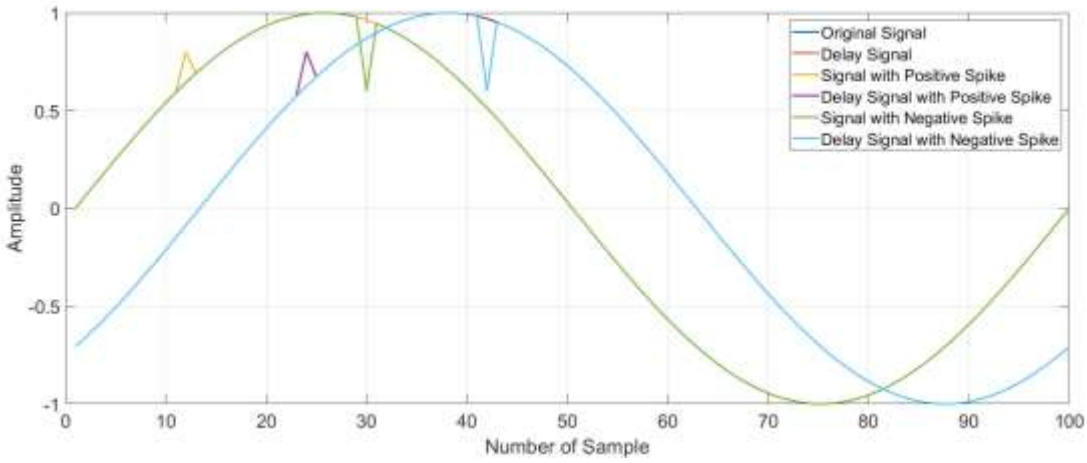

Figure 3-4: Six signals for the sine function with the same delay, two without spikes, two with positive spikes, and the last two with negative spikes.

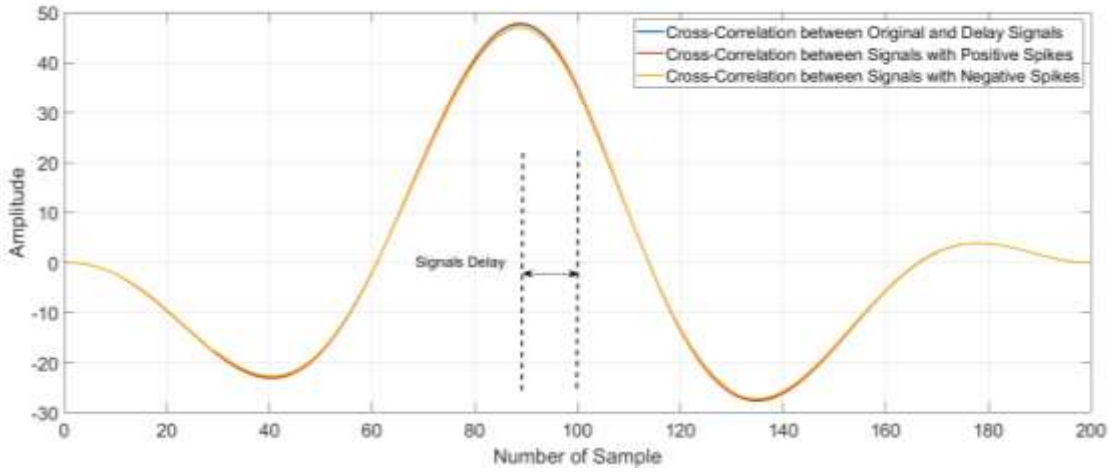

Figure 3-5: Cross-correlation between the No spikes, positive spikes, and negative spikes signals.

The cross-correlation peak is at point 89. Subtracting this from the midpoint (100) results in 11 steps. Note that one step is always missing because of the mathematical

relationship. This is due to the upwind differencing method used to find the derivative. Also, the negative spike reduces the arbitrary cross-correlation value.

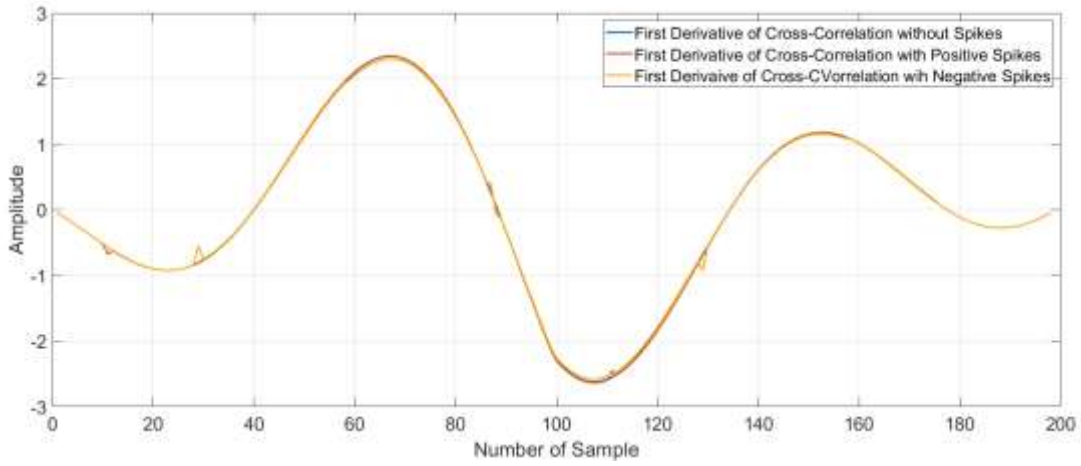

Figure 3-6: Cross-Correlation's first derivative for the three cases.

Figure 3-6 shows the first cross-correlation derivative. The spikes occur at 11 and 111 points (delay=11 from middle point (100), the actual result is 12 steps) for the positive spike (red line). Meanwhile, for the negative spike (yellow line), the peaks are at point 29 (delay is 30), and 129 (129 -100 (mid-point)) and the delay is again 30.

In the second cross-correlation derivative graph shown in Figure 3-7, positive the spikes appear at points 10, 11, 87 (13 delay steps from middle), 110, 111, and 175. The actual result is 12 steps. The reduction is due to the mathematical process for the loss of two steps.

For the negative spike, peaks are at point 28, 29 (Delay 30), 87, 128, 129, and 157.

Both cases have a peak at 87, which does not make sense in the second case. This indicates a delay between the two signals in both cases, which is 12 steps.

In the second cross-correlation derivative, the peaks indicate the feature locations and eliminate the delay. In other words, the peak at 12 which is correct for even the first signal or the second one which has a delay of 12.

In the second case, the peak is at step number 30, in both cases, for the first signal or the second one, which has a delay of 12 steps compared to the first signal. The second cross-correlation derivative eliminates the delay and shows the spikes.

The main peak near the middle shows the delay between the signals when comparing it to the middle point.

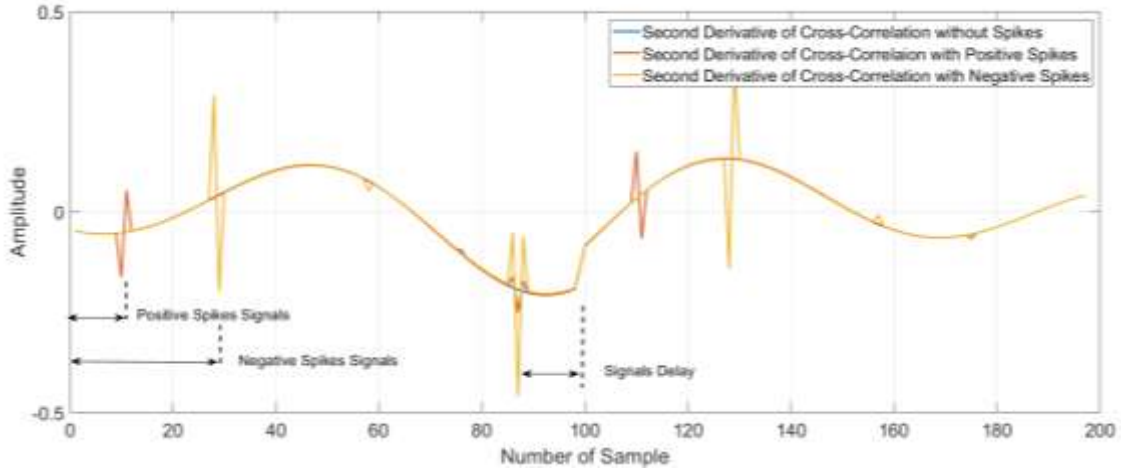

Figure 3-7: Second derivative of cross-correlation for the three cases.

3.2.3 Filters

As an introduction to the subject, noise will be considered first. This refers to unwanted signals which come with the collected data. Noise makes the identification of features difficult, since it sometimes overlaps or buries the desirable signal. Noise is produced from and not limited to: hydraulic (turbulent fluctuations), instrumentations uncertainties, unexpected changes in the system [10], such as change in the cross-sectional area of the pipe. The last of these could cause reflected waves during the water hammer phenomenon, and can be considered a noise. These detrimental signals can be treated by using filters. As an example, they enable turbulent and background noises to be separated effectively [106]. In real systems the challenge is that the noise is produced from different

components [2]. That shows the need for filtering the raw data; for instance, the transducers produce more noise and attenuation of the signal [24].

A filter is a device, either mechanical, electrical or digital, which deals with a continuous signal or sampled data. The main purpose of the filter is to pass on the desirable part of the signal and eliminate the rest. In the following description, two types of filters will be demonstrated, Moving Average Filters, and the Low/High Pass filters.

However, filtering should be adjusted to remove uncertainties, not the real changes (leaks, blocks) [45]. In addition, selection the proper filter for any circumference is still penstock decision [107].

3.2.3.1 Moving Average filters

This is the most familiar and widely used filter due to its simplicity and effectiveness. It depends on the simple idea of reproducing the output samples by averaging it on a number of samples. This produces smoother results and removes certain elements of the noise signals. As the average number increase, the results will become smoother. The filter can be calculated by this equation:

$$y(i) = \frac{1}{M} \sum_{j=0}^{M-1} x[i+j]$$

Where y is the output result, M is the sample number used for averaging, x is the signal to be filtered, i & j are indices. As seen in Figure 3-8 below, the moving average filter undergoes a noticeable alteration in smoothing the signal. However, as shown in Figure 3-8, as the averaging number points are increased, the step changes are shown with some inclination in the slopes.

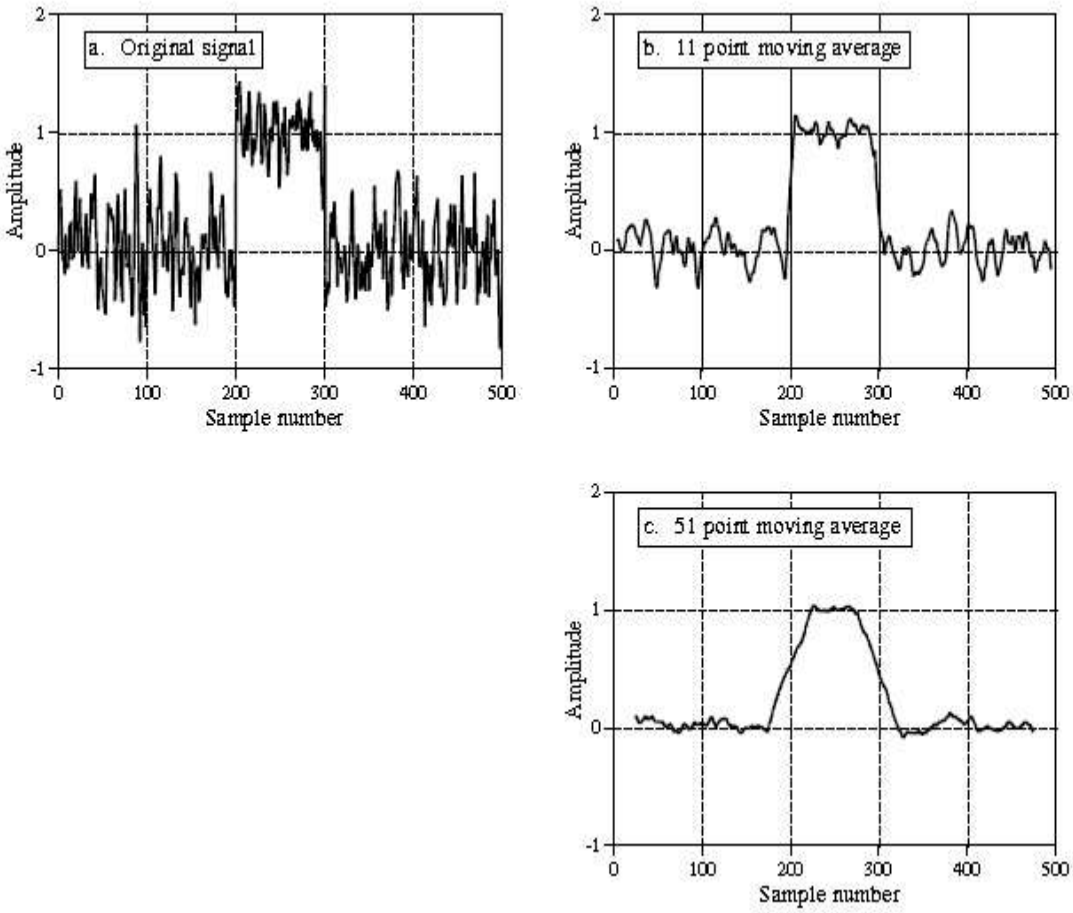

Figure 3-8 Example of moving average filter effects on rectangular pulse are buried in random noise (as in a). The outputs for 11 and 51 moving average points are shown in (b) and (c), respectively [103].

Despite its advantage, this method may treat the original, desirable, signal as noise, especially when the signal is at high frequency. So, using the principle in the frequency domain instead of the time domain is advisable to sustain the real signals. However, the stop band attenuation is extreme; in other words, it has the same effect as for the low pass filter but is considered a poor one [103].

In some cases, using a moving average for smoothing the data can give good representative samples, as in transient when the hydraulic and turbulent effects cause fluctuation.

In conclusion, in the data analysis, the average moving filter in the time domain will used; and for the frequency domain, the low/high pass filter will utilised [103]. However, it should be noted that it could treat the original signals or spikes, like those in water hammer cases, as a noise.

3.2.3.2 Low/High Pass Filter

In many cases, theoretically, researchers can estimate the system frequency range, thereby helping the hypothesis to be implemented in a realistic manner. So, 'passing' the desirable and useful data will be based on the wanted frequency values. As examples, the low-pass filter passes low frequencies and attenuates the high ones, while vice-versa is the case with high pass filter. Some filters have the flexibility to control the cut-off frequency and the steepness factor to suit the specific applications. In addition, the band-pass and the band-reject filters are types designed to pass or eliminate a specific frequency, respectively. Three of the mentioned filters are derived from the base filter which is the low-pass filter. The high-pass filter derives from reproduction of the low-pass filter, while the band-pass and the band-reject are, respectively, derived from convolution of the low and high pass filter for the first, and a subtraction for the second.

Figure 3-9 demonstrates graphically the differences between the various filters.

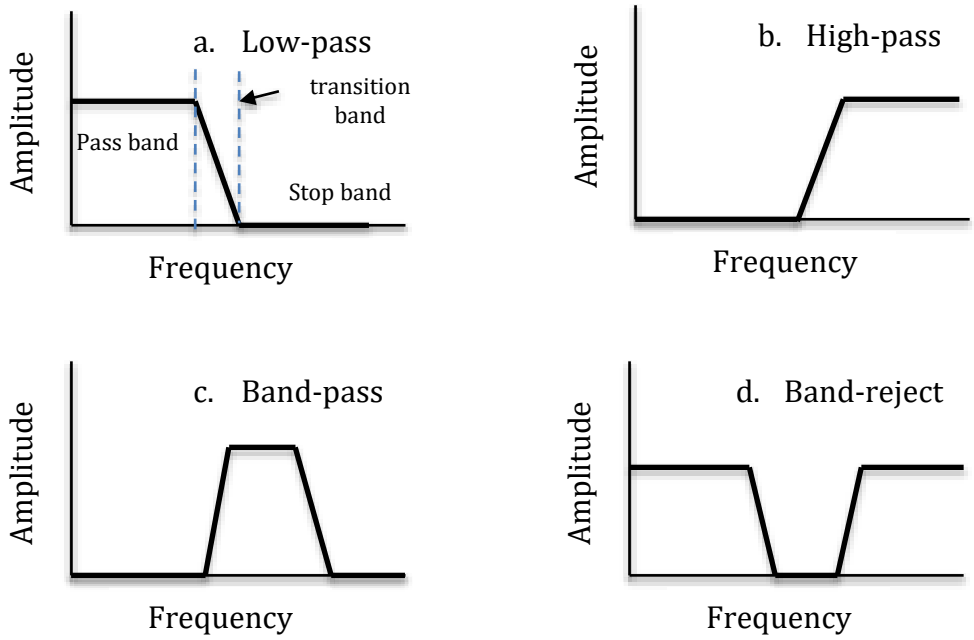

Figure 3-9 Most popular frequency domain filters [103].

The Butterworth filter is a type of the low-pass filter. It can be controlled by two parameters; the cut-off frequency and the rate of fall-off. The latter is defined by the decibel (db), which defines the ratio between two signals. The first parameter specifies the frequency at which the steepness starts. It is represented by:

$$|F(\omega)| = \frac{1}{1 + (\frac{\omega}{\omega_c})^{2n}}$$

Where the ω_c is the cut-off frequency and the n is steepness. As an example, the -30db means a reduction of the signal by a factor of 100. The cut-off frequency means the level of frequency at which the steepness starts.

3.2.3.3 Wavelet Transform (WT)

The Wavelet Transform (WT) is another method for governing the functions between the time and frequency domains. The advantage of this function compared to the Short Time Fourier Transform (STFT) is its ability to catch the nonstationary signal and reconstruct the signal inversely. The continuous Wavelet Transform can be given by:

$$W_\psi(a,b) = \int_{-\infty}^{\infty} x(t)\psi(\frac{t-b}{a})$$

The localised oscillatory function is ψ (wavelet), *x(t)* is the transform function, a is the scale parameter and b is the translation parameter. The scale parameter controls the frequency by varying time, while translation parameter move the basis function up/down at the time axis.

For technical reasons, the complex conjugate ψ^* of ψ is used. So the wavelet transform is changed to, after divided by square root of scale parameter to sustain equal energy of mother wavelet at all time scales;

$$W_\psi(a,b) = \frac{1}{\sqrt{a}}\int_{-\infty}^{\infty} x(t)\psi^*(\frac{t-b}{a})$$

The mother wavelet must have three properties. First, it must achieve this relation:

$$\int_{-\infty}^{\infty} \psi(t)dt = 0$$

That means it is oscillating, so the positive eliminates the negative and the average is zero. The second condition is the mother wavelet should have finite power,

$$\int_{-\infty}^{\infty} |\psi(t)|^2 dt = 0$$

The final property is the admissibility condition,

$$\int_{-\infty}^{\infty} \frac{|\Psi(w)|^2}{|w|}\, dw = C_\psi < \infty$$

Where $\Psi(w)$ is the Fourier Transform of the mother wavelet; this condition helps to find the inverse. This is the second feature that makes the wavelet transform a more practical technique than the STFT.

3.2.3.4 Discrete Wavelet Transform (DWT)

In the practical tests, measurements are collected at discrete time intervals. So the previous continuous mother wavelet transform can be approximated as:

$$W_{\psi}(a,b) = \frac{\Delta t}{\sqrt{a}} \sum_{j=0}^{N-1} x_j \psi^*(\frac{t_j - b}{a})$$

Where, N is the number of samples. It is important to indicate the sampling frequency, and then the time signal can be reconstructed. *N* should be chosen from *a*-*b* plane, so the x_j measurements can be reconstructed. Firstly, assume a discrete set of certain scales. Then, to reconstruct the signal, the redundancy should be eliminated so that the transform has a unique inverse. That can be applied when the orthogonal condition is achieved to define a point in a plane. The orthogonal condition requires that the two vectors should be in addition to being orthogonal, neither of them can be of zero length. This condition is represented in the following relationship:

$$\sum_{n=0}^{N-1} C_n \, C_{n2n+2m} = 0$$

Where m is an integer from 0 to $N/2$-1, and C is the mother coefficient. Another condition is that the scaling function should be represented by:

$$\sum_{n=0}^{N-1} C_n^2 = 2$$

Finally, to return the signal in accurate possible manner, another set of conditions for the mother wavelet function coefficients can be obtained from:

$$\sum_{n=0}^{N-1}(-1)^n n^m C_n = 2$$

Understanding the physical behaviour of the study subject lets the researcher select the most adaptable filter which guides the outputs to accurate system representative outputs. For this reason, in this research a proposal for a new algorithm has been developed to enhance the signal technique for the second cross correlation derivative. It has been observed that it includes some undefined peaks, and that may derive from the numerical uncertainties or other reasons in real systems.

3.3 Noise-Removal Algorithm (NRA)

This filter comes under the digital filter category, since it is a numerical algorithm and deals with sampled data.

It has been observed that undefined peaks occur with the second Derivative of the cross-correlation outputs. The peaks should indicate only the system features that can be explained. The hypothesis assumes that the noise is 'unrepeatable' either in location or amplitude. Amplitude variations are issued to make the filter be more applicable to both the experimental and real system. If the peak is repeatable at the same location and with reasonable variation, it is assumed to present features buried under a noise signals.

The backbone for this technique is building a sufficient database for normal operations events. If some singularities occur, the algorithm will detect them after a certain number of runs. Some researchers have used this idea for real field systems with predictable results [23].

3.3.1 Operating Philosophy

In a real system, the network monitoring systems show the operating fluid conditions. Those systems have a recording ability and could assist in observing the system conditions. The idea of this filter is based on utilising the normal operation

conditions, including pump startup/shutdown, or other small water hammer waves that occur frequently in the system. So, as done numerically in this research, the second cross-correlation derivative could identify the system features, even the trigger wave (the pump startup) could be considered as a smooth wave. Recording different system runs and using the signal technique will give different outputs that could be filtered by the Noise Removal algorithm (NRA) to go further in identifying small features from the amplitude of the noise.

When applying this technique on the second cross-correlation output, since the mean of this output is zero except when there is a feature, the magnitude will be far from the main. The system features could be considered as noise and removed if they were part of the network system performance. To verify the repeatability, the algorithm input is compared between five different runs. Each new run replaces the oldest one, so after five runs, if there are new features, they will be highlighted. The two criteria checked by for the algorithm are:

1. The peak exists in all five runs. Checking the peak repeatability lets the algorithm ignore the false signals.
2. If the peak has a tolerance of more than 5% compared with the other four runs it will not be counted (considered as a system feature).

If the peak achieves those two conditions, the algorithm acknowledges this peak and the user could consider it as a new feature on the system network. In this case, it could be a leak, blockage, and change in the inner diameter, or any other abnormality in the system. The code deals with the five runs as a matrix that contains five rows (runs), and the column number is customised to fit the system with a discrete number of nodes. After identifying a new feature, the code lets the user to include or eliminate it as a system feature. This advantage lets the user check whether their pipe system has undergone any alterations. Normally, the system does not have any new features, or the features are known, and whatever the result, after this step the numerical code will plot the system.

The code steps can be summarised as:

1. The new signal outputs, second cross-correlation derivative, are recorded and replace the oldest run in the sample array.
2. The code compares the peaks in the sample array and considers whether they comply with the two conditions: do they exceed the system array by 5%, and are they present at the same node (column) in the sample array.
3. Then the operator is able to include any such new peak, if any, as new features, or to acknowledge the known system abnormalities.

In summary, the algorithm deals with three inputs, the second cross-correlation derivative, the time or distance, and recorded data for comparison. In other words, it is a three-dimensional filter.

Figure 3-10 illustrates the flow chart of the code. The code is written by Matlab® (2018a).

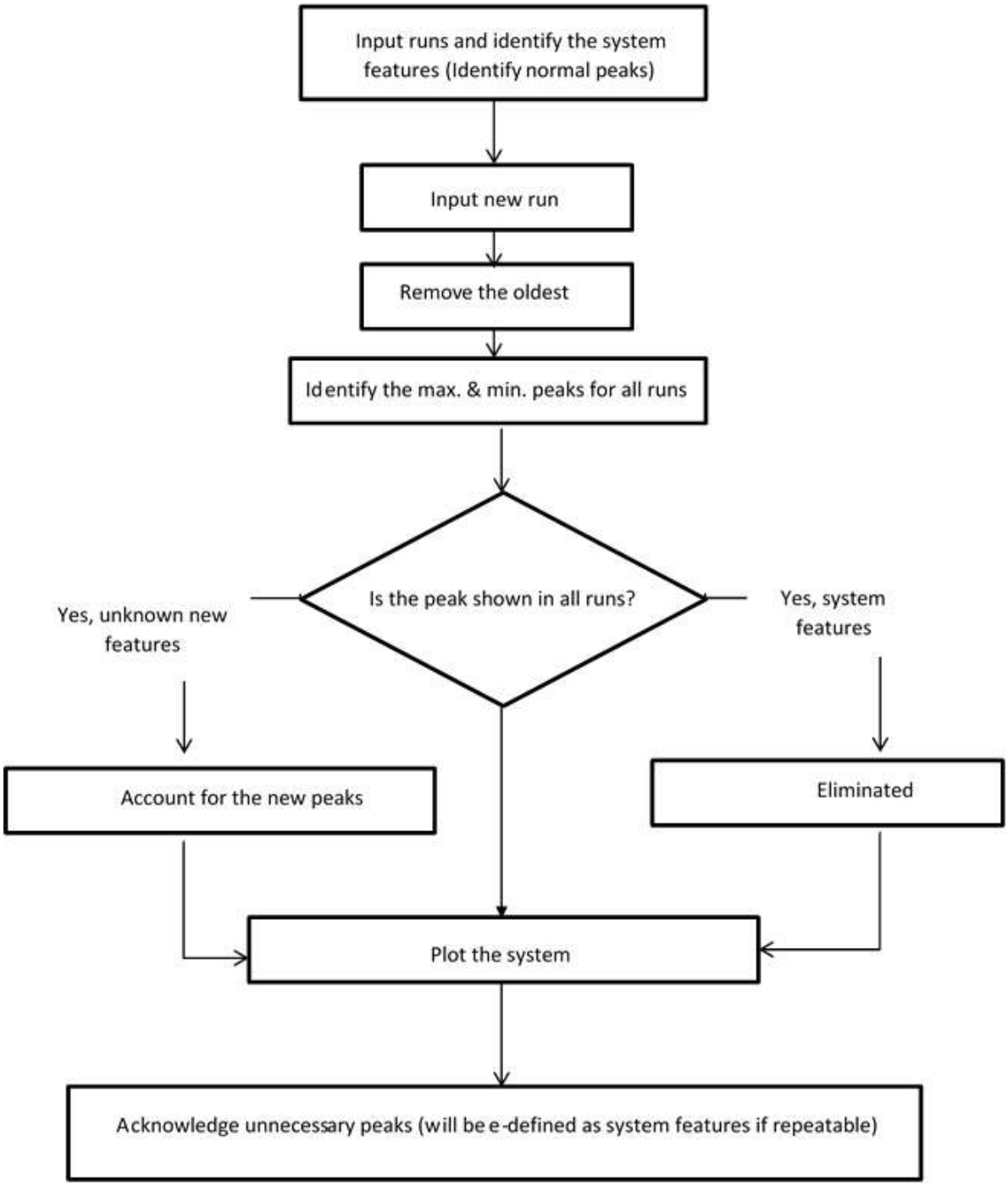

Figure 3-10: Noise Removal Algorithm (NRA) flow chart.

3.3.2 NRE filter Illustration example

In this part, a sample example will be demonstrated to explain how the algorithm works. As mentioned previously, the code deals with the second cross-correlation derivative signals. Assume a system of five nodes, which could be spatial or time points. For simplicity, the system consists of one peak at the second node and is equal to one, so the System Features (SF) will be: SF= [0 1 0 0 0]. This peak may reflect, for instance, a T-junction. The algorithm accumulates the five runs in one matrix that is called the Sample Array (SA). Let it be assumed that physically two features are created in the system network. The first is at the second node, and its second cross-correlation derivative arbitrary amplitude has increased by more than 5%. This could be explained as a blockage or a leak at the T-junction, so that the peak magnitude has altered. The second is at the fourth node and let us assume it has a value of -0.5.

Each code execution will identify if there is a leak above 5% compared with the system features array. So, after five runs, the new peaks will be available in all SA elements, and then it will be accounted for as new two peaks. The new features will be at one row of the matrix called New Features (NF). The user will be asked to include it as new features or ignore it. At this step, the user has the ability to check the system physically, if there are any harmful alterations.

If the new features are considered as system features, the SF matrix will includes them as SF= [0 1.05 0 -0.5 0], and the algorithm, in this case, will look for new features again.

This is the hypothesis of the filter and how is it works. At this research stage, the code has been checked theoretically, but the researcher is still checking the validity and performance with the actual data to be established in future.

3.3.3 Limitations

Despite not being applied on real data, the filter could have the following issues:

- A large feature could be burying a small one at the same location. For instance, at a T-junction there could be a leak, and until now the higher signal is covering or including the small one.
- Although comparing different data sets gives the ability to remove noise, the algorithm does not work instantaneously, there is a time delay issue with the above practice, and that depends on how the frequently the water hammer trigger is applied.
- As the spatial discretion becomes smaller, the noise will be more pronounced, which reduces the possibility of detecting buried singularities associated with leaks.

Chapter 4 Leak Detection Modelling by Numerical Tools

Hydraulic transient events occur in pipeline systems which result in changes to the steady state operating condition. A pressure wave travels along a pipe, and attenuates for many reasons; one of which is leakage. The occurrence and effect of these transients in systems can be expressed and solved numerically. One numerical technique for solving the governing equations is called the Method of Characteristics (MOC), which is described in the second part of this chapter. However, to describe numerically any system correctly such as the built rig or the real field system, equations are used to describe some system parameters, such as the leakage location, or a hydraulic feature, such as the pipe friction.

In this work, numerical tools have been used to simulate the real field system, and to mimic it on the new scaled rig experiment. Some equations and dimensionless numbers have been applied at different stages of this project, from the design phase, checking the rig components and up to the running of some experiments.

This chapter comprises two sections. The first part includes the equations used in this research. The second part deals with the Method of Characteristics (MOC), the mathematical tool, in detail.

4.1 The Equations

To present the study numerically, equations will be reworked to select the important parameters in this research. These were used in various situations; in the design, preliminary analysis, scaling between the rig and the real field system, pump selection, checking how far the operating and water hammer pressure was away from maximum allowable pressure for copper pipes, and other applications.

4.1.1 Joukowski Head

This was explained in chapter one. However, it will be described here again. It is a basic equation for water hammer phenomena. The maximum head generated a fluid column is decelerated can be calculated by the Joukowski equation [12].

$$\Delta H = -\frac{c}{g}\Delta V \quad (4\text{-}1)$$

Where:

ΔH: change in pressure head (m)

c: wave speed (m/s)

g: gravity acceleration (m/s^2)

ΔV: change in velocity (m/s)

This equation was applied to identify the maximum head of the system later, measuring the flow rate and obtaining the empirical acoustic speed.

4.1.2 Bernoulli & Steady-Flow Energy (SFEE) equations

Bernoulli's principle states that increasing in the velocity leads to a decrease in pressure and vice versa, and that total energy is constant for an inviscid, one dimensional and incompressible flow. The principle is based on conservation of energy. As an equation, it can be derived from the principle of conservation of energy. It includes kinetic, potential and internal energy. The following expression has been used in this research for some basic calculations for the rig and the real field data:

$$h_p + h_v + h_z = constant \quad (4\text{-}2)$$

h_p: Pressure head ($\frac{P}{\rho g}$).

h_v: Kinematic head ($\frac{V^2}{2g}$).

h_z: Potential head (Z).

When applying the first law of thermodynamics to assumption of steady flow, the above equation will be zero when applied between two points. In this case it is called 'Steady-Flow Energy Equation' (SFEE). The fluid is assumed to have a constant temperature (no internal energy is considered), density, internal energy, and viscosity. Also, no heat or work are added to the fluid.

In this research, SFEE was applied between two points: the upstream and downstream ends of the pipe, allowing for the head losses due to major and minor losses. It was used for the preliminary calculations for the real field system and the rig. It is essential to identify the required head driving the water to reach the desirable flow to enable a pump to be selected. It includes the friction losses from many parts in the rig. Also, in the real field, using measured data, the friction factor was calculated for inclusion in the numerical algorithm. It was assumed to be linear and distributed equally along system length.

4.1.3 Reynolds number

This is a dimensionless quantity that describes the ratio between inertial and viscous forces. It is applied to Newtonian fluids - fluids whose viscosity is independent of flow rate. The following expression represents it:

$$Re = \frac{\rho V d}{\mu} \qquad (4\text{-}3)$$

ρ: fluid Density (kg/m^3)

V: Velocity (m/s)

d: Characteristic Length (m).

μ: Fluid Dynamic Viscosity ($N.s/m^2$)

This number has been used many time in this research, to identify flow pattern, either laminar or turbulent; to scale between the real field and the rig; to get the friction factor from Moody diagram [108]. Its values define the flow pattern. For

Reynolds numbers between 2000 and 4000, the flow is in the transition region, below 2000 the flow is a laminar flow, and above 4000 the flow is a turbulent flow.

4.1.4 Head Losses

In the SFEE with the losses equation, the losses due to friction or from different kinds of fittings will be described in this section. The first can be presented by the following expression:

$$h_L = f\frac{LV^2}{2gd} \qquad (4\text{-}4)$$

Where:

h_L: Losses due to friction (m)

f: Darcy-Weisback friction factor

V: Velocity (m/s)

g: gravitational acceleration (m/s^2).

L: pipe length (m).

d: pipe diameter (m).

Moody [108] presented the steady state friction factor for fluid in the closed conduit estimation in simple form, in his famous paper 'Friction Factor for Pipe Flow'. His aim was to help engineers to get a good estimation in closed conduits for steady flow. From the Moody diagram [108] and for specific Reynolds number and other system specifications, the friction factor value can be obtained for the above equation.

The fitting losses can be obtained from the following expression:

$$h_L = k\frac{V^2}{2g} \quad (4\text{-}5)$$

Where:

h_L: Losses due to system fittings (m)

k : coefficient which is a function of fitting

V: Velocity (m/s)

g: gravitational acceleration (m/s^2).

Other fittings factors (like tank entrance and exits, compression fittings, valves, junctions, and expansion in the cross-sectional area) can be calculated by empirical equations or derived from expression equations in text books [15]. Head losses are assumed constant under steady state conditions [15, 108].

4.1.5 Euler Number

The Euler number is another dimensionless number related to pressure. It is the relationship between the drop pressure and the pressure associated with a flowing fluid. Its value is zero when the pressure drop is equal to zero. In other words, for a fluid system which is frictionless the Euler number has a zero value. Its expression is:

$$Eu = \frac{\Delta p}{\rho V^2} \quad (4\text{-}6)$$

Δp: The pressure difference between upstream and downstream point (Pa)

ρ: Fluid density (kg/m^3)

V: Characteristic velocity (m/s)

This number can be changed easily to a dimensionless cavitation number by considering the absolute pressure difference and ½ of kinetic energy. It was applied on the real field and the rig to simulate the real field system.

4.1.6 Flow rate with Discharge Coefficient Equation

The term has been added to the Matlab® (2018a) code as a discrete leak which is implemented using the orifice equation as an internal boundary condition [53]. It is presented as:

$$Q = (C_d A_d)_O \sqrt{2g\Delta H} \quad (4\text{-}7)$$

Where:

Q: flow rate (m^3/s)

C_d: discharge Coefficient

A_d: area of the valve (m^2)

ΔH: instantaneous drop in hydraulic gradient across the valve (m).

This expression was used in the MOC to describe the leakage at different nodes.

4.1.7 Courant Number

This number is important for the spatial mesh and the accuracy for the numerical calculations. It is a dimensionless number. The number shows the ratio between velocity times time step over the spatial discretion as follows:

$$C_r = \frac{V\Delta t}{\Delta x} \quad (4\text{-}8)$$

Where:

C_r: Courant Number

V: velocity (m/s)

Δt : time step (s)

Δx: grid cell in x- direction (m).

To improve the numerical accuracy in many applications, this ratio should be equal to or below one. Physically, it means that in water hammer, the wave propagation velocity should be bounded with a spatial discretion in a specific time step. This number should be applicable to the smallest cell if the numerical mesh has many dimensions. In this thesis, this is used for MOC solution stability [109, 110].

4.1.8 Theoretical wave speed

This equation is valid for thin pipelines without axial stress or strain [53]. Also, in a steel pipe the acoustic speed has little variation [24]. The wave speed can be calculated from the following equation:

$$c = \sqrt{\frac{K/\rho}{1 + (K/E)(D/e)}} \qquad (4\text{-}9)$$

Where:

c: wave speed (m/s)

K: bulk modulus of the liquid (Pa)

E: Young's modulus for the pipe (Pa)

ρ: fluid Density (kg/m^3).

It is assumed that the pipe has good support and is rigid. This equation is frequently used for the rig and the real field calculations.

4.2 The Method of Characteristics

4.2.1 The Method of Characteristics Principle

The method of characteristics is a mathematical technique is used to solve the partial differential equations of transient fluid flow. The first order equation is changed to a pair of ordinary differential equations, and then the solution is obtained by the method of characteristics. Solving those equations is done step by step using small-time intervals. This is an Eulerian approach. It is the most convenient method for solving transient flow equations [13] and recommended by another researcher [21] for use instead of TLC. It has been highlighted as the most accurate method in closed conduits by another [111], especially for elastic pipes [112].

Firstly, the two conservation laws are applied to the system as the follows:

Momentum equation

$$\frac{\partial Q}{\partial t} + gA\frac{\partial H}{\partial x} + RQ|Q| = 0 \qquad (4\text{-}10)$$

Continuity equation

$$\frac{\partial H}{\partial t} + \frac{c^2}{gA}\frac{\partial Q}{\partial x} = 0 \qquad (4\text{-}11)$$

Where A is the cross-sectional area, g is the gravity acceleration, c is the wave speed, H is the piezometric head, Q is the flow rate, and $R=\frac{f}{(2DA)}$, the frictional resistance for circular pipes where f is the Darcy-Weisback friction factor, D is the pipe diameter, x is the spatial discretion, and t is the time.

Numerical solution is required because of the non-linearity of the friction factor. The partial differential equations are converted to ordinary differential equations and then solved by the finite difference method with an incremental time step. More

details on the integration and conversion steps are available in Wylie and Streeter [12]. The resulting compatibility equations are:

$$H_{Pi} = C_P - B(Q_{Pi}) \qquad C^+ \qquad (4\text{-}12)$$

$$H_{Pi} = C_M + B(Q_{Pi}) \qquad C^- \qquad (4\text{-}13)$$

They are applicable for the characteristics lines $\Delta x = c(\Delta t)$ and $\Delta x = -c(\Delta t)$, respectively.

The equations are solved simultaneously to define the flow and the head, the unknown parameters at the next time step $t + \Delta t$. Some assumptions simplify the solution procedure and produce the following:

$$C_P = H_{i-1} + B\ Q_{i-1} - R\ Q_{i-1}|Q_{i-1}| \qquad (4\text{-}14)$$

$$C_M = H_{i+1} + B\ Q_{i+1} - R\ Q_{i+1}|Q_{i+1}| \qquad (4\text{-}15)$$

Where $B = \frac{c}{gA}$ and $R = \frac{f\,\Delta x}{2gDA^2}$

The pipeline is discretised into N increments ($N+1$) nodes. At each node the equations are applied to get the head and the flow at the next time step. The solution progresses from one time step to the next by defining the flow and head at each node. Figure 4-1 schematically illustrates the method of characteristics.

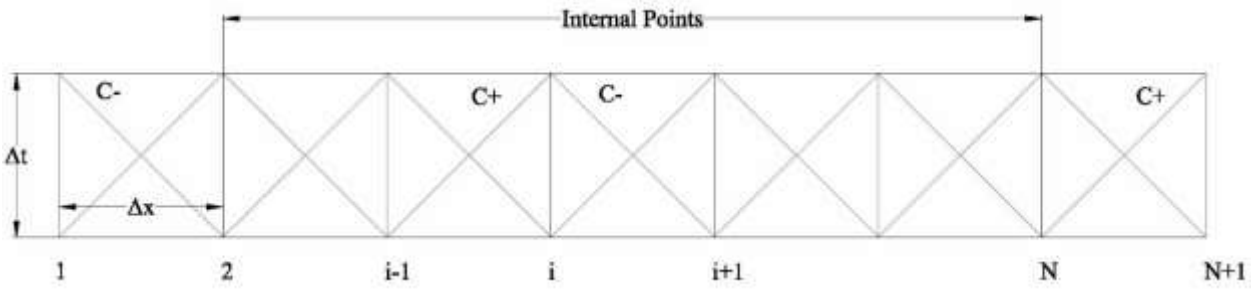

Figure 4-1: The MOC plane, points and characteristics lines [13].

This method assumes the flow is one dimensional, with the fluid having a fixed density, neglecting pipe effects, and a constant wave speed. The two dimensional

model exhibits higher energy dissipation compared to the one dimensional model [113].

The leakage can be presented numerically, as mentioned, by the flow discharge coefficient equation as follows:

$$Q = (C_d A_d)_O \sqrt{2g\Delta H} \qquad (4\text{-}16)$$

Where:

Q: flow rate (m^3/s)

C_d: discharge Coefficient

A_d: area of the valve (m^2)

ΔH: instantaneous drop in the hydraulic gradient across the valve (m).

In the MOC plane, the leak point will be presented as shown in Figure 4-2. The leak flow will calculated from equation (4-7) if ΔH is larger or equal to Zero. If ΔH is negative, the Q_{leak} is assumed to be zero.

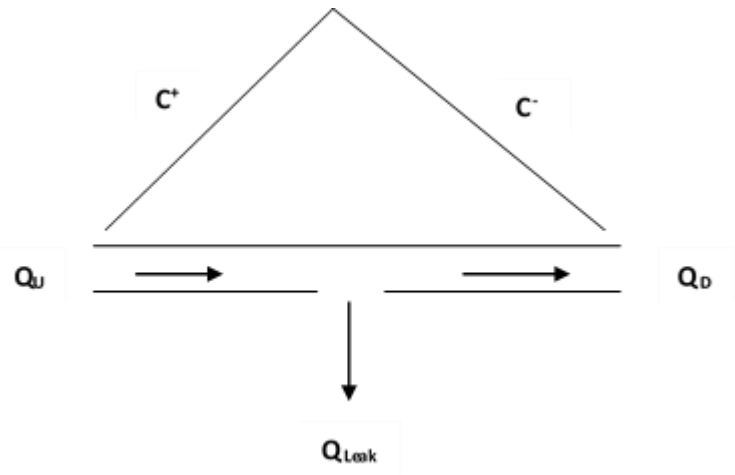

Figure 4-2: Computational leak node with the characteristics lines.

The flow upstream Q_U and down stream Q_D the leak have the following relationship: $Q_U=Q_{Leak}+Q_D$.

For the unsteady friction term, Ghidaoui *et al.* [114] suggested that if the following relationship $\frac{2D}{fV_o}/L_a$, where D is pipe diameter, f friction factor,Vo is initial velocity, L is the pipe length and a is the wave speed, is less than one, then the unsteady friction factor is not needed [115]. For the rig parameters, the figure was 0.9966, almost one.

The unsteady friction is of importance in a short length system and small diameter [115]. Also, this term causes an additional damping to the pressure wave [27, 88, 106]. There is no accurate approach for representing unsteady friction [27], and it does not represent very well the pressure wave attenuation and dispersion [105].

4.2.2 MOC Code

The Method of Characteristics (MOC) is used to model the pressure transient for the real field and the experimental rig. In this research, the MOC is written in Matlab® (2018a).

The code starts with the input data such as the steady-state flow, pipe length l, wave speed a, pipe diameter d and wall thickness e, leak coefficient (if applied) for the total time of calculation T_{max}, gravitational acceleration g, and the number of system reaches N. This number should be even to enable division of the system into equal segments. So the total nodes will be $N + 1$ starting from first node. Increasing this number will not increase the calculation accuracy significantly [116]. The pressure reading and location of leakage should allocated to those nodes. A later step is to calculate some parameters: the spatial discretion Δx, time step Δt, R resistance coefficient, and B pipeline impedance.

This is followed by the steady state solver stage that consists of solving the steady state friction effect at each node and then identifying the node pressure value.

The principle part of the numerical algorithm, the transient solver, is described below. It is divided into three parts, the upstream and downstream boundary

conditions, and the internal nodes. First, the number of time steps is obtained, and then the head and flow are calculated at the next time step. The first point is the upstream boundary condition, point 1, which is usually either the reservoir head, or the pump head. If the head is known, the flows are calculated from the relevant compatibility equation. Then the internal points are solved for all internal nodes. Finally, the last boundary is either the closed valve or open pipe end. In either case, if the head is known, the flow is obtained after solving the compatibly equation.

At the end of this time step, the procedure is repeated again after incrementing the time with one time step.

If the water hammer is caused by a valve closing, some alteration in the steady state and the transient solver result from this condition. The unsteady friction term was not included in the solver because of the limitations discussed above.

The following assumptions are inherited in the model: one dimensional fluid flow, the pipe is elastic, the fluid compressibility is negligible, and the steady state head loss is considered constant during the surge, even though these assumptions has been highlighted as not being precise by some scholars [95]. Also, the Courant number neglects the friction [95]. The shape and the attenuations of the surge wave are not well modelled when using the unsteady friction [105]. In addition, the unsteady friction contributes to the time delay [117] and is not necessary [37, 95]. Friction affects the attenuation and not the timing [101]. Despite the efforts that have been made to develop a numerical term for the unsteady friction, there are still disagreements between the numerical and experimental date. That difference is due to the nonlinear elastic behaviour of the pipe and the fluid, frequency dependence of the wall and fluid properties, and other reasons [12].

The method of characteristics is summarised in Figure 4-3.

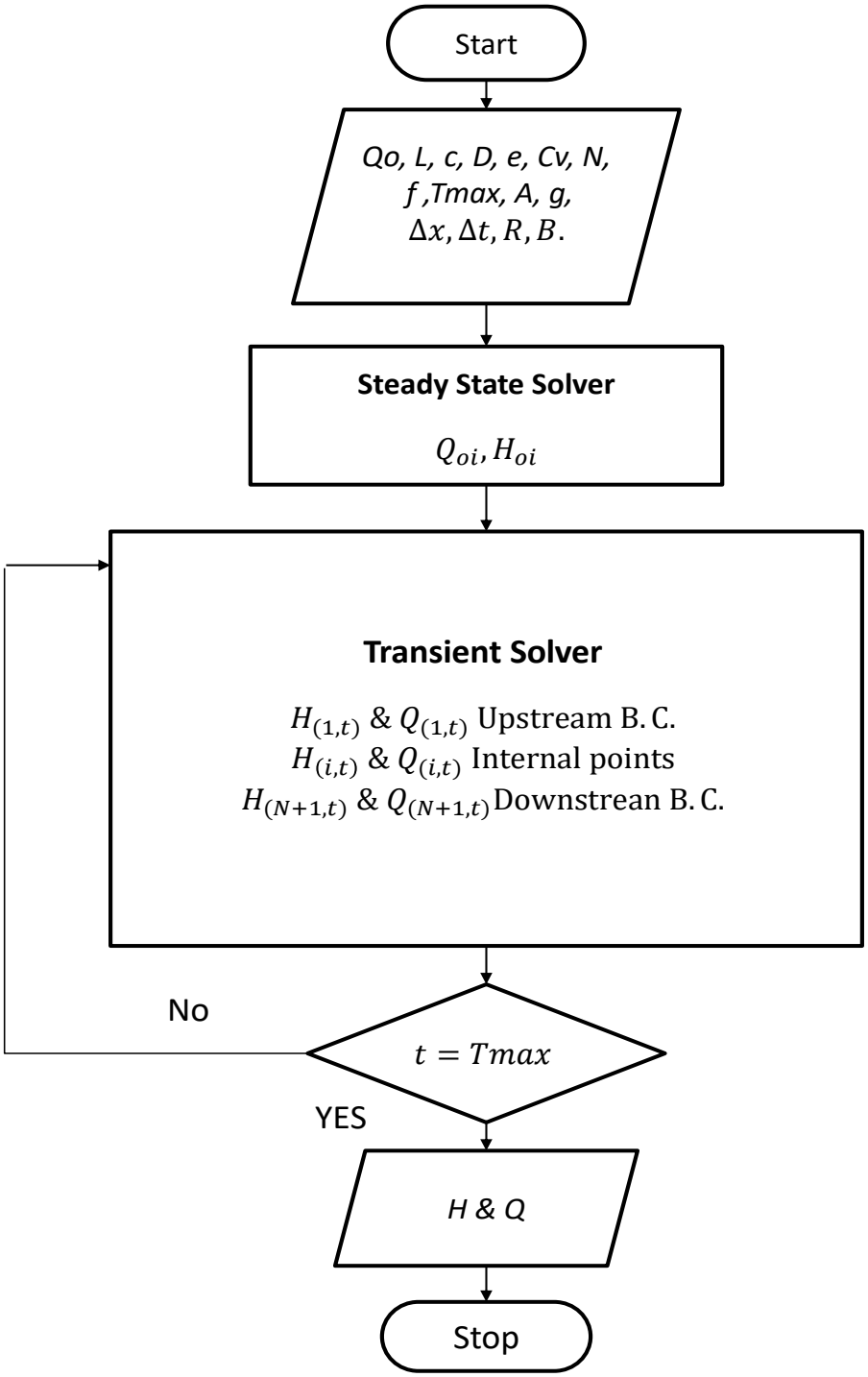

Figure 4-3: Flow chart for MOC method.

4.2.2.1 Code stability

The characteristics lines share curved line in the partial differential equations even though the speed wave is constant [12]. However, a practical exercise was done to check the stability of the numerical code. The principle is that without the trigger of a pressure surge event, the numerical code should continue to give the steady state conditions. In other words, if the valve sudden closing or pump raising are eliminated, the outputs remain the same. For example (3- 1), in Wylie and Streeter [12], the code is run for steady-state conditions, and as seen in Figure 4-4 the points at upstream of the valve, midpoint and downstream at the reservoir, remain constant.

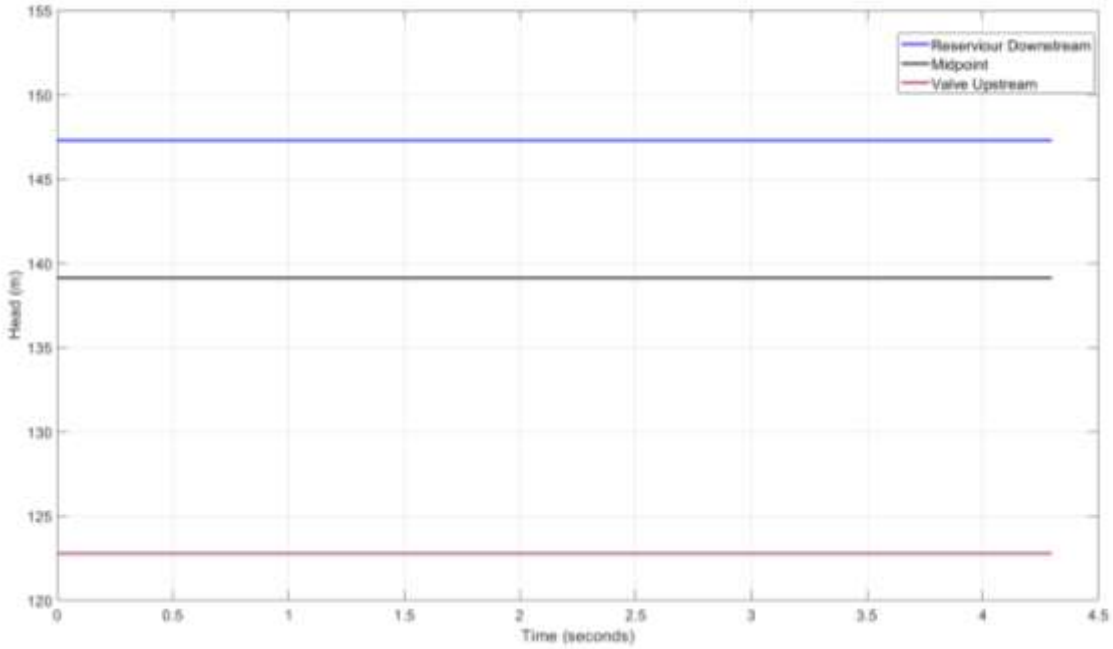

Figure 4-4: Example (3-1) in [12] parameters remain constant without the water hammer trigger.

4.2.3 Rig & Real system computational code

In the case of the rig, the code developed previously requires some modifications: location of the leak and the wave speed determine the number of nodes required. For the experimental apparatus the pipe length is 800m and the nominated spatial

discretion, the length (Δx), is 1.25m. Therefore, the number of nodes required is 640.

The real field system consists of three pipe segments of the following lengths: 300m, 15000m and 330m. The numbers of nodes are 4, 150, and 4. So the spatial distances are 75m, 100m, and 82.5m, respectively. It should be highlighted again that the real systems consists of three typical ones, and the only difference is in the submarine pipeline length which has 14 *Km*, 15 *Km* and 22 *Km*. The numerical analysis was undertaken for the mid length.

Figure 4-5 illustrates the schematic of the rig in terms of reaches.

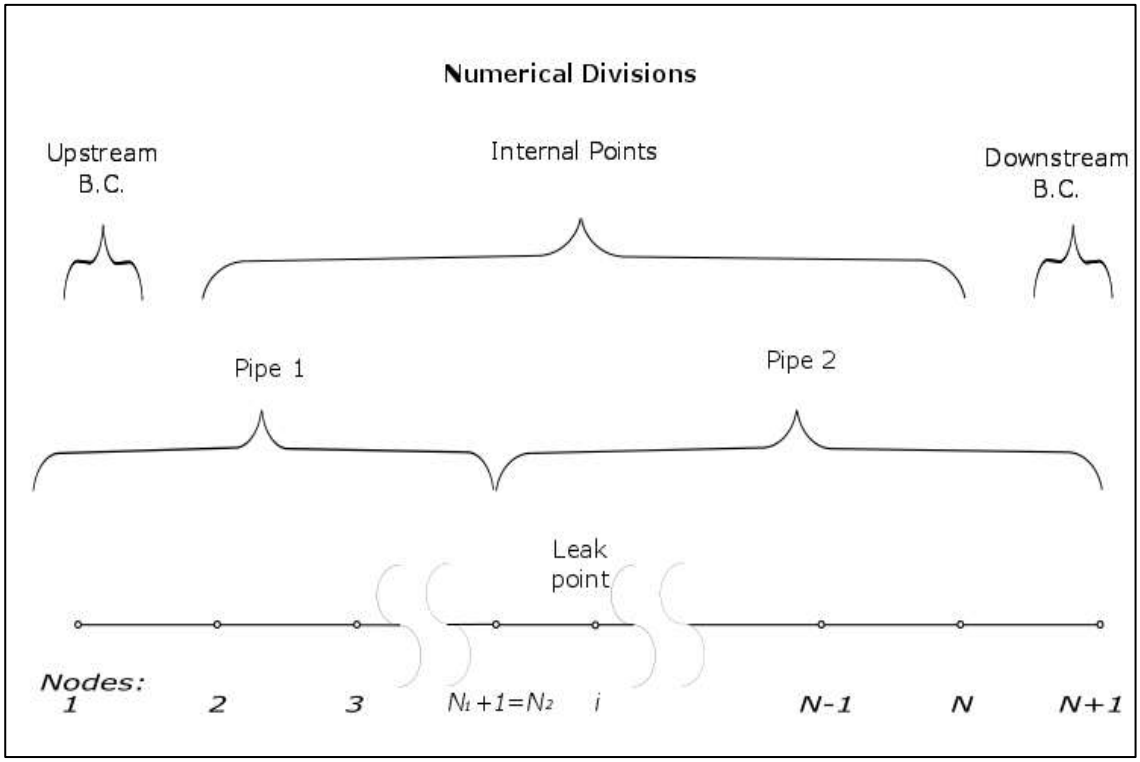

Figure 4-5: Numerical diagram for the rig.

It is obvious that to deal with the numerical issues, the rig has been divided into three boundary conditions. Furthermore, the rig consists of two parts, pipe 1 and pipe 2. As explained, the variance in internal diameter definitely affects parameters such as the wave speed and the number of reaches; hence, the numerical reaches

were divided into two, to handle those alterations in the system. As shown in Figure 4-5, the computational leak point has been varied for many tests on pipe number two. The code can deal with it after defining the leak's location.

Increasing the number of nodes in any numerical system increases the precision of the numerical output. Nevertheless, it will be source consuming. The smaller the spatial discretion, yield up better the results and improving the stability of the computation.

4.2.4 Numerical Results for the Experimental Rig and Real System

The pipe length for the test rig was $800m$. In this section, the elementary numerical outputs were checked for the leak in different positions. The code was run to check the numerical outputs at different leak locations, and applying the cross-correlation and its second derivative.

The boundary conditions were assumed as a fixed level reservoir of $20m$ and with the pipe end is open to the atmosphere. The flow rate was 1.68 $l/minute$ and the water hammer was caused by closing a downstream valve.

In Figure 4-6, a schematics shows the rig components and its dimensions. This schematic is as built dimensions in the laboratory. It is noticed there is some differences in the rig between the designed and the real construction due to many reasons will be explained in Chapter 6. The numerical outputs were done on the designed dimensions.

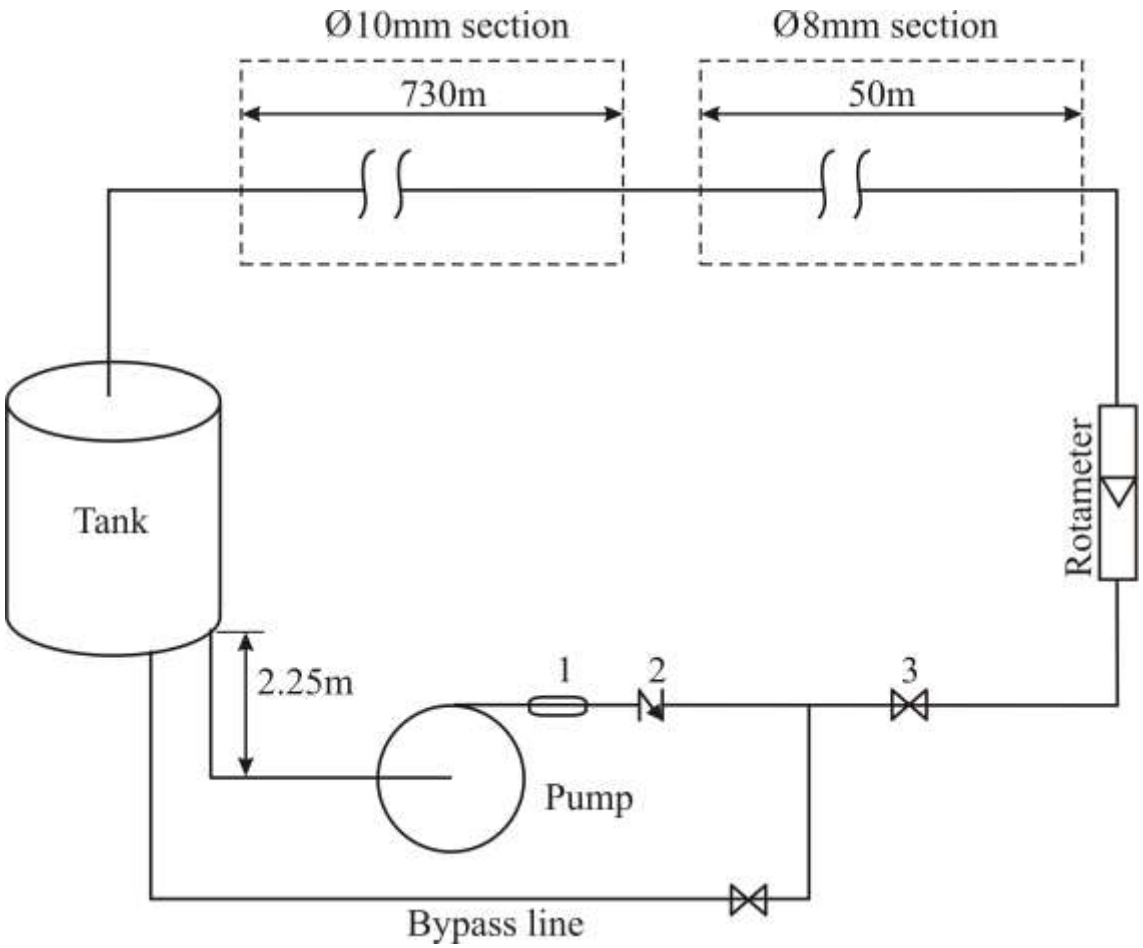

Item	PT1	PT2	L1	PT3	L2	L3	L4	L5	PT4	L6	L7	PT5
(m)	0	103	127.7	281	354	363	377	386	536	601	610	770

Figure 4-6: Schematic of the experimental rig and its components. (Number 1 anti-vibration hose, number 2 non-return valve and number 3 gate valve).

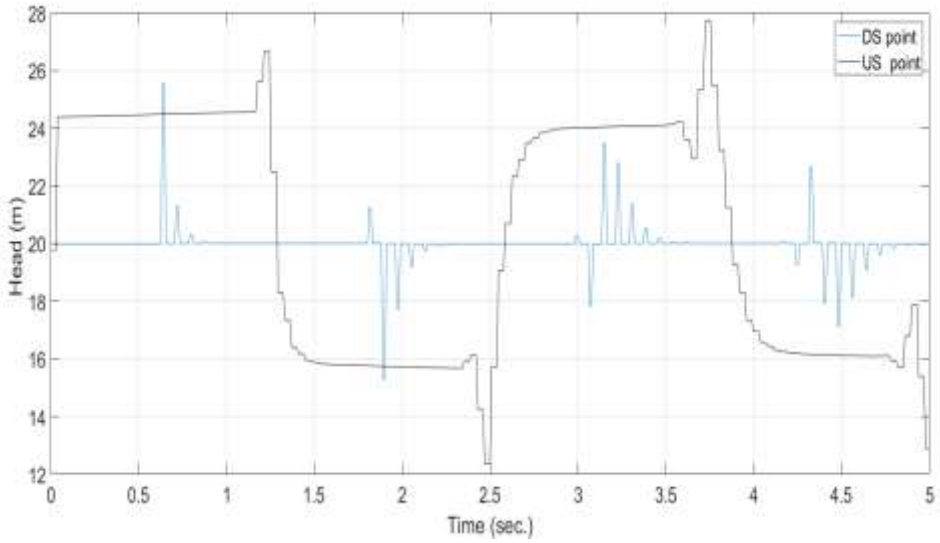

Figure 4-7: Computed transient pressure traces for the test rig. Water hammer event with change rig of two sections (8mm x 50m and 10mm x 750m)

Figure 4-7 shows the upstream and downstream computed pressure traces without a leak. The location of the computing points are just adjacent to the upstream and downstream boundary conditions by one reach.

Another computed pressure traces numerical output is revealed in Figure 4-8 for reading points at $200m$ and $800m$. The leak at node $550m$.

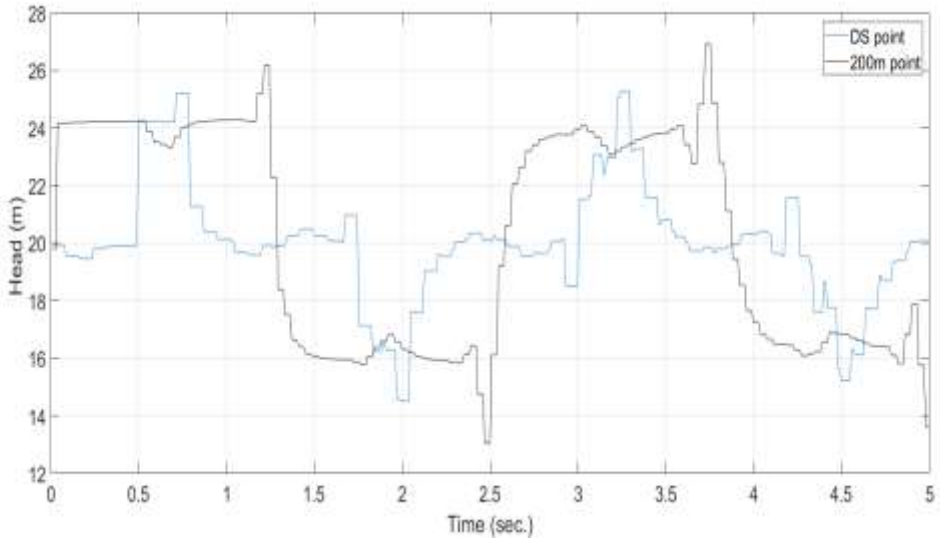

Figure 4-8: Pressure readings at 200m and 800m points for a flow with a leak at node 100m.

During numerical trials to improve the numerical code, some numerical observations were made. First, increasing the number of reaches number and the valve closing time did not show noticeable changes in the numerical output. Also, modelling the rig as two components of the same specifications was found not to affect the numerical output.

4.2.5 Numerical Results for the Real Field System

A comparison was made between the numerical results of the export terminal and the results of publication [44] to validate the numerical code output. First, the publication aims and findings will be presented. The paper aimed to model the unsteady friction term. The system consists of a pump at the upstream end and a constant level tank at the downstream end connected by a steal and PVC pipes. The steal pipe is 2 Km in length. The recorded data for pressure and flow were collected at two points along the pipe. The first was downstream of the non-return valve, downstream of the pumps; and the second was upstream of the PVC pipe. The pressure waves were triggered by the pump trip. The frequency of collected data was 50 kHz. The head loss was estimated from the steady-state condition and found to be about 0.86m and the Reynolds number was about 187,000.

They found that the constant tank level boundary condition gave a high level of pressure waves. While this may be useful to estimate the water hammer risk, it is not useful when using the transient method to diagnosis pipeline features, because the predicted values exceed the measured data. Also, that is an issue in respect to unsteady friction term for the MOC numerical code.

Initially, the export facility was modelled from the point downstream of the pump up to the floating hoses upstream of the ship and the pressure wave was caused by closing the ship valve. The length of the system was about 15,000m in total and the flexible hoses about 400m (2.6%). Figure 4-9 shows the pressure trace following the instantaneous closing for the ship valve (not practical, the closing time is 15 seconds are shown in Figure 4-10, and the first scenario case with fixed level reservoir boundary condition.

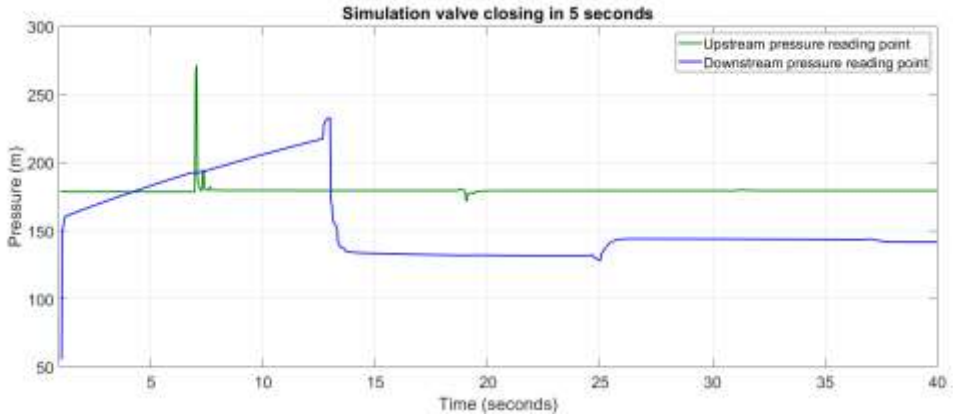

Figure 4-9: Numerical calculated heads for the upstream and downstream points of the real system.

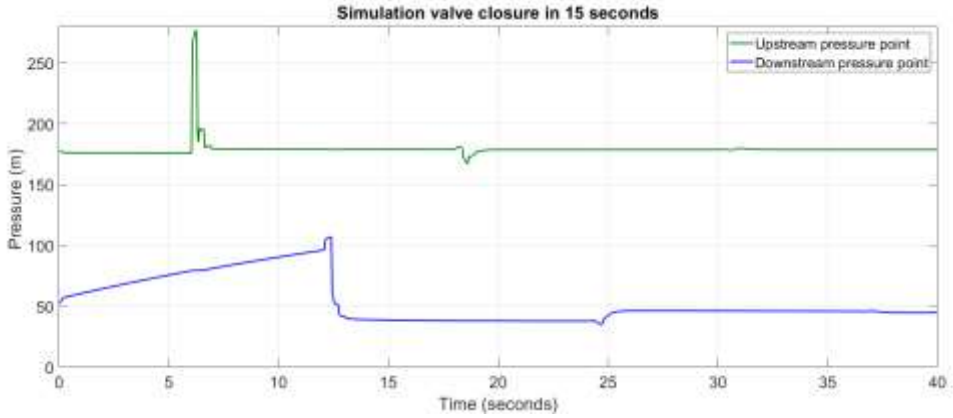

Figure 4-10: Numerical prediction of pressure heads for upstream and downstream point for the ship valve closing in 15 seconds from the numerical results.

As shown in Figure 4-10, the attenuation is clear when the valve is closed in 15 seconds when compared with Figure 4-9.

Despite the differences in system configurations, and the pressure wave causing the two points, the validity of the numerical code may be achieved.

Modelling the real-life system is complex, particularly because of the need to mimic the boundary conditions and the noise sources [44], and a lot of uncertainties are applied [57]. In addition, in reality, no 'steady' state, also the air content is not known exactly [57].

4.3 The Graph Alignment Code (Auxiliary Code)

After running the experimental rig successfully for many tests, an issue emerged after collecting certain data. When comparing two different runs for the same pressure transducer reading, like pressure point 1 without/with a leak, they coincided manually. This led the researcher to look for a code could align the two comparison charts from different runs together, as far as possible.

Two approaches were developed and applied as a code in Matlab. The first derived from the water hammer behaviour. Since the concern window starts from pressure rising up, the approach detects the gradient change starting points for both sets of data. In a later step, they will be combined together to let the water hammer event start, as closely as possible. The gradient is calculated by defining the difference between two points. To reduce the effect of noise on these values, the interval between the two points is fifty. Because of data discrepancies, the two or close points may give a false gradient. A new window will be selected, starting from the steady-state condition and coinciding with the water hammer trigger moment together. The researcher's supervisor suggested this technique.

For the second, the mean approach, the principle is to calculate the mean value for selected window of the transient event. Then the code calculates the mean values for the two sets of comparison data. Since the mean value figure could not exist exactly, in the next step, the difference between each mean value and the whole data set will be verified. The minimum difference will be located. Finally, the code coincides the two locations as much possible, as was done in the previous approach.

The hypothesis behind this is that for similar water hammer events the mean point occurs at the same time. This is applied for the same pressure point.

Both codes were more convincing and less time consuming when compared with the manual technique. The data was filtered after being loaded for both approaches at the beginning of the code.

These codes will not be needed if certain changes are made to the LabVIEW to synchronize the data with the water hammer trigger instant. Due to the late time of commissioning the experiment (March, 2017) with the scholarship period, the experimental works were expedited to get the results and do the analysis as quickly as possible. So, the work was run on the basics requirements. The tests will be improved once the conditions for data acquisition has been amended.

Figure 4-11 illustrates the two approaches. The red line is the titled pressure with a leak. After many runs, the mean approach was selected as it gives more accurate alignment.

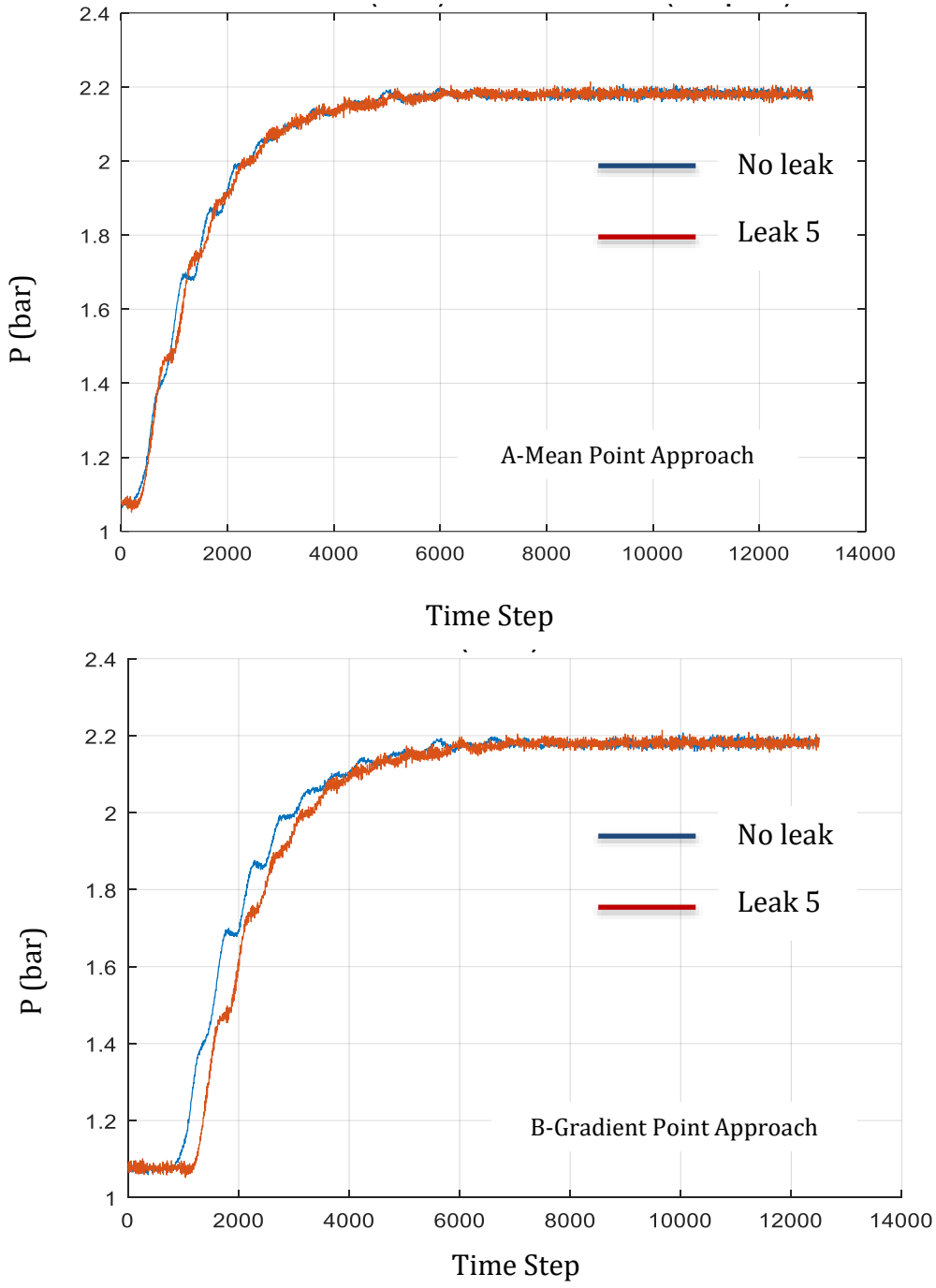

Figure 4-11: Measured data for pressure number 1 without leak (blue line) and leakage at location 5 (red line). The water hammer trigger is pump rising from 0.6 to 1.2 l/minute. Two alignment approaches, a- The mean point approach at the top and b-gradient point approach the bottom.

Chapter 5 Export Terminal System

In this chapter, the real field system configurations and parameters will be described and explained. The system was selected since it uses a simple, long distance pipeline without any connections or features in the middle. Based on this part of the Export Facilities system, the experimental rig was designed.

Most applicable studies on utilising the water hammer phenomena for detecting leaks were carried out in real water networks [23, 24] and in small facilities [27]. Although the fluids are similar, there are fewer studies on petrochemical networks than on water networks, for a variety of reasons, probably because of the hazardous nature of the products or the accessibility of the network. Meanwhile, the oil and gas industries have utilised more advanced techniques like intelligent pigging to detect the leaks. Another difference between the water and oil/gas networks is that water systems have a high percentage of leaks [89, 90]. Also, leakage is common in water pipelines whereas in oil is not [20]. Most of the experimental and field studies consider a single cross-sectional change, while in this real system and the scaled rig multi changes are considered [22].

The real system in this research covers many gaps and interesting issues in relation to water hammer phenomenon research. As an offshore oil pipeline system, a high degree of turbulence is to be expected [10].

In addition, by its nature the oil and gas pipelines industry exhibits various characteristics which do not apply in water networks, and can be summarised as follows:

1. Most of the networks are of recent construction and there is excellent documentation about the networks and their components, including the pipe dimensions and valve and pump characteristics, particularly compared to the water networks. As an example, Stoianov [27] stated that the main 36" diameter pipeline in Oxford Street, London was constructed in the 1840s and

many of the records about such pipe networks and their position have been either lost or never existed.

2. Generally, the technology in this field is modern and has the latest monitoring devices. For example, signal transmitters and flow rate meters with adequate calibration and maintenance routines are routinely installed, making the data acquisition and analysis more reliable. SCADA management systems are usually used [9] and can been integrated with leak detection approaches [118, 119].
3. Most previous water based studies, particularly at laboratory scale, were conducted on small dimension networks, while studies of oil and gas networks have considered various sizes.

The water hammer approach is a cheaper method to detect leakage compared with other methods in terms of manpower and resources. For instance, the intelligent pigging process requires operation coordination which affects the normal pipeline operation, specialist people to run the pig, and the analysis of the accumulated data. In addition, it mainly relies on specialised vendors for the supply of the required equipment. In comparison water hammer can be integrated into the system and the data analysed by one person. So, attempting to find a method using this basic concept that is practical, reliable and applicable in real systems is a major goal of this work.

5.1 Description of the Export Loading System

This section will commence with a description of the loading system in Kuwait Oil Company (KOC), which will be the subject of this study.

The parameters used during the design stage will be applied or re-evaluated to provide a good estimation of the variables to be used in the numerical modelling. Also, the irrelevant boundary conditions of the field system will be presented.

Recently, Kuwait Oil Company (KOC) has upgraded its export facilities by completing a mega project that has enhanced the export capability to handle a 3MMBLS daily production rate. This project included the Crude Export Facilities at

North Tank Farm, South Tank Farm, and North Pier Pumping & Metering station (NPP&MS) project. Hyundai Heavy Industries Co. LTD (HHI) constructed this project between 2006 and 2009. A part of the Kuwait Oil Export facilities will form the real field system in the current work.

Figure 5-1: Export Facilities Overview.

It consists of floating roof tanks, pipelines of different lengths and diameters, and interior manifolds which contain conjunction headers with different valves. This gives the system flexibility in operation, to convert the flow to the correct destination, at the right flow rate, depending on the final export destination or which pipeline is being used. In Figure 5-1 the tank farms, pipelines, the North Pier Port and Metering Skid (NPPMS), and the Catenary Anchor Leg Mooring (CALM) buoy are presented in yellow circles with number, 620, 651,612 and 619, respectively. The study part of this research starts from the pump at NPP&MS, the submarine crude line, and the CALM Buoy. As illustrated in the figure, the export facilities consist of three identical CALM Buoys, the only difference in the submarine pipe length. The location of the Kuwait Oil Export facilities is shown in Figure 5-1.

The system to be studied is explained in Figure 5-2. Also, the manifolds are shown in Figure 5-2 in the dashed squares numbered 3 and 5. In addition, in these manifolds, the pipes rise up to connect the headers pipes and then continue downward to go underground again. It should be noted that most of the pipelines are underground or on the sea bed.

Depending on the desired flow rate, the vessel at the Catenary Anchor Leg Mooring (CALM) Buoy (9) is fed either by gravity or by pumping loading. The number of tanks used to supply the crude is dependent on different factors: operational reasons, the required flow rate and the minimum suction pressure.

The elevation between the sea level and the tank bottom approximately is $111m$ (varies between one tank and another).

It is clear that there are many components of the systems to consider in the numerical modelling. The valves, headers which require changing in topology of the line and the cross-sectional pipes, affect the flow and cause many pressure drops in the system. Also the valves' operational performance (complete isolation or partial flow) are a source of uncertainty and hence difficult to model. By neglecting all of the foregoing, it can be assumed that the system components operate perfectly; however, the system still has many temperature and pressure relief valves for safety purposes. Hence, to avoid the uncertainties and the malfunctions of the components, and also to simplify the modelling, the part of the system that will be considered is downstream of the pump where there is discharge and the metering skid stream pressure transmitters up to the CALM buoy.

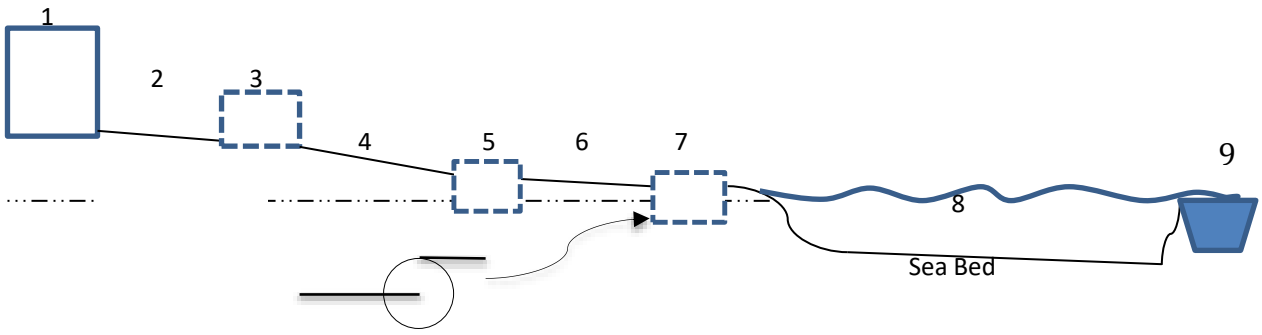

Figure 5-2: Schematic of the loading system components from Tank to CALM Buoy.

The information in Figure 5-2 is explained in details in the following table.

No.	Description	Dimensions		Note
		Diameter (in)	Length (Km)	
1	Tank	#	#	
2	Pipe line	36-48	1.3-0.6	Variation in dimensions depend on the pipeline used for loading.
3	Manifold	40, 42 & 48	0.3	
4	Pipe line	40/38, 48	8	Some pipelines have changing cross-sectional area.
5	Manifold			
6	Pipeline	48	0.5	
7	Metering & Pump station	60	0.3	
8	Submarine Pipeline	56	15,18 & 22	CALM Buoy no. 23, 24 & 20
9	CALM Buoy			

Table 5-1: Components shown in Figure 5-2 with further details.

The section of the distribution system to be studied is shown in Figure 5-3.

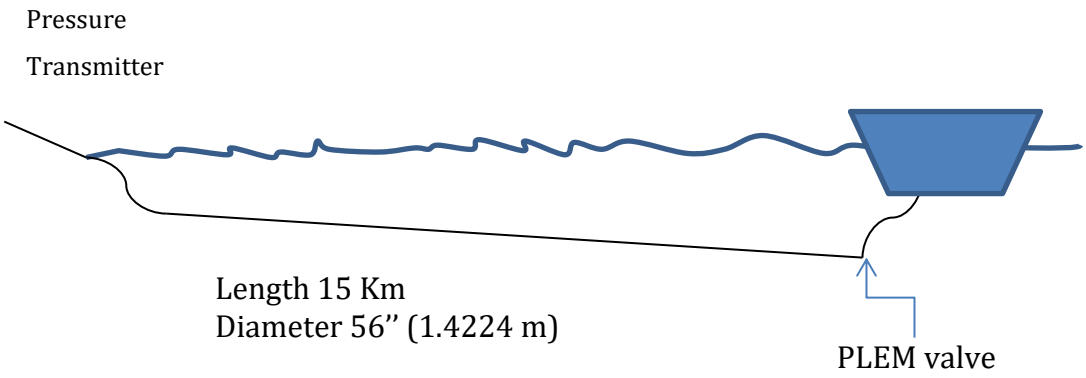

Figure 5-3: Schematic submarine line elevation of the downstream of the pump up to the CALM buoy.

The advantages of limiting the study section can be summarised as follows:

1- It avoids any malfunction of the components like a valve not closing fully, which would affect the numerical modelling. It is better in terms of leak detection to avoid these system components [43].
2- There are three almost similar submarine lines with different lengths, of 15, 18 and 22 *km* which gives the opportunity to check the validity of the numerical technique if applied.

Finally, the details of the CALM buoy components are shown in Figure 5-4. At the last point of the submarine pipeline, it divides into two hoses each containing a valve which is known as the Pipe Line End Manifold (PLEM) valve. These valves close within 5 seconds in case of an emergency such as a leak from the ship or a hose, or if the pressure becomes greater than 9 $barg$ in the PLEM [121]. This is one of the major causes of the water hammer phenomena in the system. In reality and for safety reasons, the functionality of the signal is checked routinely without operating the valves. However, the staff have been instructed to collect data on any occasions

of surge behaviour during emergency shutdowns. This rarely happens during loading for any doubtful circumferences.

The KOC has four CALM Buoys and as mentioned earlier, three of them are almost identical in components and specifications, except for the pipelines' length. These length variations are shown in item no. 8 in Table 5-1. The pipelines start from the same shore location, and different vessels can be anchored simultaneously. Referring to Figure 5-4, at the end of the submarine pipeline there are two PLEM valves linked to different hoses connected to a swivel joint. From the swivel joint two floating hoses are connected to the vessel with the CALM buoy to export oil. The swivel joint preserves the flexibility of movements of the loading; this is vital when the vessel is moving due to winds or sea currents.

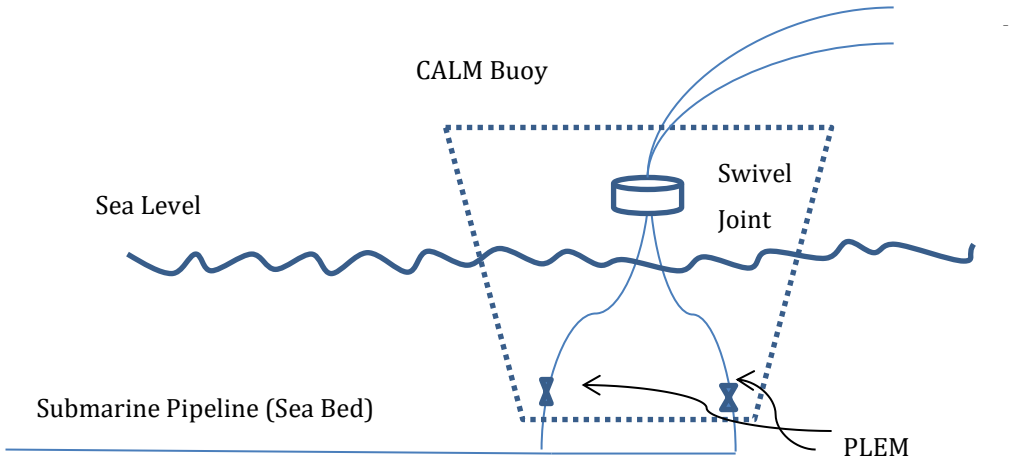

Figure 5-4: CALM Buoy Components

5.2 Comparison between the Old and New Data System

The sampling rate has increased from 1 second to 90-100 *ms*. Details about the improvement configurations for the SCADA system are included in Appendix C.

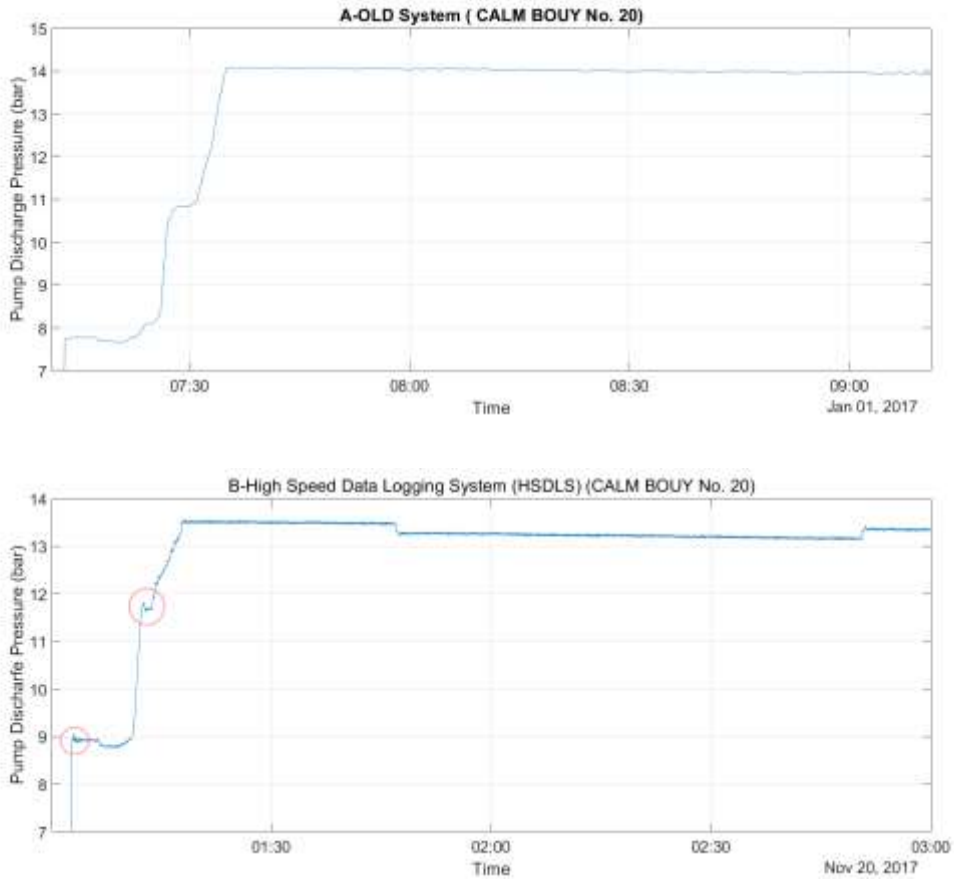

Figure 5-5: Recorded transient pressure during pump start up at pump delivery for CALM Buoy No. 20 using old (A) and new (B) data acquisition systems. Two Discharge pump readings for CALM Buoy no. 20 shows the old (A) and new system (B).

Figure 5-5 represents a comparison of the recorded of the pump pressure readings using old and new data acquisition system. Recorded transient pressure during pump at the pump delivery for CALM buoy No. 20 using old and new data acquisition systems. Examination of Figure 5-5 shows that the new recording system gives a more realistic representation of the pressure transient at the pump start up as shown in graph B in the two red circles.

Another interesting point is the intermediate pressure rise in Figure 5-5 with the old system, the range of this pressure rise is between 7.7 and 10.8bar. This step change in pressure is indicative of a transient event. This event is clearly evident the new system at about 9 and 11.7bar. Increasing the sampling rate would obviously be expected to provide more accurate information about the water hammer events.

In reality, no steady state or repeatable runs exist as illustrated in the above curves. Although recorded pressure traces being from the same location, CALM Buoy no. 20, there are numerous conditions that affect the hydraulic behaviour, including the tank storage level, number of tanks involved, tank elevations, and the number of headers and pipelines used.

However, this example shows the importance of using dimensionless parameters which enables a comparison of different operating conditions to be made by using a reference value. For instance, after dividing the value of the transient pressure by the mean steady-state figure before pumping, a comparison of individual transient events could be made.

Chapter 6 Experimental Rig Design

The experimental rig was constructed as a scale model of the actual system. This was undertaken to enable experimental validation of the numerical model.

A laboratory scale apparatus provides experimental flexibility [101] and the similarity between the large and small pipelines in transient phenomena ensures independence of size [101].

As both the model and the experiment need to be an accurate model of the real system, the numerical code has been validated initially using the classic water hammer equations with a steady state frictional term. The rig was designed with the first pipeline 8mm in diameter, 50m long and the second pipe 750m and 10mm in diameter, see Figure 6-1.

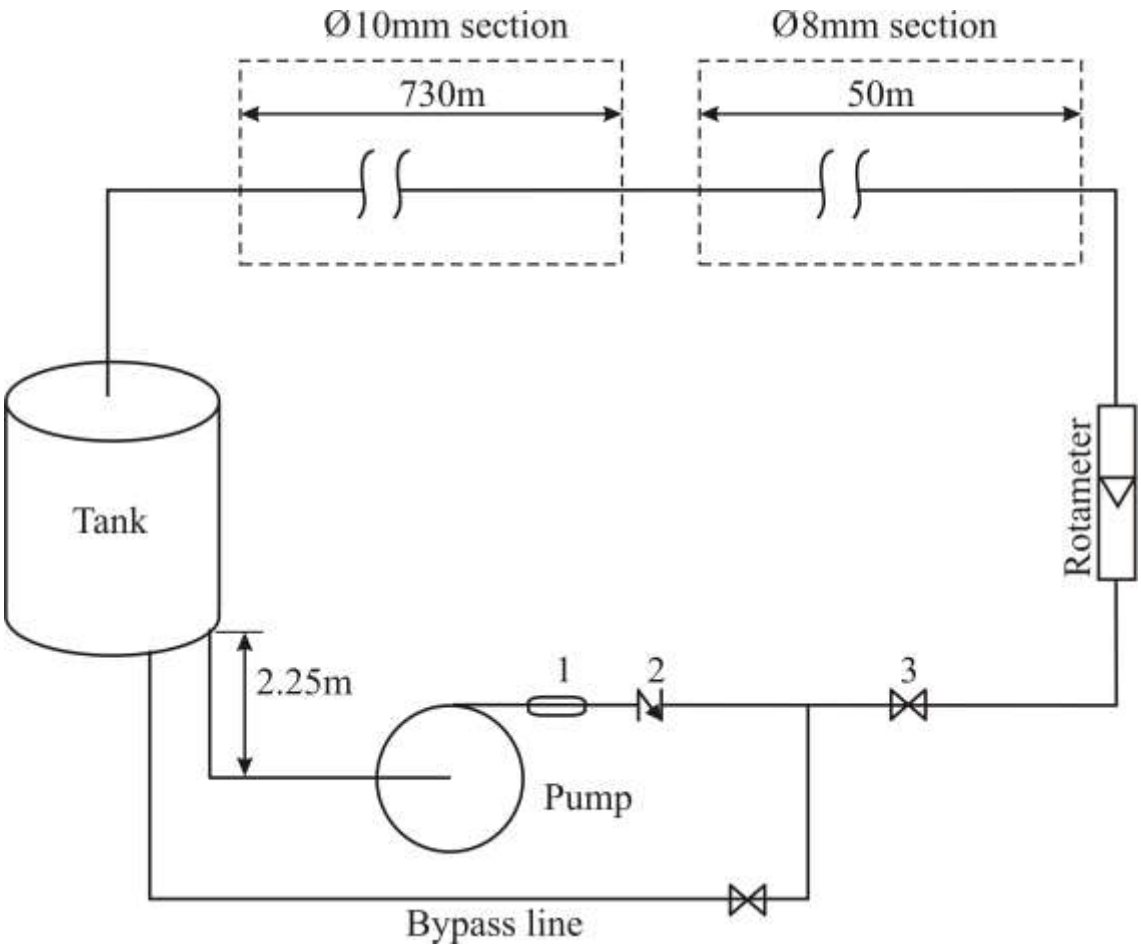

.

Item	PT1	PT2	L1	PT3	L2	L3	L4	L5	PT4	L6	L7	PT5
(m)	0	103	127.7	281	354	363	377	386	536	601	610	770

Figure 6-1: Schematic of the experimental rig and its components. (Number 1 anti-vibration hose, number 2 non-return valve and number 3 gate valve).

The pipeline material is copper. The boundary conditions were assumed as a fixed level reservoir of 30m and open to the atmosphere, at the upstream and downstream boundaries. The *Re* number of 6500 gives a flow rate of 0.0363 l/s (2.178 l/min). The numerical code models the rig as two pipelines. Firstly, the two pipes were assumed to have with the same diameter of 10mm and the computational results are shown in Figure 6-2.

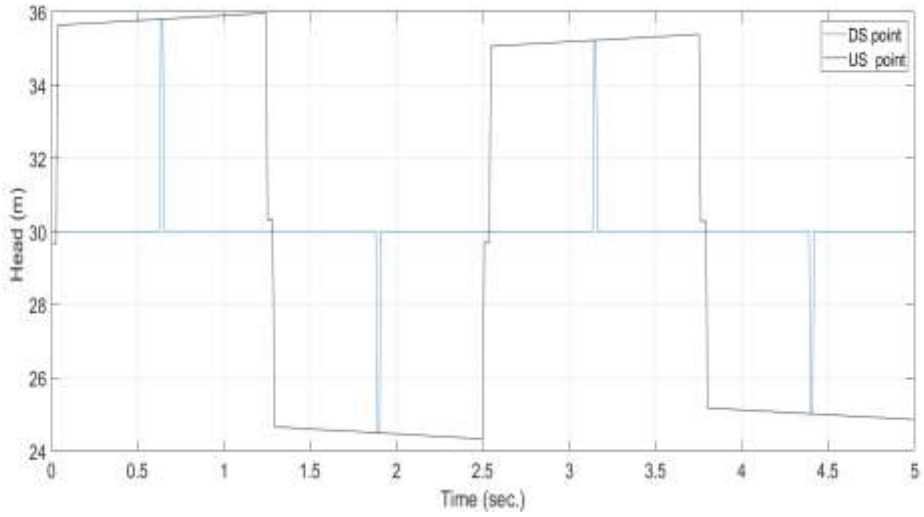

Figure 6-2: Computational Results for the rig with 30m head and open to atmosphere. (The two pipes were considered as being of 10mm diameter for the 50m and 750m lengths).

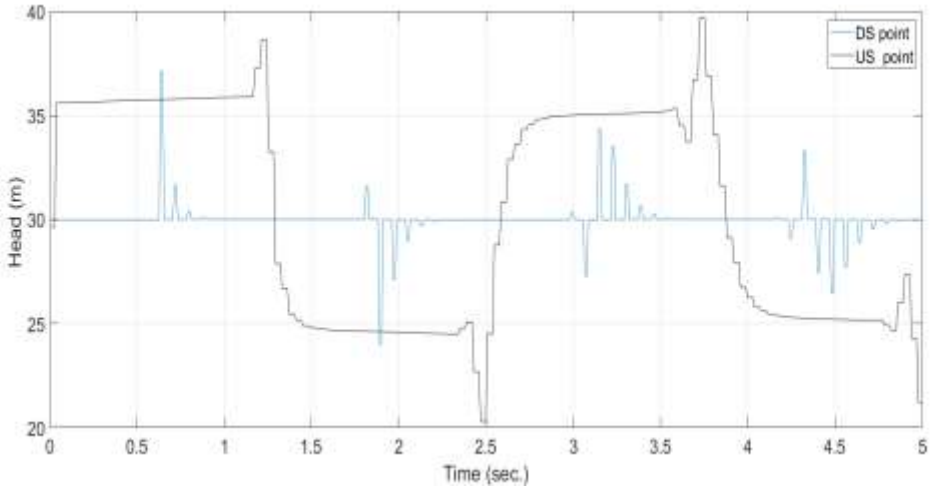

Figure 6-3: Computational predictions for experimental rig (8mm x 50m and 10mm x 750m) following valve closure at the downstream and measured at downstream the reservoir and upstream the valve.

Secondly, the corresponding computed pressure trace when allowance is made or the change in cross-section is shown in Figure 6-3, the change in the cross-sectional area effects are clear.

In addition (referring to Figure 6-2), dealing with the rig as two components of the same specifications do not affect the numerical code outputs. In other words, the numerical errors are negligible; the code outputs are no different whether the system is considered as one or two parts. This confirms the validity of the code and the trivial numerical calculation errors.

6.1 Experimental Rig Design

This section contains two parts: firstly, the calculations undertaken to design the rig to model the real field system are presented. These calculations enabled the scaled rig dimensions to be determined. Additional constraints included the relatively small space available in the laboratory, which mean that the rig had to be designed based on the space availability. Naturally, during and after the construction process the final system differed in some aspects from the original design. This was due to a variety of reasons, not only due to the congested space but also due to some unfortunate events including the damage to some coils during the building process. This meant that because the final construction differed slightly from the original design, the numerical calculations may need to be run again to reflect the actual rig configurations. The trials to recalculate the numerical coding encountered by some difficulties. The number of reaches was defined to meet the location of the connections. The three way compression connections held the pressure transducers or simulated the leak. The actual rig cannot be presented easily except if the reaches are made very short. Even so, the nodes cannot be fixed with the three way connections.

6.2 Rig Design Calculations

The rig is designed to mimic the real field system and allow validation of the leak location technique. It consists of two different cross-sectional area of copper pipe.

First, the 8 mm diameter section runs for 50 m length which is then connected to 10 mm diameter copper pipe with a length of 720m, giving some similarity to the field system, at the North Pier & Pumping Export Facility (NPP). Table 6-1 shows the two systems' parameters and some dimensionless ones which demonstrate the similarity between the systems. The rig length has been reduced by 30 m from the original design. The coils were 50 m long, 10mm diameter, and in total, there were 15 coils. The coils were connected together by straight fittings and three-way compression fittings were used to install the pressure instruments or simulate a leak. The Darcy-Weisback was used to estimate the required pump head. The rig variables presented in Table 6-1 are based on flows of 0.0363 and 0.0595 l/s, with corresponding need pressure heads of 30 and 90 m, respectively.

			NPP Export Facility			**Experimental Rig**	
L_1	**L_2**	**L_3(m)**	600	15000	400	50	720
D_1	**D_2**	**D_3(m)**	1.2192	1.4224	0.6096	0.008	0.01
c (m/s)			1051	1019	411	1298 1260	
L_1/L_2		**L_3/L_2(%)**	4		2.67	6.94	
D_1/D_2 D_3/D_2 (%)			86		42.9	80	
V_1	**V_2**	**V_3 (m/s)**	3.91	2.417	4.22 [a]	0.772[b]	0.462
c1/c2		**c3/c2**	1.03		0.4[c]	1.03	
Re_1	**Re_2**	**Re_3**	426,768	307,678	230,226	6500	4000
Joukowski Head (m)			418	251	177	96 147	60 92
R^d (coefficient Resistance)			0.3312	3.825	7.0696	20.28 12.98	
Eu			115.5			329.2	

[a]: Based on the nominal and measured volumetric rate which is 16840 m^3/s.

[b]: Based on flow rates of 0.0363 and 0.0559 litres per second, respectively.

[c]: Notice that the 3rd component is a flexible floating hose.

[d]: Dimensionless parameter is proposed by Liou [45], $R = \frac{fl}{2gDA}$.

Table 6-1: Comparison between the full-scale system and the experimental rig.

The required heads were obtained after considering the major losses deriving from the pipe friction which is proportional to the length, and the static head. Minor losses come from tank entry and the fittings. The friction loss is expressed by $h_f = \frac{flQ^2}{3.03d^5}$, where: f =friction factor from Moody diagram [108], l =length, and Q =flow rate. The other losses, for the straight fittings and the tank entrance, are obtained from $h_l = k\frac{u^2}{2g}$. The k is a factor equal to 0.44 and 0.2 for the tank entry and the straight fittings, respectively. The u and g are the velocity in m/s and gravitational acceleration in m^2/s. Instead of using the factors, some publications provide the fitting equivalent lengths [122].

For the range of flows investigated, the fitting head losses were small compared with the friction loss. The ratio was approximately 0.13% for most cases and it should be noted that the fitting losses include the 16-compression fitting and the tank entrance. Pipe friction was the major loss.

6.3 Rig Dimensions and System Configuration

In this section, rig dimensions relevant system features, such as pump and tank locations, will be described. The rig width is 3.2m, and its height is 2.5m; those dimensions ensure that the rig can contain the total length of 770 m in 98 loops of copper pipe of 10 mm and 8 mm diameters, with a nominal gap between the loops of 10 mm. This gap will be filled in some locations by pipe plastic clips of 10mm thickness (see Figure 6-4). A single loop is about 7.86 m in length. The system contains about 90 litres of water. In addition to the pipes and the frame, the rig consists of one tank, a pump, and the control/data acquisition system. The tank is fixed at the top of the rig and connected to the highest point of the pipe system. That is to ensure the air bubbles will be washed out and none will be trapped in the

system. This configuration is important to bleed any trapped air as any air bubbles will change the wave speed. For this reason, the pump was run at flow rates sufficient to expel trapped air.

Figure 6-5 shows a schematic of the main features of the pipe system. Points 1 to 5 indicate the position of the pressure transducers downstream of the pump from the first to the last pressure transducer. All the pressure transducer readings were monitored to check the system reaches a steady state without air entrainment.

Detecting small leaks by water hammer technique is easier if the measurement points are far away from the boundary conditions [43]. For that reason, most of the measurement points are located in the middle region of the rig.

The two bends in the pipeline on one side were inserted to create more length for each loop, and this also allowed the rig to be installed more easily in the laboratory. These bends saved about 0.5m in height compared to a rig built without them. It also allowed the pump to be fixed within the rig's footprint, allowing space for other workers to access different parts of the laboratory. Photographs of the experimental apparatus are presented in Figure 6-6.

The locations of the leaks and the pressure measurements are summarised in Table 6-2. The main aim of the research is to attempt to locate the position of a leak by analysing pressure traces from the rig.

Figure 6-4: Clips in column and some three-way connections.

Point	Location relative to pump down stream	Purpose	Position (% of total length)
PT1	0 m	Pressure transducer	0
PT2	103 m	Pressure transducer	13.3
PT3	281 m	Pressure transducer	36.5
PT4	536 m	Pressure transducer	69.6
PT5	770 m	Pressure Transducer	100
L1	127.7 m	Leak point	16.6
L2	354 m	Leak point	46
L3	363 m	Leak Point	47.1
L4	377 m	Leak Point	49
L5	386 m	Leak Point	50.1
L6	601 m	Leak Point	78
L7	610 m	Leak Point	79.2

Table 6-2: Pressure transducers and leak points locations.

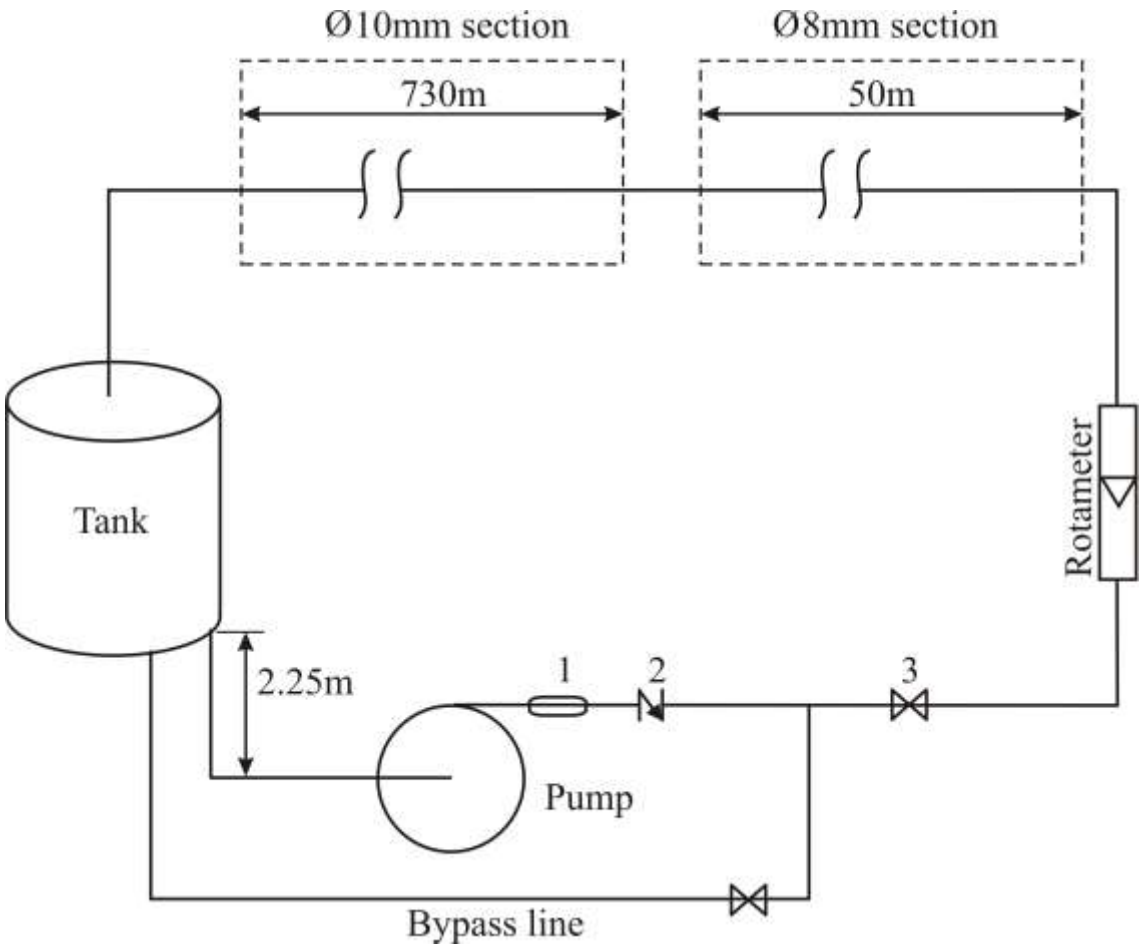

Item	PT1	PT2	L1	PT3	L2	L3	L4	L5	PT4	L6	L7	PT5
(m)	0	103	127.7	281	354	363	377	386	536	601	610	770

Figure 6-5: Schematic of the experimental rig and its components. (Number 1 anti-vibration hose, number 2 non-return valve and number 3 gate valve).

Initially, leak detection was undertaken by cross-correlation between points 1 and 5. In addition, a number of other pressure measurements were made to enable other analysis techniques to be employed. Moreover, additional monitoring points were added to collect more information about the system to make the analysis more reliable. All selected leak locations and pressure tapings were on the side of the rig opposite to the laboratory well to ensure flexibility when a leak node or pressure transducer was moved. This meant that the actual mounting points on the rig were different from those in the original design. The original points were selected so that the reflected waves from different cross-sectional areas, boundary conditions and

fittings would not overlap, so that the pressure traces relevant to each of these could be more easily identified.

Figure 6-6: Photographs of experimental apparatus in CID laboratory.

6.4 Commissioning the System

The first runs of the rig were carried out without leakage to ensure the functionality of every component. The runs started at a low flow rate to check for leaks at any point, ensure the pump was operating satisfactorily and expel any air bubbles before starting any tests. As mentioned earlier, any air bubbles in the system were identified through the rotameter. Figure 6-7 shows some air bubbles entrained for a specific flow rate.

Figure 6-7: Air bubbles at 13.8 cm flow rate (2 l/min).

Lessons that were learned during the construction and operational steps are presented at the end of this chapter.

The following subsections describe the steps undertaken to make the rig ready for experimentation.

6.4.1 Initial Runs

After ensuring that the rig was working without malfunction of any component, data were recorded from a number of initial runs. It was to be expected that the first experimental trails would encounter difficulties [126]. The rig was operated at a

number of different flow rates. Each time the pressure readings, pump duty point, flow rate input (LabVIEW), and the rotameter reading were recorded.

More than one hundred successful runs were conducted. These repeatable runs produced reference data sets for the pressure, pump operation and flow. Some difficulties due to air entrainment were encounted. Table 6-3 contains the rig parameters.

Flow (l/min.) %	**Transducer Pressure**					**Rotameter Reading (cm)**
	P1	**P2**	**P3**	**P4**	**P5**	
	(bar)					
(0.6) 28.3	1.09	0.9	0.56	0.3	0.11	2.2
(1) 37	1.72	1.33	1.001	0.515	0.11	5.3
(1.5) 50.3	3	2.29	1.71	0.85	0.11	9.6
(1.8) 58.3	3.99	3.01	2.23	1.09	0.11	12.2
(2) 63.6	4.71	3.55	2.62	1.28	0.11	13.8
(2.5) 77	6.81	5.11	3.76	1.8	0.09	17.6
(2.6) 79.9	7.29	5.46	4.02	1.92	0.09	18.3
(3) 90.3	9.34	6.99	5.14	2.44	0.1	21.3
(3.1) 93	9.88	7.39	5.44	2.58	0.1	21.8

Table 6-3: Different flow rate runs showing comparison between: LabVIEW flow rate input(Q (l/minute), pump percentage performance (%), and the rotameter readings (cm), and pressure transducers (P1,P2,P3,P4,P5).

6.4.2 Computation of the System Wave Speed

In this section four methods were used to obtain the wave speed for the system. For many reasons, researchers [13, 61] have recommended that the wave speed should be measured after completion of construction. First, the recorded pressure traces for the five transducers are compared and the differences in time for the pressure surges are calculated. Since the distances are known between the measurement locations, the velocity law $a = \Delta x/\Delta t$ is used. Second, the wave speed can be calculated by application of Joukowski law $\Delta H = c\Delta V/g$. The increment in the pressure head for each measurement point is obtained individually, and then the wave speed is calculated. The velocity for the first measurement point is different for the other four locations, since the pipe diameter is smaller for this section of the rig. The third method is similar to the first method; however, in this case a comparison of pressure traces for each of the five measurements locations is undertaken, enabling the wave speed to be computed using the velocity law above.

A fourth method has been trialled; however, the results are not clear, due to difficulties reading the pressure trace. This method depends on the time taken for the wave to travel from the trigger point to the measurement point. The length gives the time duration. The wave speed can then be computed by the formula $2(l - x)/\Delta t$, where x is the distance between the transducer and the water hammer trigger point (downstream valve in this case), and l is the total length of the rig.

Figure 6-8 illustrates all the readings for the 5K Hz test.

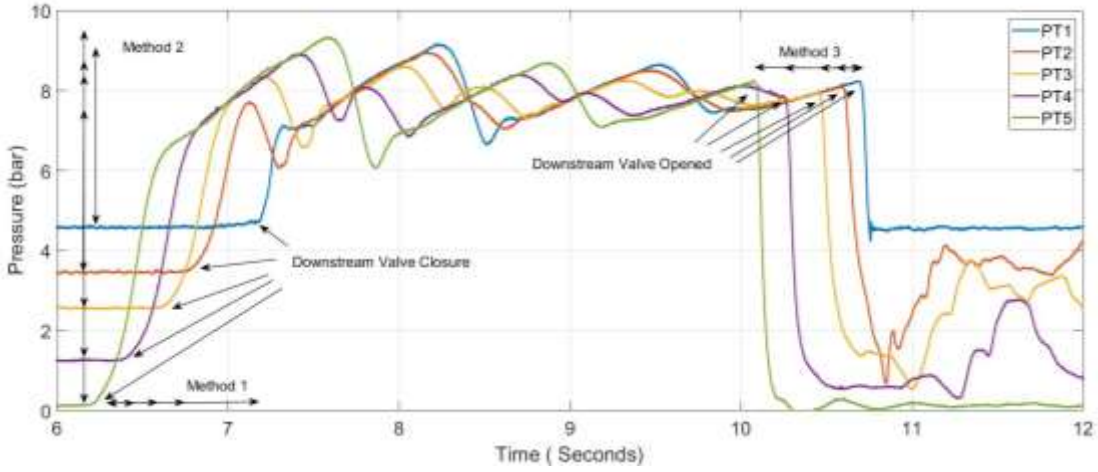

Figure 6-8: First pressure wave for the five recorded pressure transducer o measure the wave speed for the rig. The flow is Q=2l/min, (rotameter = 13.4cm). The data is filtered by 10 points moving average. The water hammer trigger was downstream valve closure then opened.

Table 6-4 presents the calculated wave speeds by the methods described above.

	***Q*=2l/min (13.4 cm)**			***Q* =1l/min. (5.4 cm)**		
Point	**Method 1 (m/s)**	**Method 2(m/s)**	**Method 3 (m/s)**	**Method 1 (m/s)**	**Method 2(m/s)**	**Method 3 (m/s)**
P5-P1	782		1256	644		1178
P5-P2	1098		1269	1082		1232
P5-P3	1358		1290	1060		1278
P5-P4	1031		1223	940		1153
P5		1318			1187	
P4		1224			1180	
P3		1225			950	
P2		1028			574	

Table 6-4: Calculations of the wave speeds (m/s) for a rate of 2 l/min and 1 l/min with a rapid closing for the downstream manual valve are calculated using different theoretical methods.

Examination of Table 6-4, shows measuring the wave speed between two transducers appears to yield wave speed values that accord reasonably closely with the theoretical values.

The theoretical wave speed is 1260 m/s and 1298 for the 10 mm and 8 mm pipes, respectively. The average wave speed for a flow of the 2 $l/minute$ using the negative wave procedure gives a wave speed of 1259.9 m/s for the pipelines as a whole.

6.4.3 Wave Speed from Negative Wave.

Based on the previous calculations, it is clear that the negative wave procedure yielded wave speeds that most closely mathematical the theoretical wave speed. Therefore, a test was undertaken on 6th of April, 2017 to pressurize the system up to approximately the maximum allowable pressure (10 *bars*), then close the downstream valve gradually until fully shut and ensure that all pressure points reached the maximum pressure. Then, the valve was rapidly opened and the readings recorded. Practically, it is difficult to pressurize the pipe system to 10 bars, since the lower (first) pressure transducer is already pressurized to near this figure. For safety reasons and to avoid undesirable consequences, this process has been terminated.

6.4.4 Checking the Rotameter Reading using the Empirical Wave Speed & Pump Characteristics Curves

Two methods were applied to check the rotameter readings. First, after obtaining the wave speed, the two flow rates were compared with the steady state velocity calculated using the measured Joukowski head. The calculations were applied to the fifth pressure transducer. From the charts ΔH was obtained, and then from Joukowski's law, the changes in velocity, Δv were obtained for the both the 1 and 2 litre per minute flow. The calculated flow rate were 1.07 *l/minutes* and 2.06 *l/minutes* for the flow rate of 1 and 2 *l/minutes*, respectively. It means the percentage differences were 7% and 3.2 %.

The other method of checking the accuracy of the rotameter involved comparing the pump chart and the first pressure transducer (close to the pump discharge). However, this required taking into the account the distance between the transducer and the pump discharge which is about 1.3m, the existence of anti-vibration hose, non-return valve, and the three-way connection, all of which cause pressure losses.

In other words, the pump discharge point should be more than the first pressure transducer which is coincided with the two figures.

6.4.5 Leak Simulation Runs

The following experiments were undertaken: 39 for various sizes of leak on different circumferences of the leak cases, and six for water hammer without a leak, making a total of 45 experiments undertaken. Leak size/no leak, leak location, and the water hammer trigger events were varied. The steady state flow rate for all cases was 0.6 l/min ($Re = 1612$). Water hammer was triggered for each case at the downstream end of the pipe, by closing the manual ball valve; or from the upstream end, by raising the pump flow rate from 0.6 l/min. to either 1.2 l/min. ($Re = 3226$), or 1.8 l/min. ($Re = 4838$). These experiments were conducted on 20th and 21st of July, 2017.

Leak size 10 mm

Leak position From downstream the pump	**Q_L ml/sec. # of runs**	**Water Hammer Trigger**	**Remarks**
L1 (127.7m)	29.3 2	1) Pump rises up from 0.6 to 1.2 l/minute. 2) Pump rises up from 0.6 to 1.8 l/minute. 3) Downstream valve closure.	Q_L=1.76 l/min.
L3 (363m)	25.05		Q_L=1.5 l/min.
L5 (386m)	19.32 2		Q_L=1.16 l/min.
L7 (610 m)	14.56 2		Q_L=0.87 l/min.

Leak size 6 mm

Leak position	**Q_L** **ml/sec.** **# of runs**	**Water Hammer Trigger**	**Remarks**
L1 (127.7m)	30.63	1) Pump rises up from 0.6 to 1.2 l/minute. 2) Pump rises up from 0.6 to 1.8 l/minute. 3) Downstream valve closure.	Q_L=1.84 l/min.
L3 (363m)	21.65 2		Q_L=1.3 l/min.
L5 (386m)	19.61		Q_L=1.17 l/min.
L7 (610 m)	Not Done		The 6mm fittings, does not fixed

Leak size 4 mm

Leak position	**Q_L** **ml/sec.** **# of runs**	**Water Hammer Trigger**	**Remarks**
L1 (127.7m)	20.77 2	1) Pump rises up from 0.6 to 1.2 l/minute. 2) Pump rises up from 0.6 to 1.8 l/minute. 3) Downstream valve closure.	Q_L=1.25 l/min.
L3 (363m)	16.67 2		Q_L=1 l/min. 1kHz & 5kHz
L5 (386m)	17.09		Q_L=1 l/min.
L7 (610 m)	13.3 2		Q_L=0.8 l/min. 1kHz & 5kHz

Leak size 1 mm

Leak position	**Q_L** **ml/sec.** **# of runs**	**Water Hammer Trigger**	**Remarks**

L1 (127.7m)	7.96	1) Pump rises up from 0.6 to 1.2 l/minute.	Q_L=0.47 l/min.
L3 (363m)	6.63		Q_L=0.398 l/min.
L5 (386m)	6.25		Q_L=0.375 l/min.

Table 6-5: Summary of experimental investigations undertaken on laboratory rig.

In addition, three pressure surge tests were recorded without a leak for three water hammer cases at frequency rates of 10 Hz and 5 kHz.

With respect to the experimental investigations, two points should be noted: first, on the experimental runs, the leak points number 2 & 4 were avoided since they were close to the pump. This could have caused the pump to be damaged, even though a shelter had been constructed above the pump. However, if needed, some additional gears will be used to avoid any spills arriving at the pump.

For leak connections numbers 1 and 3, with large leak diameter (10 mm), all the flow discharged through the leak resulting in the rig being drained of water (which was noted in the rotameter).

6.5 Challenges in Constructing and Operating the Rig

Many challenges were encountered during the design, construction and operation of this rig. Some of the challenges were expected, such as leakage from the compression fittings joints when the pipes were filled with water and later when running the pump. Others, however, were unexpected, such as forgetting the plastic covers for the discharge and suction holes of the pump. In this section, lessons learned, and pitfalls to be avoided will be highlighted for the benefit of future research as far as possible in similar future works. The key points are listed below:

1. As mentioned previously, leaks from different points along the rig were expected. However, some aspects need to be highlighted. Most of the leaks

were from the compression fittings, the difficulty arising when the connection was on the wall side, where it is hard to reach. Fortunately, since the first loop has enough clearance from the ground the technician was able go inside the rig and tighten these joints. Had this space not existed the problem would have been difficult to resolve. Hence, accessibility to all rig components should be ensured for during the rig design.

2. The pressure transducer pipe extensions were welded to a cylindrical pipe. However, when the transducer was tightened with spanners, the cylinders rotated. As a solution, flats on the cylindrical joints were machined in the mechanical workshop. This modification allowed tightening and loosening of the transducers from the connection cylinder to be achieved with less effort, as shown in Figure 6-9.

Figure 6-9: Grooved cylinder of pressure transducer extension.

3. Air bubbles caused noise during data acquisition and altered the dynamics of the system away from the design criteria. To remove the air, the pump was

run at as high a speed as possible to move the air down the pipe and out of the system. Care should also be taken in other situations where air will alter the system outputs. The pressure transducers have a small fitting opening to allow the water to enter for the pressure transducer reading. These openings could trap air bubbles and these can be difficult to eliminate. Therefore, when filling the pipes with water, the pressure transducer's fitting is filled with water carefully to keep the water in. Then, when the water level in the pipes reaches the pressure transducer's connection point, the pressure transducer is tightened to ensure no air enters the pipe. This filling approach minimises air entrainment much as possible. Unfortunately, it needs to be done every time that water is drained from the rig. Rotating the pressure transducers so they point downwards, can reduce the like hood air entrainment.

4. The available end cap had hole sizes of 4 mm, 6 mm, 8 mm and 10 mm in diameter, which were large in comparison to the pipe diameters. When this cap was installed, and due to the high pressure of the pump, the water was able to leak at high flow rate compared to the pump flow. Later, the workshop was requested to modify the end cap to make the hole as small as possible. The available size is now 1 mm which is 10% of the diameter of the second pipe and 12.5% of the first one. This is still quite large, especially since the rig is a high pressure system. It is important to obtain a smaller leak size for use in leak detection techniques.

5. Delays in the completion of the rig, either in terms of hardware such as physical infrastructure or in the software such as the data acquisition/control code, can sometimes are happened dependently.

   For instance, fitting the additional connections for the water treatment process delayed the installing and initial testing of the LabVIEW. Sometimes work was being undertaken on the pump which impacted with the development of the data acquisition and control system.

It should be noted that the changes to the mechanical configuration of the rig were based on the safety regulations for working with copper pipe. Thus, the work involved a chain of related tasks which consumed extra time and effort. In conclusion, the time delay in the construction of the new experimental rig was not anticipated. Therefore, consideration should be given to allocating more time than was provided in this case.

Chapter 7 Signal Analysis and Results

The aim of this research was to develop a technique for detecting leaks in long pipelines with turbulent flow based on water hammer principles. The water hammer could be caused, for example, by a sudden closing of a valve. In many network systems, such as the export oil system considered in this study, sudden valve closing is generally to be avoided and is only used for emergencies. Therefore, this research investigates water hammer caused by a normal operation, such as pump start-up. Despite not generating as sharp a wave compared with the rapid valve closure, pump start-up is useful for developing a tool for leak detection offering a cheap and simple method of leak detection in many pumped networks.

A numerical analysis of both the test facility, and the real field system was undertaken. Real data were obtained from both the scaled experimental set-up and the export facilities. The signal analysis, as has previously been explained, was undertaken using the cross-correlation technique and its second derivative. The results of the numerical analysis of the experimental apparatus were encouraging, whereas when the technique was applied in the laboratory, the same outcomes were not achieved, as will be presented below.

In terms of the real data the low frequency of the measurements made the technique unsuitable. The technique, is dependent on the wave speed and to detect leaks with reasonable certainty there needs to be sufficient frequency of data capture. Although the researcher's colleagues in Kuwait made every effort to increase the accuracy of the recording time they were unable to increase the sampling frequency, and the measured data was not at sufficiently small time increments. The details of this work have already been explained in section D.1.

In summary, the research described in this chapter was developed on an incremental basis. First, numerical analysis was undertaken for both the rig and the export facilities. Then, the measured data was obtained for different test runs. The

tests in the laboratory take up the largest section because many different configurations were evaluated using signal analysis.

This research, like many previous studies, focuses on the first pressure wave [36, 38, 95]. The first pressure wave is particularly important as it contains more information than the later waves.

7.1 Leak Detection Analysis in Long Pipeline Apparatus

The study was conducted in the long pipeline rig in the CID laboratory in the Civil Engineering Department, University of Sheffield. This section is divided into two parts: (a) the numerical analysis conducted prior to building the rig, and (b) the analysis of the experimental data.

7.1.1 Numerical Analysis.

Following the numerical code validation, it was applied at the experimental rig. In this section, the mathematical analysis of the selected experimental investigations is described.

7.1.1.1 Modelling the Pump Start up with/without Leak

Uncertainties in inputs for full-scale or laboratory-scale systems are inevitable [16], so using simple expressions can be useful. In order to analyse the pump start up using a cross-correlation second derivative technique, the pump start-up was simulated by the following equation (instead of fixed reservoir head, 20m):

$$HR = 2 + \frac{t}{Full\ Load\ Time} 10 \qquad (7\text{-}1)$$

Where HR is the upstream head in metres and t is the time in seconds. Allowing for the pump performance curve, it was assumed, as shown in the equation, that the relationship is linear. It was also assumed that the system pressurized at a 2 m head and the pump would raise the pressure up to a 12 m head pressure. The full load

time was estimated at 0.05, 1 and 5 seconds. Simplification of the boundary conditions can be implemented with reasonable results [12]. In all cases the results were recorded to verify any differences in the outputs. The downstream boundary condition was assumed to be open to the atmosphere (head = $0m$). After several numerical attempts, the time step was 9.902×10^{-4} $seconds$ was selected, while the spatial distance is 1.25 m. Two leak locations were tested at the 100 m and 380 m nodes. The pressure measurements were recorded at upstream and downstream locations, 1.25 m (node 2) and 798.75 m (node 63), respectively. Figure 7-1 shows A schematic for the experimental rig with the measurements and leak points.

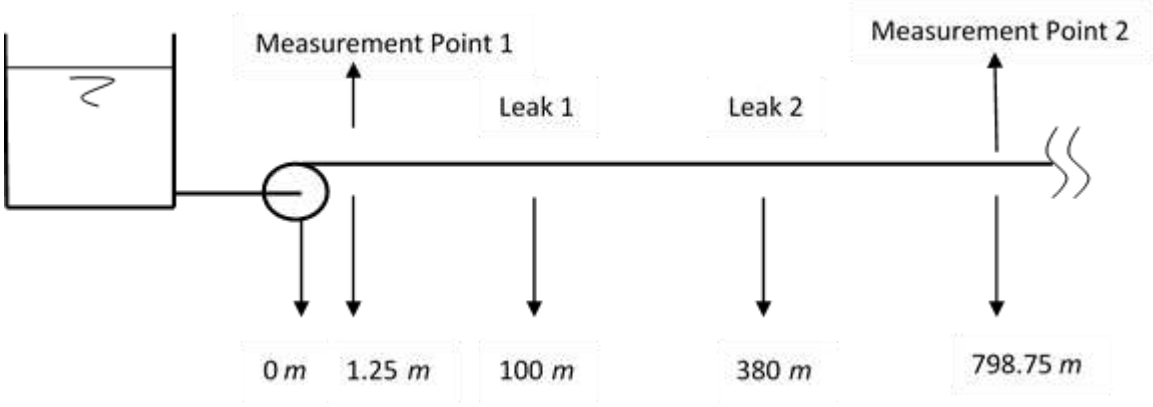

Figure 7-1: Experimental Rig Schematic for the numerical test of 100m and 380m leak points.

It was observed that there were differences between the second cross-correlation results: with/without leaks, for different start-up times, and different leakage rates at 100 m and 380 m leaks. Differences were observed on the calculated traces both downstream of the pump and upstream the pipe end. The leak flow rate was assumed to be 5% of the steady state flow. A comparison of the second derivative of the cross-correlation for the 0.5 second pump start-up between no leak and leak at 100m downstream the pump, is shown in Figure 7-2. The blue line is for the no leak case, while the red line for a leakage at 100 m. The peaks indicated by the circle show the cross-correlation second derivative response in case of a leakage, while

the blue line does not show any peaks on the same time. The peaks of the second cross-correlation derivative are given in Table 7-1

From the tables, it can be seen that the results are as expected. In the two tables the difference between no leak and leak are very clear in peak numbers from 2-5. The time step is small enough to regard the errors as trivial.

It was also observed that, even though the start-up time (5 *seconds*) was much longer that the characteristic time of the system (1.26 *seconds*), it could show similar singularities.

Startup Pump time		**0.5s**	**0.05 s**	**0.5 s**	**1s**	**5s**
Leak (%)	**Numerical pressure wave reflection Distances (m)**	**0%**	**5%**	**5%**	**5%**	**5%**
Time (sec.)		**Arbitrary Amplitude**	**Arbitrary Amplitude**	**Arbitrary Amplitude**	**Arbitrary Amplitude**	**Arbitrary Amplitude**
0.03968	50	6.483 x10^5	6.22 x10^7	5.778 x10^7	5.744 x10^7	5.352 x10^7
0.08036	101	None	-2.131 x10^6	-1.877 x10^6	-2.021 x10^6	-2.007 x10^6
0.08234	104	None	2.131 x10^6	2.444 x10^6	2.304 x10^6	2.04 x10^6
0.1587	200	None	-1.73 x10^6	-1.364 x10^6	-1.502 x10^6	-1.518 x10^6
0.1607	202	None	1.67 x10^6	1.924 x10^6	1.782 x10^6	1.549 x10^6
0.6369	825	-1.358 x10^7	-1.303 x10^7	-1.339 x10^7	-1.336 x10^7	-1.272 x10^7
0.6389	850	1.358 x10^7	1.303 x10^7	1.339 x10^7	1.365 x10^7	1.274 x10^7
3.735	4750	-3.382 x10^6	-3.539 x10^6	-3.288 x10^6	-3.487 x10^6	-3.558 x10^6
4.37	5550.3	-1.717 x10^7	-1.67 x10^7	-1.67 x10^7	-1.653 x10^7	-1.634 x10^7
5.002	6325	-2.326 X 10^8	-2.326 x10^8	-2.326 x10^8	-2.326 x10^8	-2.179 x10^8

Table 7-1: Different start-up outputs, with the pressure readings are at upstream and downstream points and leak is on 100m from upstream.

Startup Pump time		0.5s	0.05 s	0.5 s	1s	5s
Leak (%)	**Numerical pressure wave reflection Distances (m)**	**0%**	**5%**	**5%**	**5%**	**5%**
Time (sec.)		**Arbitrary Amplitude**	**Arbitrary Amplitude**	**Arbitrary Amplitude**	**Arbitrary Amplitude**	**Arbitrary Amplitude**
0.03968	50	5.779×10^{5}	6.191×10^{7}	5.742×10^{7}	5.717×10^{7}	5.324×10^{7}
0.3026	381	None	-2.073×10^{6}	-1.84×10^{6}	-1.99×10^{6}	-1.982×10^{6}
0.3046	384	None	2.074×10^{6}	2.404×10^{6}	2.272×10^{6}	2.013×10^{6}
0.6032	760	None	-1.637×10^{6}	-1.57×10^{6}	-1.443×10^{6}	-1.478×10^{6}
0.6052	762.5	None	1.58×10^{6}	1.564×10^{6}	1.722×10^{6}	1.506×10^{6}
0.6369	825	-1.358×10^{7}	-1.293×10^{7}	-1.318×10^{7}	-1.321×10^{7}	-1.261×10^{7}
0.6389	850	1.358×10^{7}	1.293×10^{7}	1.317×10^{7}	1.349×10^{7}	1.264×10^{7}
3.735	4750	-3.382×10^{6}	-3.542×10^{6}	-3.254×10^{6}	-3.459×10^{6}	-3.541×10^{6}
4.37	5550.3	-1.717×10^{7}	-2.113×10^{7}	-1.669×10^{7}	-1.65×10^{7}	-1.632×10^{7}
5.002	6325	$-2.326 \text{ X } 10^{8}$	-2.262×10^{8}	-2.312×10^{8}	-2.315×10^{8}	-2.168×10^{8}

Table 7-2: Different Start-up outputs, with the pressure readings are at upstream and downstream points and leak is on 380m from upstream.

In Figure 7-2, some results of the second derivative cross-correlation are shown.

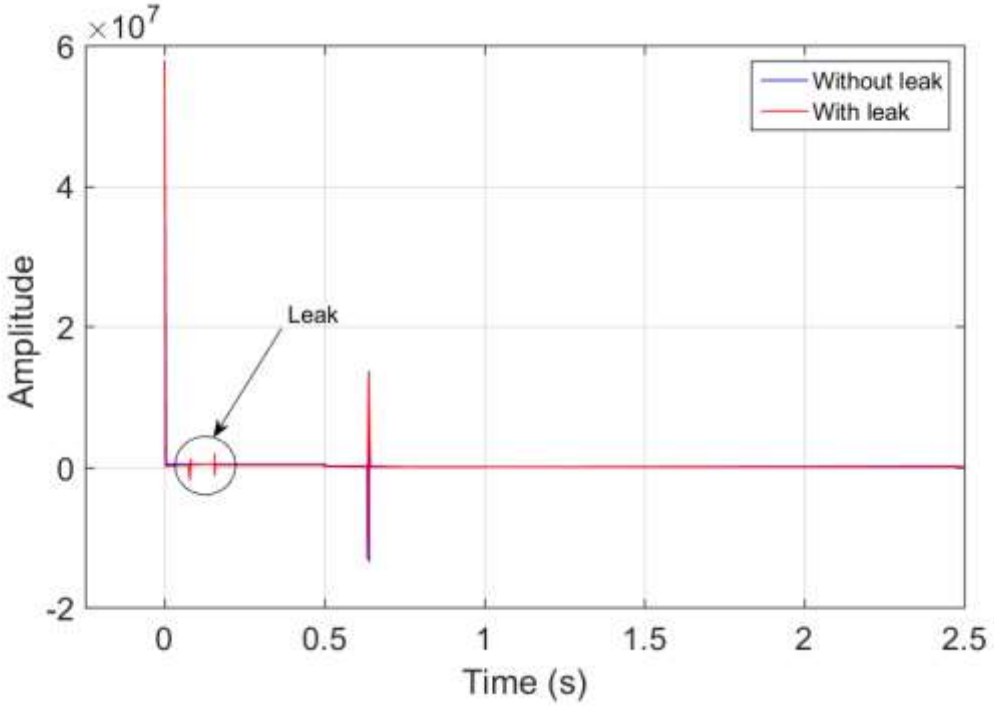

Figure 7-2: Second derivative for numerical pump start-up time of 0.5 seconds, without (blue line) and with leak at 100m (red line).

After these trials, it was concluded that a pump start-up wave could be used to detect leakage. These findings suggest that this type of water hammer event can be used at the laboratory and field scale.

7.2 Analysis of the Computational Output for the Experimental Rig, as Constructed

As previously explained in chapter six, the final experimental rig was a modification of the original design. Thus, the numerical modelling was undertaken on the as constructed rig. The original pipe length was 800m. Therefore, the model rig was computational divided into either 64 or 640 segments, with a resulting spatial discretion of 12.5 *m* or 1.25 *m*, respectively. The leak points were located on the node positions.

However, the length of the actual laboratory pipeline was reduced to 770 *m*. The locations of the measurement points or leaks (3-way compressions fittings) were

correspondingly altered. The number of nodes for the modified length were kept as close as possible to the number in the original pipeline configuration, i.e. 700 node with a spacing of 1.1m. Table 7-3 compares the numerical spacing with the actual spacing.

	PT1	PT2	L1	PT3	L2	L3	L4	L5	PT4	L6	L7	PT5
Distance along pipe (actual rig) (m)	0	103	127.7	281	354	363	377	386	536	601	610	770
Distance along pipe (numerical model)	0	103.4	127.6	280.5	354.2	363	377.3	386.1	535.7	600.6	610.5	770
Node No.	0	94	166	255	322	330	343	351	487	546	555	700

Table 7-3: Leak and transducers locations for the numerical model & experimental rig.

The signal analysis described in a former section is repeated in the following sections, taking into account the slight differences between the experimental rig and the numerical model illustrated in Table 7-3.

7.3 Experimental Rig Analysis

The experimental plan was to start with the analysis of large leaks and then to reduce the size of leaks until the smallest possible leak detection level was reached. The first leak was 10 mm in diameter. This size would be considered as a rupture or a physical junction, rather than a leak, especially since the system has a diameter of

only 8 mm. However, even when the diameter of the leaks was reduced, the rig was drained downstream of the leak points on many occasions. That was due to the network characteristics such as the pressure, pipe length, small pipe diameter and high friction losses. The rig was tested in many configurations by changing parameters such as: the leak location, leak size, and water hammer event (valve closure or altering the pump rate). Since the numerical results for the pump rising up were encouraging, it was decided to increase the flow from 0.6 up to 1.2 $l/minute$ which would more closely reflect the flows in the real system. Valve closure as a trigger for a transient event was also examined. Leak size and location of leaks were the variables examined. The leak size was reduced from 10 mm to 4 mm, but the leak flow rate was still almost above the input flow rate. However, later, the technician managed to drill a hole of $1mm$ diameter in the end cap joint which was the smallest used in this study.

While the results of all leaks sizes will be presented, attention will be focused on the $1mm$ leak at a variety of different locations.

Initially, transients were induced in the pipe without any leakage and this was benchmark for the leakage experiments. The experiments were undertaken for three water hammer triggers:

1. downstream valve closure,
2. as increase in the pump flow rate from 0.6 to $1.2l/minute$, and
3. as increase in the pump flow rate from 0.6 to 1.8 $l/minute$.

The steady state flow in all cases was 0.6 $l/minutes$. Figure 7-3 shows the results for those tests. Video clips were captured of the flow rate changed from 0.6 to 1.2 $l/minute$, that is the pump performance increasing from 28.3% up to 42.3 %. The time for the pressure surge was recorded with a stop watch and was approximately 0.55 $seconds$.

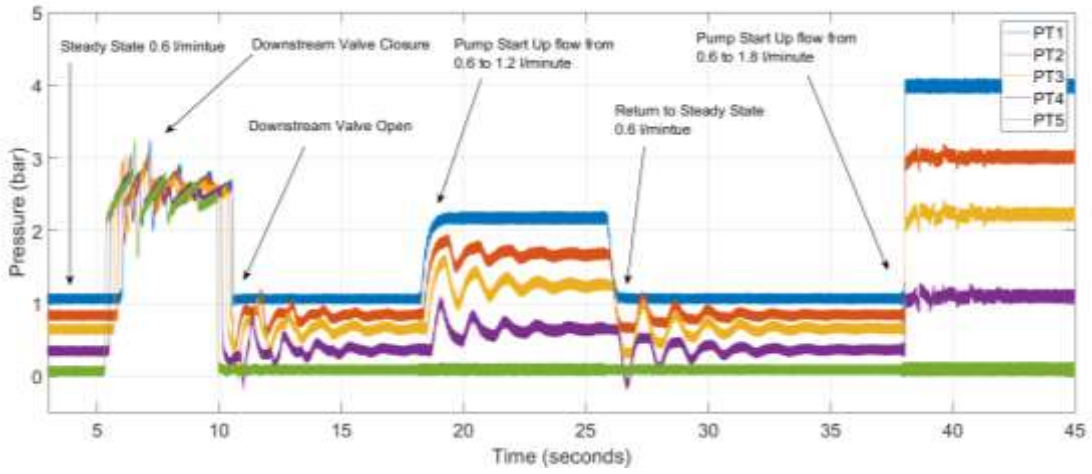

Figure 7-3: Recorded pressure trace for three water hammer triggers for the steady state flow of 0.6 $l/minute$. Downstream valve closure, increasing the flow rate from 0.6 l/min. to 1.2 l/min. and to 1.8l/min.

The details of the experiments on the water hammer event are listed in the following Table 7-4.

Leak Size (mm)	**Leak position (m) (distance from upstream boundary)**	**Leak flow Q_l $(\frac{ml}{s})(\frac{l}{min.})$**
10	L1 (127.7)	29.3 (1.758)
	L3 (363)	25.05 (1.503)
	L5 (386)	19.32 (1.1592)
	L7 (610)	14.56 (0.8736)
6	L1	30.63 (1.8378)
	L3	21.65 (1.299)
	L5	19.61 (1.1766)
4	L1	20.77 (1.2462)
	L3	16.67 (1.0002)
	L5	17.09 (1.0254)
	L7	13.3 (0.798)

1	L1	7.833 (0.47)
	L3	6.833 (0.41)
	L5	4.67 (0.28)

Table 7-4: Measured pressure transients experiments for pump start –up from steady state of 0.6 l/min. to 1.2l/min.

From the above table it is clear that for most of the leak sizes the leak flow exceeded the steady state flow rate of 0.6 litre per minute, regardless of the leak's location. To be more precise, the leak could be considered as a branch or rupture in the network rather than a leak. The reliability of any leak detection system is dependent on how small a leak is that can be detected.

In the next section, pressure transients for different leak sizes will be considered. The leak was located at L5 (386 m) for all of these tests. Figure 7-4 shows the pressure rise due to an increase in flow rate from 0.6 to 1.2 $l/minute$. Each of the four plots represents a different leak size. Each plot includes the five pressure transducers readings. The data is raw, as no filtering process has been applied and the sampling frequency is 5 kHz. Leak point 5 was located at 386 m, which means that this point is downstream of the pressure transducer 3 by 23 m, and upstream of transducer 4 by 20 m. Since these two points were closest to the leak location, the greatest effect will be seen on these two transducers for the transient or reflection waves. When tracking $P4$ through the plots, it could be seen that its value fluctuated and reached a negative value for both the 10 and $6mm$ leak. Clearly, the steady pressure value increased as the leak size decreased. Since pressure transducer $P5$ was close to a point on the rig at the atmospheric pressure, there was no noticeable change in pressure for any of the leak cases investigated.

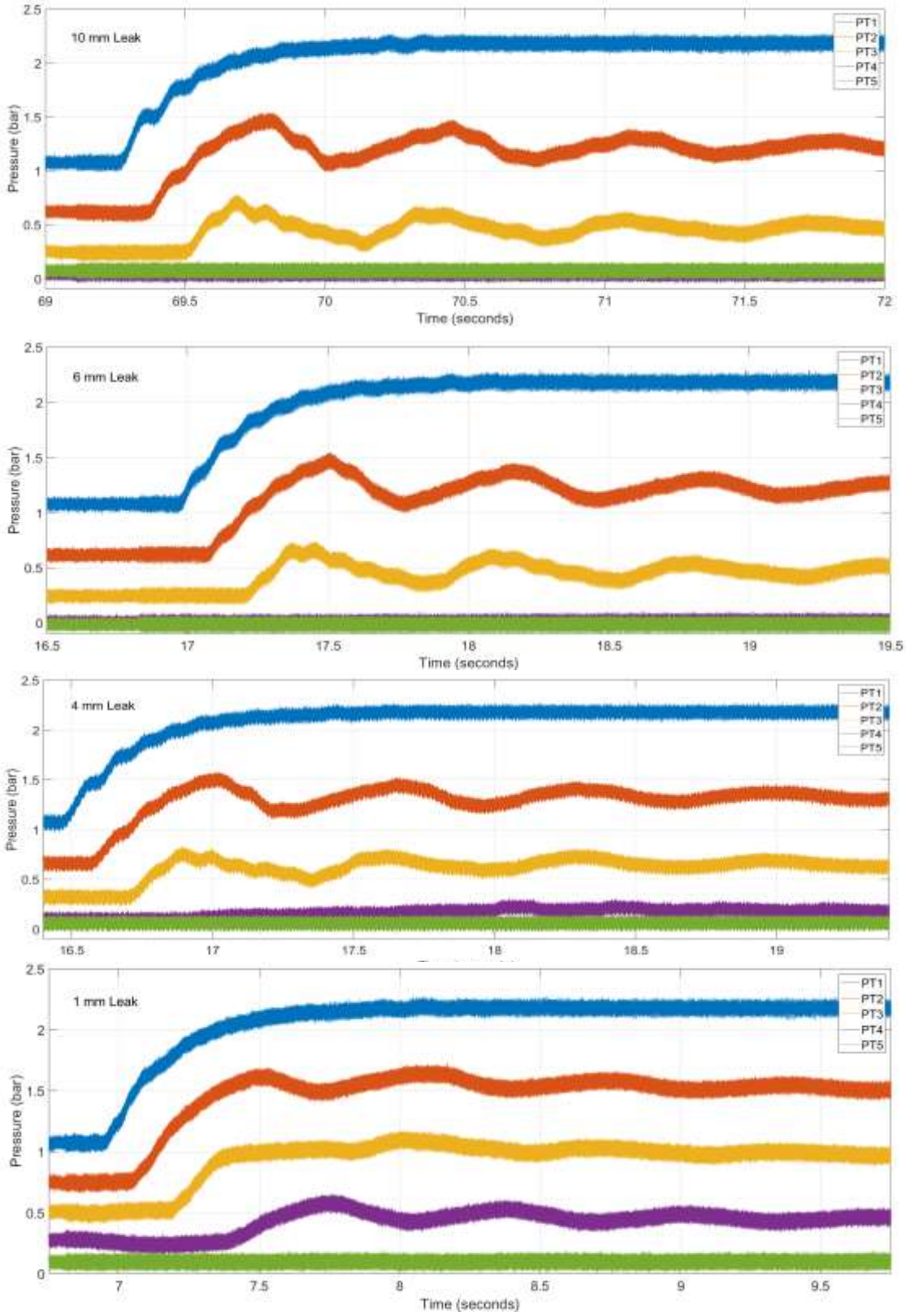

Figure 7-4: Measured pressure transients for pump rise from 0.6 to 1.2 l/minute, for leak location no. 5 (L5) with 10, 6, 4,1mm leak size.

Examination of Figure 7-4 shows that the pressure transients for all four leak cases examined were similar. In the case of transducer 4, the pressure for the 6 mm hole was slightly larger than for the 10 mm hole. For the 10 mm size hole, the pressure at point 4 was less than the pressure at point 5. Transducer $P1$ shows the reflection wave effect for the three largest leaks. Despite the measuring point being close to the pump, the leaks were sufficiently large to send reflection waves back down the pipe. As the leak size was reduced, the curve became more stable and smoother and the effect of the reflections disappeared.

For the second and third transducers, the effect of the large leak reduced the periodic wave time in both cases. So, the oscillations due to water hammer are at almost twice the frequency of wave without leak.

To identify the system features, especially leaks, many trials were undertaken at the $L5$ position, starting with large leaks and then decreasing to smaller sizes. Also a number of different filtering approaches were used, and attempts made to mimic the water hammer signal, to enhance the cross-correlation technique and consequently its second derivatives. Later sections will concentrate on the 1 mm Leak at position $L3$.

7.4 Cross-correlation and its derivative analysis

Cross-correlation and its derivatives have been widely used to find the time delay in interrelated signals. This method allows the cross-correlation functions to be used to find more than merely the delay or offset between signals. As reported in the literature review (Chapter 2), it can be used for leak detection in fluid systems. In this research the same approach will be used to detect leaks or find system features. The main advantage of using cross-correlations is in finding the offset in time between two signals. In this work, the raw data have been filtered with a low-pass filter and the moving average. The parameters for each filter have been changed many times refining the data to ensure suitability for cross-correlation. For instance, the analysis was based on a wide range of moving average points range, such as 50 or 200 points. Also, for the low-pass filter, the filter order and the cut-off have been altered on many occasions to assess the outputs. It was found the low-pass filter of

order 32 and cut-off frequency of 500 *Hz* are suitable parameters, since these parameters can retain more features of the raw data. Also, in the cross-correlation analysis of the foregoing parameters, these parameters provide more details and are assumed to be smooth relative to the other parameter' outputs. Some results for trials with different low-pass parameters will be presented. The water hammer traces are recorded at high frequency, enabling the moving average filter to smooth the raw data in such a way that some of the noise is eliminated.

Some examples of the cross-correlation and its derivatives, along with some comments about the findings are presented below.

7.4.1 Downstream valve closure measured data

The measured transient pressures following sudden downstream valve closure, measurement by transducers P2 & P3, is presented in this section. First, the filtered data are shown in Figure 7-5. The next figure, Figure 7-6, shows the cross-correlations for the two pressure transducers at the frequencies of 500Hz & 750Hz. The offset between the peak and the midpoint is of the same order of magnitude as the filter order, 32. This means that the cross-correlation relationship does not identify the delay in signals as was anticipated from the modelling. So it is that the second derivative cannot be relied on to identify the leak detection or other system features in this research setting that is shown in Figure 7-7, in the lower graph. No specific frequency can be observed and the delay is again the filter order.

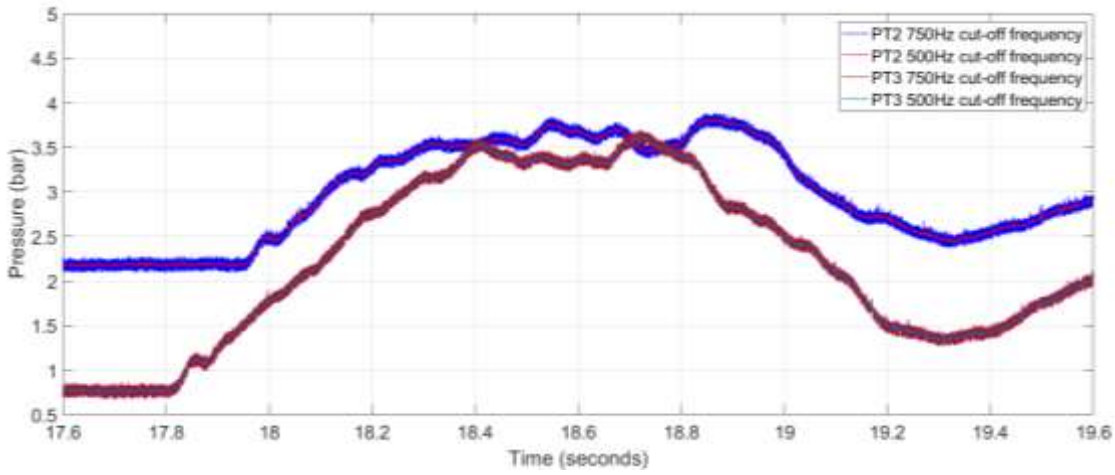

Figure 7-5: The filtered data for P2 and P3 with cut-off frequencies of 500Hz and 750Hz.

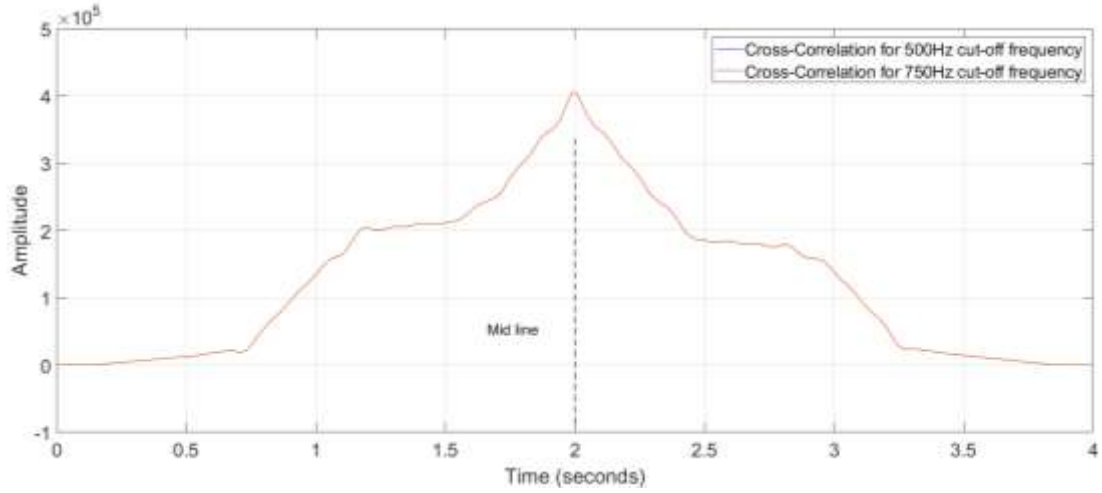

Figure 7-6: The cross-correlation between the P2-P3 for the different frequencies (500, 750).

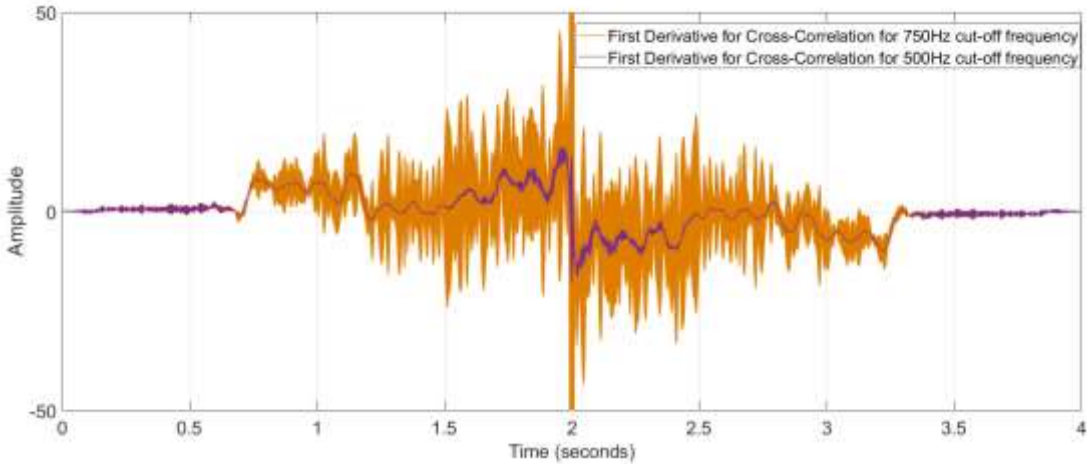

(a) First Derivative of cross-correlation between Measured PT2 and PT3.

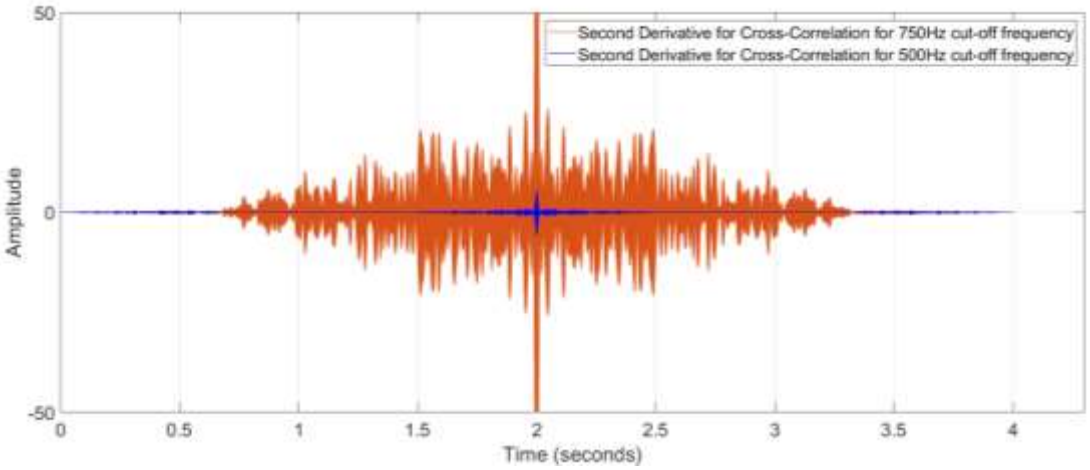

(b) Second Derivative of cross-correlation between Measured PT2 and PT3.

Figure 7-7: First and second derivatives of the cross-correlation between P2-P3 (500Hz,750Hz cut-off frequencies).

A number of trials were performed to find the delay, three time windows were selected, from steady state to the trigger of the transient, to at least find the signal delay initially. Concentrating on the steady state and the changes in pressure traces at the beginning of the water hammer event, the obvious delay event occurs between the signals. Therefore, the analysis depended on making important for the specific window. The time offset between the signals is the thresholds step for the leak detection approach. Unfortunately, these trials were not useful. The time windows in all the selected cases were chosen to be less than

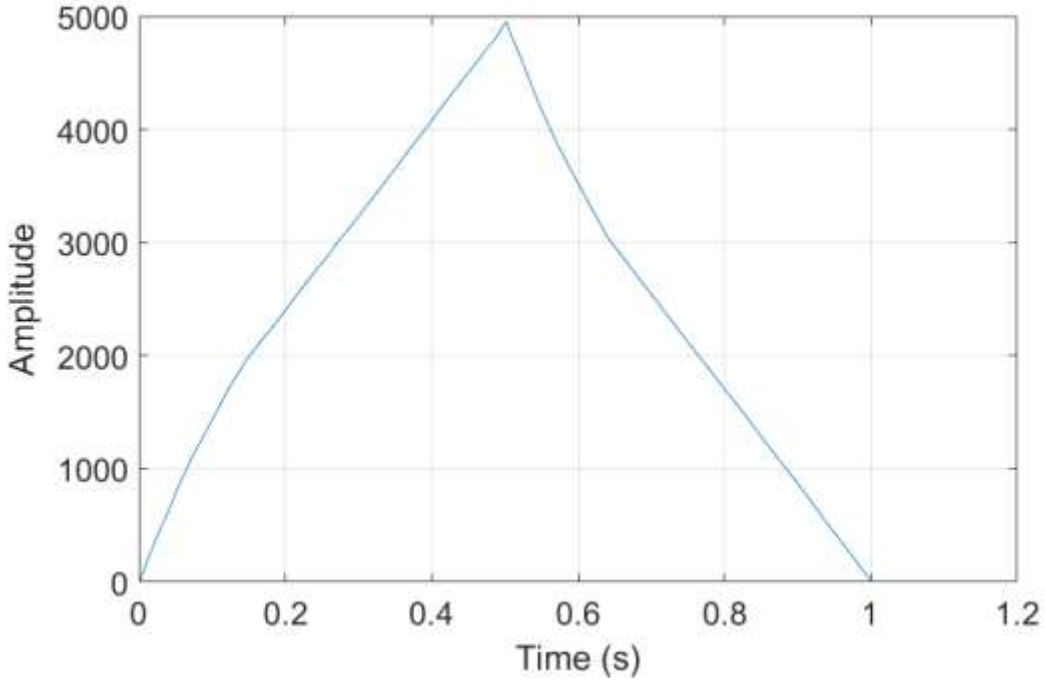
5000
4000
3000
2000
1000
0
Amplitude
0
0.2
0.4
0.6
0.8
1
1.2
Time (s)

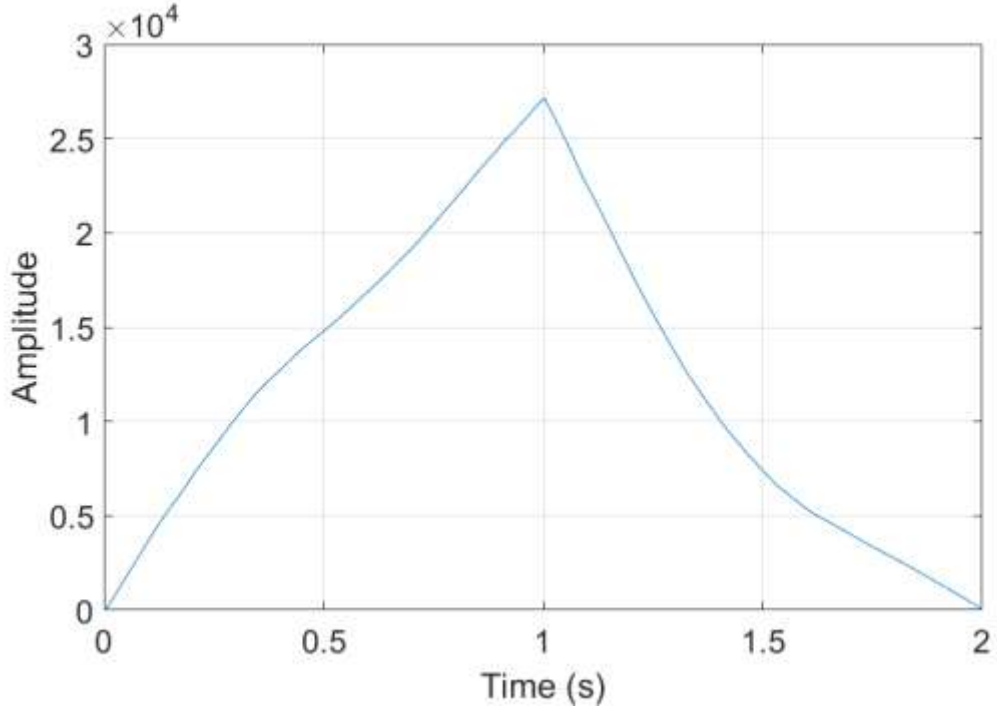
×10^4
3
2.5
2
1.5
1
0.5
0
Amplitude
0
0.5
1
1.5
2
Time (s)

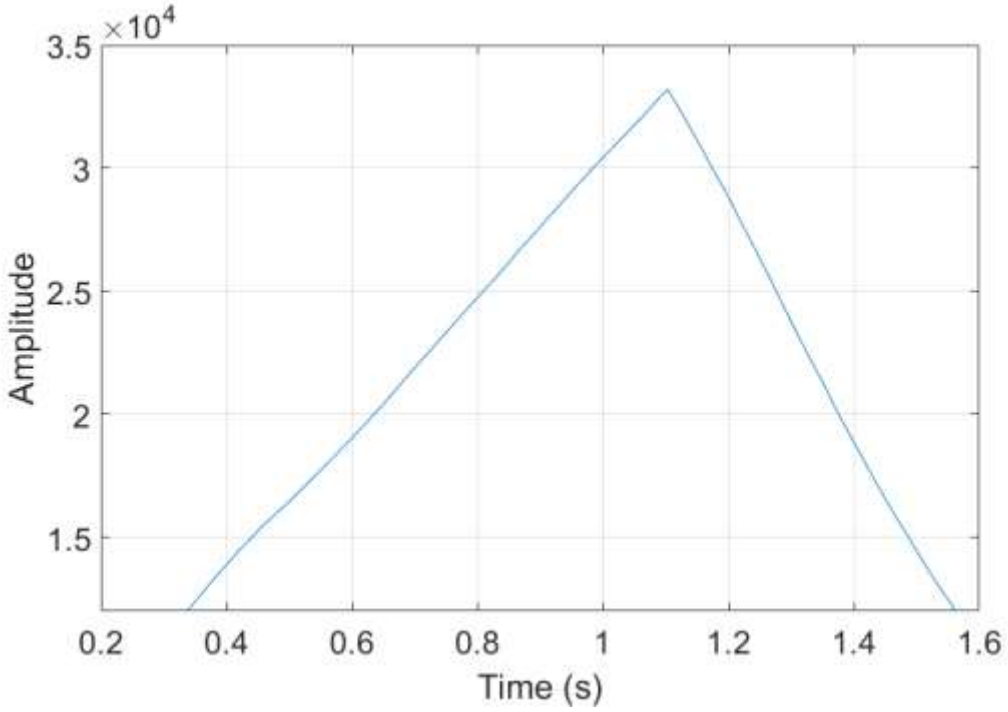

Figure 7-8: The cross-correlation relationship between P2 and P3 for different time windows (0.5, 1 and 1.1 seconds).

the characteristics time. Figure 7-8 reveals the cross-correlation results for three time windows.

In other words, the cross-correlations could not even find the delay let alone identify the system features through its second derivative. This point will be demonstrated later and explanations given for the unexpected output of this research in relation to a technique that has been used successfully in other disciplines.

7.5 Power Spectrum & Spectrogram analysis for 1mm diameter leak at locations, L1, L3 and L5

The spectrum power density function in Matlab was used to analyse frequencies of interest. The case examined was the water hammer produced by increasing the flow rate from 0.6 to 1.2 $l/minute$ (see Figure 7-9). Recall that leak number 1, L1 is located between P2 and P3, while leaks L3 and L5 are located between P3 and P4. The pressure transients for pressure transducer will be shown on the same plot, to show the effect of measurement location on the magnitude of the pressure. The y-axis is the pressure in bars and the x-axis is the time in seconds. The transducers P1 and P5 are close to the pump discharge and are approximately at atmospheric pressure, so the changes at these points due to the leakage effect are weak. The effect of the leak at both measurement locations is not at all clear. The two signals are almost identical, especially those from P5. Notice that from Figure 7-10, the leak flow rates at L1, L3 and L5 are 0.47, 0.41 and $0.28l/minute$, respectively. The raw data are filtered with a low-pass filter of order 32 and cut-off frequency of 500. The Matlab function is 'fir1' is used [127].

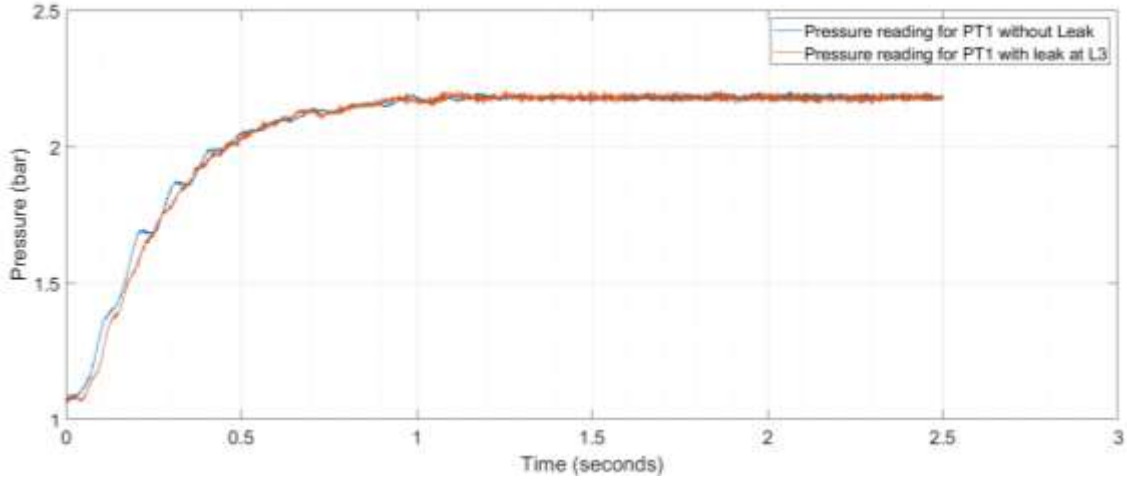

(a) **Recorded pressure transients at pressure transducer PT1.**

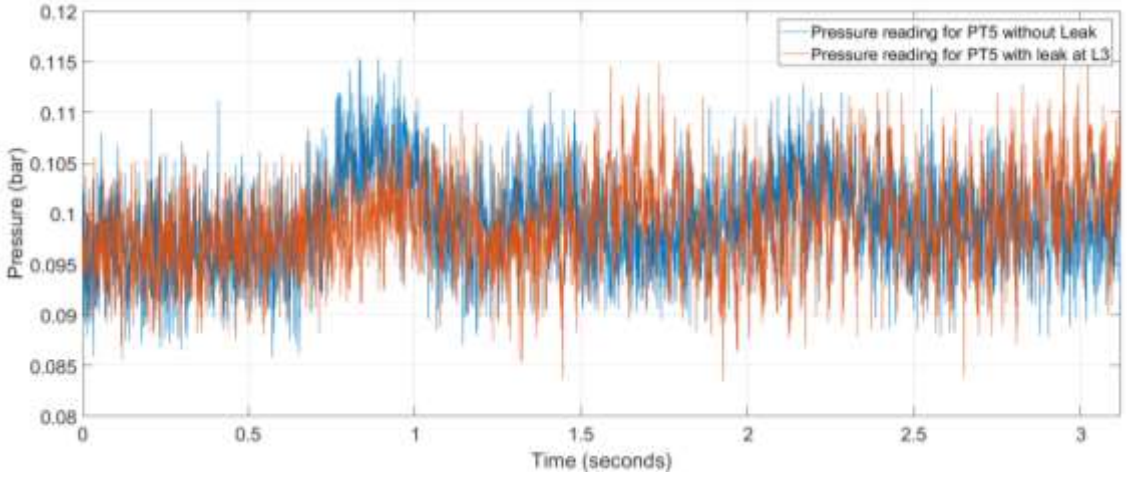

(b) **Recorded pressure transients at pressure transducer PT5.**

Figure 7-9: Recorded pressure transients at pressure transducers P1 & P5 for increase in flow from 0.6 to 1.2 l/minute. Blue line without leak & orange line with leak at location 3 (L3) at 363m downstream the pump.

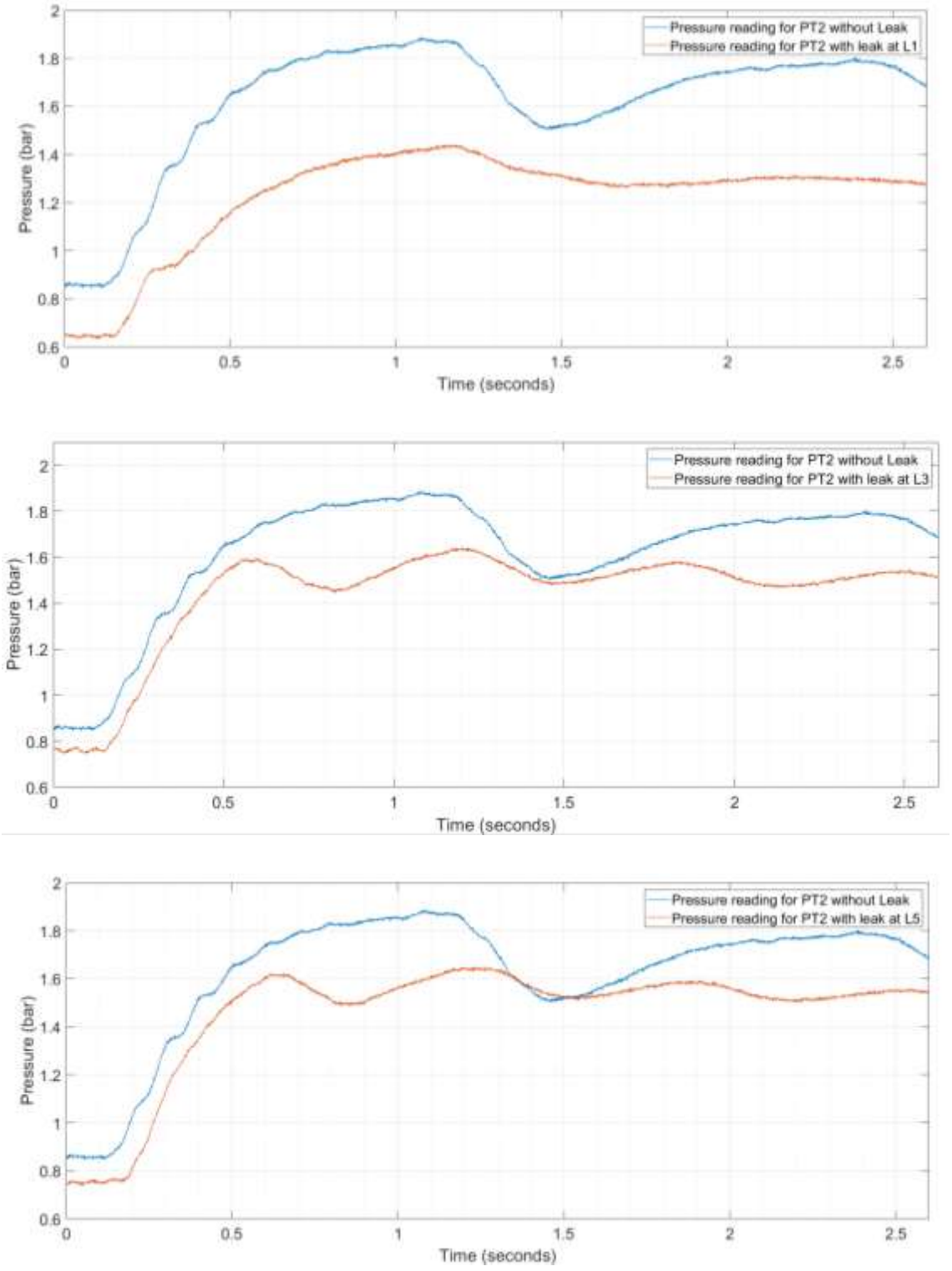

Figure 7-10 Recorded pressure transients at pressure transducers PT2 for increase in flow from 0.6 to 1.2 l/minute without and with leak at locations L1 (127.7m), L3(363m) and L5 (386m) downstream the pump.

From Figure 7-10 in the L1 case the pressure wave is seen to attenuate with time and its effect is clear. In the cases of L3 and L5, the characteristic time of reflection

for both cases has been reduced approximately by half. That is because the reflection wave from the leak is large, since the flow rate is almost between 47 and 68 percent of the flow through the system. L3 and L5 are at $354m$ and $363m$, which constitutes almost about half of the rig's length (total is $770m$), so the second valleys of the L3 and L5 almost coincide with the first valley for the no leak readings. Another thing to notice is that since L3 is closer than L5 to P2 , the second valley of L3 happens in a shorter time period than for L5. This is in line with what one would expect, as, in effect, the pipe length has been shortened.

In Figure 7-11, for P3, the L1 effect has less variation in pressure due to the leak, since it is upstream P3, the characteristic time does not affect the results in as clear a manner, and its distance does not coincide with any leak point. Thus the number of peaks and valleys are the same. However, for the L3 and L5 case, the leaks were large enough to smooth the pressure curves. Also, the peaks and valleys can be seen.

The P4 readings are shown in Figure 7-12, the L1 case follows the same pattern as the No leak compared to the previous two similar cases, P2 and P3, with the differences in the readings being to the pressure transducer and leak locations. Also, for L3 and L5 the reflection wave reaches P3 after 0.6127 of a seconds, causing the first valley and reducing the characteristic reflection time to almost half. The difference in the second valley time is also noticeable between L3 and L5.

From these demonstrations and figures, it is clear that the experimental system is working and gives reasonable outputs. However, the threshold for the leak detection approach, as mentioned, was the signal analysis. In addition to the cross-correlation and its derivative, the Matlab signal analyser tool box, the Power spectrum and the spectrogram features were used to study each signal individually. Some results from these analyses will now be demonstrated.

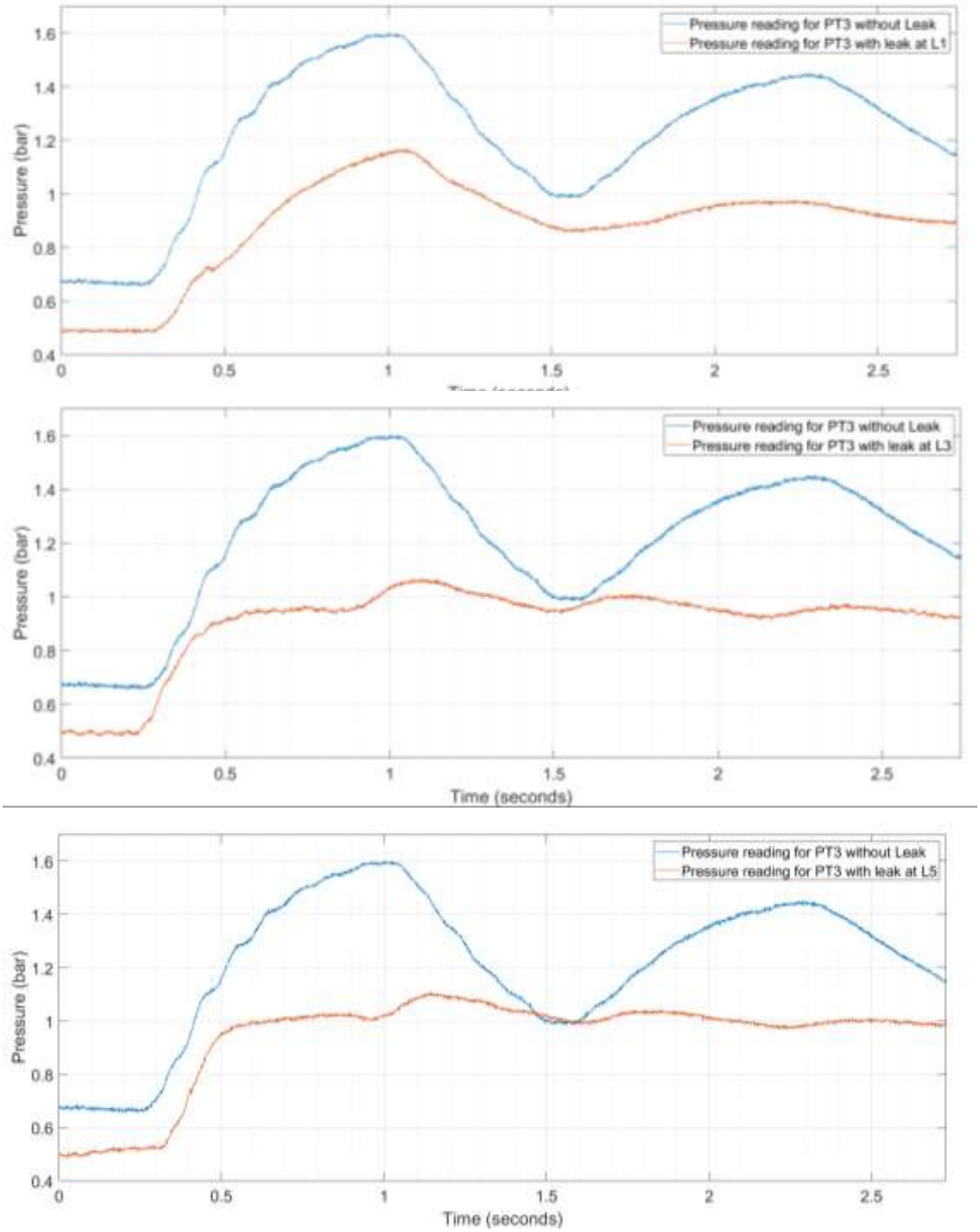

Figure 7-11: Recorded pressure transients at pressure transducers PT3 for increase in flow from 0.6 to 1.2 l/minute without and with leak at locations L1 (127.7m), L3(363m) and L5 (386m) downstream the pump.

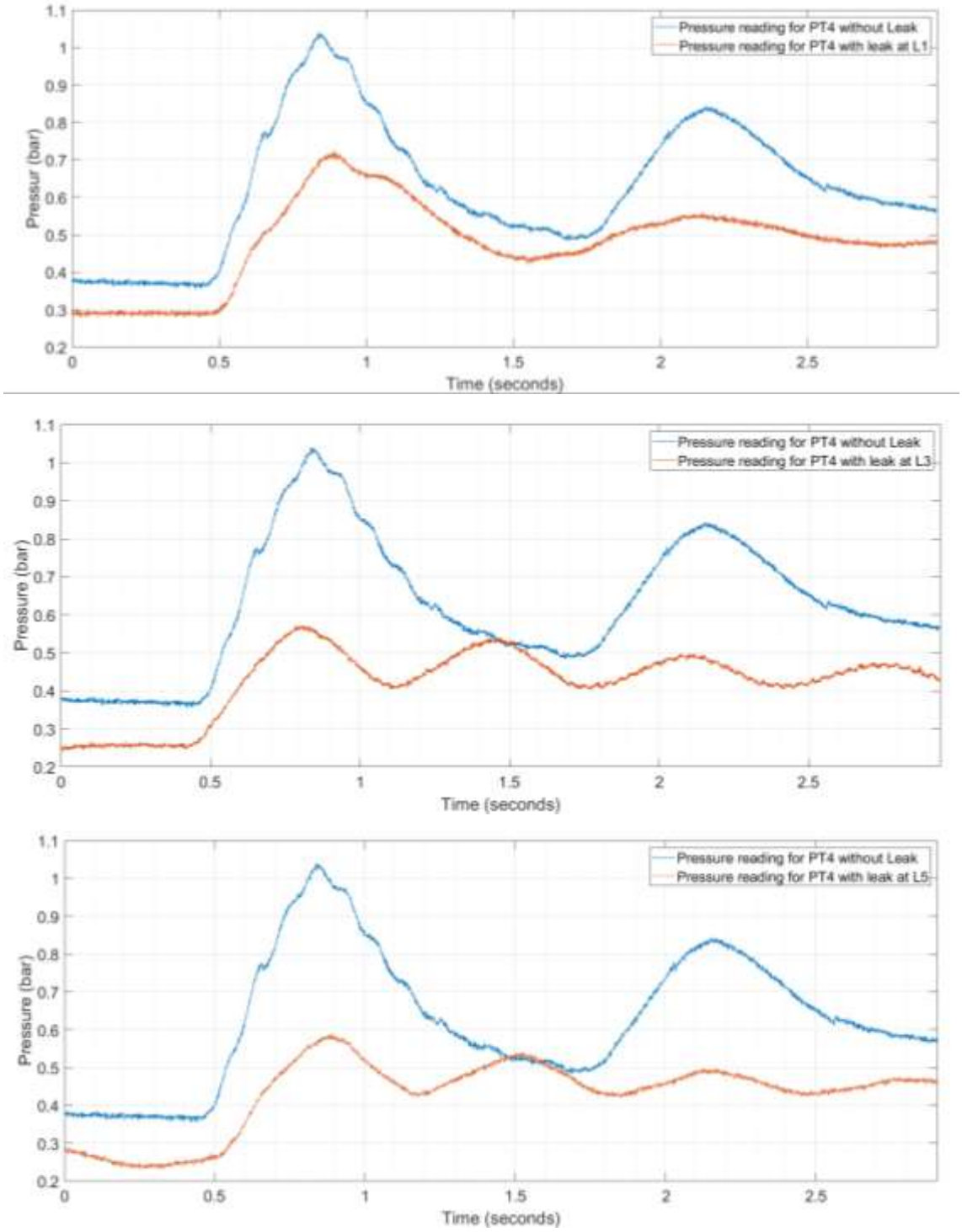

Figure 7-12: Recorded pressure transients at pressure transducers PT24for increase in flow from 0.6 to 1.2 l/minute without and with leak at locations L1 (127.7m), L3(363m) and L5 (386m) downstream the pump.

The physical signal has many frequency components. By decomposing the signal into a series of discrete frequencies, it is possible to show the value of each level. When this analysis is done by distribution of the power of the signal, it is called the Spectrum Power Density.

A representation of a spectrum of frequencies for a signal in a visual pattern is called a Spectrogram. The y-axis has the distribution of frequency intensity, while the x-axis is the time domain. The variation in colours in the chart shows different intensities of the signal.

The power density and spectrogram results have many useful applications when dealing with a signal that has many frequencies requiring identification. The Matlab Tool box and signal analyser [127], will be applied on some of the above pressure data.

The pressure readings for the L3 case will now be presented. Since these leak locations are between P3 and P4, the analysis is performed both on data with and without a leak. First**,** Figure 7-13 contains two sets of six charts. The first three charts are for P3 without a leak and the remainder include a leak at L3. Each case has three charts: the first shows the sample readings, the middle one is the power spectrum chart and the last is the spectrogram. Since the expected important frequencies will be in a specific range, the spectrum power a-axis has been trimmed to focus on the range from zero to 0.35, looking for expected frequencies.

For both methods, this analysis does not show any clear features which could be relied on when looking for the leak or other system features. For the power spectrum, the value oscillates within a limited range that does not indicate any noticeable frequency. Also, when comparing between no-leak and the leak case, the charts exhibit almost the same pattern.

In the spectrogram charts, the findings are the same, and no precise details can be concluded. However, it is noticed that in the L3 case, a blue line representing -160 *db* is clearer when compared with the no leak case.

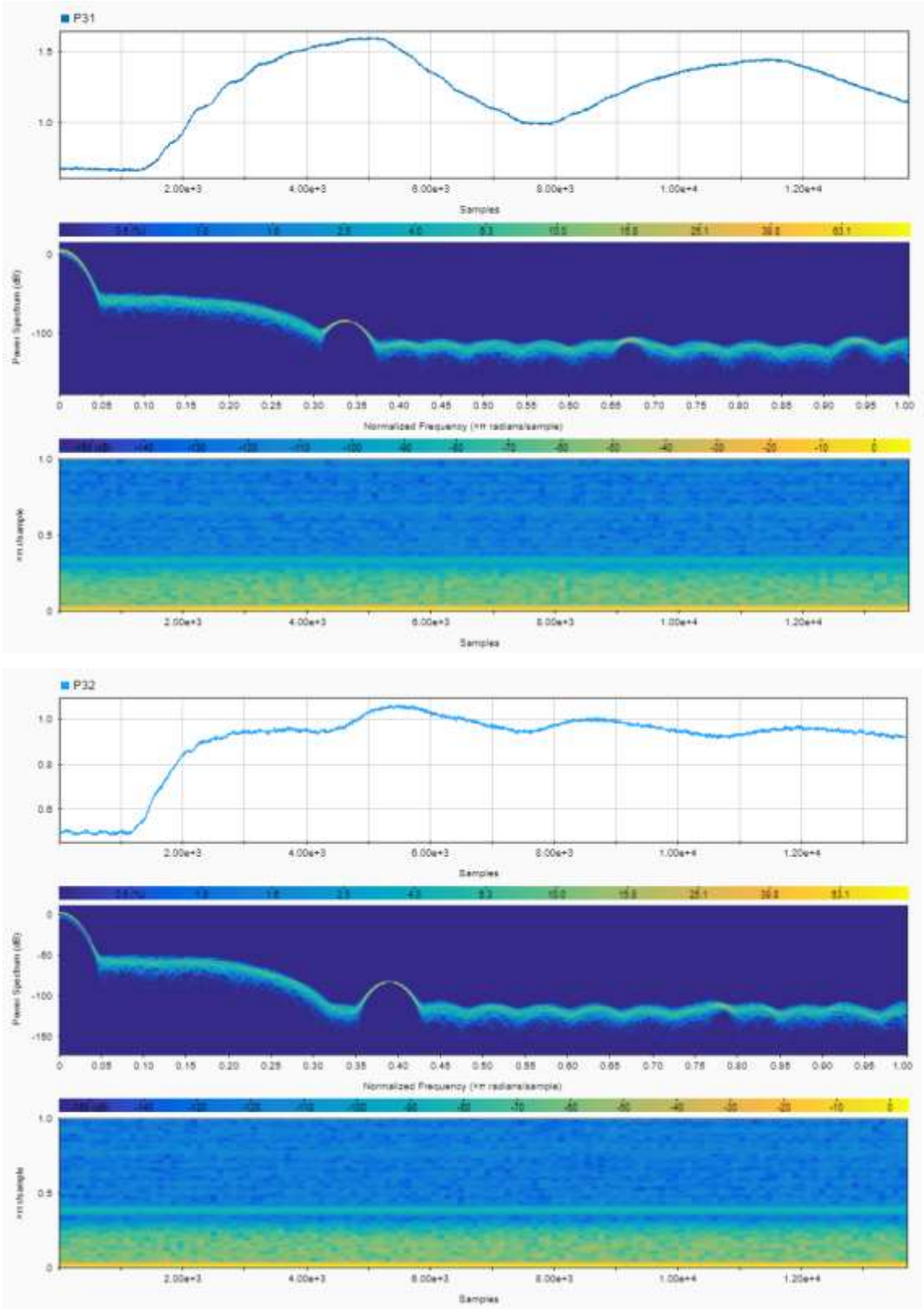

Figure 7-13: P3, Power Spectrum and Spectrogram for (Top) without leak (bottom) with leak at L3 for pump flow rate increasing from 0.6l/minute to 1.2l/minute.

In Figure 7-14 illustrates the application of the approach for P4. Despite the differences in the pressure readings between P3 and P4 in both cases, with and without a leak, the results of the power spectrum and spectrogram analyses are almost the identical. The desired and useful frequencies cannot be discovered.

Even when different signal analysis techniques were applied in this research on the laboratory apparatus outputs, no robust results were produced. In the discussion section, some explanations will be given regarding the leak definition with those techniques. It is the probable that the leak signals were attenuated or buried in other frequencies.

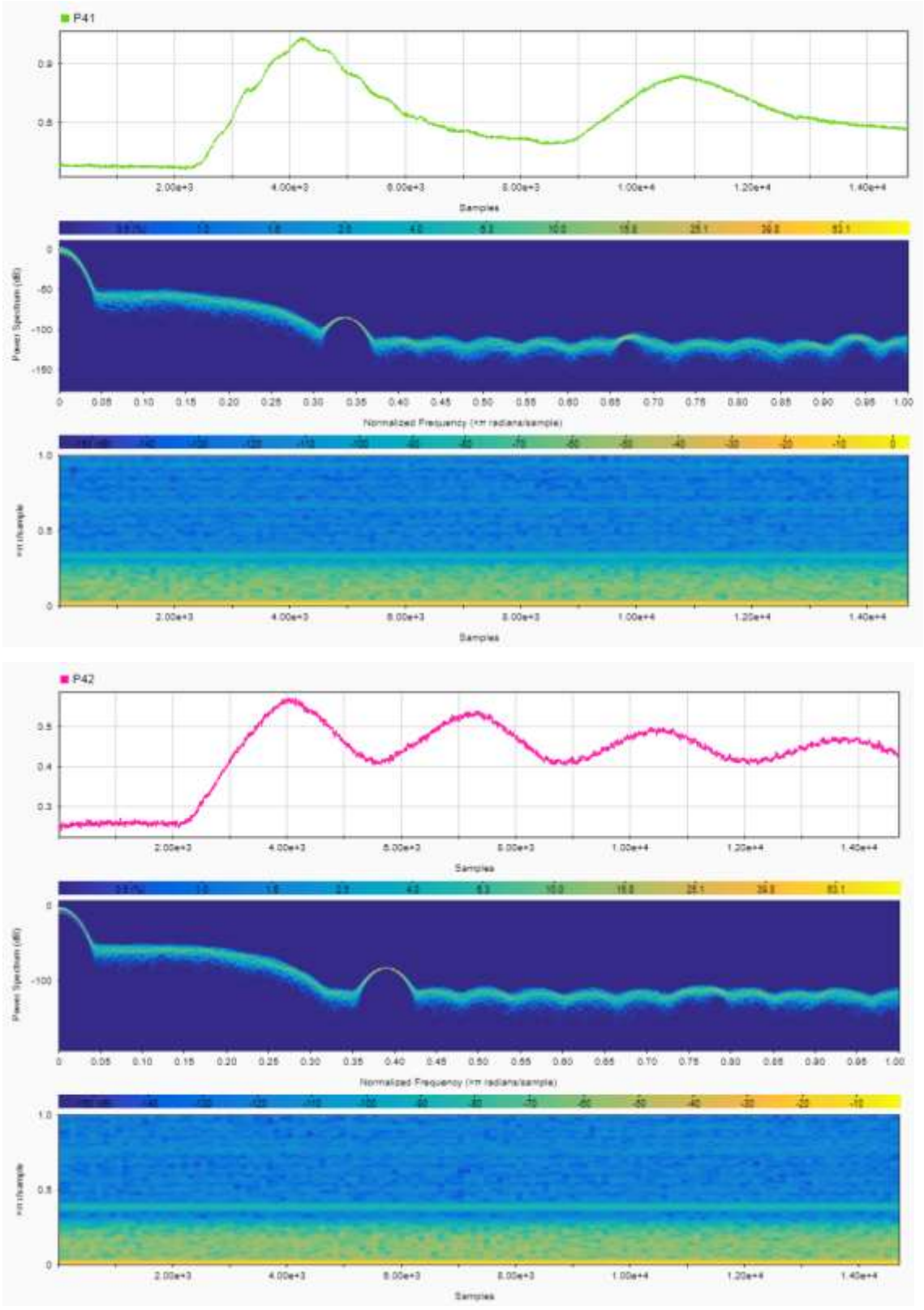

Figure 7-14: P4, Power Spectrum and Spectrogram for (top) without leak (bottom) with leak at L3 for pump flow rate increasing from 0.6l/minute to 1.2l/minute.

7.6 Verifications and Enhancement of the Signal Analysis

Due to the lack of information that was obtained from the data analysis, some further attempts have been tried to develop the technique. One method involved shifting the data to start from the same point. It was then possible to compute the cross-correlation between different transducer points. The other method was to mimic part of the water hammer to strengthen the correlations between the signals. This technique was partially successful in obtaining the time delay between the signals. However, it did not show the other system features. In addition, it was not successful for many of the other cases.

Verification of for technique was implemented on simple signals with/without leaks to simulate the study features in a simple way.

In the next sections, each process will be explained briefly with examples given.

7.7 Shifting the Data to Zero and Applying cross-correlation for No leak.

The water hammer experiment was undertaken by controlling the pump to change the steady-state flow from 0.6 $l/minute$ to 1.2 $l/minute$ in 0.55 seconds. The data collection for the five pressure transducers was moved to start from zero as seen in Figure 7-15. The data were filtered by a low-pass filter (order 32).

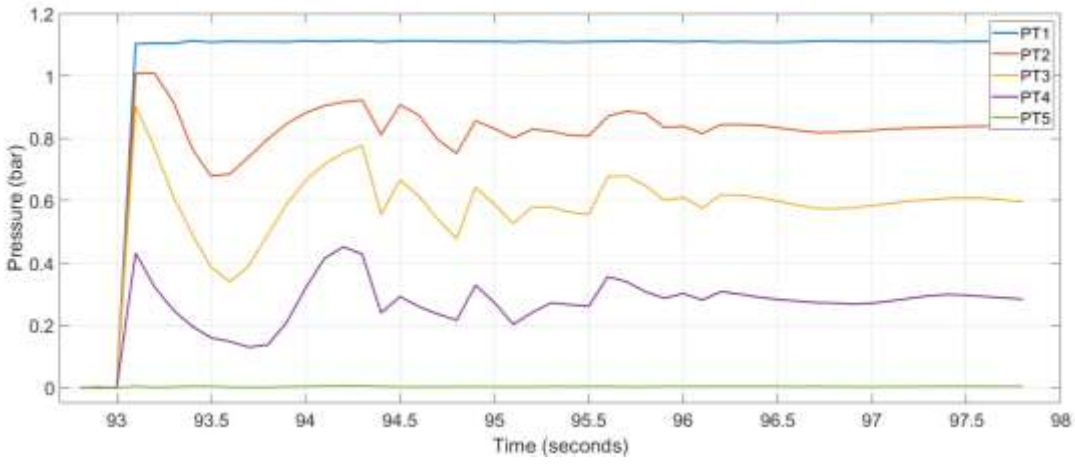

Figure 7-15: Shifting the recording pressure traces for the five transducers to stat from the same time: water hammer induced by increasing pump flow rate from 0.6 to 1.2 l/minute.

Physically, this shifting could be comparing to pump sharp start-up. In practise, a sharp water hammer wave is easier to identify and then to analyse. The cross correlation results for a filtered data of order 32 are presented below in Figure 7-16 first graph, a zoomed view of the cross-correlation is shown. Examination of Figure 7-16 (a) shows that no distinct feature on graph (such as a sudden spike) is evident. Hence, no progress in the signal analysis in the signals could not be formed.

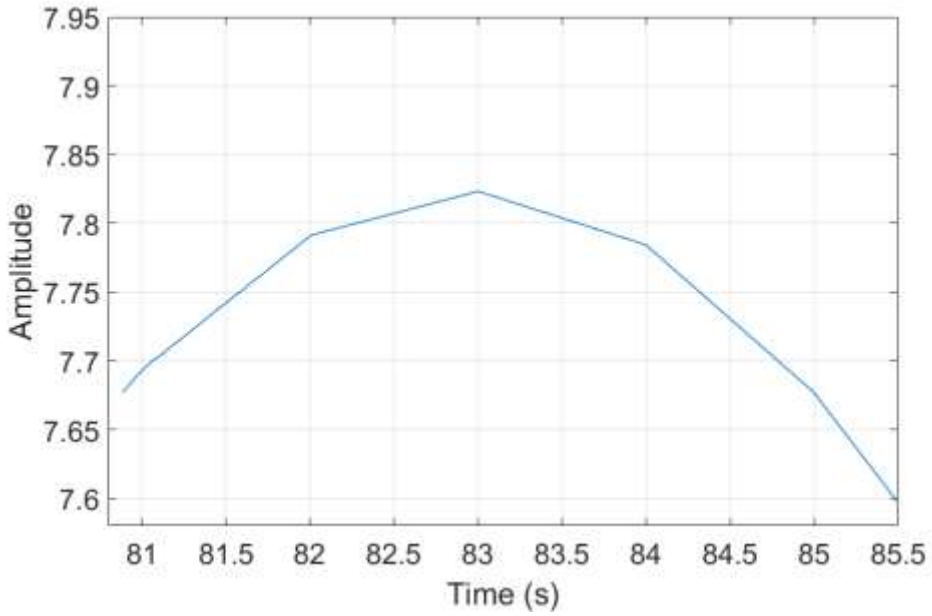

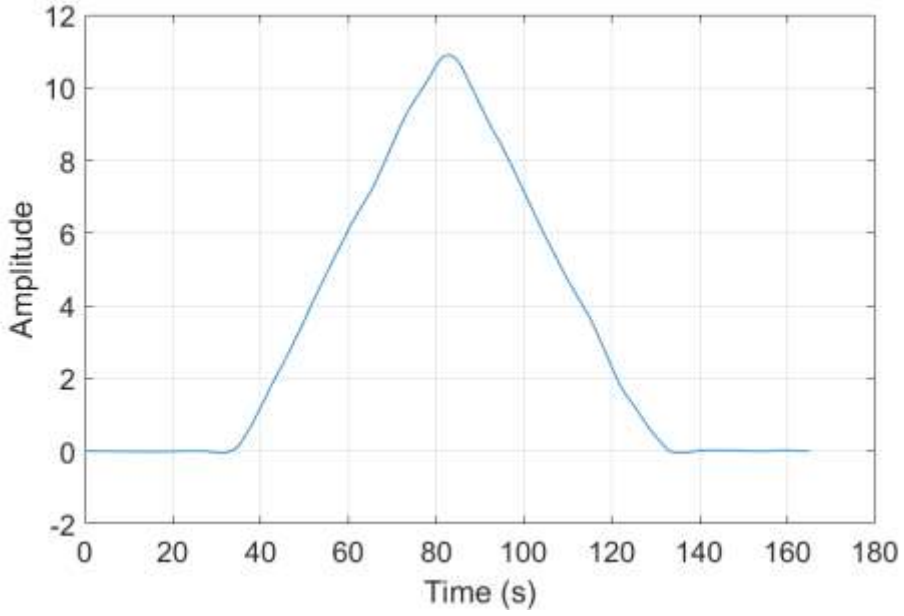

Figure 7-16: Cross-correlation between P3 and P4, and the lower chart between P2 and P4.

7.8 Enhancing the Cross-Correlation by Extending the Data

Since using the moving average method and the low-pass filter did not produce the expected analytical results from the cross-correlation and the second derivative, one of the ideas considered and applied to enhance the cross-correlation analysis was to use a technique known as' the extended line', as illustrated in Figure 7-17, which is applied after the signal filtering steps. The extended lines are based on parallel changes between two readings. For example, since the zoom of interest is primarily on the first wave, therefore the remaining data is trimmed and parallel lines are added to mimic the change in the behaviour between two points. The time delay is calculated and maintained since this is what should happen in reality and theoretically. The results of this technique were as predicted, improving the cross-correlation output on the delay and showing new peaks in some cases. Nevertheless, the peaks could not be correlated with any system features.

This approach was applied to various water hammer leak tests. For example, a leak at position 3 with steady state flow of 1.8 $l/minute$ and the water hammer is

triggered by shutting the manual downstream valve. The cross-correlation was done between P2 and P3, and also P3 and P4.

This approach depends on some alterations in the signal to improve the cross-correlation principle for extending the data with coherent signals with specific delay. The extension should make the correlation between the signals more robust, so the noise effect may be reduced and some outputs could be useful.

Referring to Figure 7-17, the period is time has been estimated for the two signals, the steps are as follows:

1. Divide the periodic of the time wave in half so that only the pressure surge is kept for further analysis.
2. Delete the remaining data from the trace and from the half point (point 1) draw diagonal line to 75% of the half period (point 2). The pressure of point 2 should be the initial steady pressure before the transient event.
3. The remaining 25% of the enhanced period should be the same as the start value, i.e. steady state pressure.
4. For the second pressure trace, the data should not be cut at the mid-point of the upsurge but further along the trace considering the time delay between the two signals.
5. The line for the second trace is drawn between the last point in the previous step (mid-point plus the time delay) and at the same slope as the previous line.
6. The second point can be obtained from the solving the line equation. The slope is now known and the line should be stopped at the initial value of signal two, so that the time can be defined.
7. After this time, the pressure value should be considered constant until the end of the total periodic time.

The aim of returning the values to the initial value for a short period of time (25% in the first signal and maybe less in the case of the second one) is to mimic the

transient and improve the cross-correlation analysis. In summary, the enhanced lines sustain the time delay between the signals and the slope to maintain the signals' coherency.

The above steps are summarised in Figure 7-17, which shows four graphs, each one having two arbitrary similar signals.

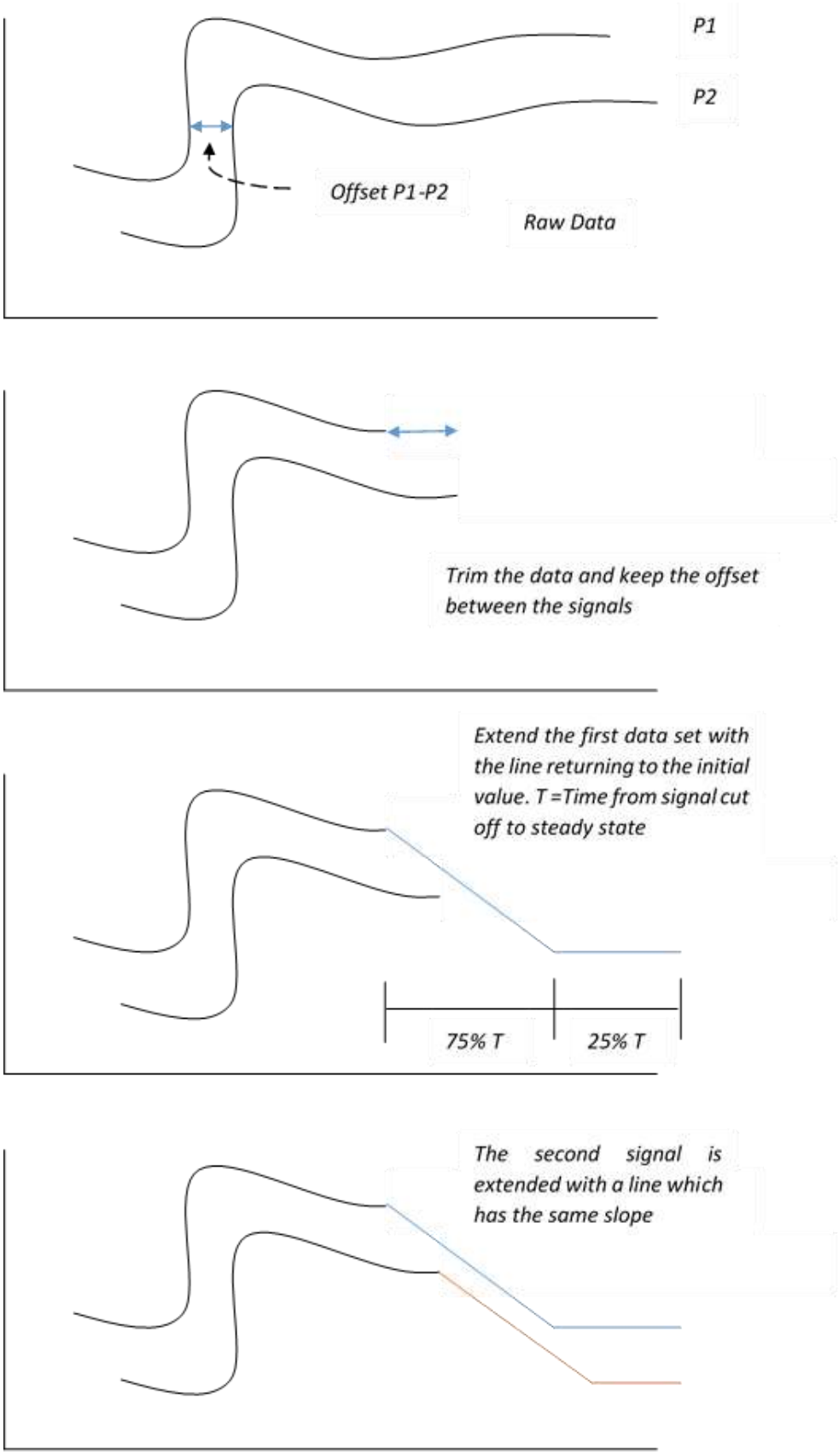

Figure 7-17: Schematic of the enhanced lines steps method.

The second derivative of the cross-correlation has been improved by using this approach. Despite the small offset shown near the middle because of the low-pass filter order, the offset between the signals is clearly evident. That is predictable, since the extended data retains the delay between the signals.

The following examples explain the approach. The two examples are transient events due to the pump start-up from zero to $1.8 l/minute$ and closing the down stream valve for this steady state flow rate. First, the upstream event shown in Figure 7-18 shows the enhanced pressure readings for $P2$, $P3$ and $P4$. It is clear from Figure 7-18 that $P3$ has two different extended lines, because when comparing with $P2$, this will be the delayed signal, while with $P4$ the opposite is the case. As shown in Figure 7-18, sometimes maintaining the slope and returning to initial value is not possible, as in this figure. Sustaining the slope seems to be more reasonable and more important.

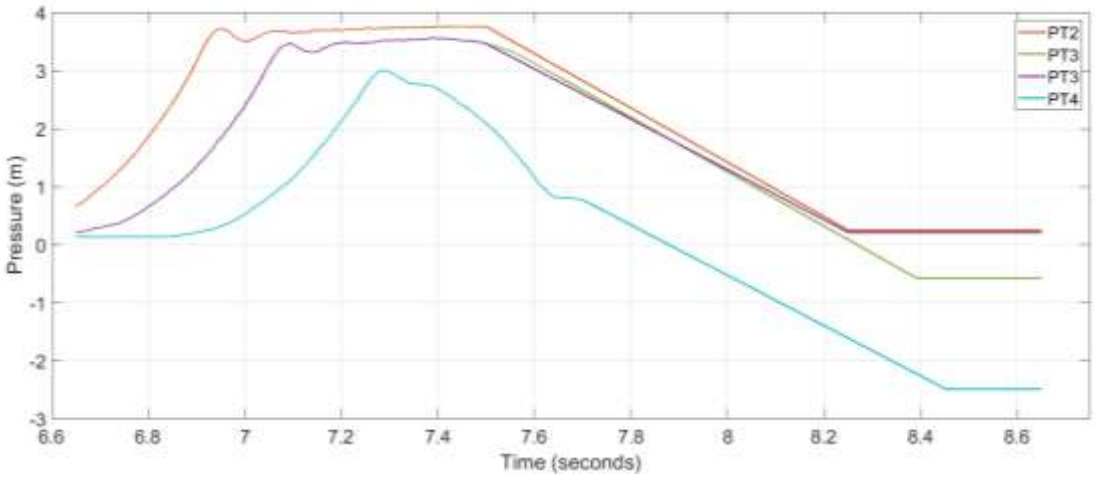

Figure 7-18: Enhanced measured pressure traces, for PT2, PT3, and PT4 for pump start-up from rest to 1.8 l/minute.

In Figure 7-19 and Figure 7-20 the second derivatives of cross-correlation for $P2 - P3$ and $P3 - P4$ are shown respectively, for the case of a leak at L3 and also no leak at L3.

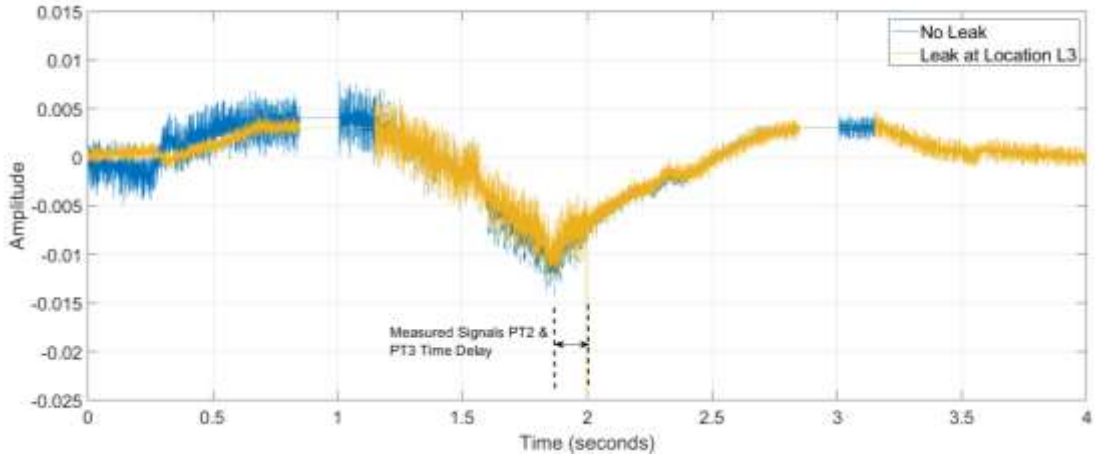

Figure 7-19: Second derivative for the cross-correlation between P2-P3 with enhanced extended lines.

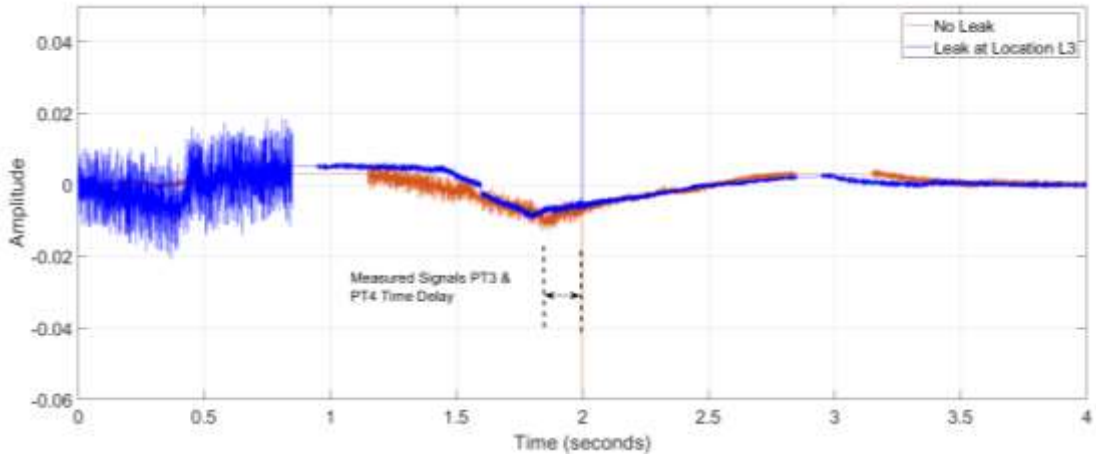

Figure 7-20: Second derivative for the cross-correlation between P3-P4 L3 for the cases of no leak at L3 and leak at L3 water hammer due to pump star-up.

In the two figures, Figure 7-19and Figure 7-20 above, a noticeable improvement was achieved in the signal analysis to find the time delay between the two signals. However, the leak position it is not evident.

In conclusion with this enhanced line approach, whilst it has been applied successfully to the upstream water hammer to show the time delay between the signals, which we already know, the important feature, the position of the leak,

cannot be found using this technique. However, in respect of the downstream transient, the time delay between the signals cannot be even identified in the second derivative of cross-correlation of the outputs.

Chapter 8 Discussion

Use of water hammer as leak detection technique has been widely reported in the literature and can be thought of as a successful signal analysis approach. This work attempted to simulate a real field working system and apply the technique to a new scaled rig built for this purpose. In reality, and due to operation and safety of the pipeline systems water hammer generated by the sudden closure of a valve is not permitted in these systems. It can only be used in emergency situations. Therefore, using the pump start up process is a more reasonable and applicable water hammer event. However, a pressure wave caused by the valve movement, enlarges the system's singularities [2, 36]. The laboratory scale rig is $770m$ long and is constructed from small diameter (8 and 10 mm) pipe. Also, the pipe material is thin walled copper as opposed to the relatively thick (though still technically 'thin walled') stainless steel used in the real system. In addition, the flow regime is turbulent with a high steady operating pressure in the pipe. To achieve the aim of the study, a laboratory-scale rig exhibiting these properties was constructed in ones of the University's laboratories. The rig is unique in terms of material, hydraulic capabilities and physical dimensions.

Unfortunately, all the selected signal analysis techniques were unsuccessful on the rig. They failed to clearly identify features such as the position of a leak due to a variety of reasons. One of those is the hydraulic turbulence of the flow which mashes the signal from a leak. Unsteady turbulent behaviour is complex to understand [128]. Also, since the rig is constructed from small diameter pipe, friction losses are high. Consequently, the signal attenuates more rapidly than that in a larger diameter pipe. In addition, the rig is quite long, another reason that could allow useful details to be lost. To help find explanations for the lack of success in leak detection, the factors affecting the signal quality reports by previous researchers will be presented.

The effect of high friction has been described by researchers, such as Liou [46] in relation to high inlet Mach numbers, and Beck *et al.* [39] in relation to small diameter pipes. The pressure waves were more attenuated in comparison to large pipes with the same pressure wave.

Another effect, reported by Ferras *et al.* [129], is the shape of the rig. They noticed that the mechanical behaviour of straight pipes was different to coils. In coil rig changes occur in the pressure wave shape and the time delay. In the experimental rig used in this study, and because of the congested space, it was bent to fit in. This is another difference between the model rig, which is in a long straight line, and the actual rig, which has 97 loops, on each of which there are two bends. On each loop the bends have two semi-circles and two quarter-circles. The bend to diameter ratios are 86 and 43 for the semi and quarter circle, respectively. These bends could cause vibrations due to Fluid Structure Interaction [53, 130], and thus could affect the analysis. The existence of bends and high friction could contribute to wave transmission and reflection. The wave energy is damped due to friction and inelastic behaviour [15]. Furthermore, the rig is not reinforced completely, like underground pipelines. Therefore, the rig could be subject to large dynamic forces during pressure wave occurrence [131]. If the pipe moves because of pressure surge, the motion of the pipe is likely to result in mechanical damping in addition to the viscous damping [132].

Furthermore, the uncertainty produced by complex features such as branches and topography produce many complex waves which complicates pressure transients analysis [2].

Another possible explanation is that the smallest leak size is large compared to the pipes diameters (12.5 and 10 %). The high pressure allows a minimum leak flow at point 5 that is 46.7% of the steady state flow of 0.6 $l/minute$. This flow is also quite large and physically it would be considered a pipe rupture and the reflected wave produced from the leak location could mask many other features downstream of the leak location. The flow regime behaves differently for small and large leak flow rates [133]. Additionally, changes in the flow regime can distort the pressure wave [134].

Furthermore, the assumptions in the numerical model may not represent the empirical settings precisely. The numerical analysis assumed that the leak flow rate remaining constant during the steady and transient states. However, it is clear that the oscillating pressure wave in the pipe affects the leak flow rate. The rate will vary, especially at points which are far from the high pressure pump. To reiterate, it was found that, in many cases, the section of the rig downstream from the leak was drained during some of the leak tests. Modelling the leak as an orifice may inadequate [27], in addition to the existence of uncertainties in the boundary conditions [16], pipe coefficients, and method of solution in general [135].

The cross-correlation technique was selected due to its previous successful applications ease of implementation. In this research the signal analysis by cross-correlation and its derivatives did not successfully, locate pipe leaks. In complex systems, features such as the number of components or change in the pipe material and diameter produce sophisticated reflection patterns that limit the cross-correlation analysis [2]. Dispersion is a problem in applying the cross-correlation on actual systems [47]. In a recent study done by Butterfield *et al.* [94] a variety of signal processing techniques were tested to find a suitable leak detection form. They concluded that, to avoid the attenuation or dispersion of the pressure signal, some models of signal processing may be more successful than others. Therefore, the importance of trying many techniques to find the best combination of techniques should not be underestimated. They conclusion is that no one improve the statement technique is suitable for all systems [26]. This point is a penstock for any analysis. Despite the differences between the two researches' leak identification approaches, in signal analysis, the same procedure could be the solution to avoid inaccurate outputs. The threshold in any leak detection form is finding a suitable signal processing technique to highlight the desirable features. Furthermore, the soft wave is very complex [1], which means need more focus on this aspects is required.

In terms of the analysis process, it is better to identify the background noise before applying any technique. The background noise, in this case, would be the steady-

state flow without leaks. Also, some pipeline features have reflections that are similar [105].

For the cross-correlation delay, the filter order has an effect on the offset. In all cases, the cross-correlation outputs have delay steps equal in number to the filter order. Accounting for the time delay between the signals involves subtracting a number equal to the product of the order number by the time step, to enhance the analysis.

Although the analysis for the rig still needs further development, the run outputs seem to be mimic real network systems reasonably well, hence they are scalable.

8.1 Testing the Cross-Correlation Analysis Behaviour with Simple Signals

In order to demonstrate the signal analysis by cross-correlation, a simple example is tested numerically to find how the delay between signals could be reduced if the signal is not treated with a suitable technique. Seven matrices are used, each with ten points, assuming that the different signals have similarity in behaviour and a specific time delay. The aim of this example is to examine a signal which is correlated with a slightly different one in order to see the alterations on the cross-correlation.

Table 8-1 contains the propsal signals.

Signal Name	Signal parameters
Original Signal	2 2 5 5 5 5 5 2 2 2
Signal One	1 1 1 3 3 3 3 1 1 1
Signal Two	1 1 1 1 3 3 3 3 3 1 1
Signal Three	1 1 1 3 3 3 3 3 3 1 0*
Signal Four	1 0* 3 3 3 3 3 1 0
Signal Five	1 0 2* 3 3 3 3 3 1 0
Signal Six	3* 0 2 3 3 3 3 3 1 0

Table 8-1: The proposed different signals parameters.

The signals one and two are delayed by one step and two steps, respectively. Later, signal one becomes changed and the changed element is denoted by a strike (*).

The signals are shown in Figure 8-1.

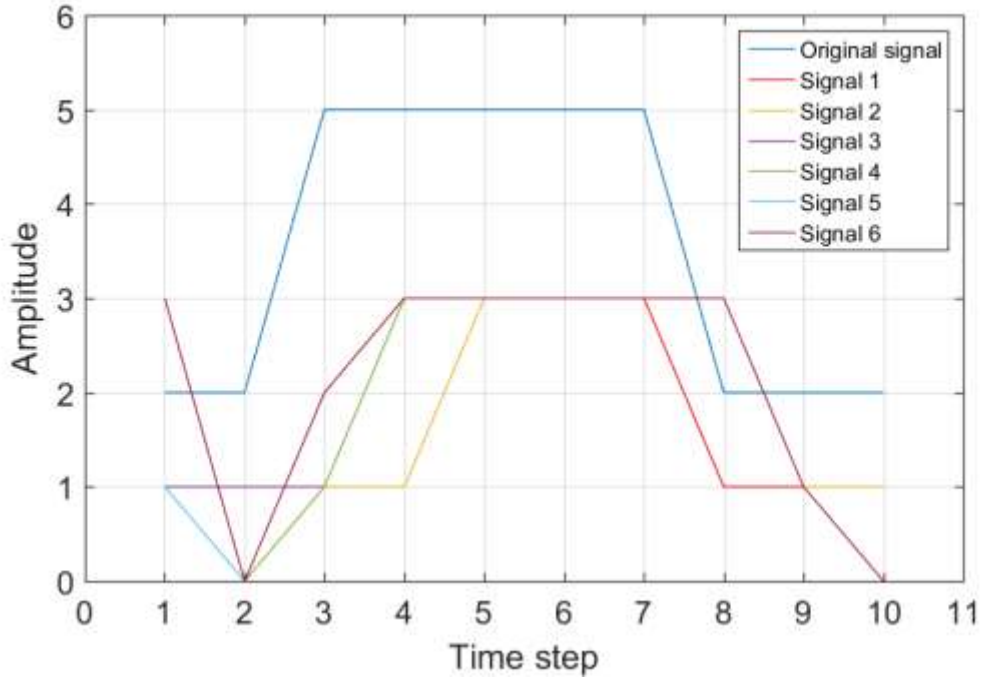

Figure 8-1: Different simple matrices to mimic a water hammer event.

From the Figure 8-1, it can be seen that the original signal is the blue line, while the orange line (signal one) is delayed by one step. The yellow line, signal two, is delayed by two steps. The changes in the five matrices are an attempt to simulate alteration of the signals by features such as noise, system characteristics, hydraulic effects, or other factors. In Figure 8-2, five curves are shown for the cross-correlation between the original signal and the other five suggested signals. The mid-point is at reading 10 on the x-axis. For the signal with two steps delay, the orange line reaches its peak on 8, which means the delay from the centre is two is correct. For the other one point with offset, the peak in the chart is on the 9 value which means 1 step delay. However, for the last matrix, signal six, its peak is on the midpoint, which means the delays have vanished.

When tracing the values it is noticed that in the stage assumed to be similar to the steady state prior to the water hammer event, the values are highly fluctuating. The value starts at 2, while the other matrices start at 1. On examination of Figure 8-1, it can be seen that in the stage representing the steady-state prior to the water hammer event the y-value starts bat 3 while the other matrices have starting y-values of 1. Then suddenly it drops to zero and then rises to 2. The oscillations of those first three points have a significant massive effect on the cross-correlation outputs, even though the remaining points behave in acceptable. The blue line in Figure 8-2 represents this relationship and it can be seen that there is no offset for this data.

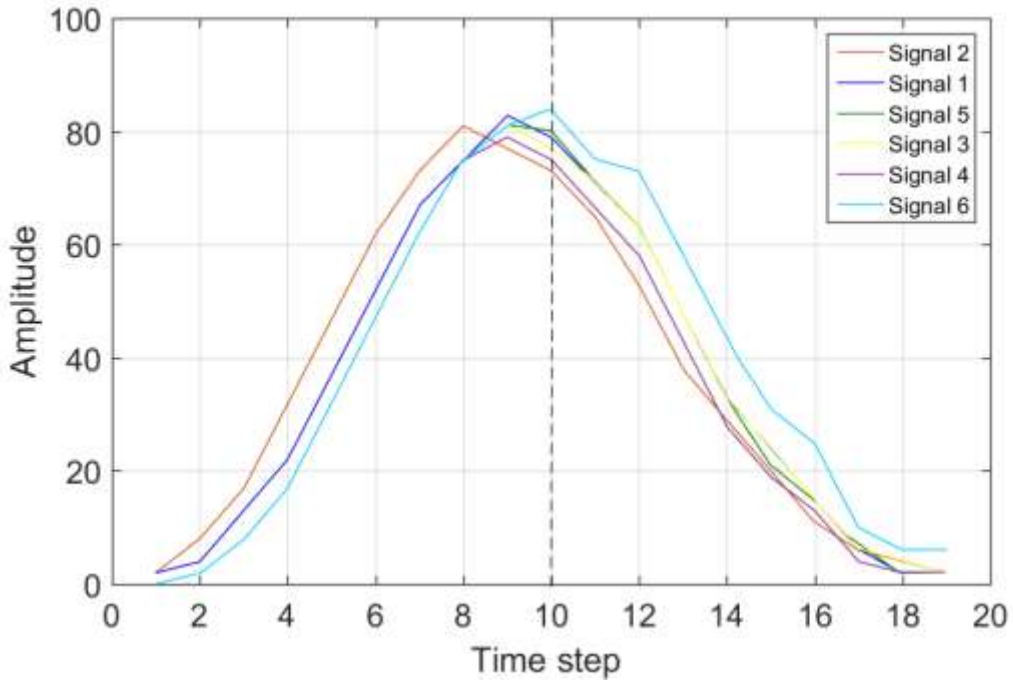

Figure 8-2: The cross-correlation between the original signal and the other six signals.

Since the cross-correlation principle mathematically depends on the multiplication of the two signals and the maximum has been shown to occur at the moment where the two signals coincide, having large oscillations may eliminate the values of these outputs, and shows the signal without offset. As seen in the cross-correlation graph, all the peaks have their correct delay (most have one, but one example has two steps), except that signal 6 which shows no delay. That is because the steady state

time period has been altered by changing the first data point to a higher value. Thus, the steady-state fluctuations affect the cross-correlation outputs and the offset has vanished. The forgoing example illustrates that a cross-correlation analysis can be ineffective when there are fluctuations in the signal prior to the transient event.

Chapter 9 Conclusions & Future Work

This work was undertaken to examine some leak detection water hammer approaches to real field systems. A water hammer event produces a wave in the system, and system features like leaks or junctions, reflect the wave generated, enabling it to be captured and analysed. The wave caused by a pump rising was selected since it would be easier and more efficient to apply on a real network system.

The research started by constructing a new rig scale model of the real system, to enable pressure transient data to be recorded. The physical and hydraulic properties of the rig were scaled to mimic the real system. A computational model of the rig was developed and the output of the model was analysed using the second derivative of the cross-correlation. The governing equations were solved by method of characteristics approach using Matlab code developed for this purpose. The pressure transient associated with pump start-up was modelled, and the second cross-correlation derivative showed promise in identifying leak locations. The leaks were at the 100m and 380 m locations and the second cross-correlation derivative technique identified the locations with reasonable precision. Additional leaks and pressure transducers were installed on the laboratory rig.

After constructing the laboratory rig and undertaking the numerical analysis, the experimental programme was commenced. The leak test examined the effect of leak location, leak size and the waterhammer trigger events. The test runs focussed on pump start-up as the transient event. A leak diameter of 1mm was the most used size leak examined.

The analyses of the cross-correlation and its derivative showed some limitations. Therefore, other techniques including the analysis of the spectrum power density and spectrogram were tried without significant progress being achieved. Therefore, using the cross-correlation technique and its principles, some further trials were conducted. These included: (i) using enhanced data lines and (ii) shifting the data. The first of these showed the offset between the signals perfectly; however, there

was no improvement in the relation to the second cross-correlation derivative. For the second approach, neither the cross-correlation nor its derivative was improved.

The cross-correlation analysis results are indicative of some limitations in relation to the rig configuration.

It is probable that the length of the rig, high friction, bends, the number of connections, and its small pipe diameter attenuated the water hammer waves. In addition, data has a lot of hydraulic noise, which is likely to result in the useful spikes or details either being buried or distorted within the signal. However, the scaled experimental rig is a more realistic representation of the field system than the numerical model.

In the export facilities 'the real field system in this thesis', despite the technology and resources available, the desirable sampling rate was low due to the large number of sensors connected to the SCADA system. This reduced the scanning time and made the sampling rate low. Accordingly, considerable effort was made by researcher's colleagues January, 2018 to increase the data acquisition scan time from 1 $second$ up to 90-100 $milli\ second$. This sampling rate is, nevertheless, still below the required sampling frequency of 1 kHz. Since the laboratory rig is scale model of the flied system, further enhancement of the laboratory apparatus could enable the research findings to be applied on the full-scale systems.

As a result of the numerical and experimental findings of this study, it is reasonable to conclude that success in leak detection will depend on implementing appropriate signal processing. Developing a signal processing procedure that tracks the change in pressure during the transient event and, at the same time, does not discount new spikes or singularities could produce a water hammer leak detection approach for real field systems. An initial concept in relation to this technique has been presented in section 3.3 with a simple application. It is designed to adapt the operating systems

through taking into account the water hammer behaviour peaks on the second cross-correlation derivative.

In summary, the current work could be developed in the future in the following areas: signal processing, the experimental rig and the real system.

Focusing on signal processing to detect any singularities in pressure waves based on the database available could be more successful. This could involve designing a filter or algorithm to detect any changes in the system caused by reflected wave. Analysis of measured transient data is likely to form the basis of any leak detection system.

9.1 Future Work

The results of this research lead to various recommendations for future work this research has attempted to use fluid transients as a leak detection tool with limited success. It has used 'soft' pressure wave arising from pump start up as the water hammer trigger in long elastic pipe. The main obstacle has been the adaption of signal processing filters to discern the characteristics features of the raw data. As demonstrated by Butterfield *et al.* [94], whatever the approach or the research system, finding the most appropriate raw data processing is the main issue in empirical or real systems.

In the real field system, the sampling frequency was too low to enable signal processing to be applied. The sampling frequency needs to be sufficient high to capture the characteristics of the pressure wave.

The following two sections provide suggestions for future work on signal processing and the experimental rig.

9.2 Future work on signal processing

Since the signal analysis did not detect the expected features in the rig, so, more sophisticated methods should be applied to find features in the signal which can be recognised as reflection points in the rig.

Furthermore, future research should be focus on developing the following aspects of the proposed algorithm:

- Instead of sustaining the remaining new peaks, after being approved by the user, the average values at the nodes for all five runs could be calculated and used as the system features.
- The hypothesis technique (second cross-correlation & the filter) could be used as a guide to indicate changes in the system, after construction (compared with the theoretical design); some changes may have harmful consequences while others may be natural (like small bending of the pipe after construction).
- The effects could be compared by applying the algorithm with/without well-known filters like: 5 moving points filter, low-pass filter, and high-pass filter.
- If it works perfectly without other filters, could this proposed filter be considered as an alternative for all the others or could it be used in combination?
- Could it be developed to deal with continuous signals? In this case it should be a mechanical or electrical filter.
- This filter could be integrated into a real network monitoring system such as SCADA, so that the operator could have the chance to check new features and avoid any harmful changes in the system.
- Based on the simple example for the cross-correlation, which demonstrated that the delay between signals could be zero, further work could be carried out to investigate this occurrence and try to find a solution.
- It may be that the best performance of the proposed algorithm could be achieved by accumulating a reasonable amount of the data for dimensionless parameters such as the pressure and flow and finding any changes in the system behaviour for the same water hammer trigger.

9.3 Future works on the experimental rig

This research has been undertaken on a particular experimental setup, and there are many other possible settings of the rig that researchers can use for new studies. In the following paragraphs some suggestions are provided for expanding the research based on the experimental setups.

The rig has a capability for extension by an additional 150m of copper pipes on the existing rods, allowing a total length of 920m. In addition, a flexible hose can be connected to the copper pipe. In addition to changing the diameter of the rig, this would also allow a change in material, which would offer another parameters relating to the pressure wave phenomena to be investigated. The particular attenuation in the flexible hose would change the pressure signal, which would be a new field to study.

The rig has thirteen three-way compression fittings on different locations. Those can be used to fix additional pressure transducers, simulate other leaks, or be used as new branches and connections for other equipment. Also, changing the pressure transducers and the leak locations would provide a further line of investigation.

Since the rig has been constructed as a scale model of pipe system of large diameter, with long length, it could be used to simulate a large distribution network system. The three-way connections could be branches with either continuous or intermittent flow rate.

References

1. Stouffs, P. and M. Giot, *Pipeline leak detection based on mass balance: Importance of the packing term.* Journal of loss prevention in the process industries, 1993. **6**(5): p. 307-312.

2. Colombo, A.F., P. Lee, and B.W. Karney, *A selective literature review of transient-based leak detection methodownstream.* J. hydro-environment research, 2009. **2**(4): p. 212-227.

3. Davis, P.M., et al., *Performance of European cross-country oil pipelines Statistical summary of reported spillages in 2012 and since 1971*. 2013, CONCAWE.

4. Cech, M., et al., *Performance of European cross-country oil pipelines*

   Statistical summary of reported spillages in 2015 and since 1971. 2017.

5. Lay-Ekuakille, A., A. Trotta, and G. Vendramin. *FFT-based spectral response for smaller pipeline leak detection*. in *Instrumentation and Measurement Technology Conference, 2009. I2MTC'09. IEEE*. 2009. IEEE.

6. KOC, I.C.T., *Condition Assessment of KOC Buried Pipeline*. 2006, Kuwait Oil Company.

7. *Crude Oil System*. 2018.

8. BBC, *BP: Gulf of Mexico oil spill 'shared responsibility'*. 2013.

9. Devold, H., *Oil and Gas Production Hand book An Introduction to Oil and Gas prodduction, transport, refining, and petrochemical industry*. 2013: ABB, Oil and Gas.

10. Stafford, M. and N. Williams, *Pipeline leak detection study*. 1996, HSE Books.

11. Purcell, P.J., *Moddelling a tarnsient event at an event hydroelectric scheme*, in *12th International Comference on Pressure Surges*. 2015: Dublin, Ireland.

12. Wylie, E.B., V.L. Streeter, and L. Suo, *Fluid transients in systems*. Vol. 1. 1993: Prentice Hall Englewood Cliffs, NJ.

13. Thorley, A.R.D., *Fluid Transients in pipeline Systems*. 2004: Professional Engineering Publishing.

14. Zarzycki, Z., et al., *Simulation of transient flows in a hydraulic system with a long liquid line.* Journal of Theoretical and Applied Mechanics, 2007. **45**(4): p. 853-871.

15. Massey, B.S. and J. Ward-Smith, *Mechanics of fluids*. 9th ed. Vol. 1. 2012: Spon Press.

16. Zhang, Q., et al., *Stochastic analysis of water hammer and applications in reliability-based structural design for hydro turbine penstocks.* Journal of Hydraulic Engineering, 2011. **137**(11): p. 1509-1521.

17. McInnis, D. and B.W. Karney, *Transients in distribution networks: Field tests and demand models.* Journal of Hydraulic Engineering, 1995. **121**(3): p. 218-231.

18. Collins, R.P., et al., *How severe can transients be after a sudden depressurization.* Journal: American Water Works Association, 2012. **104**(4).

19. Taghvaei, M., et al. *leak and feature detection in water distribution network taghvaei beck boxall* in *10th International Conference on Pressure Surges, Edinburgh, UK*. 2008.

20. Taghvaei, S.M., *Leakage detection in pipeline networks*. 2007, University of Sheffield, Department of Mechanical Engineering.

21. Ghazali, M.F., *Leak detection using instantaneous frequency analysis*. 2012, University of Sheffield.

22. Meniconi, S., B. Brunone, and M. Ferrante, *Water-hammer pressure waves interaction at cross-section changes in series in viscoelastic pipes.* Journal of fluids and structures, 2012. **33**: p. 44-58.

23. Starczewska, D., J. Boxall, and R. Collins. *A method to characterise transients from pressure signals recorded in real water distribution networks*. in *12th International Conference on Pressure Surges*. 2015. BHR Group.

24. Vardy, A.E. and H. Mackenzie. *Use of pressure surge for pipeline condition monitoring*. in *11th International Pressure Surge Conf., Lisbon, Portugal* 2012.

25. Boulos, P.F., et al., *Hydraulic transient guidelines for protecting water distribution systems.* Journal (American Water Works Association), 2005. **97**(5): p. 111-124.

26. Covas, D., H. Ramos, and A.B. De Almeida, *Standing wave difference method for leak detection in pipeline systems.* Journal of Hydraulic Engineering, 2005. **131**(12): p. 1106-1116.

27. Stoianov, I.I., *Advanced techniques for detecting, locating and quantifying leaks in water transmission pipelines*. 2008, Imperial College London.

28. Geiger, G., D. Vogt, and R. Tetzner, *State-of-the-art in leak detection and localization.* Oil Gas European Magazine, 2006. **32**(4): p. 193.

29. Geiger, G., T. Werner, and D. Matko. *Leak detection and locating-a survey*. in *PSIG Annual Meeting*. 2003. Pipeline Simulation Interest Group.

30. Scott, S.L. and M.A. Barrufet, *Worldwide assessment of industry leak detection capabilities for single & multiphase pipelines*. 2003: Offshore Technology Research Center College Station.

31. Liou, C.P. *Pipeline leak detection based on mass balance*. in *Pipeline Infrastructure II*. 1993. ASCE.

32. Murvay, P.-S. and I. Silea, *A survey on gas leak detection and localization techniques.* Journal of Loss Prevention in the Process Industries, 2012. **25**(6): p. 966-973.

33. Pettit, G. and B. Morgan, *A tool to estimate the failure rates of cross-country pipelines.* Hazards XXI: Process Safety and Environmental Protection in a Changing World. IChemE, London, 2009: p. 294-302.

34. *Intelligent Pig Components*. 2015.

35. Contractor, D., *The reflection of waterhammer pressure waves from minor losses.* Journal of Basic Engineering, 1965. **87**(2): p. 445-451.

36. Meniconi, S., et al., *Small amplitude sharp pressure waves to diagnose pipe systems.* Water Resources Management, 2011. **25**(1): p. 79-96.

37. Meniconi, S., B. Brunone, and M. Ferrante, *In-line pipe device checking by short-period analysis of transient tests.* Journal of Hydraulic Engineering, 2010. **137**(7): p. 713-722.

38. Beck, S., et al., *Pipeline network features and leak detection by cross-correlation analysis of reflected waves.* Journal of hydraulic engineering, 2005. **131**(8): p. 715-723.

39. Beck, S., et al., *Pipeline system identification through cross-correlation analysis.* Proceedings of the Institution of Mechanical Engineers, Part E: Journal of Process Mechanical Engineering, 2002. **216**(3): p. 133-142.

40. Mpesha, W., S.L. Gassman, and M.H. Chaudhry, *Leak detection in pipes by frequency response method.* Journal of Hydraulic Engineering, 2001. **127**(2): p. 134-147.

41. Ferrante, M. and B. Brunone, *Pipe system diagnosis and leak detection by unsteady-state tests. 1. Harmonic analysis.* Advances in Water Resources, 2003a. **26**(1): p. 95-105.

42. Kreyszig, E., *Advanced Engineering Mathematics, 2006*. 9 th ed. John Whiley & Sons. 2006.

43. Kossatz, H., *An application of real-time unsteady flow simulation in a leakage detection software*, in *10th International Pressure Surge Conf., Edinburgh, UK*. 2008.

44. Soares, A.K., D.I. Covas, and H.M. Ramos, *Damping analysis of hydraulic transients in pump-rising main systems.* Journal of Hydraulic Engineering, 2012. **139**(2): p. 233-243.

45. Liou, J.C. and J. Tian. *Leak Detection: A Transient Flow Simulation Approach*. in *Pipeline Engineering AME Petroleum Division Publication PD V60, 1994 Proceedings of the Energy Source Technology Conference*. 1994

46. Liou, C.P., *Mass imbalance error of waterhammer equations and leak detection.* Journal of fluids engineering, 1994 **116**(1): p. 103-109.

47. Taghvaei, M., S. Beck, and W. Staszewski, *Leak detection in pipelines using cepstrum analysis.* Measurement Science and Technology, 2006. **17**(2): p. 367.

48. Randall, R.B., *Frequency analysis*. 1987: Brül & Kjor.

49. Beck, S., J. Foong, and W. Staszewski, *Wavelet and cepstrum analyses of leaks in pipe networks*, in *Progress in Industrial Mathematics at ECMI 2004*. 2004, Springer. p. 559-563.

50. Ferrante, M., B. Brunone, and S. Meniconi, *Wavelets for the analysis of transient pressure signals for leak detection.* Journal of hydraulic engineering, 2007. **133**(11): p. 1274-1282.

51. Ferrante, M. and B. Brunone, *Pipe system diagnosis and leak detection by unsteady-state tests. 2. Wavelet analysis.* Advances in Water Resources, 2003b. **26**(1): p. 107-116.

52. Jung, B.S. and B.W. Karney, *Systematic surge protection for worst-case transient loadings in water distribution systems.* Journal of Hydraulic Engineering, 2009. **135**(3): p. 218-223.

53. Bergant, A., et al., *Parameters affecting water-hammer wave attenuation, shape and timing—Part 1: Mathematical tools.* Journal of Hydraulic Research, 2008. **46**(3): p. 373-381.

54. Bergant, A., et al., *Parameters affecting water-hammer wave attenuation, shape and timing—Part 2: Case studies.* J. Hydraulic Research, 2008. **46**(3): p. 382-391.

55. Bergant, A., et al., *Further investigation of parameters affecting water hammer wave attenuation, shape and timing: part 1: mathematical tools: report on applied and numerical analysis*. 2003: Department of mathematics and computer science, University of technology.

56. Bergant, A., et al. *Further investigation of parameters affecting water hammer wave attenuation, shape and timing. Part 2: Case studies*. in *Proceedings of the 11th International Meeting of the IAHR Work Group on the Behaviour of Hydraulic Machinery under Steady Oscillatory Conditions, Stuttgart, Germany*. 2003.

57. Duan, H.-F., Y.-K. Tung, and M.S. Ghidaoui, *Probabilistic analysis of transient design for water supply systems.* Journal of Water Resources Planning and Management, 2010. **136**(6): p. 678-687.

58. Bruce, A. *Reliability analysis of electric utility SCADA systems*. in *Power Industry Computer Applications., 1997. 20th International Conference on*. 1997. IEEE.

59. Zhang, L.-b., et al., *Designing a reliable leak detection system for West Products Pipeline.* Journal of Loss Prevention in the Process Industries, 2009. **22**(6): p. 981-989.

60. Mackenzie, H., R. Campbell, and A.E. Vardy. *Use of pressure surge for unblocking hydrocarbon pipelines*. in *Proc., 12th Int. Conf. on Pressure Surges, Dublin*. 2015.

61. Kaplan, M., V.L. Streeter, and E.B. Wylie, *Oil pipeline transients.* 1966.

62. Kaplan, M., V.L. Streeter, and E.B. Wylie, *Computation of oil pipeline transients.* Journal of the Pipeline Division, 1967. **93**(3): p. 59-74.

63. Tijsseling, A., *Fluid-structure interaction in liquid-filled pipe systems: a review.* Journal of Fluids and Structures, 1996. **10**(2): p. 109-146.

64. Bergant, A., et al., *Parameters affecting water-hammer wave attenuation, shape and timing—Part 2: Case studies.* Journal of Hydraulic Research, 2008. **46**(3): p. 382-391.

65. Wang, X.-J., M.F. Lambert, and A.R. Simpson, *Detection and location of a partial blockage in pipeline systems using damping of fluid transients*, in *Critical Transitions in Water and Environmental Resources Management*. 2004. p. 1-10.

66. Kossatz, H. *Surge protection of a marine terminal: an analysis of relief system' dynamic response*. in *10th International Pressure Surge Conf., Edinburgh, UK*. 2008.

67. Colombo, A. and B.W. Karney, *Pipe breaks and the role of leaks from an economic perspective.* Water Science and Technology: Water Supply, 2003. **3**(1-2): p. 163-169.

68. Chaudhry, M.H., *Applied hydraulic transients*. 3rd ed. 2014: Springer.

69. Brunone, B., *Transient test-based technique for leak detection in outfall pipes.* Journal of water resources planning and management, 1999. **125**(5): p. 302-306.

70. Stoianov, I., et al., *Wavelet processing of transient signals for pipeline leak detection.* 2002.

71. Pudar, R.S. and J.A. Liggett, *Leaks in pipe networks.* Journal of Hydraulic Engineering, 1992. **118**(7): p. 1031-1046.

72. Vitkovsky, J.P., *Inverse analysis and modelling of unsteady pipe flow: Theory, applications and experimental verification*. 2001, Adelaide University, Department of Civil and Environmental Engineering.

73. Vítkovský, J.P., A.R. Simpson, and M.F. Lambert, *Leak detection and calibration using transients and genetic algorithms.* Journal of water resources planning and management, 2000. **126**(4): p. 262-265.

74. Vítkovský, J.P., A.R. Simpson, and M.F. Lambert. *Minimization algorithms and experimental inverse transient leak detection*. in *2002 Water Resources Planning and Management Conf*. 2002.

75. Liggett, J.A. and L.-C. Chen, *Inverse transient analysis in pipe networks.* Journal of Hydraulic Engineering, 1994. **120**(8): p. 934-955.

76. Nash, G.A. and B.W. Karney, *Efficient inverse transient analysis in series pipe systems.* Journal of Hydraulic Engineering, 1999. **125**(7): p. 761-764.

77. Covas, D. and H. Ramos. *Hydraulic transients used for leakage detection in water distribution systems*. in *Proc. 4th Intl. Conf. on Water Pipeline Systems, United Kingdom*. 2001.

78. Covas, D., et al. *Water pipe system diagnosis by transient pressure signals*. in *Water Distribution Systems Analysis Symposium 2006*. 2006.

79. Haghighi, A., D.I.C. Covas, and H.M. Ramos, *Modified inverse transient analysis for leak detection of pressurized pipes*, in *11th Internationsal Conference on Pressue Surge*. 2012: Lisbon, portugal

80. Kapelan, Z.S., D.A. Savic, and G.A. Walters, *A hybrid inverse transient model for leakage detection and roughness calibration in pipe networks.* Journal of Hydraulic Research, 2003. **41**(5): p. 481-492.

81. Nicholas, R.E. *Leak detection on pipelines in unsteady flow*. in *Proc. Ann. Meeting of ASME: Forum on Unsteady Flow, New York*. 1990.

82. Nicholas, R. *Leak detection by model compensated volume balance*. in *Pipeline Engineering Symposium*. 1987.

83. Jönsson, L. and M. Larson, *Leak detection through hydraulic transient analysis*, in *Pipeline systems*. 1992, Springer. p. 273-286.

84. Lee, P.J., et al., *Leak location using the pattern of the frequency response diagram in pipelines: a numerical study.* Journal of Sound and Vibration, 2005a. **284**(3-5): p. 1051-1073.

85. Lee, P.J., et al., *Frequency domain analysis for detecting pipeline leaks.* Journal of Hydraulic Engineering, 2005b. **131**(7): p. 596-604.

86. Duan, H.-F., et al., *Leak detection in complex series pipelines by using the system frequency response method.* Journal of Hydraulic Research, 2011. **49**(2): p. 213-221.

87. Brunone, B. and M. Ferrante, *Pressure waves as a tool for leak detection in closed conduits.* Urban Water Journal, 2004. **1**(2): p. 145-155.

88. Wang, X.-J., et al., *Leak detection in pipelines using the damping of fluid transients.* Journal of Hydraulic Engineering, 2002. **128**(7): p. 697-711.

89. Taghvaei, M., S. Beck, and W. Staszewski, *Leak detection in pipeline networks using low - profile piezoceramic transducers.* Structural Control and Health Monitoring, 2007. **14**(8): p. 1063-1082.

90. Ghazali, M., et al., *Instantaneous phase and frequency for the detection of leaks and features in a pipeline system.* Structural Health Monitoring, 2011. **10**(4): p. 351-360.

91. Arbon, N.S., et al. *Field validation of transient analysis for in-line valve condition assessment*. in *Proc., 10th Int. Conf. on Pressure Surges*. 2008. BHR Group, Cranfield, UK.

92. Butterfield, J.D., R.P. Collins, and S.B. Beck. *Feature extraction of leaks signals in plastic water distribution pipes using the wavelet transform*. in *ASME 2015 International Mechanical Engineering Congress and Exposition*. 2015. American Society of Mechanical Engineers.

93. Butterfield, J., et al., *Experimental investigation into vibro-acoustic emission signal processing techniques to quantify leak flow rate in plastic water distribution pipes.* Applied Acoustics, 2017a. **119**: p. 146-155.

94. Butterfield, J.D., et al., *Prediction of leak flow rate in plastic water distribution pipes using vibro-acoustic measurements.* Structural Health Monitoring, 2017b: p. 1475921717723881.

95. Chaudhry, M.H. *Analysis and control of hydraulic transients: practical aspects and considerations*. in *Proc., 12th Int. Conf. on Pressure Surges, Dublin*. 2015.

96. Collins, R., J. Boxall, and S.B. Beck, *Onset Detection Of ransient Waves using a Novel Experimental Data Set*, in *11th International Pressure Surge Conf., Lisbon, Portugal* 2012: Lisbon, Potrugal.

97. Ghazali, M., et al., *Comparative study of instantaneous frequency based methods for leak detection in pipeline networks.* Mechanical Systems and Signal Processing, 2012. **29**: p. 187-200.

98. Motazedi, N. and S. Beck, *Leak detection using cepstrum of cross-correlation of transient pressure wave signals.* Proceedings of the Institution of Mechanical Engineers, Part C: Journal of Mechanical Engineering Science, 2017: p. 0954406217722805.

99. Louati, M. and M.S. Ghidaoui. *On the Behaviour of High Frequency Acoustic Waves in Pressurized Inviscid Fluid in a Conduit*. in *12th International Conference on Pressure Surges*. 2015.

100. Ferrante, M., B. Brunone, and S. Meniconi, *Leak-edge detection.* Journal of hydraulic research, 2009. **47**(2): p. 233-241.

101. Bergant, A. and U. Karadžić. *Developments in valve-induced water-hammer experimentation in a small-scale pipeline apparatus*. in *Proceedings of the 12th International Conference on Pressure Surges (Dublin)(Cranfield,)*. 2015.

102. Lange, F.H., *Correlation techniques*. 1987, N.J. : Van Nostrand, Englewood Cliffs.

103. Smith, S.W., *The scientist and engineer's guide to digital signal processing*. 2015.

104. Motazedi, N. and S. Beck. *The use of the cross-correlation of two signals as a transient leak detection method Motazedi*. in *Proc., 12th Int. Conf. on Pressure Surges* 2015. Dublin.

105. Covas, D., et al., *Water hammer in pressurized polyethylene pipes: conceptual model and experimental analysis.* Urban Water Journal, 2004. **1**(2): p. 177-197.

106. Brunone, B., et al., *Velocity profiles and unsteady pipe friction in transient flow.* Journal of water resources planning and management, 2000. **126**(4): p. 236-244.

107. Urbanek, J., et al., *Leak detection in gas pipelines using wavelet-based filtering.* Structural Health Monitoring, 2012. **11**(4): p. 405-412.

108. Moody, L.F., *Friction factors for pipe flow.* Trans. Asme, 1944. **66**: p. 671-684.

109. Covas, D., et al., *The dynamic effect of pipe-wall viscoelasticity in hydraulic transients. Part I—Experimental analysis and creep characterization.* Journal of Hydraulic Research, 2004. **42**(5): p. 517-532.

110. Covas, D., et al., *The dynamic effect of pipe-wall viscoelasticity in hydraulic transients. Part II—Model development, calibration and verification.* Journal of Hydraulic Research, 2005. **43**(1): p. 56-70.

111. Wood, D.J., et al., *Numerical methods for modeling transient flow in distribution systems.* Journal (American Water Works Association), 2005. **97**(7): p. 104-115.

112. Ramos, H. and D. Covas, *Water pipe system response under dynamic effects.* Journal of Water Supply: Research and Technology-Aqua, 2006. **55**(4): p. 269-282.

113. Leite, P., et al., *Evaluation of flow resistance in unsteady pipe flow: numerical developments and first experimental results.* 2012.

114. Ghidaoui, M.S., et al., *A review of water hammer theory and practice.* Applied Mechanics Reviews, 2005. **58**(1): p. 49-76.

115. Duan, H.-F., et al., *Unsteady friction and visco-elasticity in pipe fluid transients.* Journal of hydraulic research, 2010. **48**(3): p. 354-362.

116. WICHOWSKI, R., *Comparative analysis of water-hammer calculation by the approximate and the complete methods of characteristics.* Periodica Polytechnica. Civil Engineering, 1991. **35**(1-2): p. 107.

117. Vardy, A. and A. Tijsseling. *Method of characteristics:(Why) is it so good?* in *Proc., 12th Int. Conf. on Pressure Surges, Dublin*. 2015.

118. Da Silva, H.V., et al., *Leak detection in petroleum pipelines using a fuzzy system.* Journal of Petroleum Science and Engineering, 2005. **49**(3-4): p. 223-238.

119. Laurentys, C., et al., *Design of a pipeline leakage detection using expert system: A novel approach.* Applied Soft Computing, 2011. **11**(1): p. 1057-1066.

120. Institue, A.P., *Manual of Petroleum Measurement Standard Chapter-Vocabulary*. 1994.

121. LTD., H.H.I.C., *Surge Analysis For New Crude Loading Systen at NPP & MS*. 2006: Kuwait.

122. KME Group, *Yorkshire Tube Systems*. 2008.

123. Wilo, *Wilo-Helix VE 2..., 4..., 6..., 10..., 16...* 2015.

124. SCATTERGOOD & JOHNSON, L., *Gems Pressure Transducer Clibration Chart*. 2015.

125. UK Copper Board. *Copper Tubes in demostic heating system*. 2013; Availaboratoryle from: UKcopperboard.co.uk Note:Copper Initiative replaces the activities carried out by the UK Copper Board.

126. Covas, D.I., et al. *Measurement of hydraulic transients in a metal pipe rig: effects of free-air, cavitation and pipe axial-deformation*. in *11th International Pressure Surge Conf., Lisbon, Portugal* 2012.

127. *MathWorks*. Availaboratoryle from: https://uk.mathworks.com/.

128. Brown, F., D.L. Margolis, and R.P. Shah, *Small-amplitude frequency behavior of fluid lines with turbulent flow.* Journal of Basic Engineering, 1969. **91**(4): p. 678-693.

129. Ferras, D., et al., *Hydraulic transients in straight and coil pipe rigs*, in *12th International Pressure Surge Conf.* 2015: Dublin, Ireland.

130. Tijsseling, A.S., et al., *Skalak's extended theory of water hammer.* Journal of sound and vibration, 2008. **310**(3): p. 718-728.

131. Simão, M., J. Mora-Rodriguez, and H. Ramos. *Interaction between hydraulic transient events and structure vibration*. in *Proc., 12th Int. Conf. on Pressure Surges, Dublin*. 2015.

132. Williams, D., *Waterhammer in non-rigid pipes: precursor waves and mechanical damping.* Journal of Mechanical Engineering Science, 1977. **19**(6): p. 237-242.

133. Clarke, L., et al., *Measurement of fluid flow rates through cracks.* International journal of pressure vessels and piping, 1997. **71**(1): p. 71-75.

134. Brown, F.T., *The transient response of fluid lines.* Journal of Basic Engineering, 1962. **84**(4): p. 547-553.

135. Rougier, J. and M. Goldstreamtein, *A Bayesian analysis of fluid flow in pipe - lines.* Journal of the Royal Statistical Society: Series C (Applied Statistics), 2001. **50**(1): p. 77-93.

Appendix A Experimental Rig Manual

A.1 Introduction

This manual includes details of the rig components, dimensions, operating philosophy, control/data acquisition and limitations. The last is important to be followed by the user to be aware of the limitations of the rig to avoid operational hazards and ensure the safe operating of the rig.

A.2 Rig components

A.2.1 Pump

The pump is high pressure centrifugal Wilo type model Helix VE 211-1/16/E/KS. It is high efficacy multistage pump with numerous control modes. The pump can deliver up to 90*m* head of pressure. In the chart presented in Figure A-0-1, the flow against head, shaft power, efficiency, and NPSH values.

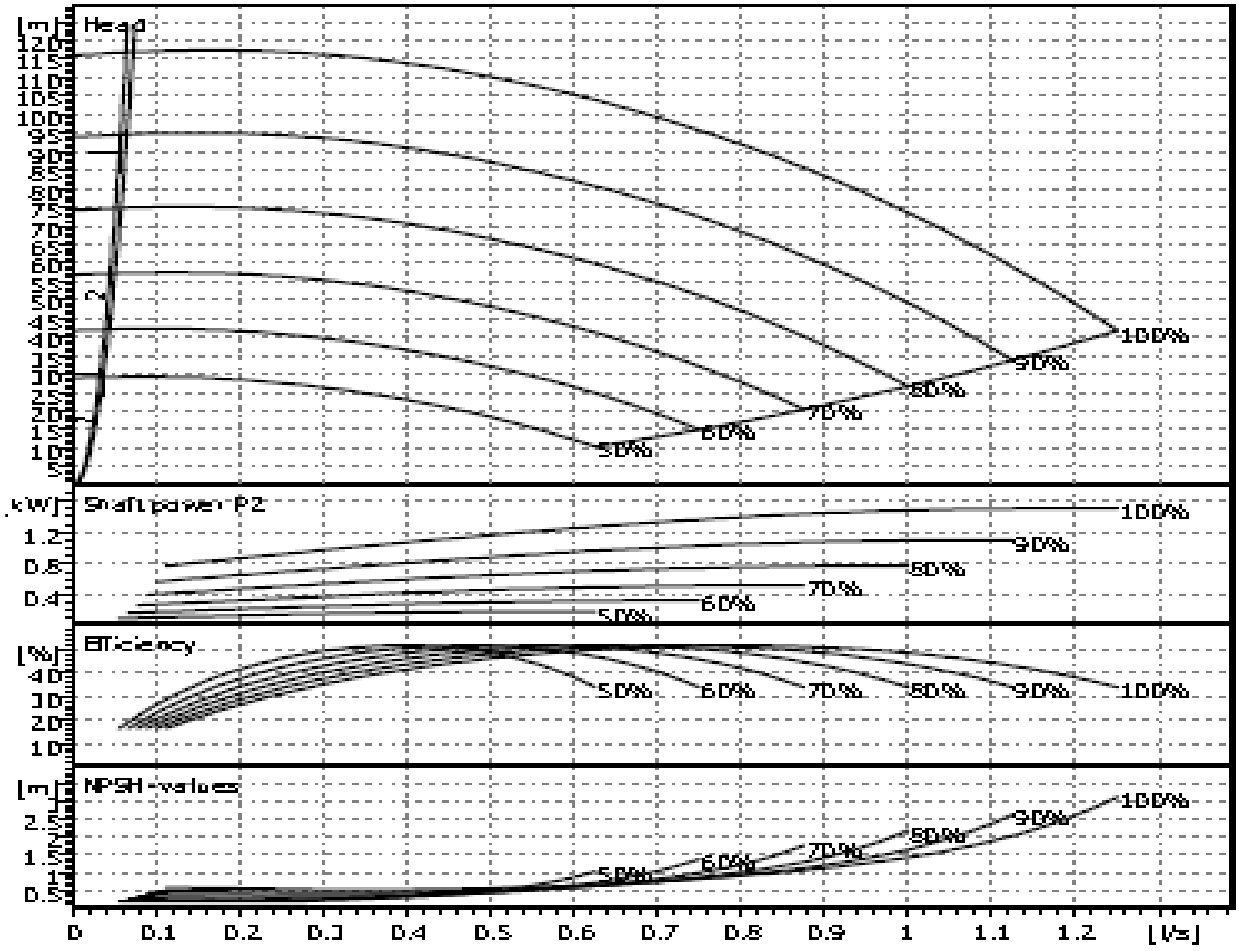

Figure A-0-1: Pump flow rate against head, shaft power, efficiency, and NPSH values[123].

A.2.2 Rotameter

Rotameter calibration done on two days for different rotameter readings. The temperature was 20°C in the laboratory. As shown in the Figure A-0-2, the rotameter reading is along the horizontal axis while the flow rate in both litre per second and per minute is presented on the vertical axis. Calibration of the rotameter by measuring the mass of water in grammes collected in a bucket for a time period 2 minutes. The masses used to calibrate the rotameter were weighted on a scale to ensure their accuracy.

In addition, the tube size is 14 and the floating is from steel type. The tube diameter is 14.2 mm and the weight is 16.5 gm.

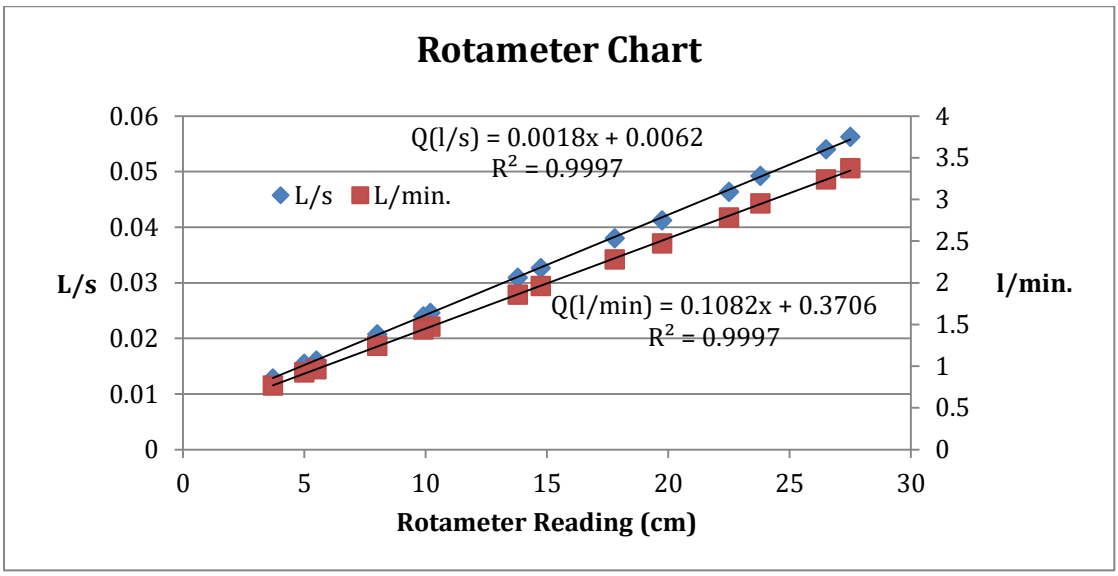

Figure A-0-2: Calibration of flow rotameter.

The flow through the rig could be estimated by four methods:

1. Rotameter readings.
2. Pump Characteristics curves.
3. Joukowski equation using an empirical wave speed.
4. Darcy-Weisback equation.

The flows estimated by each of these methods coincided with each other within the bounds of acceptable accuracy. The comparison between the mentioned methods were undertaken and calculated for a rotameter flow rate of 2 *l/minutes*. The equivalent flow rates were 2.13 *l/minutes* (6.5%) for the pump chart, 2.06 l/minutes (3.02%) for the Joukowski equation, and 2.2 *l/minutes* (10%) for the Darcy-Weisback equation.

A.2.3 Pressure Transducer

The pressure transducers are Gems model 1/4" digital pressure transmitter 4 to 20mA output signal and it can measure pressure from 0 to 10bar. The Pressure transducers have the following original calibration data from the vendor which is converted into chart, as shown in Figure A-0-3.

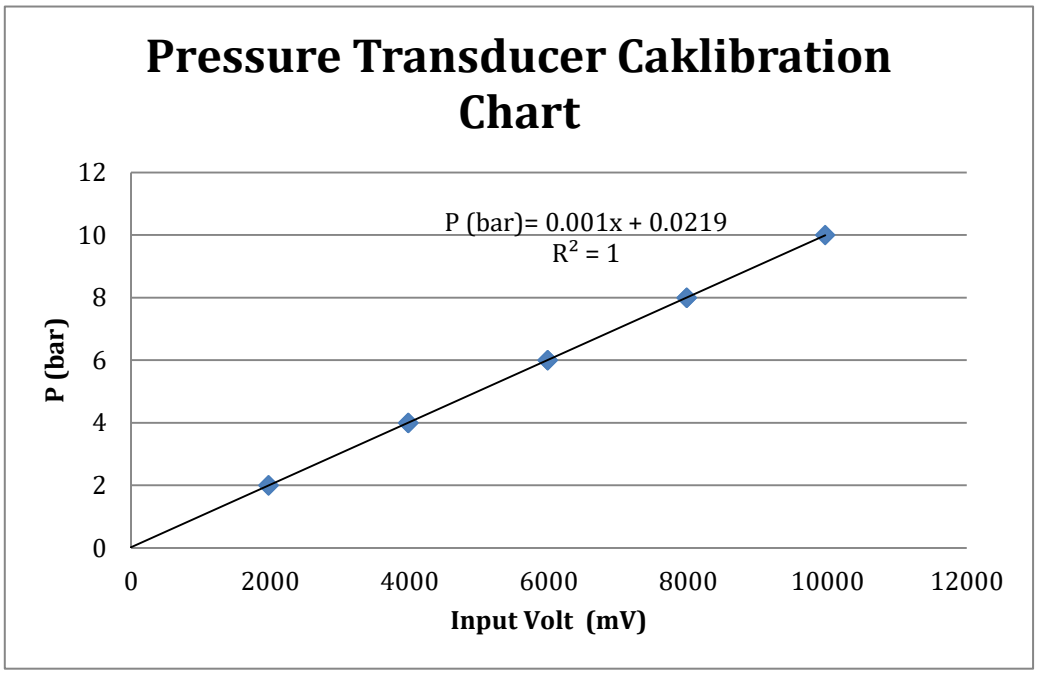

Figure A-0-3: Pressure Transducers calibration data [124].

A.2.4 Control and Data acquisition system

The data acquisition system should be adequate to ensure research objectives are achieved. Therefore, the equipment is used in this study had to be able to measure pressure transients at sufficiently high frequency to locate leaks along the pipe. Initial calculations were undertaken to identify the required frequency with respect to the pipe length. In real system, the ten-meter tolerance is equivalent to half a meter. The proportional between the precision length to the total real filed length is the equivalent to the experimental rig. This concluded the half meter of tolerance for the rig. By using this spatial distance and taking into account the rig dimensions and its wave speed, that gives a required sampling frequency of 5000*Hz*. The selected input module is '' National Instrument NI-9203''. It has 8 channels with total frequency of 200K *Hz*. Significantly is exceeding the required 5000 Hz. The output module is NI-9265 which has four channels and output current from 0 to 20 *mA.*

The chassis is NI-9174 which contains the two modules and integrated with LabVIEW program to control the pump and recording the data simultaneously. The program is installed on a laptop which collects and analyses the data.

Initially, some experimental runs at a steady state flow ranging from 0.6 up to 2 l/s were undertaken without any leak. This step was undertaken to estimate wave speed of the system and ensure the accuracy of the theoretical predictions and the measured data. Transients were induced by manually closing a ball valve and simultaneous recording of the pressure at the five different points along the pipe. The wave speed was calculated by measuring time taken by the wave reached the measuring points together with the rig length. The average wave speed of the system for the five readings was computed to be 1259.9 m/s, which accords with the theoretical value of 1260m/s.

No automatic synchronization between the start of transient measurements and the triggering of the transient event. It was done manually and later a numerical code was written to align the various pressure traces. When the timer of the data code reached zero, then the valve was closed at the same time. The inlet pressure is 4.71 bars for the flow of 2 *l/minute*.

A.2.5 The LabVIEW control modes

In this section, the various modes to control the experimental rig and collect the data will be demonstrated individually. Each mode's purpose and method of operation will be explained. Furthermore, LabVIEW interfaces will be shown in detail. All panels have the ability to alter the flow rate, show the five pressure transducer readings, the sampling rate, and graphical pressure/time trace for each of the five pressure transducers.

However, there are some differences in the modes of operation. The first interface is shown in Figure A-0-4. This panel enables the data sampling rate to be varied from 10 Hz to 5k Hz when selecting the start manual shut-off button.

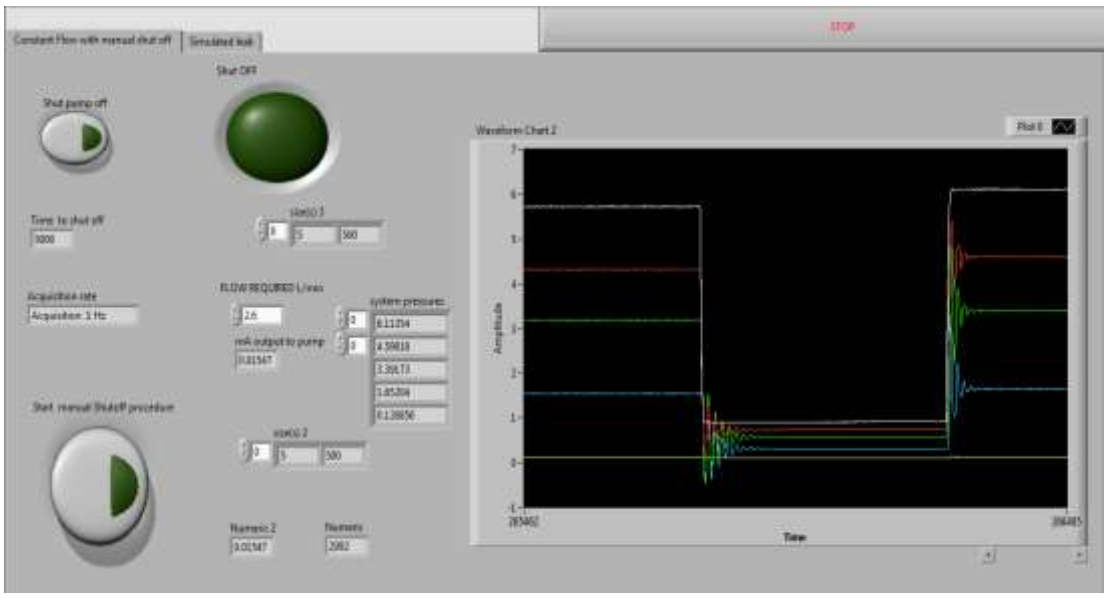

Figure A-0-4: LabVIEW Data acquisition system with constant Flow with Manual shut-Off interface.

The second panel is presented in Figure A-0-5. The panel operates the pump ramping with selected time. This feature has been added to the system control to explore the effect on the water hammer of changing the flow rate with designated time. Unfortunately, the pump response was not linear to the input time; therefore, the tests were done on instantaneous ramping.

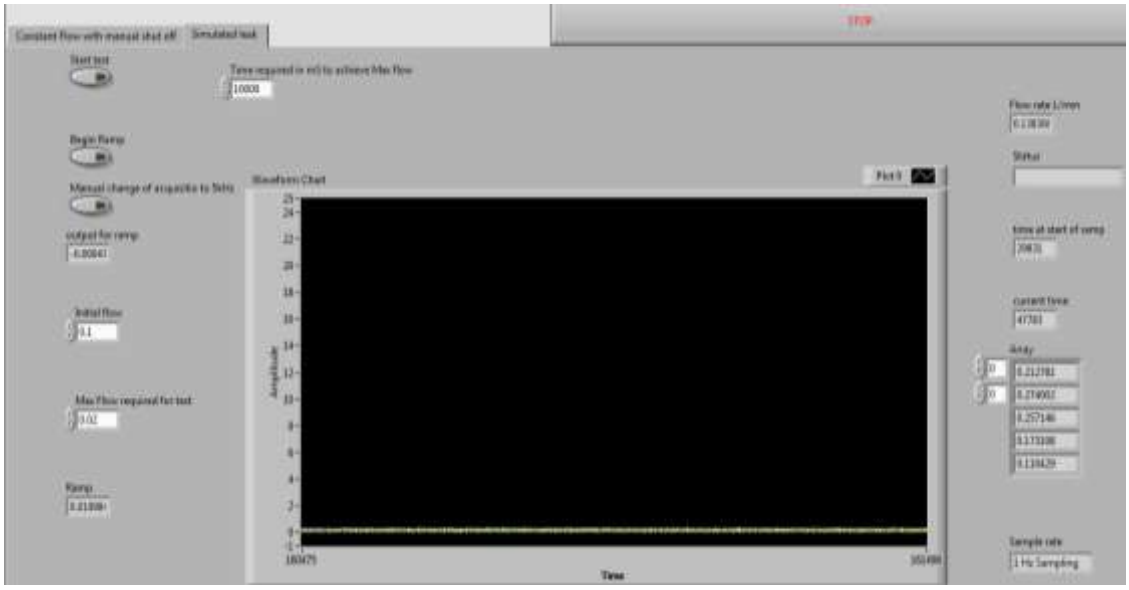

Figure A-0-5: LabVIEW Data acquisition system with simulated Leak interface.

A.2.6 Limitations

When operating this rig, it is important that the maximum transient pressures do not exceed permissible limits. The pressure transducer is limited to 10 bar. Thus, in steady-state flow the maximum flow through the pump is 2 *l/minute* for a head of 90 *m.* However, it is also important to ensure that the Joukowski pressure for a sudden closure does not exceed 10 *bars.* Since the maximum Joukowski head for downstream valve closing is about 9.5 *bars,* a maximum flow rate of 1.8 *l/minute* was considered appropriate for these investigations. The bypass connection could be used to release excess pressure, if required.

A.2.7 Operating Procedures

Before operating the system checks were carried out:

1. When the rig was being refilled, the pump air valve should be open to release the air. After the pipe has been filled, the valve was closed. To protect the pump, carrying out this procedure was prudent every time before switching it on.
2. All valves were checked to be in correct position fro the required test.
3. When the pump was running, any air entrained in the flow could be seen through the rotameter. If present, it was essential to de-air the pipeline before starting any experiments.
4. Provided there was sufficient water in the tank, could be run at varying flow rates to remove the air.
5. The pressure transducer measurements the pump operating pressure head, the flow rate as measured by the LabVIEW software, and the rotameter readings should all correlate with the data presented in Table 6-3. That means all equipment was working in harmony within an acceptable tolerance. If any deviation in the readings was observed, the gears or the rig settings, should be checked.

The operation of the experimental rig should proceed as follows:

1. Switch on the LabVIEW, DAQ system and the pump.
2. Select the required mode.
3. Run the LabVIEW and set the desirable flow rate in the interface.
4. The software will record the data for each single run, whatever the time length.
5. The LabVIEW has an option to record the data at a frequency of either 10 Hz or 5k Hz.

Appendix B Applied MOC code Example

At the beginning, to ensure that the code was working perfectly, the system in Bergent *et al.* [64] was simulated and the results were identical. In this section the test pipeline system consists of two tanks connected by a copper pipe with length of 37.2m. The inner diameter and the wall thickness are 22mm and 1.6mm, respectively. The pipe has two different connection levels with the tanks, it connecting with tank 1 at 2.03m and with tank 2 at datum level. The system details are illustrated in Figure B-1.

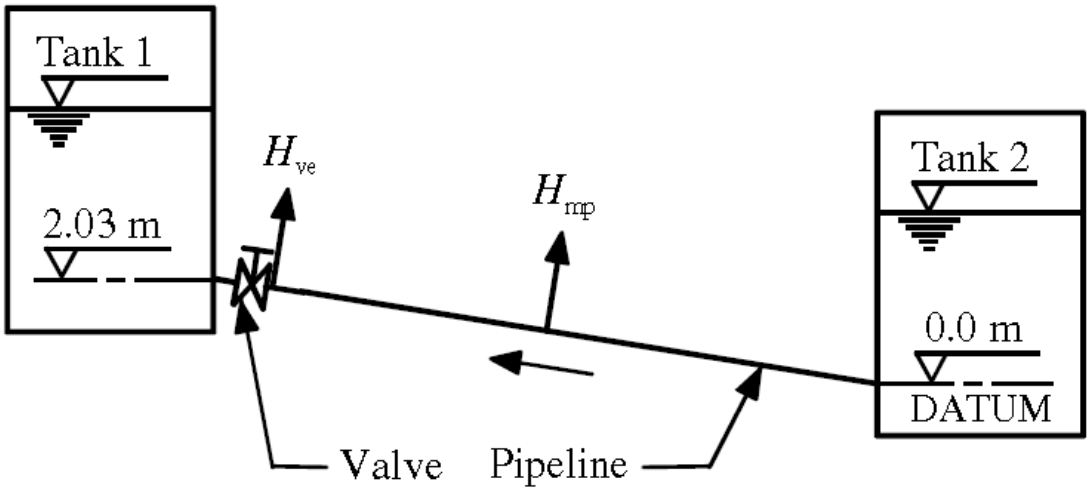

Figure B-1 : Test apparatus [64].

The initial flow is 0.0076 x 10^{-3} m^3/s (Re=4360). The leak has a diameter of 0.52mm, and the weighted area $C_d A_{Or}$=15.25 x $10^{-8} m^2$. The leak flow is 5% of the steady-state flow and its area is 0.056% of the pipe cross-sectional area. The wave speed is 1319m/s. For numerical code purposes, the system was divided into 32 segments. The leak node was at distance of 13.95m (3/8th) upstream of the valve. The computed transient pressure trace following sudden closure of the valve, is shown in Figure B-2,. The blue line is the pressure at the valve, while the green line represents the pressure at the midpoint.

In addition, the code was checked with Wylie & Streeter [12] , example 3-1. The outputs were identical, between the code developed by the author and that from benchmark code.

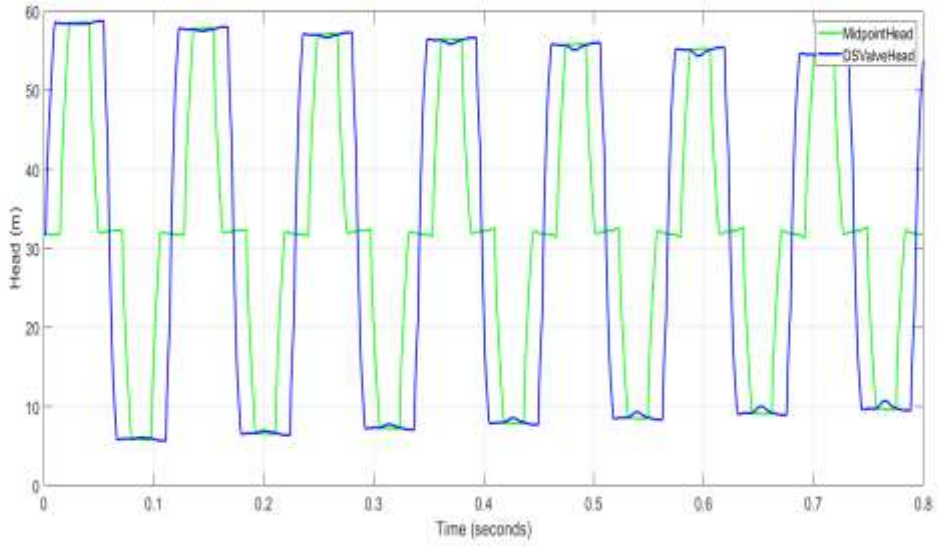

Figure B-2: Computed pressure trace following valve closure for the Bergant [64] case study. Leak point at 3/8th of total length (13.95m) upstream from the valve.

Figure B-3 shows the result of shifting the leak node point from the downstream to upstream side with the same ratio of length (3/8th). The effect of the leak was similar to the previous case in magnitude; however, the signs were opposite.

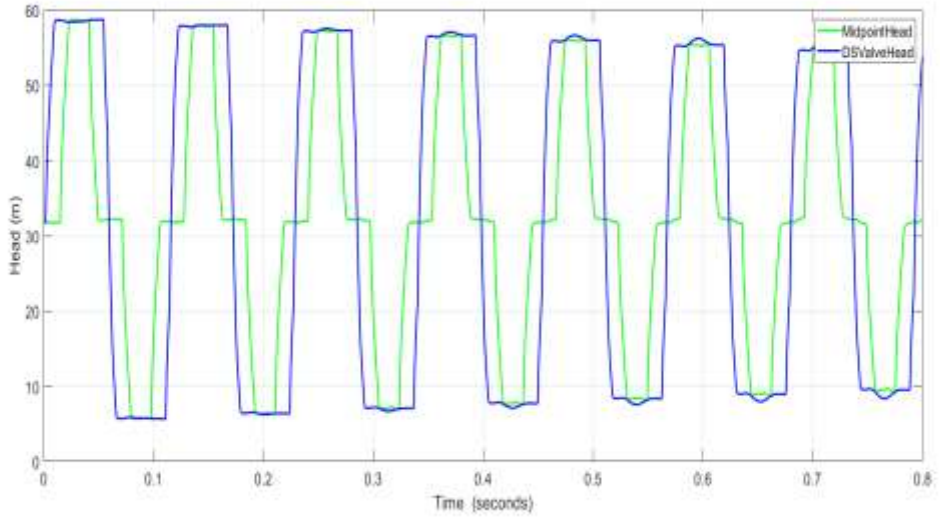

Figure B-3: Leak at 3/8th point from the upstream reservoir.

Appendix C Matlab Codes

In this section the codes has been used for the MOC numerical calculations, filtering the experimental data, and alignment different runs; are included. Note that, the percentage symbol '%' in Matlab is a comment sentences, not an execution one. So, mostly is used for explanations and make the code easy to follow, or either reveals the statement usage. In other occasions, sometimes the comment symbol is used to write another condition. For example, the experimental rig has different inputs from other applied cases, like the real filed or published case. So, instead of writing the code for each case, the initials conditions are kept under the comments until it is used. The same procedure is done on the upstream and downstream points. The conditions, open to atmosphere and closing valve are written for the downstream point.

Note: due to typing format, some comment sentences in the code are in two lines. It copied to Matlab without the percentage mark'%', the software consider it as an execution statement. So in general, when a statement in the following codes are in green colour, that is means, it is belong to a comment statement not an execution one.

The MOC codes have another type which dealing with steps as functions for example, the steady-state and the transient event. The input data is in text file. The two type of codes do the same function, so here for simplicity, the script files are shown.

C.1 Rig Leak Code

It can be used for the rig or the Bergent *et al.* [64] example, based on the input data. The input data can be changed to simulate the rig, real field parameters. This caused by changing the input data and used the 'uncomment' features in the Matlab code to enable the calculated case. The input data are:

1. Pipes: length, wall thickness, Young's modulus, and diameter.

2. Reservoir head: It fixed and represents the water elevation above the datum.
3. Leak: leak node number, leak orifice coefficient.
4. Others: maximum calculation time, valve orifice coefficient, acceleration of gravity, wave speed, valve closing time.

The program reads the input data and then calculated the steady state. Then, it calculates the transient event. The outputs are the head and the flow for all computational nodes.

```
% L: Pipe Length (m), g: gravitational acceleration = 9.81 (m/s^2)
% E: Modules, HR: Reservoir Head (m),H0 : Valve Head (m)
% N: integer (no. of pipe segments (even)),Ti: initial time valve
(sec.)
% D: Time step (sec.) Dx: internal distance between sections (m),
% H(i): Pressure Head (m) for section (i) , Q(i): volumetric Flow Rate
% (m^3/s) for section (i), R: Resistance coefficient, F: Darcy-
% Weisback
% friction factor, Ti: initial Tau value, Tf: final Tau value
% tc: valve operation time (sec.), a: wave speed (m/s)
% DHf: each Head loss due to friction for each Dx
% B=a/(G*A) pipeline impedance, R=Resistance Coefficient
%

clear all              %
close all              %   to clear any previous data
clc                    %

% %%%%%%%%Temporary data until open a read file%%%%%%%%%%%%

%%%%Bergent Parameters %%%%%
% L=37.2; a=1319; D=0.022; f=0.078; HR=32; tc=0.009; ti=1;tf=0;
Tmax=0.8; E=0.75;
% Q0=0.000076;CdA0=0.000274; g=9.81; N=32; A=pi*(D/2)^2; t=0; %
Cd=0.72, get from ClkAor (Bergant)
% %Q for the rig, the leak will be at 3/8 (13.95m) from DOWNSTREAM ;
at node 13

%%%% Rig Parameters %%%%
L=800; a=1260; D=0.01; f=0.039; HR=20; tc=0.009; ti=1;tf=0; Tmax=5;
E=0.75;
CdA0=0.009; g=9.81; N=64; A=pi*(D/2)^2; t=0;NLK=9;CdALK=0.0000001365;
%
Q0=0.0000028; % Q for the rig, the leak will be at 1/8 (100m) ; at
node 9

% read the data from fil Simple.dat, will be created later.%%%%%%%%

%%%% fid=fopen(Simple.dat), ) %
%%%% L,a,D,F,,,,,,,,=fread(fid,'Simple')
% Calculate the Dt and Dx
Dx=L/N ;
```

```
Dt=Dx/a;

% Calculate B & R

R=f*L/(2*g*D*A^2*N) ; % Resistance coefficient,
B=a/(g*A);  % Pipe-line impedance

% Steady State Solver
%Q0=CdA0*sqrt(2*g*HR);


Hf=4*f*L*Q0^2/(A^2*D*2*g);


DHF=HR-Hf;
     % Assume the variables are in matrix of position and time, i.e
            % H(x,t) and Q(x,t)

        % Since Matlab accepts only positive integer as array index,
we
        % avoid the Zero, assume t=0 will be t=1 then to show the
results,
         % subtract 1.

   for i=1:N;             % Since start from 1, so add 1 to N. (avoid
the zero because of MATLAB error)
    H(1,1)=HR;          % should be at reservoir B C but copy here to
maintain seq.

        if i==10 % 1/8 node (100m) OR 22 3/8(13.95m) if Bergent
% Using the percentage of Q0 at the first step has done By Bergent
(2008),
% then the orifice eq. for transient solver
%             QLK(1)= 0.000000152*sqrt(2*g)*sqrt(H(12,1)); % eq
Qlk=Cd*A(lk)sqr(2g*(H(lk)-Z))
%              Q(13,1)=Q0-QLK(1); % (Stoianov,2008, P281)Cd=0.68
%              Q0=Q(13,1); % after the leak point, Q0 will change,
Q(11,t)=QLK(t)+Q(13,t)
       QLK(1)=0.05*Q0;    % Similar to the transient solver, when the
       Q(10,1)=Q0-QLK(1); % transient calculate for node 4, the
Q(2,5,t) should equal the upstream
       Q0=Q(10,1);         % flow before the leak, so Q(2,6,t) after
the downstream the leak.

        end

        H(i+1,1)=H(1,1)-i*R*Q0^2; % to get H for each point at steady
state
        Q(i,1)=Q0;

        Q(i+1,1)=Q0; % just to increase the array to have the same
size
                     % H, so it can be table & write together at
same
```

```
                        % spreadsheet (xlsx file)
        QNS(1)=Q0;
    end


    %%%%%%%%% End SS leak code %%%%%

    %%%%%%%%%% Code for SS without leak %%%%%
%     QNS(1)=Q0 ;
%
%      H(i+1,1)=HR-i*R*Q0^2;%Hf*i/N; % to get H for each point at
steady state
%
%
%      Q(i,1)=Q0;
%
%      Q(i+1,1)=Q0;
%      QNS=Q0;
%     end
%%%%%%%% Code for SS Without leak %%%%%%%%

%%%% Transient Solver %%%%%%%%

NoTimeSteps=Tmax/Dt; % change the time to time steps no.s then convert
it
                     % again, to be included in the plots and data,
                     % Q(2,1)i.e @ discrete 2 time 0
NoTimeSteps=round(NoTimeSteps); % Convert to integer.

tc=tc/Dt;    % to convert time steps to real time, *Dt
                              % in tau eq.

%%%%%%%% LEAK at node 21 on 13.95m from DOWNSTREAM Bergent OR 9 Rig
%%%%%%%%%

%QLK=zeros (1,NoTimeSteps); % Reallocate the variable to avoid
%changing the array size.
Q9D=zeros (1,NoTimeSteps); % Reallocate the variable to avoid
%changing the array size.
Q9U=zeros (1,NoTimeSteps); % Reallocate the variable to avoid
%changing the array size.
Q9U(1)=Q(8,1);  % Since at node 12 (leak node) the upstream flow is
%different from
Q9D(1)=Q(10,1);  % the downstream flow. These should be valid in SS
%and transient
QLKU(1)=Q(NLK-1,1);  % Used for general Distrecte_Leak_Solver
QLKD(1)=Q(NLK+1,1);  %
%QLK(1)=0.0000038;
% H=zeros (1,NoTimeSteps);
% Q=zeros (1,NoTimeSteps);
%%%%%%%%%%%%%%%%%%

  hold on

  % Solve for the different points with the time
  % step
for t=2:NoTimeSteps;
```

```
% 1st: Reserviour B C
H(1,t)=HR; % as in the example 3-1
Q(1,t)=(HR-H(2,t-1)+B*Q(2,t-1))/(B+R*abs(Q(2,t-1)));


%second internal points
for i=2:N % N increased by 1 (see Line 43) to avoid the zero index,ie
% H(0)

H(1,t)=HR; % Actually the H(0) to avoid the Zero as index

%%%%% Commands for Discrete Leak Solver%%
%if i==NLK-1 % since the calculation begin at the node upstream the
leak node directly.
% Discrete_Leak_Solver (single node)
%[H,Q,QLK,QLKU,QLKD,i ] =
Discrete_Leak_Solver(H,Q,B,R,CdALK,t,i,NLK,QLK,QLKU,QLKD);

 if i==8 %  REMEMBER i=NLK-1
       % Since the coefficients related to i=11, so the head
       % calculated here while the flow for 11 calculated in previous
       % node(=5) with leak equation.

   CP=H((i-1),t-1)+B*Q((i-1),t-1);%
   BP=B+R*abs(Q((i-1),t-1));%
   CM=H((i+1),t-1)-B*Q9U(t-1); %    The flow for the -ve
charachteristics
   BM=B+R*abs(Q9U(t-1)); %         is Q9U(t)

H(i,t)=(CP*BM+CM*BP)/(BP+BM);
Q(i,t)=(CP-CM)/(BP+BM);

elseif i==9    % Leak Node , i= NLK
% NOT WORKING, gives Qlk>Q0, so used the percentage of Q0 at the %
first step assume 5%Q0 & DLK=3%D (like Bergent, 2008),
% H5+Clk*Alk*sqrt(2*g)BP*BM/(BP+BM)*sqrt(H5)+(CP*BM+CM*BP)/(BP+BM)
% solve for H5+b*sqrt(H5)+c Quadratic equation, let
CP=H((i-1),t-1)+B*Q((i-1),t-1);
BP=B+R*abs(Q((i-1),t-1));
CM=H((i+1),t-1)-B*Q((i+1),t-1);
BM=B+R*abs(Q((i+1),t-1));

 b=(0.0000001365^2*BP*BM)/(BP+BM);
c=0.0000001365^2*(CM*BP+CP*BM)/(BM+BP); % REMEMBER; the # should be
reviewed for the

 QLK(t)=(-b+sqrt((b)^2+4*c))/2;% H5 is actual sqrt(H5)
  H(9,t)=(QLK(t))^2/0.0000001365^2; %%%H at NLK
  %QLK(t)= 0.000000673*H12; % eq Qlk=Cd*A(lk)sqr(2g*(H(lk)-
%Z))(Bergent 2008)
  % Redefind Q(11,t) at the same time, to include the leak node,
   Q9U(t)=(CP-H(9,t))/BP;%%%%%%%% H at NLK
   % Also redeined Q(13,t) is including.
   Q9D(t)=(H(9,t)-CM)/BM;
```

```
 Q(9,t)=Q9U(t)+Q9D(t); % just for reference, not including in
%computational for adjacent points
                          % See above for node 11 and below for node
13
   %%% Ensure that, Q12U(t)-QLK(t)-Q12D(t)=0; valid for all time steps
   %%% Use C+ equation to defined H(13,t) based on the node 13 (leak),
   %%% since each time step node 12 redefine Q(11,t) & Q(13,t)

    elseif i==10    % i=NLK+1
       % Since the coefficients related to i=13, so the head
       % calculated here while the flow for 4 calculated in previous
       % node(=5) with leak equation.

   CP=H((i-1),t-1)+B*Q9D(t-1);% The flow for the -ve characteristics
   BP=B+R*abs(Q9D(t-1));%     is Q12D(t)
   CM=H((i+1),t-1)-B*Q((i+1),t-1); %
   BM=B+R*abs(Q((i+1),t-1)); %

  H(i,t)=(CP*BM+CM*BP)/(BP+BM);
  Q(i,t)=(CP-CM)/(BP+BM);

   else % General eqautions
CP=H((i-1),t-1)+B*Q((i-1),t-1);
BP=B+R*abs(Q((i-1),t-1));
CM=H((i+1),t-1)-B*Q((i+1),t-1);
BM=B+R*abs(Q((i+1),t-1));

H(i,t)=(CP*BM+CM*BP)/(BP+BM);
Q(i,t)=(CP-CM)/(BP+BM);
end

end
% 3rd D/s point, assume sudden closing, QNS=0.


%Q(11,t)=0.2074; % TO CHECK THE TRASIENT SOLVER, FIXED THE DOWNSTREAM
CODITIONS
%H(11,t)=H(11,1);

CP=H(N,t-1) +B*Q(N,t-1);
BP=B+R*abs(Q(N,t-1));


if t<tc
    tau=ti-(ti-tf)*(t/tc)^E;

else tau=tf;
end



Cv=tau^2*Q0^2/(2*H(N,t));% shifted up to check% derivate from the
valave given equation(Ex 3-1)
QNS(t)=-BP*Cv+sqrt((BP*Cv)^2+2*Cv*CP);
H(N+1,t)=CP-BP*QNS(t);
Q(N+1,t)=QNS(t);      % compute the last point and defined it as (N+1)
is necessary for time computation
```

```
                        %  for each time step.

% when assume sudden closing, active the following:
% QNS(t)=0;
% CP=H(N,t) +B*Q(N,t);
% BP=B+R*abs(Q(N,t));
% H(N+1,t)=CP-BP*QNS(t) ;
% Q(N+1,t)=0;



%
%                                % Plot and write the data
%
% plot(t*Dt,H(16,t),'k*',t*Dt,H(33,t),'bd')%,t*Dt,tau,'+'); %drawnow
),hold % ) to be ploted later QNS
%
% title('Example Bergent (2008)')
% ylaboratoryel(' Head (m)')
% xlaboratoryel ('Time (sec.)')
% legend('Head at Valve','Head at Mid point')% 'Tau');
%
% % axis ([-0.1 0.4 -20 100]) % set the graph scale
%
% NoTimeSteps=Tmax/Dt; % Again: change the time to time steps no.s
then convert it
%                      % again, to be included in the plots and data,
%                      % Q(2,1)i.e @ discrete 2 time 0
% if t==100
%     termine; % used to select execution time.
% end

end


                              % Plot and write the data

plot((1:NoTimeSteps)*Dt,H(65,1:NoTimeSteps),(1:NoTimeSteps)*Dt,H(16,1:
NoTimeSteps),'g');%,'k*',t*Dt,H(33,1:NoTimeSteps),'bd')%,t*Dt,tau,'+')
; %drawnow ),hold % ) to be plotted later QNS

title('Rig with leak at 1/8 th node (100m))')
ylaboratoryel(' Head (m)')
xlaboratoryel ('Time (sec.)')
legend('Head at Valve','Head at Mid point')% 'Tau');

% axis ([-0.1 0.4 -20 100]) % set the graph scale

%NoTimeSteps=Tmax/Dt; % Again: change the time to time steps no.s then
convert it
                     % again, to be inlcuded in the plots and data,
                     % Q(2,1)i.e @ discrete 2 time 0
```

```
%This function save the data in excel file.
%


dlmwrite('Transient_Q_Rig_Leak.csv',Q);
dlmwrite('Transient_H_Rig_Leak.csv',H);
%filename='Transient_Output.xlsx';
%sheet=1;
%xlswrite(filename,H,sheet,'A1');% Start the array with A1 cell at
%xlswrite(filename,Q,sheet,'B1');
```

C.2 Real Field Code

It is similar to the above, MOC numerical code but for the real field. It is without a leak node. Note: the execution time takes about four hours, due to length of the pipes and the number of its segments.

The input data are:

1. Pipes: number of pipes, length, wall thickness, Young's modulus, and diameter.
2. Reservoir head: It fixed and represents the water elevation above the datum.
3. Leak: leak node number, leak orifice coefficient.
4. Others: maximum calculation time, valve orifice coefficient, acceleration of gravity, wave speed, valve closing time.

The program reads the input data and then calculated the steady state. Then, it calculated the transient event. The outputs are the head and the flow for all computational nodes.

```
   Export Facilities Modelling
%this code to model the export operation facilities CB 23 which %consists
of shore Pipe line, Subsea pipelines, two flexible hoses %each components
is treated as a segment have the following numbers %1 for shore pipeline,
2 for the subsea one and 3 and 4 for hoses.

% Boundary Conditions:
%Bc's upstream is taken from the nominal data as fixed reservoir and
%the D/S of the system s open to atmosphere. The connection between %the
%subsea pipeline (2) and the two hoses (3) and (4) is a junction  %the
```

```
equation of continuity Q(2,NS,T)=Q(3,1,t)+Q(4,1,t) and the head %are
equal; H(2,NS,t)=H(3,1,t)=H(4,1,t)

% Time Step:
% based on external calculation by selecting the time step of the
%shortest component which is he flexible hose. Details are including %
on WinWord file have the same title.

% all variables for H and Q will be arrays with three indexes are the %
component, segment and time. While the Resistance coefficient, pipeline
impedance, length and other variables will have only the component
figure.
%

% Transient initially will be caused by closing the ship valves which
%closing in 15 seconds.


% L: Pipe Length (m), g: gravitational acceleration = 9.81 (m/s^2)
% E: Modules, HR: Reservoir Head (m),H0 : Valve Head (m)
% N: integer (no. of pipe segments (even)),Ti: initial time valve (sec.)
% D: Time step (sec.) Dx: internal distance between sections (m),
% H(i): Pressure Head (m) for section (i) , Q(i): volumetric Flow
%Rate(m^3/s) for section (i), R: Resistance coefficient, F: Darcy-
%Weisback friction factor, Ti: initial Tau value, Tf: final Tau %value
tc: valve operation time (sec.), a : wave speed (m/s)
% DHf: each Head loss due to friction for each Dx
% B=a/(G*A) pipeline impedance, R=Resistance Coefficient
%i= component no.  , j= segments of each component
% u & v wave scarettring variables (sqrt(power(j))

clear all              %
close all              %   to clear any previous data
clc                    %


%%% All variables can be defined with index figure, so that the
%%%programming can be followed. i.e H=NaNs(Nx,Nt) or H=NaNs(Nx,Nt).
%%%or fixed value H(i,j,t)=99.99

%L(1:4)=999.9;a(1:4)=999.9; N(1:4)=999.9;f(1:4)=999.9;D(1:4)=
Npipes = 4;
% 1st Component, shore pipe line
L(1)=300;
a(1)=1051;
D(1)=1.2192;
f=0.018;
HR=180 ;
g=9.81;
N(1)=4;
A(1)=pi*(D(1)/2)^2;

t=0;

% second component, subsea line
```

```
L(2)=15000; a(2)=1019; D(2)=1.4224; f=0.018;  N(2)=150;
A(2)=pi*(D(2)/2)^2;

% 3rd & 4th component flexible hoses
L(3)=400  ; L(4)=L(3); a(3)=411.5;a(4)=a(3); D(3)=0.6096;D(4)=D(3);
f=0.018;
N(3)=4;N(4)=N(3); A(3)=pi*(D(3)/2)^2; A(4)=A(3);

% Ship valve

tc=15; ti=1;tf=0; Tmax=100; E=0.75; CdA0=0.009;
% Tmax selected based on Dt to give an integer time step. (Normally
%30 sec. for analysis the pump start, increased to 100 seconds,
% it should be at least 890 seconds (the pump start up time)


% Calculate the Dt and Dx, the WinWord file for more information.
Dt=0.1098;



% calculate B & R & steady State Solver for all segments and steady
%state solver

NoTimeSteps=Tmax/Dt; % change the time to time steps no.s then
                     % convert it again, to be included
                     % in the plots and data,
                     % Q(2,1)i.e. @ discrete 2 time 0

NoTimeSteps=round(NoTimeSteps);
Tmax=NoTimeSteps*Dt;

H=zeros(Npipes,length(N),NoTimeSteps);


for i=1:Npipes;
Dx(i)=L(i)/N(i) ;

R(i)=f*L(i)/(2*g*D(i)*A(i)^2*N(i)) ; % Resistance coefficient,
B(i)=a(i)/(g*A(i));  % Pipe-line impedance

% Steady State Solver
Q0=16860/3600;   % Refer to the design pumping volumetric flow rate

Q03=Q0/2;
Q04=Q03;

     % Assume the vaibles are in matrix of position and time, i.e
            % H(x,t) and Q(x,t)

        % Since Matlab accepts only positive integer as array index,
        % I avoid theZero, assume t=0 will be t=1 then to show
        % the results, subtract 1.


    for j=1:N(i);
```

```
    if i==1
    H(1,1,1)=HR;    %%%%%%NOTE: t=0 does Matlab accept that%%%%%%%
% should be at reservoir B C but copy here to maintain seq.
    H(i,j+1,1)=HR-j*(0.811); % to get H for each point at steady
                             % state
    Q(i,j,1)=Q0;          % & i+1 to keep H(1,1,t)=152 later.
    H(i,N(i)+1,1)=HR-N(i)*(0.811);
    Q(i,j+1,1)=Q0;


    elseif i==2
        H(2,1,1)=H(1,5,1);
        H(i,j+1,1)=H(2,1,1)-j*(0.811); % to get H for each point at
                                       %steady state
        Q(i,j,1)=Q0;

        H(i+1,1,1)=H(2,1,1)-N(i)*(0.811);
        H(i+2,1,1)=H(2,1,1)-N(i)*(0.811);
        % Q(i,j+1,1)=Q0/2; % at this node the pipe divided into two
                         % sections include i=3 then i=4
    else                %

% take pressure drop from the last segment, previous DHF
        H(i,j+1,1)=H(i,1,1)-j*(11.925); % divide calculated hf/N,
                                        %while hf include 50m
                                        %elevation (including sea
                                        %depth0 sections.


        Q(i,j,1)=Q0/2;
        Q(3,5,1)=Q0/2;
        Q(4,5,1)=Q0/2;
        QNS=Q03;
    end
    end
end









tc=tc/Dt;    % to convert time steps to real time, /Dt
              % in tau eq. so can divide t (see below)




  hold on

  % Solve for the different points with the time
  % step
for t=2:1:NoTimeSteps;
```

```
for i=1:4

% 1st: Reservoir B C

if i==1
%H(1,1,t)=HR;
H(1,1,t)=81.6+t/8105*80.6; % Simulate the pump start and the US
%reservoir pressure rise from 8 bar to 15.9 bar, in 14.8 mins (890
%seconds) ( t/NoTimeSteps, gives in seconds). Simulate linear
%relation for the pump

Q(1,1,t)=(HR-H(1,2,t-1)+B(i)*Q(1,2,t-1))/(B(i)+R(i)*abs(Q(1,2,t-1)));

%elseif i==2             %%%%%%%%%%%%%%%%%%%%%%%% TO BE REVIEW TO
INCLUDE JUNCTIONS FOR i=2,3 and 4
%   CP=H(1,4,t-1)+B(1)*Q(1,4,t-1);%
%   BP=B(1)+R(1)*abs(Q(1,4,t-1));  %
%   CM=H(2,2,t-1)-B(2)*Q(2,2,t-1); %
%   BM=B(2)+R(2)*abs(Q(2,2,t-1));

%H(2,1,t)=(CP*BM+CM*BP)/(BP+BM); % Initial the  1st points for next
%Q(2,1,t)=(CP-CM)/(BP+BM);       % segment




%else      % for 3d and 4th segments which end with valves.

%    CP=H(2,150,t-1)+B(2)*Q(2,150,t-1);% Similar to DOWNSTREAM Bc
(above),
%    BP=B(2)+R(2)*abs(Q(2,150,t-1));  % However here in general form.
%    CM=H(3,2,t-1)-B(3)*(2*Q(3,2,t-1)); % Note: Similar results for
the below when adding
%    BM=B(3)+R(3)*abs(2*Q(3,2,t-1));  % Q(3&4,1,-1) together like
below.

%H(3,1,t)=(CP*BM+CM*BP)/(BP+BM); % Initial the  1st points for next
%Q(3,1,t)=(CP-CM)/(BP+BM);       % segment

% To find the branch 4, assume similarity of both in operations
condition.
%H(4,1,t)=H(3,1,t)               % Initial the 1st points for next
%Q(4,1,t)=Q(3,1,t)               % segment




end

%second Internal points

CP=0;CM=0;BP=0;BM=0;  % During debugging check the error when occur.

for j=2:N(i) % N increased by 1 to avoid the zero index, in the C.
             %eq's below
```

```
H(1,1,t)=HR; % Actually the H(0) to avoid the Zero as index

CP=H(i,(j-1),t-1)+B(i)*Q(i,(j-1),t-1);
BP=B(i)+R(i)*abs(Q(i,(j-1),t-1));
 if  j<150 % since the index increase above the max. index, this
condition is sitting to avoid Matlab error.
 CM=H(i,(j+1),t-1)-B(i)*Q(i,(j+1),t-1); %    General
 BM=B(i)+R(i)*abs(Q(i,(j+1),t-1)); %              Equations

 else  CM=H(i+1,1,t-1)-B(i+1)*(Q(i+1,1,t-1)+Q(i+2,1,t-1));% to avoid
MATLAB error because of that.
       BM=B(i+1)+R(i+1)*abs(Q(i+1,1,t-1)+Q(i+2,1,t-1));% To deal at
DOWNSTREAM BC, avoid increasing index (array)


 end

H(i,j,t)=(CP*BM+CM*BP)/(BP+BM);
Q(i,j,t)=(CP-CM)/(BP+BM);


end

% 3rd D/s points for each components, i.e.; 1,2,3 and 4.


if i==1
    CP=H(i,4,t-1)+B(i)*Q(1,4,t-1);
    BP=B(i)+R(i)*abs(Q(i,N(i),t-1));
    CM=H(2,2,t-1)-B(2)*Q(2,2,t-1);
    BM=B(2)+R(2)*abs(Q(2,2,t-1));

H(2,1,t)=(CP*BM+CM*BP)/(BP+BM);  % Initial the 1st point for next
Q(2,1,t)=(CP-CM)/(BP+BM);        % segment

elseif i==2
    CP=H(2,150,t-1)+B(2)*Q(2,150,t-1);% Similar to DOWNSTREAM Bc
(above),
    BP=B(2)+R(2)*abs(Q(2,150,t-1));  % However here in general form.
    CM=H(3,2,t-1)-B(3)*2*Q(3,2,t-1); % 2*Q..since at the junction the
two Q's
    BM=B(3)+R(3)*abs(2*Q(3,2,t-1));   % are identical

H(3,1,t)=(CP*BM+CM*BP)/(BP+BM); % Initial the  1st points for next
Q(3,1,t)=(CP-CM)/(BP+BM);       % segment

% To find the branch 4, assume similarity of both in operations
condition.
H(4,1,t)=H(3,1,t)               % Initial the 1st points for next
Q(4,1,t)=Q(3,1,t)               % segment


else      % for 3d and 4th segments which end with valves.
```

```
if t<tc

   tau=ti-(ti-tf)*(t /tc)^E;
else tau=tf;
end

CP=H(i,N(i),t-1) +B(i)*Q(i,N(i),t-1);
BP=B(i)+R(i)*abs(Q(i,N(i),t-1));



Cv=tau^2*Q03^2/(2*H(i,N(i),t-1));% shifted up to check% derivate from
                                  %the valve given equation (Ex 3-1)
QNS(t)=-BP*Cv+sqrt((BP*Cv)^2+2*Cv*CP);
HNS(t)=CP-BP*QNS(t);
Q(3,5,t)=QNS(t);
Q(4,5,t)=QNS(t);
H(3,5,t)=HNS(t);
H(4,5,t)=HNS(t);
end




% when assume sudden closing, active the following:
%QNS(t)=0;
%CP=H(3,N(i),t-1) +B(i)*Q(i,N(i),t-1);
%BP=B(i)+R(i)*abs(Q(i,N(i),t-1));
%HNS(t)=CP-BP*QNS(t);


 end

%%% Calculate the wave scarettring variables at different points.

% Y(i)=pi*(D(i)/2)^2/a(i); %  calculate the a Admittance
% u3=sqrt(Y(i)/2)*(883*g*H(3,2,t))+sqrt(1/(2*Y(i)))*Q(3,2,t)*A(3);  %
P=Density*g*HNS
% v3=sqrt(Y(3)/2)*(883*g*H(3,2,t))-sqrt(1/(2*Y(i)))*Q(3,2,t)*A(3);
% u2=sqrt(Y(2)/2)*(883*g*H(1,2,t))+sqrt(1/(2*Y(2))*Q(1,2,t))*A(2);  %
P=Density*g*HNS
% v2=sqrt(Y(2)/2)*(883*g*H(1,2,t))-sqrt(1/(2*Y(2))*Q(1,2,t))*A(2);

                                % Plot and write the data

plot(t*Dt,HNS(t),'bx-',t*Dt,H(2,1,t),'k+-'); drawnow  %,t*Dt,tau,'ro')
%t,HNS,'kx'),hold % t,QNS,'p--') to be plotted later %QNS
 %plot(t*Dt,u3,'bo',t*Dt,v3,'kx');
% plot(t*Dt,u(2),'bo',t*Dt,v(2),'k+');

title('Pressure Headownstream @ different Points');
ylaboratoryel('Head (m) ');
xlaboratoryel ('Time (sec.)');
```

```
legend ('D/S point','U/S shore pipeline ');

% axis ([0 4.35 120 130]) % set the graph scale
t=t/Dt;
NoTimeSteps=Tmax/Dt; % Again: change the time to time steps no.s then
convert it
                     % again, to be included in the plots and data,
                     % Q(2,1)i.e @ discrete 2 time 0


end
%}
```

C.3 Cross-Correlation and its second derivative Code

This code reads the data from LabVIEW files recorded after the experimental runs. Before analysing the raw data, the code filters it with low-pass. The data process by the cross-correlation and its derivatives. The outputs data then can be drawn or analysis.

```
%clear all             % to clear any previous data
%close all             % close all figures windows.
%clc
%a=(H(64,1:NoTimeSteps)); %node 64 before the last point, H=0 when
consider the pump start up effect.
%b=(H(16,1:NoTimeSteps));

 %a=[0 0 0.5 0.7 0 ];
 %b=[0 0.5 0.7 0 0 ];

%%%%%% This to read the collecting data and analysis directly%%%%
% a=xlsread('C:\Users\hsharbi\Google Drive\Documents\Collecting
Data\KOC\5 Seconds Data\Data37_Calm 20 Feb 18_2.xls','CALM
20','F2036..F3701');
% b=xlsread('C:\Users\hsharbi\Google Drive\Documents\Collecting
Data\KOC\5 Seconds Data\Data37_Calm 20 Feb 18_2.xls','CALM
20','H2036..H3701');
% Dt=5; % Delta time is 30 seconds for some collecting data
% Tmax= 8325; % total loading time in seconds, different between cases
66900
% NoTimeSteps=Tmax/Dt; % change the time to time steps no.s then
convert it
%                      % again, to be included in the plots and data,
%                      % Q(2,1)i.e @ discrete 2 time 0
% NoTimeSteps=round(NoTimeSteps); % Convert to integer.
%%%%%%%%%%%%%%%%%%%%%%%%%%%%%%%%%%%%%%%%%%%%%%%%%%%%%%%%%%%%%%%%
```

```
%%%%% This to read the experimental rig data and analysis
directly%%%%
data = dlmread('C:\Users\hsharbi\Google Drive\Experimental Runs\NO
LEAK , SS 0.6 DOWNSTREAM WH, 0.6-1.2 US WH,0.6-1.8 US WH, 1.8
DOWNSTREAM WH (without text easy to read).txt','',[0 1 273226 5]);%
[row (1st =0) col row col]
% Read the data 1st column time no' 9 should be divide by sample rate)
% then the 5 pressure transducers.

%NOTE: DO NOT filter the data twice.
% averaging all points central by 200 points
avg_data=movmean(data,200,1); % 200 the central moving average, zeros
                              %are cncled and the average
                              % calculate on number of non-zero
                              %points. 1 deals with columns rather
                              % than rows.

a=data(:,3); % P1
b=data(:,4); % P2


% Low pass filter for all data

order=32; % increase figure get smoother.
cut_off=500/2500; % cut off freq 2000 to normalize / Nyquist Freq(=
Sampling Freq/2)
filtdata=fir1(order,cut_off);%  low-pass frequency filter.
af=conv(a,filtdata); % convolution law to filter the raw data 1st
pressure.
bf=conv(b,filtdata); % convolution law to filter the raw data second
pressure.


Dt=0.0002; % Frequency 5000kHz Dt=0.0002 & for 1kHz Dt=0.001 sec.
NoTimeSteps=size(data,1);

NoTimeSteps=round(NoTimeSteps); % Convert to integer.
%%%%%%%%%%%%%%%%%%%%%%%%%%%%%%%%%%%%%%%%%%%%%%%%%%%%%%%%%%%%%%%%
%function [result] = myXCorr(A , B)
%Implementation of the Cross Correlation Function


N=size(a,1); % when use the code for the numerical analysis (MOC
code), the N=size(a,2), M=size(b,2) and it is working ??
M=size(b,1); % check?? Take the no. of rows as sample no.. If data in
one row, should be convert.
%
result = zeros(1, N + M - 1 );
result=xcorr(af,bf);

% or
% len = size(result,2);
% for m = 1 : len  %code if xcorr function not exist.
%    arg = (m - N);
%
%    if(arg < 0)
%        negativeCondition = 1;
%        limit = N + arg;
```

```
%    else
%        negativeCondition = 0;
%        limit = N - arg;
%    end
%
%    for n = 1:limit
%            if(negativeCondition == 0)
%             result(m) = result(m) + a(arg + n) * b(n);
%            else
%             result(m) = result(m) + a(n) * b(n - arg);
%            end
%    end
% end
% or Nioulfar Code
% np=M;
% R33 = zeros(np,1);
%             for m=1:np+1
%                 for n=1:np-m+1
%                     R33(m) = R33(m)+a(n)*b(n+m-1);
%
%                 end
%             end




%lag = -(N-1):1:N-1;% -503:1:5grid 03;%   , general code

%plot(lag*Dt, result);
%plot(lag, mResult);

D1=diff(result)/Dt; % diff function calculate the difference between
the array and divide it by integer,
D2=diff(D1)/Dt;     % default (1) so divide by Dt to differentiate,
                    %NOTE: R1 will be N-1 number & R2 N-2
%plot((4:NoTimeSteps*2)*Dt,D2) % start from 4 ( the new x-axis is N-
%2,nno's of sample)% 362 to let the x-axis (time) and the second %der.
CC have the same lengths




%hold on
% plot(filtdata);
% plot(filtdata);
plot((4:(NoTimeSteps+8)*2)*Dt,D2);% figure added to time step depends
on the filter order, like 16, 32, ..
```

C.4 Alignment Code

This code was created to align two different data from different experimental runs, like run with leak and without leak for the same water hammer transient event. This

function was created to align two data from different runs together. The two approaches, the gradient and the mean approach, are included and the last one is active. The code in addition to the main purpose, charts alignment, it includes the low-pass filter and moving average filter. The data first reads form the LabVIEW data files.

```
  %%%%%%%%%%%%%%%% Align Function %%%%%%%%%%%%%%%%%%%%

% since the data from different experimental runs are collected
%manually,
% this script to align the data automatically.
clear

data1 = dlmread('C:\Users\hsharbi\Google Drive\Experimental Runs\NO
LEAK , SS 0.6 DOWNSTREAM WH, 0.6-1.2 US WH,0.6-1.8 US WH, 1.8
DOWNSTREAM WH (without text easy to read).txt','',[0 0 273226 4]);%
[row (1st =0) col row col]
data2 = dlmread('C:\Users\hsharbi\Google Drive\Experimental Runs\L3
(1mm) 0.6-1.2 (2) 20-11-17.txt','',[0 0 20000 4]);% [row (1st =0) col
row col]
%data2 = dlmread('C:\Users\hsharbi\Google Drive\Experimental Runs\L5
(1mm) 0.6-1.2.txt','',[0 0 70500 4]);% [row (1st =0) col row col]
%data2 = dlmread('C:\Users\hsharbi\Google Drive\Experimental Runs\L1
4mm 0.6SS WH DS, WH UP 0.6-1.2,0.6-1.8.txt','',[0 0 236450 4]);% [row
(1st =0) col row col]
%data2 = dlmread('C:\Users\hsharbi\Google Drive\Experimental Runs\L5
4mm 0.6SS WH DS, WH UP 0.6-1.2,0.6-1.8.txt','',[0 0 188100 4]);% [row
(1st =0) col row col]
% Note: the first column in LaboratoryVIEW, does not present the time

% NOTE: Do NOT filter the data twice.
%%%%%%%%%%%%%%%%%%%%%%%%%%%%%%
% Averaging all points central by 200 points
% avg_data1=movmean(data1,200,1); % 200 the central moving average,
both sides, the function consider only the cells with values
%                                % calculate the number of non-zero
points.
%                                % 1 deals with columns rather than
rows.
% avg_data2=movmean(data2,200,1);

%%%%%%%%%% OR %%%%%%%%%%%%%%%
% Low pass filter for all data
%

P11=data1(:,1);P21=data1(:,2);P31=data1(:,3);P41=data1(:,4);P51=data1(
:,5);

P12=data2(:,1);P22=data2(:,2);P32=data2(:,3);P42=data2(:,4);P52=data2(
:,5);

order=32; % increase figure get smoother.
cut_off=500/2500; % cut off freq 2000 to normalize / Nyquist Freq(=
Sampling Freq/2)
```

```
filtdata=fir1(order,cut_off);%  low-pass frequency filter.
P11=conv(P11,filtdata);
P21=conv(P21,filtdata);P31=conv(P31,filtdata);P41=conv(P41,filtdata);P
51=conv(P51,filtdata);
P12=conv(P12,filtdata);
P22=conv(P22,filtdata);P32=conv(P32,filtdata);P42=conv(P42,filtdata);P
52=conv(P52,filtdata);
avg_data1=[P11,P21,P31,P41,P51];
avg_data2=[P12,P22,P32,P42,P52];

% Select the desirable event window %
subplot(2,1,1); % break here to see the chart and select star and end
times
plot(avg_data1);grid;
title('No leak. WH events: SS 0.6l/min DOWNSTREAM, 0.6-1.2 l/min. UP,
0.6-1.8 l/min. UP, and SS 1.8l/min. DOWNSTREAM');
xlaboratoryel('Time Step');ylaboratoryel('bar');
subplot(2,1,2);
plot(avg_data2);grid;
title('L3 1mm. WH event:0.6-1.2 l/min. UP');
xlaboratoryel('Time Step');ylaboratoryel('bar');

% based on the above plots the WH event window will be selected
individually.
% by identify the start time, start#, and the end# will be start time
+
% 12500 (2.5 second).

%STOP BELOW TO ENTER WINDOW TIME. INPUT start1 & start2 manually.
NOTE: the start time should be > 500 steps,
% in difference from the SS region to avoid -ve index in following
% calculations. start#: beginning of considering time window.

NoTimeSteps1=(start1+12500-start1)-50;  % is added in gradient
calculations NOTE: ENTER START1 & START2 MANUALLY AFTER SEEN THE
PREVIOUS  PLOT
NoTimeSteps2=(start2+12500-start2)-50;   % to ensure suitable
comparison interval and reduce the noise effect.



   %%% Pick up the start of WH to match the
   %%%% charts either by gradient or
   %%%% Max/Min/mean approach

                              %%%%% Gradient Approach%%%%

% Find the change in gradient for P1 in data 1
% for i=1:NoTimeSteps1 % avoid zero and exceeding the matrix
dimension.
%     gradient1(i)=(data1(start1+i+50,1)-data1(start1+i,1))/50; %After
averaging every 20 steps have points,
%                                              % so select 50 to cover
wider
%                                              % window. GRADIENT IS
```

```
%                                                % CALCULATED for P1
% end
% % Find the change in gradient for P1 in data 2
% for i=1:NoTimeSteps2 % avoid zero and exceeding the matrix
dimension.
%     gradient2(i)=(data2(start2+i+50,1)-data2(start2+i,1))/50; %After
averaging every 20 steps have points,
%                                                % so select 50 to cover
wider
%                                                % window. GRADIENT IS
%                                                % CALCULATED for P1
% end
%
%    subplot(2,1,1); % break here to see the chart and select star and
end times
% plot(gradient1);grid;
% title('No leak gradient');xlaboratoryel('Time
Step');ylaboratoryel('Arbitry Altitude')
% subplot(2,1,2);
% plot(gradient2);grid;
% title('L5 4mm gradient');xlaboratoryel('Time
Step');ylaboratoryel('Arbitry Altitude')
%
%     [Max1,locs1]=max(gradient1); %Find the max gradient, should
select small time window for 2.5 seconds
%     [Max2,locs2]=max(gradient2);
%
%      % Based on P1 WH locations, the time steps are selected for P2,
P3 ..
%     P11=avg_data1(start1+abs(locs1-500):start1+locs1+12500,1);
%     P12=avg_data2(start2+abs(locs2-500):start2+locs2+12500,1);
%
%    P21=avg_data1(start1+abs(locs1-500):start1+locs1+13000,2);% The
addition number to ensure the P2,P3,
%    P22=avg_data2(start2+abs(locs2-500):start2+locs2+13000,2); %P4
and P5 have suffient time
%
%     P31=avg_data1(start1+abs(locs1-500):start1+locs1+13700,3);
%     P32=avg_data2(start2+abs(locs2-500):start2+locs2+13700,3);
%
%     P41=avg_data1(start1+abs(locs1-500):start1+locs1+14700,4);
%     P42=avg_data2(start2+abs(locs2-500):start2+locs2+14700,4);
%
%     P51=avg_data1(start1+abs(locs1-500):start1+locs1+15600,5);
%     P52=avg_data2(start2+abs(locs2-500):start2+locs2+15600,5);
%


%%%%%%%%%%%%%%%% Max OR Mean Approach %%%%%%%%%%%%%%%%%%%%%%%%

 % Find the max OR mean value in P1 and try to match different runs


%[P11max,locs1]=max(P11(start1:start1+12500));[P12max,locs2]=max(P12(s
tart2:start2+12500));

P11=avg_data1(start1:start1+12500,1); % abs() to avoid -ve values.
    P12=avg_data2(start2:start2+12500,1);
```

```
 DiffCalc1=abs(mean(P11)-P11);DiffCalc2=abs(mean(P12)-P12);% find the
diff. between the mean all P values

locs1=find(DiffCalc1==min(DiffCalc1));locs2=find(DiffCalc2==min(DiffCa
lc2));% define the locations of min. diff.
 %  Then match the two pressure, delete the difference in time.

   Dx=locs2-locs1; % define the spatial difference & modify the strat2
to coincided together.
   % Based on P1 WH locations, the time steps are selected for P2, P3
..
    P11=avg_data1(start1:start1+12500,1); % abs() to avoid -ve values.
    P12=avg_data2(start2+Dx:start2+Dx+12500,1);

    P21=avg_data1(start1:start1+13000,2);% The addition number to
ensure the P2,P3,
    P22=avg_data2(start2+Dx:start2+Dx+13000,2); %P4 and P5 have
suffienct time

    P31=avg_data1(start1:start1+13700,3);
    P32=avg_data2(start2:start2+Dx+13700,3);

    P41=avg_data1(start1:start1+Dx+14700,4);
    P42=avg_data2(start2+Dx:start2+Dx+14700,4);

    P51=avg_data1(start1:start1+15600,5);
    P52=avg_data2(start2+Dx:start2+Dx+15600,5);
```

C.5 Noise Removal Algorithm

This code was explained briefly in this section. It is principle to record 5 different runs data as a matrices. Then it check the peaks with two criteria, fisrt , it is repeated in the 5 runs. Secondly, check if the peak is high with certain percentage. If these two conditions are achieved, then the code will acknowledge this peak as new feature. The operator has a choice to decline or consider it as a new feature.

```
%function  [ NF,SF ] = Denoise_Filter( D2,SF,R2,R3,R4,R5 )
%       Denoise_Filter
%   is used to remove the random noises (not reputable) based on the
%   variable amplitude in the y-axis and time or location in the x-
%axis.
%   D2: the variable will be accumulated in the data base (temporary,
```

```
%   the second derivative of cross correlation).
%   NF: new system features (peaks).
%   SF: known system features, must be an input

 R1=R2;
 R2=R3;      % these steps to relocate the data and cancel the oldest
one,
 R3=R4;      % and include the new one (D2)
 R4=R5;
 R5=D2;

 NoNodes=length(R1); % define the no of nodes, must be equal for all
runs
                  % (Data) to compare the peaks at same locations or
time steps.
 NoData=5;

 SampleArray=[R1;R2;R3;R4;R5];
 Peak(NoData,NoNodes)=zeros; %  preallocated the array to avoid size
%changing.
 NF_logical(NoData,NoNodes)=zeros; % preallocated the array to avoid
%size changing.
 NF(NoNodes)=zeros;

                %% Identify Peaks
% The peaks go through two filters, first in the below if loop, then
after
% the following statement.
 for No1=1:NoData
     for No2=1:NoNodes
       if  abs(SampleArray(No1,No2)-SF(No1,No2))>0.05*SF(No1,No2); %
1st FILTER
    % This command is more generated than (SampleArray(No1,No2)~=0)
    % this relationship (not equal) could be %changed to include
    % percentage (ex.  rather than equal to zero
    % Since, this code begin with the second
    % derivative cross-correlation.
           Peak(No1,No2)=SampleArray(No1,No2); % to include the peaks
%only.
       end
     end
 end
 %% second FILETER
 SF_logical=SF~=0;

% for i=1:NoNodes
   NF_logical=Peak~=SF; % return the array location (row,column) by
%integer 1, others zeros. NF_logical, to distinguish between the NF
%matrix & logical array defined the location of known features.

  [row,col]=find (NF_logical~=0 & SF_logical==0); % defind the
%location of nonzero elements and at the same time not a system
%features end

%%%%%% ------------------------------------------------------------
---------
```

```
 % The following should be applied when all the 5 runs have the same
%peak, ex the first column are almost equal, means the sample at that
point has a new feature.
NPlocation=length(row);
NF=SF;  % this step ensure to contain the old SF peaks, and remaining
        %is zero, but the following if statement add the new all runs
        %peaks.

for i=1:NPlocation

        if abs(Peak(row(i),col(i))-
(SF(row(i),col(i)))>0.05*(SF(row(i),col(i)))) &&
all(NF_logical(:,col(i))==1);
            % second condition '(:,col(i)' to be sure that it is
            %availaboratoryle at
            % all 5 runs.
        NF(:,col(i))=Peak(row(i),col(i)); % Defined the new peaks as
                                          %NF (new system features)
        else

        end

end
% PV=Peak(row,col); % defined the peak values

 % NF will indicate the location, while peak array contains the real
 % values. The new features NF will be output for this function.
 %. Then outside this function, the option to change it to system
 %features (SF) can be implemented.

% ------------------------------------------------------------------
--
% To consider the NF as SF, a function a& may GUI is needed to control
by
% operator or can be deleted. After this stage the SF could be
%updated and the NF will be nill in order to capture new features at
%with new runs.
%
% SF=NF;
```

Appendix D Enhanced The Real Field Data System

D.1 Collecting Data and Installing the High Speed Data Logging System (HSDLS)

The oil is pumped at a rate of approximately 14500 metric ton per hour, or alternatively by gravity feed due to elevation of the header tank above the sea. This provide sufficient head to deliver a flow rate which varies between 10500 and 11200 MT/hr. The gravity feed depends on the CALM Buoy being utilised and the number of tanks being loaded.

Data is fed from various locations to the SCADA system. Downstream of the pump, the metering skid contains seven streams. From each of these, pressures and the flows can be obtained. Depending on the required flow rate, the optimum number of streams will be operated. For simplification and to reduce discrepancies, the pressure transmitter downstream of the discharge of the pump will be used here. In addition, at location 8, in Table 5-1 the subsea pipe is divided into two hoses and there are pressure transmitters at each hose which should give the same reading. After collecting the data from these locations, the data is reanalysed to present a single reading.

SCADA system has the ability to collect the data, control all the readings and also to control elements in the system. In long pipelines networks, it is recommended as the best data acquisition system [10]. Since the facility has a significant number of elements (1618 items), the collecting data scan time is suitable for normal operation and maintenance operation, despite the signals from transducers being mostly continuous. The current scan time, or sampling rate is 1 reading of each type per second.

In water-hammer leak detection approaches, the sampling rate is related to the acoustic speed of the system, hence high frequency sampling is required. For example, a reasonable sampling rate is 1 kHz, that is 1000 readings per second is typically required in measuring fluid transient. This frequency is much slower than the data acquisition rate from this system.

This information about the low data acquisition rate in the real system was conveyed to the Export Maintenance Team by the author. Without affecting any normal operation or introducing maintenance issues, the scan rate was increased ten of old, from 1 second to 90-100 *ms*. The work was completed in mid-January, 2018. Figure D-1 and Figure D-2 illustrate the old and the new system, respectively. The data are displayed to 8 decimal points.

Field Loop Wiring Report Format (data per second)

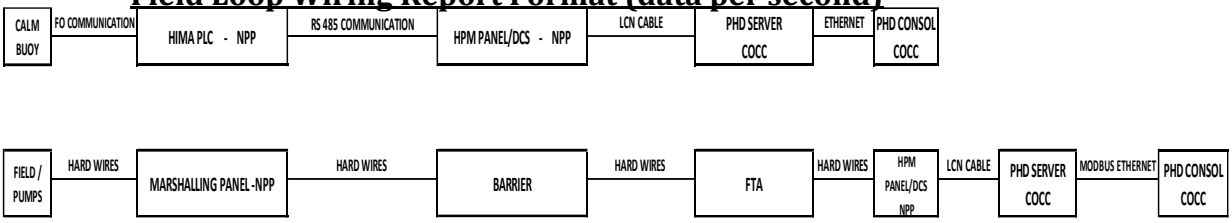

PHD SYSTEM DATA						
Sr. No.	DateTime	612PI600A	612PI600B	612PI600C	612PIG20P20	612PIP20D
		BAR	BAR	BAR	BAR	BAR
		BUOY # 20 CRUDE PRESSURE A	BUOY # 20 CRUDE PRESSURE B	BUOY # 20 CRUDE PRESSURE C	PUMP # 20 INLET LINE	PUMP # 20 OUTLET LINE
1	23-12-2017 3:47	4.700000	4.6	4.5	8.466642	10.03412
2	23-12-2017 3:47	4.715000	4.616667	4.516667	8.464684	10.0652
3	23-12-2017 3:47	4.730000	4.633333	4.533333	8.462726	10.09629
4	23-12-2017 3:47	4.745000	4.65	4.55	8.460767	10.12737
5	23-12-2017 3:47	4.760000	4.666667	4.566667	8.458808	10.15845
6	23-12-2017 3:47	4.775000	4.683333	4.583333	8.456849	10.18954
7	23-12-2017 3:47	4.790000	4.7	4.6	8.454891	10.22062
8	23-12-2017 3:47	4.805000	4.716667	4.616667	8.452932	10.25171
9	23-12-2017 3:47	4.820000	4.733333	4.633333	8.450974	10.28279
10	23-12-2017 3:47	4.835000	4.75	4.65	8.449016	10.31388

Figure D-1: Field loop & report format before implementing High Speed Data Trending System.

Field Loop Wiring Report Format (data per 100 millisecond)

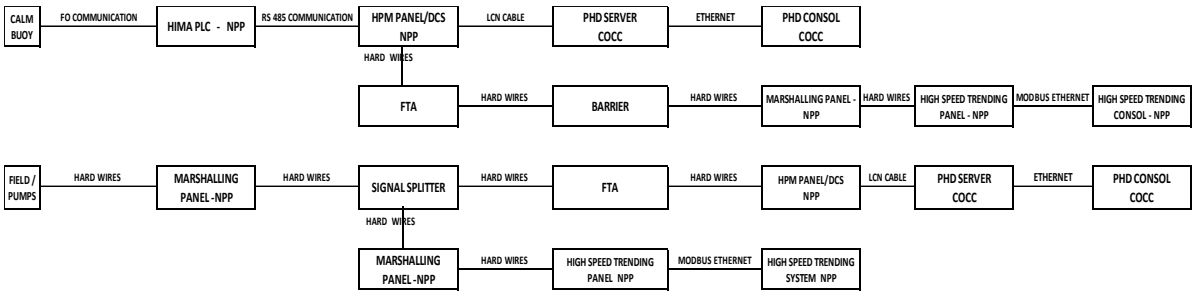

HIGH SPEED DATA LOGGING SYSTEM (NEW SYSTEM)						
Sr. No.	DateTime	612PI600A	612PI600B	612PI600C	612PIG20P20	612PIP20D
		BAR	BAR	BAR	BAR	BAR
		BUOY # 20 CRUDE PRE	BUOY # 20 CRUDE PRES	BUOY # 20 CRUDE PRE	PUMP # 20 INLET LINE	PUMP # 20 OUTLET LINE
1	2017-12-23 03:47:00.093	004.9148440	004.6062498	004.5140619	008.4506245	010.1724997
2	2017-12-23 03:47:00.197	004.9148440	004.6062498	004.5140619	008.4506245	010.1724997
3	2017-12-23 03:47:00.297	004.9148440	004.6062498	004.5140619	008.4481249	010.1887503
4	2017-12-23 03:47:00.397	004.9148440	004.6062498	004.5140619	008.4481249	010.1887503
5	2017-12-23 03:47:00.500	004.9187498	004.6031251	004.5203128	008.4531250	010.1937504
6	2017-12-23 03:47:00.597	004.9187498	004.6031251	004.5203128	008.4531250	010.1937504
7	2017-12-23 03:47:00.700	004.9148440	004.6062498	004.5203128	008.4425001	010.1937504
8	2017-12-23 03:47:00.800	004.9148440	004.6062498	004.5203128	008.4425001	010.1937504
9	2017-12-23 03:47:00.900	004.9117188	004.6062498	004.5203128	008.4375000	010.2049999
10	2017-12-23 03:47:01.000	004.9117188	004.6062498	004.5203128	008.4375000	010.2049999

Figure D-2: Field loop & report format after implementing High Speed Data Trending System.

The system consists of three main parts: splitter, PLC and the SCADA. The splitter is used to split the signals, one is given to PLC/SCADA for data logging and the other is for Digital Control System DCS. The PLC Programmer Logic Control has six analogue inputs cards and each supports four channels 4-20 mA inputs. A 16-bit analogue converter is used to convert these signals into digital form. PLC can communicate with SCADA system using MODBUS protocol. Finally, the SCADA takes the input signal from PLC using the MODBUS protocol and saves the data into an SQL database. The SCADA system is also responsible for the display, control, alarms and reports generation.

The HSDLS architecture is shown in Figure D-3. It shows that the new branch of the HSDLS system starts from the splitter as an intersection point between the old and

new system. Then the analogue inputs are taken to the PLC and then the data monitoring system.

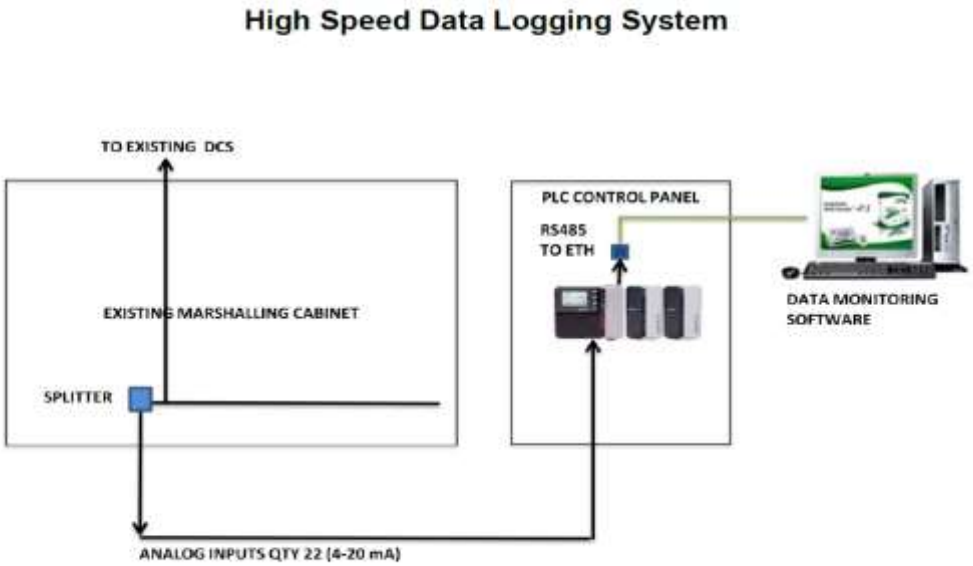

Figure D-3: The HSDLS architecture.

Unfortunately, the improvements raise two issues that make the field data difficult to analyse. The first and the main issue is that the sample frequency does not meet the leak detection criteria for complying with the system wave speed. So, the scanning frequency is a source of uncertainty [12]. Secondly, the work was completed in January, 2018 which was at a late stage of the researcher's scholarship period. In addition, the sampling rate is important because it governs the accuracy of the spatial resolution [27].